FTD-ID(RS)T-0361-82

# FOREIGN TECHNOLOGY DIVISION

THEORY OF THE RADIATION OF SURFACE ANTENNAS

by

L.N. Zakhar'yev, A.A. Lemanskiy, K.S. Shcheglov

SEP 0 7 1982

E

82 09 07 388

# UNEDITED MACHINE TRANSLATION $\sigma_{\zeta}$ mon

FTD-ID(RS)T-0361-82                    2 August 1982

MICROFICHE NR: FTD-82-C-001040

THEORY OF THE RADIATION OF SURFACE ANTENNAS

By: L.N. Zakhar'yev, A.A. Lemanskiy, K.S. Shcheglov

English pages: 357

Source:  Teoriya Izpucherniya Poverkhnostnykh Antenn,
         Publishing House "Sovetskoye Radio",
         Moscow, 1969, pp. 1-231,

Country of origin: USSR
This document is a machine translation.
Requester: USAMICOM
Approved for public release; distribution unlimited.
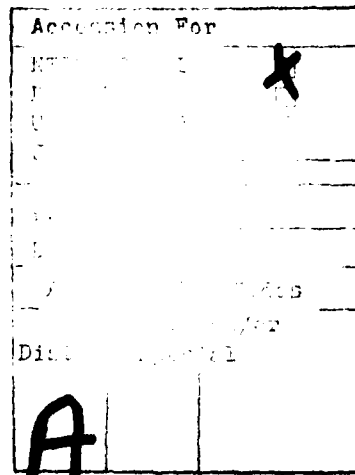
Table of Contents

# U. S. BOARD ON GEOGRAPHIC NAMES TRANSLITERATION SYSTEM

| Block | Italic | Transliteration | Block | Italic | Transliteration |
|-------|--------|-----------------|-------|--------|-----------------|
| А а | *А а* | A, a | Р р | *Р р* | R, r |
| Б б | *Б б* | B, b | С с | *С с* | S, s |
| В в | *В в* | V, v | Т т | *Т т* | T, t |
| Г г | *Г г* | G, g | У у | *У у* | U, u |
| Д д | *Д д* | D, d | Ф ф | *Ф ф* | F, f |
| Е е | *Е е* | Ye, ye; E, e* | Х х | *Х х* | Kh, kh |
| Ж ж | *Ж ж* | Zh, zh | Ц ц | *Ц ц* | Ts, ts |
| З з | *З з* | Z, z | Ч ч | *Ч ч* | Ch, ch |
| И и | *И и* | I, i | Ш ш | *Ш ш* | Sh, sh |
| Й й | *Й й* | Y, y | Щ щ | *Щ щ* | Shch, shch |
| К к | *К к* | K, k | Ъ ъ | *Ъ ъ* | " |
| Л л | *Л л* | L, l | Ы ы | *Ы ы* | Y, y |
| М м | *М м* | M, m | Ь ь | *Ь ь* | ' |
| Н н | *Н н* | N, n | Э э | *Э э* | E, e |
| О о | *О о* | O, o | Ю ю | *Ю ю* | Yu, yu |
| П п | *П п* | P, p | Я я | *Я я* | Ya, ya |

*ye initially, after vowels, and after ъ, ь; e elsewhere.
When written as ё in Russian, transliterate as yё or ё.

## RUSSIAN AND ENGLISH TRIGONOMETRIC FUNCTIONS

| Russian | English | Russian | English | Russian | English |
|---------|---------|---------|---------|---------|---------|
| sin | sin | sh | sinh | arc sh | $\sinh^{-1}$ |
| cos | cos | ch | cosh | arc ch | $\cosh^{-1}$ |
| tg | tan | th | tanh | arc th | $\tanh^{-1}$ |
| ctg | cot | cth | coth | arc cth | $\coth^{-1}$ |
| sec | sec | sch | sech | arc sch | $\operatorname{sech}^{-1}$ |
| cosec | csc | csch | csch | arc csch | $\operatorname{csch}^{-1}$ |

| Russian | English |
|---------|---------|
| rot | curl |
| lg | log |

## GRAPHICS DISCLAIMER

All figures, graphics, tables, equations, etc. merged
into this translation were extracted from the best
quality copy available.

THEORY OF THE RADIATION OF SURFACE ANTENNAS.

L. N. Zakhar'yev, A. A. Lemanskiy, K. S. Shcheglov.

Page 2.

In the book are examined the characteristics of the antennas, arranged/located on the surface of conductive bodies. Based on the examples to half-plane, key, circular and elliptical cylinders are given strict evaluations of the effect of edges, impedance of surface and finite dimensions of body to the radiation pattern of surface antenna. The results of investigation, reduced to the engineering formulas and the graphs/curves, can be used during the design of antennas, which do not create aerodynamic drag, or for calculating of line-source antennas and gratings of arbitrary range.

The book is intended for scientific workers and specialists in the region of antennas and applied electrodynamics, and also graduate students and students.

Page 3.

INTRODUCTION.

Theory and practice of antennas are developed in close
cooperation with many branches of contemporary science and
technology. The development of jet aviation and missile construction,
a rapid increase in the velocities of flight vehicles led to the fact
that as the onboard antennas together with the classical ones
(mirror, lens) increasing use find the surface antennas, i.e.,
antennas, which are located near or directly on the surface of
projectile and forming radiation pattern with the essential effect of
this surface. The fundamental advantage of surface antennas consists
in the fact that during their use as the onboard antenna systems do
not impose the restriction themselves to the aerodynamic shapes of
flight vehicles. At the same time surface antennas make it possible
to very effectively form/shape the required radiation patterns.

The theory of surface antennas encompasses a wide circle of the
questions, connected with the solution of internal problem, by
subsequent performance calculation of antenna radiation, by the
analysis of the effect of the medium (for example, the layer of
plasma), which surrounds antenna, on its characteristics. At present

there is a considerable volume of works [1] - [9], published in the Soviet and foreign literature, dedicated to different aspects of theory and surface of antennas technique. The book "Theory of the radiation of surface antennas" is dedicated to the solution of exterior problem for the antennas, which are located on the bodies of various forms. During the solution of exterior problem it is assumed that the antenna emits in the free space and field distribution in antenna aperture known. The obtained results of calculation correspond to amplitude-phase field distribution of sufficiently general view and therefore they can be used for the development of surface antennas of different types (slotted, impedance, etc.).

Page 4.

Aerodynamic objects are exclusively manifold and frequently accept complex forms, so that the solution of exterior problem in the general case is impossible. At the same time many aerodynamic objects or their individual sections can be sufficiently well approximated by surfaces which admit the analytical solution of electrodynamic problem. In the present work are examined the radiation characteristics of the surface antennas, arranged/located on the half-plane, key, to band, circular and elliptical cylinder, to sphere and spheroid.

From the vast class of surface antennas are not examined
virtually only conical antennas. The latter fact is connected with
the fact that the numerical calculation of the radiation field of
conical antennas according to precise formulas is extremely complex,
especially in the most interesting case of the asymmetric excitation
of the surface of cone. The approximate results known to the authors
of calculating conical antennas are obtained predominantly without
taking into account the effect of the point of cone, which is correct
in that region where the effect of vertex of a conical surface is
unessential. Since in the book are investigated the diffraction
phenomena, connected with shaping of the field of surface antennas,
the authors considered it advisable to restrain from the examination
of antennas, which are located on the surface of cone.

The questions in question in the book, are united by the fact
that they all are reduced to finding of the fields of those created
by radiation sources which are located near or directly on the
surface of one or the other body. For the solution of problems of the
type indicated can be used the different methods: the method of
Green's functions [10], reciprocity theorem in combination with the
solutions of appropriate diffraction problems [11], the method of
integral equations [10]. In this book as the basis of the analysis of
the radiation characteristics of surface antennas is assumed the
single approach, connected with the use/application of a reciprocity

theorem. As far as other precise, and also approximate methods of the solution of the problems in question are concerned are mentioned the works, in which these methods are utilized.

Page 5.


With the fulfillment of work the authors strove, mainly, for development/detection and analysis essential features of the radiation characteristics of surface antennas, and also for the development of the simple calculation procedures, which make it possible to manage without cumbersome calculations. For this purpose in the work together with strict ones extensively are used the approximate and asymptotic methods, complex problems are reduced to the simpler (or at least they are compared with them). If it was impossible to simplify problem was performed the detailed calculation whose results contain information, necessary during the construction of antenna. Work carries designing-theoretical character. Since at its base lies/rests a strict method, data of experiment were drawn only for the illustration.


In the book are placed mainly original materials, and also series/row of the results, published in the Soviet and foreign literature. The part of the results (Chapter 3 and 8) is obtained by the authors together with Z. I. Shteynfel'd. The numerical

calculations, widely utilized for the analysis of the radiation characteristics of surface antennas, are carried out under the management/manual of N. I. Dmitriyeva.

Page 6.


1.


FUNDAMENTAL CALCULATION RELATIONSHIPS


In present chapter is set forth the main apparatus necessary for performance calculation of radiation of surface antennas according to the reciprocity theorem. Here, as in all remaining chapters, is utilized the rationalized system of unity MKC. It is assumed that the dependence of electromagnetic field on the time takes form $\exp(-i\omega t)$.


1.1. According to Lorenz's lemma (for example, see [12]) electromagnetic fields $\vec{E}$, $\vec{H}$ and $\vec{E}_1$, $\vec{H}_1$, created by outside currents with bulk densities of $\vec{j}$ and $\vec{j}_1$, satisfy the relationship/ratio

$$\text{div}\,[\vec{E},\ \vec{H}_1] - \text{div}\,[\vec{E}_1,\vec{H}] = \vec{j}\vec{E}_1 - \vec{j}_1\vec{E}. \qquad (1.1)$$

Let us examine the system of two emitters, arranged/located arbitrarily relative to surface of S of the ideally conductive body (Fig. 1.1). As the emitter, which creates field $\vec{H}_1$, $\vec{H}_1$, let us select elementary electric dipole with the single moment/torque $\vec{p}$, which is located at certain point of space M. As another emitter, which creates field $\vec{E}$, $\vec{H}$, let us take antenna with the aperture, limited by surface $S_A$. Let us assume that they are known of the tangential field

component $\vec{E}_\tau$, $\vec{H}_\tau$ in antenna aperture.

Page 7.

Let us use Lorenz's lemma (1.1) to fields $\vec{E}_1$, $\vec{H}_1$, $\vec{E}$, $\vec{H}$, created by the sources in question in space V, limited by surfaces $S$, $S_A$ and spherical surface $S_0$ it is sufficient large radius (Fig. 1.1). According to (1.1) in space V

$$\operatorname{div} [\vec{E}, \vec{H}_1] - \operatorname{div} [\vec{E}_1, \vec{H}] = -\vec{j}_1 \vec{E}. \qquad (1.2)$$

Integrating expression (1.2) by space of the V taking into account theorem of Gauss-Ostrogradskiy and boundary conditions on surface of S, and also radiation condition, we obtain the following relationship/ratio:

$$\int\limits_{S_A} \{[\vec{E}_\tau, \vec{H}_1] - [\vec{E}_1, \vec{H}_\tau]\}\, \vec{n}_e\, ds = -\int\limits_{V_1} \vec{j}_1 \vec{E}\, dv_1. \quad (1.3)$$

In expression (1.3):

$\vec{n}_e$ - normal to $S_A$, external with respect to space V;

$V_1$ - space, in which is concentrated outside current with a density of $\vec{j}_1$.

In the case in question the source of outside current is elementary dipole and therefore

$$-\int\limits_{V_1} \vec{j}_1 \vec{E}\, dv_1 = 4\pi\, \vec{p}\vec{E}\,(M).$$
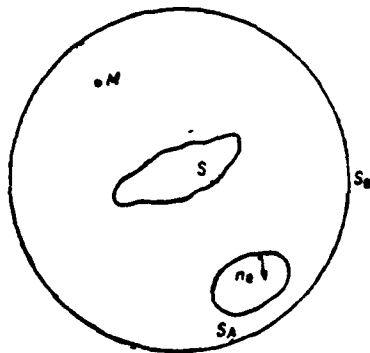
Fig. 1.1. To the derivation of reciprocity theorem.


Page 8.


Thus, component $E_p(M) = \vec{p}\vec{E}(M)$ of electric vector $\vec{E}$ of the field, created at the arbitrary point of space M of antenna, which is located near or directly on surface of S of conductive body, satisfies the relationship/ratio:

$$E_p(M) = \frac{1}{4\pi} \int_{S_A} \{[\vec{E}_r, \vec{H}_1] - [\vec{E}_1, \vec{H}_r]\} \vec{n}_e ds. \qquad (1.4)$$

Applying Lorenz's lemma to fields $\vec{E}$, $\vec{H}$ and $\vec{E}'$, $\vec{H}'$, by the antenna and elementary magnetic dipole, created by surface, which are located at point M and having the single dipole moment $\vec{q}$, we will obtain analogous relationship/ratio for component $H_q(M)$ of the magnetic vector of the field of antenna at point M:

$$H_q(M) = \frac{1}{4\pi} \int_{S_A} \{[\vec{E}_r, \vec{H}'] - [\vec{E}', \vec{H}_r]\} \vec{n}_e ds. \qquad (1.5)$$

Relationships/ratios (1.4) and (1.5) are the analytical expression of reciprocity theorem. These relationships/ratios show that the field of surface antenna at the arbitrary point of space M can be designed, if are assigned tangential components $\vec{E}_\tau, \vec{H}_\tau$ of field in antenna aperture and are known the values of the auxiliary fields $\vec{E}_1, \vec{H}_1; \vec{E}'$, $\vec{H}'$, created on surface $S_A$ by elementary electrical and magnetic dipoles, which are located at point M. Field distribution in antenna aperture in each specific case is determined as a result of the solution of internal electrodynamic problem. Fields $\vec{E}_1, \vec{H}_1; \vec{E}', \vec{H}'$ are the solutions of the diffraction problems, which correspond to the excitation of the body of the form in question by electrical and magnetic dipoles, which are located at point M (Fig. 1.1). Dipoles must be oriented in the same directions, as designed components $E_p\vec{p}, H_q\vec{q}$ of vectors $\vec{E}$ and $\vec{H}$.

Page 9.


If it is necessary to determine the radiation pattern of surface antenna, point M one should extend to infinity and then as the auxiliary vectors $\vec{E}_1, \vec{H}_1; \vec{E}', \vec{H}'$ it is necessary to take the solutions of the problems about the diffraction of the respectively polarized plane waves, which fall to surface of S of the body in question from the assigned direction. Since in the remote zone of antenna field $\vec{E}, \vec{H}$ carries the character of locally plane wave, for

calculating the radiation pattern it suffices to use one of the relationships/ratios [by expression (1.4) given above or (1.5)].

If antenna aperture $S_A$ coincides with the section of surface S of conductive body, expression (1.4), (1.5) they are simplified, since

$$[\vec{E}_{\imath}, \vec{H}_{\imath}]\, \vec{n}_e |_S = [\vec{E}', \vec{H}_{\imath}]\, \vec{n}_e |_S = 0,$$

they take the following form:

$$E_p(M) = \frac{1}{4\pi} \int\limits_{S_A} [\vec{E}_{\imath}, \vec{H}_{\imath}]\, \vec{n}_e ds, \qquad (1.6)$$

$$H_q(M) = \frac{1}{4\pi} \int\limits_{S_A} [\vec{E}_{\imath}, \vec{H}']\, \vec{n}_e ds. \qquad (1.7)$$

Latter/last relationships/ratios show that for calculating the antenna radiation pattern, arranged/located directly on surface of S of conductive body, it suffices to know only components of the magnetic vector of the diffraction field of plane wave, tangents to surface of S.

1.2. Radiation patterns of the surface antennas, arranged/located on the bodies of cylindrical form.

Before passing to the examination of the solutions of the diffraction problems which will be used for the calculation of the radiation patterns of surface antennas according to the reciprocity theorem, let us touch several general/common/total questions,

connected with the analysis of the radiation characteristics of antennas, which are located on the bodies of cylindrical form.

Page 10.

The solution of three-dimensional vector diffraction problem, necessary for finding the three-dimensional/space radiation pattern of surface emitter, even in the case of the bodies of cylindrical form presents known difficulties. However, if is solved the two-dimensional problem about scattering of plane wave from the cylindrical body, the solution of the spatial diffraction problem of obtaining not difficult [13].

Let on cylindrical body fall the plane wave, which arrives from the direction, which is characterized by angles $\vartheta$, $\varphi$:

$$\vec{E}_i = \vec{e}_i \exp\left[-i\varkappa (z \cos\vartheta + x \sin\vartheta \cos\varphi + y \sin\vartheta \sin\varphi)\right],$$

$$\vec{H}_i = \vec{h}_i \frac{1}{Z_0} \exp\left[-i\varkappa (z \cos\vartheta + \right.$$

$$\left. + x \sin\vartheta \cos\varphi + y \sin\vartheta \sin\varphi)\right], \qquad (1.8)$$

where $\vec{e}_i, \vec{h}_i$ - the unit vectors of the polarization of the plane wave: $Z_0$ - impedance of free space; $k = 2\pi/\lambda$ - wave number.

The possibility of reducing of spatial diffraction problem to flat/plane is caused by the fact that the dependence of the electromagnetic field on coordinate z in the incident wave takes the

simple form. It is almost obvious (for example, see [14]), that in the diffraction field $\vec{E}$, $\vec{H}$ the dependence on z takes the same form, as in the incident wave, i.e.

$$\vec{E} = \vec{e}(x, y)e^{-i\kappa z \cos\theta},$$
$$\vec{H} = \vec{h}(x, y)e^{-i\kappa z \cos\theta}. \qquad (1.9)$$

Further examination is conveniently conducted for two fundamental types of polarization $E_{\perp}$ and $E_{\parallel}$, electrical and magnetic vectors of the incident wave corresponding to orientation in the direction, perpendicular to the axis of cylindrical body.

Page 11.


In the case of perpendicular polarization $E_{\perp}$, component $E_z = 0$, and remaining components of vector $\vec{E}$ satisfy the equation of Helmholtz

$$\Delta E_{x, y} + \kappa^2 E_{x, y} = 0,$$

which taking into account (1.9) takes the following form:

$$\Delta_t e_{x, y} + \kappa^2 \sin^2\theta e_{x, y} = 0,$$

where

$$\Delta_t = \frac{\partial^2}{\partial x^2} + \frac{\partial^2}{\partial y^2}. \qquad (1.10)$$

Equation (1.10) is required to solve for the condition

$$[\vec{n}_o, \vec{e}]|_S = 0, \qquad (1.11)$$

if bounding surface S ideally conducting, and the condition for the excitation

$$\vec{E}_i = \vec{e}_i \exp[-i\kappa \sin\theta (x \cos\varphi + y \sin\varphi)]. \qquad (1.12)$$

Let us compare the problem in question with the two-dimensional problem about the incidence/drop on the cylindrical body of plane wave with wave vector $\vec{\varkappa}$, of that polarized in the plane of incidence. Components $E_x^0, E_y^0$ of electric vector $\vec{E}^0(x, y, \varkappa)$ of the diffraction field, which corresponds to two-dimensional problem, satisfy the equation

$$\Delta_\tau E^0_{x, y} + \varkappa^2 E^0_{x, y} = 0, \qquad (1.13)$$

to the boundary condition

$$|\vec{n}_e, \vec{E}^0| |_S = 0 \qquad (1.14)$$

and to the condition for the excitation

$$\vec{E}_i^0 = \vec{e}_i^0 \exp\left[-i\varkappa\left(x \cos\varphi^0 + y \sin\varphi^0\right)\right]. \qquad (1.15)$$

Comparing relationships (1.10)-(1.12) and (1.13)-(1.15), which uniquely determine the solutions of spatial and two-dimensional problems, it is not difficult to ascertain that conditions (1.10)-(1.12) and (1.13)-(1.15) will become equivalent, if we in expressions (1.13) and (1.15) assume

$$\varkappa = \varkappa \sin\vartheta, \quad \varphi^0 = \varphi.$$

Page 12.


Thus, the components of vectors $\vec{E}$, $\vec{H}$ of the field, corresponding to spatial diffraction problem, are expressed as field component $\vec{E}^0(x, y, \varkappa)$, $\vec{H}^0(x, y, \varkappa)$ in two-dimensional problem with the aid of the following relationships/ratios:

$$E_{x,\,y} = E^0_{x,\,y}(x, y, \kappa \sin \vartheta)e^{-i\kappa z \cos \vartheta},$$
$$E_z = 0, \tag{1.16}$$
$$H_{x,\,y} = \pm \frac{\cos \vartheta}{Z_\bullet} E^0_{y,\,x}(x, y, \kappa \sin \vartheta)e^{-i\kappa z \cos \vartheta}, \tag{1.17}$$
$$H_z = \sin \vartheta H^{)}_z(x, y, \kappa \sin \vartheta)e^{-i\kappa z \cos \vartheta}.$$

In the case of polarization $E_\parallel$ analogous reasonings lead to the following expressions, which connect field component $\vec{E}$, $\vec{H}$ and $\vec{E}^\bullet$, $\vec{H}^\bullet$:

$$H_{x,\,y} = H^0_{x,\,y}(x, y, \kappa \sin \vartheta)e^{-i\kappa z \cos \vartheta};$$
$$H_z = 0, \tag{1.18}$$
$$E_{x,\,y}' = \mp Z_\bullet \cos \vartheta H^0_{y,\,x}(x, y, \kappa \sin \vartheta)e^{-i\kappa z \cos \vartheta},$$
$$E_z = \sin \vartheta E^0_z(x, y, \kappa \sin \vartheta)\,e^{-i\kappa z \cos \vartheta}. \tag{1.19}$$

Relationships/ratios (1.16)-(1.19) make it possible to determine the solution of spatial diffractive problem, if is known the solution of the two-dimensional problem of diffraction.


As the illustration of the use/application of formulas (1.16)-(1.19) let us give calculation according to the reciprocity theorem of the three-dimensional/space radiation pattern of the elementary slotted emitter, which is located at certain point Q(x, y, z) on the surface of the conducting cylindrical body (Fig. 1.2) and excited by the field

$$\vec{E}_\tau = \{e_1, e_2, e_3\}.$$

The source in question creates in the remote zone in direction $\vec{k}$ (Fig. 1.2) certain field $\vec{E}$. Expressions (1.16)-(1.19) make it possible to determine with the aid of the reciprocity theorem any

component of this field, if are known the solutions of the
two-dimensional problems about the diffraction of plane waves on the
cylindrical body, which correspond to polarizations $E_{\perp}$ and $E_{//}$.


Page 13.


In order to find the components of field $\vec{E}$, let us introduce two
single orthogonal vectors $\vec{p}_1$ and $\vec{p}_2$, such, that

$$|\vec{p}_1|=|\vec{p}_2|=1, \quad \vec{p}_1\vec{p}_2=0,$$
$$\vec{p}_1\vec{\varkappa}=\vec{p}_2\vec{\varkappa}=0, \quad \vec{p}_1\vec{z}_0=0. \qquad (1.20)$$

It is obvious that the projections of vector $\vec{E}$ of the unknown field
to directions $\vec{p}_1$, $\vec{p}_2$ completely characterize the radiation/emission
of slot in the remote zone:

$$\vec{E}=(\vec{E}, \vec{p}_1)\,\vec{p}_1 + (\vec{E}, \vec{p}_2)\,\vec{p}_2. \qquad (1.21)$$
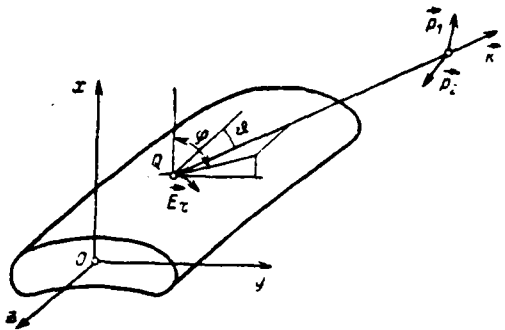
Fig. 1.2. To problem of diffraction on cylindrical body.

The vectors

$$\vec{p_1} = \{\sin\varphi; \ -\cos\varphi; \ 0\},$$

$$\vec{p_2} = \{\cos\vartheta\cos\varphi; \ \cos\vartheta\sin\varphi; \ -\sin\vartheta\}$$

are selected in such a way that the first of them coincides with the

sense of the vector $\vec{E}$ of the plane wave

$$\vec{E}_{01} = Z_0\,[\vec{\kappa}, \vec{H}_{01}]; \ \vec{H}_{01} = [\vec{\kappa}, \vec{p_1}], \qquad (1.22)$$

not having components $E_{01z}$ (polarization $E_\perp$), but the second vector s

- by sense of the vector $\vec{E}$ of the plane wave

$$\vec{E}_{02} = Z_0\,[\vec{\kappa}, \vec{H}_{02}]; \ \vec{H}_{02} = [\vec{\kappa}, \vec{p_2}], \qquad (1.23)$$

in which $H_{02z} = 0$ (polarization $E_{\parallel}$). According to relationships/ratios

(1.16)-(1.19) the solutions of the problems about the diffraction of

plane waves (1.22), (1.23) can be expressed through the solutions of

corresponding two-dimensional problems. Using reciprocity theorem and

formulas (1.16)-(1.19), it is not difficult to obtain the following expression for the three-dimensional/space radiation pattern of elementary slotted emitter, which is located on the cylindrical surface:

$$\vec{E} = \frac{\exp(-i\kappa z \cos\vartheta)}{4\pi} \left\{ \left( \left[ \vec{E}_\tau, \vec{e}_x \frac{\cos\vartheta}{Z_\bullet} \times \right. \right. \right.$$

$$\times E^0_{\perp y}(x, y, \kappa\sin\vartheta) - \vec{e}_y \frac{\cos\vartheta}{Z_\bullet} E^0_{\perp x}(x, y, \kappa\sin\vartheta) +$$

$$\left. + \vec{e}_z \sin\vartheta H^0_{\perp z}(x, y, \kappa\sin\vartheta) \right] \vec{n}_e \right) \vec{p}_1 +$$

$$+ (\left[ \vec{E}_\tau, \vec{e}_x H^0_{\parallel x}(x, y, \kappa\sin\vartheta) + \right.$$

$$\left. \left. + \vec{e}_y H^0_{\parallel y}(x, y, \kappa\sin\vartheta) \right] \vec{n}_e) \vec{p}_z \right\}. \qquad (1.24)$$

where $\vec{E}^\bullet_\perp$, $\vec{H}^\bullet_\perp$; $\vec{E}^\bullet_\parallel$, $\vec{H}^\bullet_\parallel$ - solution of the two-dimensional problems about the diffraction of the perpendicularly and in parallel polarized plane waves on the body in question.

Thus, for calculating solid coverage of slotted emitter on the cylindrical surface it is necessary to know the field in slot $\vec{E}_\tau$ and the solutions of two scalar problems, which correspond to the excitation of this surface by plane waves with polarizations $E_\perp$ and $E_\parallel$.

Page 15.

Analogously can be calculated the radiation pattern of elementary electrical radiator/resonator/element, located at point

Q(x, y, z) and oriented in the direction of normal to the surface of cylindrical body. Calculation shows that in this case

$$\vec{E} = \frac{1}{4\pi} e^{-i\kappa z \cos \vartheta} \{ (E^0_{\perp x}(x, y, \kappa \sin \vartheta) \vec{e}_x +$$
$$+ E^0_{\perp y}(x, y, \kappa \sin \vartheta) \vec{e}_y, \vec{n}_e) \vec{p}_1 + (- Z_0 \cos \vartheta \times$$
$$\times H^0_{\parallel y}(x, y, \kappa \sin \vartheta) \vec{e}_x + Z_0 \cos \vartheta H^0_{\parallel x}(x, y, \kappa \sin \vartheta) \times$$
$$\times \vec{e}_y + \sin \vartheta E^0_{\parallel z}(x, y, \kappa \sin \vartheta) \vec{e}_z, \vec{n}_c) \vec{p}_2 \}. \quad (1.25)$$

In the examination of radiation patterns in the main section, i.e., in the plane, perpendicular to the axis of cylindrical body, it is assumed that assigned field distribution $E_t$ on the surface of cylinder does not depend on coordinate z. Since in actuality is excited only the finite segment of cylindrical body and the character of the excitation in a specific manner depends on coordinate z, it is necessary to establish/install the limits of the applicability of the obtained results.

In connection with this let us examine the arbitrary conducting cylindrical body, in certain section $\Sigma$ of surface of which is assigned electric field $\vec{E}_t$ with components $E^0_z$ and $E^0_s$ in the coordinate directions z and s (Fig. 1.3).
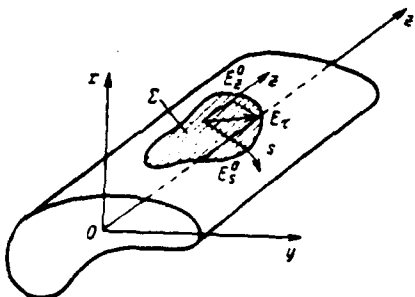
Fig. 1.3. On the calculation of the main section of radiation pattern.


Page 16.


The radiation pattern of the examined surface emitter can be obtained from formula (1.6), if we assume $\vec{p}=\vec{e}_z$ for the parallel and $\vec{p}=\vec{e}_\varphi$ for the perpendicular polarization ($\vec{e}$ - unit vector):

$$E_z = \frac{1}{4\pi} \int_\Sigma E_z^0 H_\varphi d\sigma, \qquad (1.26)$$

$$E_\varphi = \frac{1}{4\pi} \int_\Sigma E_z^\varphi H_z d\sigma, \qquad (1.27)$$

where $H_\varphi$ and $H_z$ - components of magnetic field on the surface of the cylinder, excited by the respectively polarized plane wave, which falls from the direction $\varphi$ in plane xOy (Fig. 1.3). Since the incident wave flat/plane and field $\vec{H}$ on coordinate z does not depend, expressions (1.26), (1.27) can be rewritten as follows (omitting constants):

$$E_z(\varphi) = \int_{s_1}^{s_2} \left[ \int_{z_1}^{z_2} E_z^0(z,s)\,dz \right] H_s(s,\varphi)\,ds; \qquad (1.28)$$

$$E_\varphi(\varphi) = \int_{s_1}^{s_2} \left[ \int_{z_1}^{z_2} E_s^0(z,s)\,dz \right] H_z(s,\varphi)\,ds. \qquad (1.29)$$

From the latter/last relationships/ratios it follows, that for all field distributions in antenna aperture, such, that

$$\int_{z_1}^{z_2} E_{s,z}^0(s,z)\,dz = C\psi_{s,z}(s). \qquad (1.30)$$

the radiation patterns in the main section will be identical, if functions $\psi_{s,z}(s)$ coincide.

In expression (1.30) C - arbitrary constant value, and integration limits can be selected infinite in view of the fact that $E_{s,z}^0 = 0$ on the surface of conductive body everywhere with exception of antenna aperture. A special case of the distribution, which satisfies condition (1.30), is distribution of the type

$$E_{s,z}^0(s,z) = A(s)B(z). \qquad (1.31)$$

Page 17.

Actually/really, substituting (1.31) in (1.30), we obtain

$$\psi(s) = A(s); \quad C = \int_{-\infty}^{+\infty} B(z)\,dz. \qquad (1.32)$$

For example, field distribution in the infinitely thin slot satisfies condition (1.32), since the law of field distribution across the slot

does not depend on field distribution along it and can be found
sufficiently accurately from the solution of the corresponding
electrostatic problem. This indicates, in particular, that the
radiation pattern of the thin slot, cut in the conducting cylinder of
lengthwise generatrix, in the main section does not depend on the
sizes/dimensions of slot and form of field distribution along it.
Latter/last confirmation is correct for the thin slot of variable
width, since in expressions (1.26) and (1.27) in the case of the thin
slot it is possible immediately to integrate over s considering that
$H_{z,s}$ is virtually constant in the width of slot.

Thus, for the determination of the radiation patterns in the
main section, which correspond to field distributions which satisfy
conditions (1.30) or (1.31), instead of the spatial problem
sufficiently solving flat/plane, which, as a rule, considerably
simplifies examination. In conclusion it should be noted that the
information of the spatial problem about the surface emitters to
two-dimensional problem proves to be possible not only in the case of
cylindrical, but also for the arbitrary convex body with a small
surface curvature. True, this simplification is possible only for the
"linear" antennas, arranged/located over the "large cross section" of
convex body, i.e., along the line on which the planes, tangents to
the body surface, are parallel to one straight line, and only for the
main section of radiation pattern, i.e., for the plane, perpendicular

to this straight line.

Page 18.

In this case, as it follows from works [15, 16], radiation pattern by main section is evinced with the aid of the reciprocity theorem as follows:

$$E_s = \int_{s_1}^{s_2} E_z^0(s) f(\xi) e^{i\kappa s} ds \qquad (1.33)$$

during the parallel polarization;

$$E_\varphi = \int_{s_1}^{s_2} E_s^0(s) g(\xi) e^{i\kappa s} ds \qquad (1.34)$$

during the perpendicular polarization.

Functions $f(\xi)$ and $g(\xi)$, entering expressions (1.33) and (1.34), will be examined in the following paragraph. The parameter $\xi$ in formulas (1.33), (1.34) depends only on the radius of curvature of body surface in section xOy (Fig. 1.3). This means that in the case of the convex slightly bent/slightly curved surface the radiation pattern of the line-source antenna in question in the main section depends only on surface curvature in this section. The property indicated has very important value during performance calculation of the radiation/emission of the line-source antennas, arranged/located on the bodies of complex form, making it possible to obtain necessary

DOC = 82036101          PAGE 25


results from the solutions of the simpler problems about the
emitters, which are located on the bodies of cylindrical form.

1.3. Scattering plane wave on the conductive bodies of various forms.

In S1.1 it was shown that for the determination of the field of
surface antenna it is necessary to know solution of $\vec{E}_1$, $\vec{H}_1$ (or $\vec{E}'$,
$\vec{H}'$) the corresponding diffraction problem. Since subsequently
according to the reciprocity theorem will be designed mainly the
radiation patterns of surface antennas, let us give the solutions of
the problems about the diffraction of plane waves on the bodies of
various forms. In the case of cylindrical bodies we will be
restricted to the examination of the two-dimensional problems of
scattering for two fundamental types of the polarization ($E_\perp$ and $E_\parallel$)
of applied field.

Diffraction of plane wave on the half-plane.

The problem about the diffraction of plane wave on the ideally
conducting half-plane is solved by Sommerfield [17] with the aid of
the method of the branched solutions. The solution of problem
represented in the locked form is expressed as Fresnel's integrals.

Page 19.

If the incident plane wave has single amplitude and is propagated in the direction, perpendicular to the edge/fin of screen and which forms angle $\varphi$ with the plane of screen $y=0$ (Fig. 1.4), the components of diffraction fields, which correspond to polarizations $E_\perp$ and $E_\parallel$, can be represented as follows at the arbitrary point of space $r$, $\varphi'$.
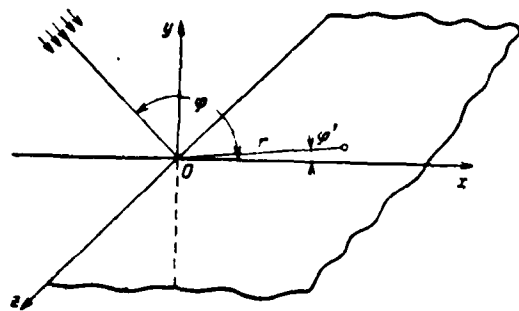
Fig. 1.4. To scattering of plane wave on the half-plane.

Page 20.

Perpendicular polarization (magnetic vector of primary field is parallel to the edge of half-plane):

$$H_z(r,\varphi') = \tfrac{1}{2}\exp[-i\kappa r\cos(\varphi-\varphi')]\{1+\sqrt{2}e^{-i\frac{\pi}{4}}\times$$

$$\times F_1\left(2\sqrt{\tfrac{\kappa r}{\pi}}\cos\tfrac{\varphi-\varphi'}{2}\right)\} + \tfrac{1}{2}\exp[-i\kappa r\cos(\varphi+\varphi')]\times$$

$$\times\left\{1+\sqrt{2}e^{-i\frac{\pi}{4}}F_1\left(2\sqrt{\tfrac{\kappa r}{\pi}}\cos\tfrac{\varphi+\varphi'}{2}\right)\right\}. \quad (1.35)$$

$$-\tfrac{1}{Z_0}E_r(r,\varphi') = \tfrac{1}{2}\sin(\varphi-\varphi')\exp[-i\,\kappa r\cos(\varphi-$$

$$-\varphi')]\left\{1+\sqrt{2}\,e^{-i\frac{\pi}{4}}F_1\left(2\sqrt{\tfrac{\kappa r}{\pi}}\cos\tfrac{\varphi-\varphi'}{2}\right)\right\}+$$

$$+\tfrac{1}{2}\sin(\varphi+\varphi')\exp[-i\,\kappa r\cos(\varphi+\varphi')]\times$$

$$\times\left\{1+\sqrt{2}e^{-i\frac{\pi}{4}}F_1\left(2\sqrt{\tfrac{\kappa r}{\pi}}\cos\tfrac{\varphi+\varphi'}{2}\right)\right\}+$$

$$+\sqrt{\tfrac{2}{\pi\kappa r}}e^{i\left(\kappa r+\frac{\pi}{4}\right)}\sin\tfrac{\varphi}{2}\cos\tfrac{\varphi'}{2}. \quad (1.36)$$

$$-\tfrac{1}{Z_0}E_\varphi(r,\varphi') = \tfrac{1}{2}\cos(\varphi-\varphi')\exp[-i\kappa r\cos(\varphi-\varphi')]\times$$

$$\times\left\{1+\sqrt{2}e^{-i\frac{\pi}{4}}F_1\left(2\sqrt{\tfrac{\kappa r}{\pi}}\cos\tfrac{\varphi-\varphi'}{2}\right)\right\}+\tfrac{1}{2}\cos(\varphi+\varphi')\times$$

$$\times\exp[-i\kappa r\cos(\varphi+\varphi')]\left\{1+\sqrt{2}e^{-i\frac{\pi}{4}}\times\right.$$

$$\times F_1\left(2\sqrt{\tfrac{\kappa r}{\pi}}\cos\tfrac{\varphi+\varphi'}{2}\right)\Big\}+$$

$$+\sqrt{\tfrac{2}{\pi\kappa r}}e^{i\left(\kappa r+\frac{\pi}{4}\right)}\cos\tfrac{\varphi}{2}\cos\tfrac{\varphi'}{2}. \quad (1.37)$$

The parallel polarization (electric vector of primary field is parallel to the edge of half-plane):

$$E_z(r, \varphi') = \frac{1}{2} \exp\left[-i\kappa r \cos(\varphi - \varphi')\right] \times$$

$$\times \left\{1 + i\sqrt{2}e^{-i\frac{\pi}{4}} F_1\left(2\sqrt{\frac{\kappa r}{\pi}}\cos\frac{\varphi - \varphi'}{2}\right)\right\} -$$

$$- \frac{1}{2}\exp\left[-i\kappa r \cos(\varphi + \varphi')\right]\left\{1 + \sqrt{2}\,e^{-i\frac{\pi}{4}} \times \right.$$

$$\left. \times F_1\left(2\sqrt{\frac{\kappa r}{\pi}}\cos\frac{\varphi + \varphi'}{2}\right)\right\}. \qquad (1.38)$$

$$Z_o H_r(r, \varphi') = \frac{1}{2}\sin(\varphi - \varphi')\exp\left[-i\kappa r \cos(\varphi - \varphi')\right] \times$$

$$\times \left\{1 + \sqrt{2}\,e^{-i\frac{\pi}{4}} F_1\left(2\sqrt{\frac{\kappa r}{\pi}}\cos\frac{\varphi - \varphi'}{2}\right)\right\} -$$

$$- \frac{1}{2}\sin(\varphi + \varphi')\exp\left[-i\kappa r \cos(\varphi + \varphi')\right]\left\{1 + \right.$$

$$\left. + \sqrt{2}\,e^{-i\frac{\pi}{4}} F_1\left(2\sqrt{\frac{\kappa r}{\pi}}\cos\frac{\varphi + \varphi'}{2}\right)\right\} +$$

$$+ \sqrt{\frac{2}{\pi\kappa r}}\,e^{i\left(\kappa r + \frac{\pi}{4}\right)}\cos\frac{\varphi}{2}\sin\frac{\varphi'}{2}. \qquad (1.39)$$

$$Z_o H_\varphi(r, \varphi') = \frac{1}{2}\cos(\varphi - \varphi')\exp\left[-i\kappa r \cos(\varphi - \varphi')\right] \times$$

$$\times \left\{1 + \sqrt{2}\,e^{-i\frac{\pi}{4}} F_1\left(2\sqrt{\frac{\kappa r}{\pi}}\cos\frac{\varphi - \varphi'}{2}\right)\right\} -$$

$$- \frac{1}{2}\cos(\varphi + \varphi')\exp\left[-i\kappa r \cos(\varphi + \varphi')\right] \times$$

$$\times \left\{1 + \sqrt{2}\,e^{-i\frac{\pi}{4}} F_1\left(2\sqrt{\frac{\kappa r}{\pi}}\cos\frac{\varphi + \varphi'}{2}\right)\right\} +$$

$$+ \sqrt{\frac{2}{\pi\kappa r}}\,e^{i\left(\kappa r + \frac{\pi}{4}\right)}\sin\frac{\varphi}{2}\sin\frac{\varphi'}{2}. \qquad (1.40)$$

Page 21.

In expressions (1.35)-(1.40)

$$F_1(v) = \int_0^v e^{i\frac{\pi}{2}t^2}\,dt$$

- the integral of first-order Fresnel;

$$\kappa = 2\pi/\lambda.$$

Relationships/ratios (1.35)-(1.40) together with the reciprocity theorem make it possible to calculate the radiation patterns of the radiation sources, arbitrarily arranged/located relative to the surface of half-plane.

Diffraction of plane wave on the key.

For calculating the antenna radiation patterns, arranged/located on the key, we will use the solution of the problem of diffraction, obtained by Oberhettinger [18], which is correct for the arbitrary aperture angle of key. In the case, interesting us, which corresponds to an incidence in the plane wave on the surface of key (Fig. 1.5), the components of diffraction fields take following form [18].

Page 22.

Perpendicular polarization:

$$H_z(r, \varphi') = \sum_{n=0}^{\infty} \varepsilon_n J_{\frac{n\pi}{\alpha}}(\kappa r) e^{-i\frac{n\pi^2}{2\alpha}} \times$$

$$\times \left[ \cos\frac{n\pi}{\alpha}(\varphi - \varphi') + \cos\frac{n\pi}{\alpha}(\varphi + \varphi') \right], \qquad (1.41)$$

$$E_r(r, \varphi') = \frac{i\pi Z_0}{\alpha \kappa r} \sum_{n=0}^{\infty} n\varepsilon_n J_{\frac{n\pi}{\alpha}}(\kappa r) e^{-i\frac{n\pi^2}{2\alpha}} \times$$

$$\times \left[ \sin\frac{n\pi}{\alpha}(\varphi - \varphi') + \sin\frac{n\pi}{\alpha}(\varphi + \varphi') \right]; \qquad (1.42)$$

$$E_\varphi(r, \varphi') = i Z_0 \sum_{n=0}^{\infty} \varepsilon_n J'_{\frac{n\pi}{\alpha}}(\kappa r) e^{-i\frac{n\pi^2}{2\alpha}} \times \qquad (1.43)$$

$$\times \left[ \cos\frac{n\pi}{\alpha}(\varphi - \varphi') + \cos\frac{n\pi}{\alpha}(\varphi + \varphi') \right].$$

Parallel polarization:

$$E_z(r, \varphi') = \sum_{n=0}^{\infty} J_{\frac{n\pi}{\alpha}}(\kappa r) e^{-i\frac{n\pi^2}{2\alpha}} \times$$

$$\times \left[ \cos\frac{n\pi}{\alpha}(\varphi - \varphi') - \cos\frac{n\pi}{\alpha}(\varphi + \varphi') \right], \qquad (1.44)$$

$$H_r(r, \varphi') = -\frac{i\pi}{\alpha Z_0 \kappa r} \sum_{n=0}^{\infty} n J_{\frac{n\pi}{\alpha}}(\kappa r) \times$$

$$\times e^{-i\frac{n\pi^2}{2\alpha}} \left[ \sin\frac{n\pi}{\alpha}(\varphi - \varphi') - \sin\frac{n\pi}{\alpha}(\varphi + \varphi') \right]; \qquad (1.45)$$

$$H_\varphi(r, \varphi') = \frac{1}{iZ_0} \sum_{n=0}^{\infty} J'_{\frac{n\pi}{\alpha}}(\kappa r) e^{-i\frac{n\pi^2}{2\alpha}} \times$$

$$\times \left[ \cos\frac{n\pi}{\alpha}(\varphi - \varphi') - \cos\frac{n\pi}{\alpha}(\varphi + \varphi') \right]. \qquad (1.46)$$

Fig. 1.5. To scattering of plane wave by key.


Page 23.


In expressions (1.41)-(1.46)


$J_{\frac{n\pi}{\alpha}}(\kappa r)$ — Bessel function:

$$\varepsilon_n = \begin{cases} 1 \text{ при } n = 0; \\ 2 \text{ при } n \neq 0; \end{cases}$$

Key: (1). with.


$\alpha$ - external wedge angle;

$$J'_{\frac{n\pi}{\alpha}}(\kappa r) = \frac{\partial}{\partial (\kappa r)} J_{\frac{n\pi}{\alpha}}(\kappa r);$$

$\varphi$ — direction of arrival of plane wave:
$r, \varphi'$ — coordinates of observation point (Fig. 1.5)
Diffraction of plane wave on the circular cylinder.


The solution of the problem of diffracting the plane wave on the circular cylinder is determined according to the method of separation

of the variable/alternating r, $\varphi'$, z (Fig. 1.6) in the equation of Helmholtz and takes following form [19] for the types of the polarization of applied field in question.

Perpendicular polarization $(E_\perp)$:

$$H_z(r, \varphi') = \exp\left[-i\kappa r \cos(\varphi - \varphi')\right] -$$

$$- \sum_{n=-\infty}^{\infty} (-i)^n \frac{J'_n(\kappa a)}{H_n^{(1)'}(\kappa a)} H_n^{(1)}(\kappa r) e^{in(\varphi-\varphi')}; \quad (1.47)$$

$$-\frac{1}{Z_0} E_r(r, \varphi') = \sin(\varphi - \varphi') \exp\left[-i\kappa r \cos(\varphi - \varphi')\right] -$$

$$-\frac{1}{\kappa r} \sum_{n=-\infty}^{\infty} n(-i)^n \frac{J'_n(\kappa a)}{H_n^{(1)'}(\kappa a)} H_n^{(1)}(\kappa r) e^{in(\varphi-\varphi')}, \quad (1.48)$$

$$-\frac{1}{Z_0} E_\varphi(r, \varphi') = \cos(\varphi - \varphi') \exp\left[-i\kappa r \cos(\varphi - \varphi')\right] -$$

$$- i \sum_{n=-\infty}^{\infty} (-i)^n \frac{J'_n(\kappa a)}{H_n^{(1)'}(\kappa a)} H_n^{(1)'}(\kappa r) e^{in(\varphi-\varphi')}. \quad (1.49)$$

Page 24.

Parallel polarization $(E_\parallel)$:

$$E_z(r, \varphi') = \exp\left[-i\kappa r \cos(\varphi - \varphi')\right] -$$

$$- \sum_{n=-\infty}^{\infty} (-i)^n \frac{J_n(\kappa a)}{H_n^{(1)}(\kappa a)} H_n^{(1)}(\kappa r) e^{in(\varphi-\varphi')}, \quad (1.50)$$

$$Z_0 H_r(r, \varphi') = \sin(\varphi - \varphi') \exp\left[-i\kappa r \cos(\varphi - \varphi')\right] -$$

$$-\frac{1}{\kappa r} \sum_{n=-\infty}^{\infty} n(-i)^n \frac{J_n(\kappa a)}{H_n^{(1)}(\kappa a)} H_n^{(1)}(\kappa r) e^{in(\varphi-\varphi')}; \quad (1.51)$$

$$Z_0 H_\varphi(r, \varphi) = \cos(\varphi - \varphi') \exp\left[-i\kappa r \cos(\varphi - \varphi')\right] -$$

$$- i \sum_{n=-\infty}^{\infty} (-i)^n \frac{J_n(\kappa a)}{H_n^{(1)}(\kappa a)} H_n^{(1)'}(\kappa r) e^{in(\varphi-\varphi')}. \quad (1.52)$$
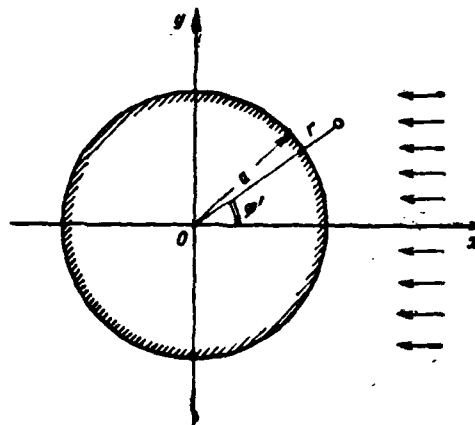
Fig. 1.6. To scattering of plane wave on the circular cylinder.


Page 25.


In expressions (1.47)-(1.52):


$H_n^{(1)}(\kappa a)$, $J_n(\kappa a)$, $H_n^{(1)'}(\kappa a)$, $J'_n(\kappa a)$ — the Hankel function, Bessel function, and their derivatives of argument ka;


a - radius of cylinder;


r, $\varphi'$ - coordinate of observation point (Fig. 1.6);


$\varphi$ - angle of incidence in the plane wave (in Fig. 1.6 $\varphi=0$).

Diffraction of plane wave on the elliptical cylinder.

The solution of the problem of diffracting the plane wave on the ideally conducting elliptical cylinder (Fig. 1.7), given, for example, in work [20], can be represented as follows.
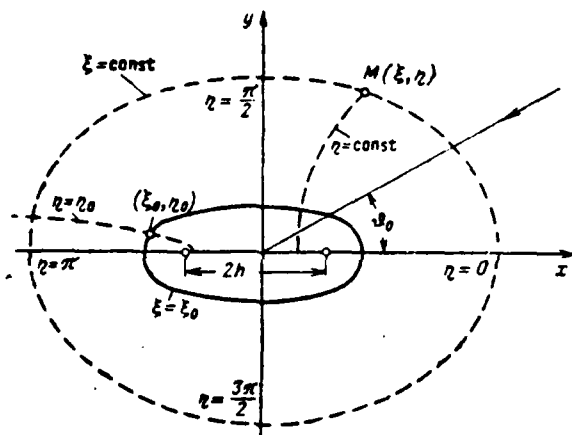
Fig. 1.7. To scattering of plane wave on the elliptical cylinder.

Page 26.

Perpendicular polarization $(E_\perp)$:

$$H_z(\xi,\ \eta) = \exp\left[-i\kappa h\left(\operatorname{ch}\xi\cos\eta\cos\vartheta_0 + \operatorname{sh}\xi\sin\eta\sin\vartheta_0\right)\right] -$$
$$- 2\sum_{n=0}^{\infty}\{C_n^{(1)}\operatorname{Me}_n^{(1)}(\xi,\ q)\,ce_n(\eta,\ q)\,ce_n(\vartheta_0,\ q) +$$
$$+ S_n^{(1)}\operatorname{Ne}_n^{(1)}(\xi,\ q)\,se_n(\eta,\ q)\,se_n(\vartheta_0,\ q)\}; \qquad (1.53)$$

$$-\frac{1}{Z_0}\sqrt{\tfrac{1}{2}(\operatorname{ch}2\xi - \cos 2\eta)}\,E_\xi(\xi,\ \eta) = (\operatorname{ch}\xi\sin\eta\cos\vartheta_0 -$$
$$- \operatorname{sh}\xi\cos\eta\sin\vartheta_0)\exp\left[-i\kappa h\left(\operatorname{ch}\xi\cos\eta\cos\vartheta_0 +\right.\right.$$
$$\left.\left.+ \operatorname{sh}\xi\sin\eta\sin\vartheta_0\right)\right] -$$
$$-\frac{2}{i\kappa h}\sum_{n=0}^{\infty}\{C_n^{(1)}\operatorname{Me}_n^{(1)}(\xi,\ q)\,ce'_n(\eta,\ q)\,ce_n(\vartheta_0,\ q) +$$
$$+ S_n^{(1)}\operatorname{Ne}_n^{(1)}(\xi,\ q)\,se'_n(\eta,\ q)\,se_n(\vartheta_0,\ q)\}; \qquad (1.54)$$

$$-\frac{1}{Z_0}\sqrt{\tfrac{1}{2}(\operatorname{ch}2\xi - \cos 2\eta)}\,E_\eta(\xi,\ \eta) = (\operatorname{sh}\xi\cos\eta\cos\vartheta_0 +$$
$$+ \operatorname{ch}\xi\sin\eta\sin\vartheta_0)\exp\left[-i\,\kappa h\left(\operatorname{ch}\xi\cos\eta\cos\vartheta_0 + \operatorname{sh}\xi\sin\eta\sin\vartheta_0\right)\right] +$$
$$+\frac{2}{i\kappa h}\sum_{n=0}^{\infty}\{C_n^{(1)}\operatorname{Me}_n^{(1)'}(\xi,\ q)\,ce_n(\eta,\ q)\,ce_n(\vartheta_0,\ q) +$$
$$+ S_n^{(1)'}\operatorname{Ne}_n^{(1)}(\xi,\ q)\,se_n(\eta,\ q)\,se_n(\vartheta_0,\ q)\}. \qquad (1.55)$$

Parallel polarization $(E_\parallel)$:

$$E_z(\xi, \eta) = \exp\left[-i\,\varkappa h\,(\mathrm{ch}\,\xi\cos\eta\cos\vartheta_o + \mathrm{sh}\,\xi\sin\eta\sin\vartheta_o)\right] -$$

$$-2\sum_{n=0}^{\infty}\{C_n^{(2)}\,\mathrm{Me}_n^{(1)}(\xi,\ q)\,\mathrm{ce}_n(\eta,\ q)\,\mathrm{ce}_n(\vartheta_o,\ q) +$$

$$+ S_n^{(2)}\,\mathrm{Ne}_n^{(1)}(\xi,\ q)\,\mathrm{se}_n(\eta,\ q)\,\mathrm{se}_n(\vartheta_o,\ q)\}; \qquad (1.56)$$

$$Z_o\sqrt{\frac{1}{2}\,(\mathrm{ch}\,2\xi - \cos 2\eta)}\,H_\xi(\xi,\ \eta) =$$

$$= (\mathrm{ch}\,\xi\sin\eta\cos\vartheta_o - \mathrm{sh}\,\xi\cos\eta\sin\vartheta_o)\exp\left[-i\,\varkappa h\,(\mathrm{ch}\,\xi\cos\eta\cos\vartheta_o + \right.$$
$$\left. + \mathrm{sh}\,\xi\sin\eta\sin\vartheta_o)\right] -$$

$$-\frac{2}{i\,\varkappa h}\sum_{n=0}^{\infty}\{C_n^{(2)}\,\mathrm{Me}_n^{(1)}(\xi,\ q)\,\mathrm{ce}'_n(\eta,\ q)\,\mathrm{ce}_n(\vartheta_o,\ q) +$$

$$+ S_n^{(2)}\,\mathrm{Ne}_n^{(1)}(\xi,\ q)\,\mathrm{se}'_n(\eta,\ q)\,\mathrm{se}_n(\vartheta_o,\ q)\}. \qquad (1.57)$$

$$Z_o\sqrt{\frac{1}{2}\,(\mathrm{ch}\,2\xi - \cos 2\eta)}\,H_\eta(\xi,\ \eta) =$$

$$= (\mathrm{sh}\,\xi\cos\eta\cos\vartheta_o + \mathrm{ch}\,\xi\sin\eta\sin\vartheta_o)\times$$

$$\times\exp\left[-i\,\varkappa h\,(\mathrm{ch}\,\xi\cos\eta\cos\vartheta_o + \mathrm{sh}\,\xi\sin\eta\sin\vartheta_o)\right] +$$

$$+\frac{2}{i\,\varkappa h}\sum_{n=0}^{\infty}C_n^{(2)}\,\mathrm{Me}_n^{(1)'}(\xi,\ q)\,\mathrm{ce}_n(\eta,\ q)\,\mathrm{ce}_n(\vartheta_o,\ q) +$$

$$+ S_n^{(2)}\,\mathrm{Ne}_n^{(1)'}(\xi,\ q)\,\mathrm{se}_n(\eta,\ q)\,\mathrm{se}_n(\vartheta_o,\ q). \qquad (1.58)$$

Page 27.

In expressions (1.53)-(1.58):

$$C_n^{(1)} = \frac{\mathrm{Ce}_n'(\xi_0, q)}{p_n \, \mathrm{Me}_n^{(1)'}(\xi_0, q)};$$

$$S_n^{(1)} = \frac{\mathrm{Se}_n'(\xi_0, q)}{s_n \, \mathrm{Ne}_n^{(1)'}(\xi_0, q)};$$

$$C_n^{(2)} = \frac{\mathrm{Ce}_n(\xi_0, q)}{p_n \, \mathrm{Me}_n^{(1)}(\xi_0, q)};$$

$$S_n^{(2)} = \frac{\mathrm{Se}_n(\xi_0, q)}{s_n \, \mathrm{Ne}_n^{(1)}(\xi_0, q)};$$

$$p_n = \begin{cases} \dfrac{1}{A_0^{(2m)}} \mathrm{ce}_{2m}(0, q)\,\mathrm{ce}_{2m}\left(\dfrac{\pi}{2}, q\right), & \overset{(1)}{\text{если}} \ n = 2m \\[2ex] \dfrac{-1}{\sqrt{q}\, A_1^{(2m+1)}} \mathrm{ce}_{2m+1}(0, q)\,\mathrm{ce}'_{2m+1}\left(\dfrac{\pi}{2}, q\right), & \\[1ex] \text{если}\ n = 2m + 1; \end{cases}$$

$$s_n = \begin{cases} \dfrac{1}{q B_2^{(2m+2)}} \mathrm{se}'_{2m+2}(0, q)\,\mathrm{se}'_{2m+2}\left(\dfrac{\pi}{2}, q\right), & \overset{(1)}{\text{если}} \ n = 2m, \\[2ex] \dfrac{1}{\sqrt{q}\, B_1^{(2m+1)}} \mathrm{se}'_{2m+1}(0, q)\,\mathrm{se}_{2m+1}\left(\dfrac{\pi}{2}, q\right), & \\[1ex] \text{если}\ n = 2m + 1; \end{cases}$$

Key: (1). if.

$\xi, \eta$ — the coordinate of observation point in the elliptical coordinate system, shown in Fig. 1.7;

$\xi_0$ - value of coordinate $\xi$, which corresponds to the surface of elliptical cylinder;

$\vartheta_0$ - angle of incidence in the plane wave;

$q = (kh)^2/4$, $2h$ - distance between the foci of elliptical cylinder;

$ce_n(\eta, q)$, $se_n(\eta, q)$ — angular Mathieu functions;

$$Ce_n(\xi, q), \quad Se_n(\xi, q), \quad Me_n^{(1)}(\xi, q) \, Ne_n^{(1)}(\xi, q)$$

- radial Mathieu functions of the first and third orders,

$$A_0^{(2m)}, \quad A_1^{(2m+1)}, \quad B_1^{(2m+1)}, \quad B_2^{(2m+2)}$$

- the first Fourier coefficients in the expansions of the angular functions

$$ce_{2m}(\eta, q), \quad ce_{2m+1}(\eta, q), \quad se_{2m+1}(\eta, q), \quad se_{2m+2}(\eta, q)$$

in the series/rows of the trigonometric functions.


Page 28.


Primes in the preceding expressions noted the derivatives of angular and radial functions of $\eta$ and $\xi$ respectively.


Diffraction of plane wave on the sphere.


The solution of the problem of diffracting plane electromagnetic wave on ideally conducting sphere [21] is convenient to represent with the aid of potentials P and Q, introduced by Foch [22].
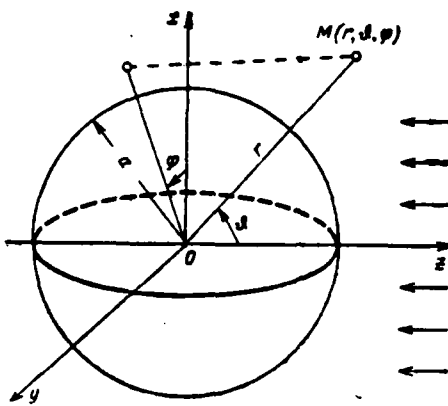
Fig. 1.8. To scattering of plane wave on the sphere.

Page 29.

If plane wave falls on the sphere in direction z<0 (Fig. 1.8) and it has components

$$E_x^i = -Z_* H_y^i = e^{-i\kappa z},$$

the components of the diffraction field $\vec{E}$, $\vec{H}$ are expressed as follows [23]:

$$E_r = \cos \varphi \left( \frac{\partial^2}{\partial r^2} + \kappa^2 \right) \left( r \frac{\partial P}{\partial \theta} \right), \qquad (1.59a)$$

$$E_\theta = \cos \varphi \left\{ \frac{1}{r} \frac{\partial}{\partial r} \left( r \frac{\partial^2 P}{\partial \theta^2} - i \kappa \frac{1}{\sin \theta} \frac{\partial Q}{\partial \theta} \right) \right\}, \qquad (1.59б)$$

$$E_\varphi = - \sin \varphi \left\{ \frac{1}{r} \frac{1}{\sin \theta} \frac{\partial}{\partial r} \left( r \frac{\partial P}{\partial \theta} \right) - i \kappa \frac{\partial^2 Q}{\partial \theta^2} \right\}, \qquad (1.59в)$$

$$H_r = - \sin \varphi \left( \frac{\partial^2}{\partial r^2} + k^2 \right) \left( r \frac{\partial Q}{\partial \theta} \right); \qquad (1.59г)$$

$$H_\theta = \sin \varphi \left\{ i \kappa \frac{1}{\sin \theta} \frac{\partial P}{\partial \theta} - \frac{1}{r} \frac{\partial}{\partial r} \left( r \frac{\partial^2 Q}{\partial \theta^2} \right) \right\}; \qquad (1.59д)$$

$$H_\varphi = \cos \varphi \left\{ i \kappa \frac{\partial^2 P}{\partial \theta^2} - \frac{1}{r \sin \theta} \frac{\partial}{\partial r} \left( r \frac{\partial Q}{\partial \theta} \right) \right\}; \qquad (1.59e)$$

$$P = \frac{1}{i \kappa^2 r} \sum_{n=1}^{\infty} \frac{2n+1}{n(n+1)} (-i)^n \left[ \psi_n(\kappa r) - \right.$$
$$\left. - \frac{\psi'_n(\kappa a)}{\zeta'_n(\kappa a)} \zeta_n(\kappa r) \right] P_n'(\cos \theta),$$

$$Q = \frac{1}{i \kappa^2 r} \sum_{n=1}^{\infty} \frac{2n+1}{n(n+1)} (-i)^n \left[ \psi_n(\kappa r) - \right.$$
$$\left. - \frac{\psi_n(\kappa a)}{\zeta_n(\kappa a)} \zeta_n(\kappa r) \right] P_n(\cos \theta).$$

From the latter/last expressions it follows that:

$$E_r = \cos \varphi R'(\theta); \quad E_\theta = \cos \varphi \, \Theta'(\theta); \quad E_\varphi = - \sin \varphi \Phi'(\theta),$$
$$H_r = - \sin \varphi R(\theta); \quad H_\theta = \sin \varphi \Theta(\theta); \quad H_\varphi = \cos \varphi \Phi(\theta). \qquad (1.60)$$

In expressions (1.59) and (1.60):


r, ϑ, φ - the coordinate of observation point in the coordinate

system, shown in Fig. 1.8;


a - radius of sphere;

$P_n(\cos \vartheta)$ —

∧ Legendre's complete;

$$\psi_n(x) = \sqrt{\frac{\pi x}{2}} J_{n+\frac{1}{2}}(x); \quad \zeta_n(x) = \sqrt{\frac{\pi x}{2}} H^{(1)}_{n+\frac{1}{2}}(x)$$

- spherical Bessel and Hankel functions.


Page 30.


Methods of the solution of the problems of diffraction on the bodies of complex form.


The results of performance calculations of radiation of surface antennas, led in chapters 3-9, are obtained in essence with the aid of precise methods. However, the bodies on which are arranged/located surface antennas, frequently have very complex layout, and then does not succeed in obtaining exact solution. In connection with this special importance acquire the approximate and numerical methods of the theory of diffraction.


From the point of view of practical calculations the simplest approximate method of the solution of problems of the type in question is Kirchhoff's method [24], at base of whom lie/rest the representations of geometric optic/optics. Let at point Q, distant up to the arbitrary distance from surface of S of cylindrical body, be placed the radiation source, which creates field with polarization

$E_\perp$ or $E_\parallel$. Let us designate U unique component of diffraction field in the direction, parallel to the axis of cylindrical body $(U=H_z-$ for polarization $E_\perp$, $U=E_z$ - for polarization $E_\parallel$). The precise value U(P) at observation point P can be calculated by the formula of Kirchhoff [24]:

$$U(P) = U_\bullet(P, Q) - \frac{1}{4\pi} \int_S \left\{ U \frac{\partial}{\partial n_e} \left[ \frac{e^{i\kappa\rho}}{\rho} \right] - \frac{e^{i\kappa\rho}}{\rho} \frac{\partial U}{\partial n_e} \right\} ds, \quad (1.61)$$

where $U_\bullet(P, Q)$ - the field of radiation source at observation point; $U_\bullet=0$, if point P is located in the shadow zone; $\rho$ - distance between the point on surface of S and precise of observation; $n_e$ — external normal to the surface of S.

If points P and Q are located in the plane, perpendicular to the axis of cylindrical body,

$$U(P) = U_\bullet(P, Q) - \frac{i}{4} \int_L \left\{ U \frac{\partial}{\partial n_e} H_{\bullet 1}^{(1)}(\kappa\rho) - H_\bullet^{(1)}(\kappa\rho) \frac{\partial U}{\partial n_e} \right\} dl,$$
$$(1.62)$$

where L - duct/contour in the section of surface of S by the plane, passing through points P and Q.

Page 30.

Formulas (1.61) and (1.62) show that for a strict calculation of value U(P) it is necessary to know the precise values of U and $\partial U/\partial n_e$ on the body surface. However, if surface S has complex form,

the precise values U and $\partial U/\partial n_e$ cannot be found.

The method of Kirchhoff, which makes it possible to find approximate value u(P), consists in the fact that values U(F) and $\partial U(F)/\partial n_e$ at each point F on the illuminated part of surface S of opaque body take as the equal ones to:

$$U(F) = u(F),$$
$$\frac{\partial}{\partial n_e} U(F) = \frac{\partial}{\partial n_e} u(F), \qquad (1.63)$$

where u(F) - field on plane $\Sigma$, tangent to surface of S at point F.

If point F is located in the shadow zone,

$$U(F) = \frac{\partial}{\partial n_e} U(F) = 0. \qquad (1.64)$$

During computation U(F) and $\partial U(F)/\partial n_e$ according to formula (1.63) it is assumed that electromagnetic field on plane $\Sigma$ satisfies the same boundary conditions as on surface of S. We gave the fundamental principles which will be required subsequently for the calculations according to Kirchhoff's method (see Chapter 5). The detailed presentation of Kirchhoff's method the reader can find, for example, in the book of Baker and Copson [24].

If the conductive body on which is located surface antenna, is limited by arbitrary convex surface with the radii of curvature, greater in comparison with the wavelength, the antenna radiation patterns can be designed with the aid of the relationships/ratios,

given in Foch's works [15, 16]. Let us give the short presentation of the results of these works in the form, convenient for the solution of the problem about the surface emitter.

Let to the arbitrary convex body (Fig. 1.9), the surface curvature of which is changed continuously, from the direction $\varphi$ in plane xOy fall plane wave. Let us accept for simplicity, that tangential plane to the body at the points for which z=0, is parallel to axis Oz. The section of this body by plane xOy forms certain the curve L(s).

Page 32.

Parameter s - the arc length, calculated off the origin of coordinates along by the curve L(s), moreover s increases with an increase in coordinate y. We will as before examine two polarizations $E_\perp$ and $E_\parallel$. Point $s_\bullet$ (Fig. 1.9) divides the curve L(s) into two parts, one of which is located in the region of light/world, and another - in the shadow zone. In work [15] it is shown that the magnetic field on the surface of conductor at any point s curved L(s) has the following value.

Polarization $E_\perp$:

$$H_s = H_0 g\,(\mathfrak{k})\,e^{i\,\pi(s-s_0)}. \qquad (1.65)$$

Polarization $E_\parallel$:

$$H_t = H_0 f(\xi) e^{i \pi (\varphi - \omega t)}. \qquad (1.66)$$

In expressions (1.65), (1.66):

$$|\xi| = \sqrt[3]{\varkappa / 2R^2} |s - s_0|;$$

$H_0$ - magnetic intensity of the incident wave at the point of contact of tangency $s_0$[1];

R - radius of curvature of surface of the scattering body in the section by plane xOy.

FOOTNOTE [1]. If the curve L(s) locked, on it is two end-points $s_0$. in this case in formulas (1.54), (1.55) must be considered only that point $s_0$ which is nearer to point s. ENDFOOTNOTE.
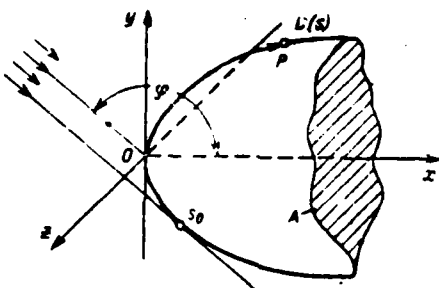
Fig. 1.9. To scattering of plane wave on tne convex body.

Page 33.

The sign of the parameter $\xi$ is negative, if the incident wave illuminates point s, and positive, if point s is located in the shadow. Functions $f(\xi)$ and $g(\xi)$ are expressed as Airy's integral $w(\tau)$ [25] according to formulas [15]:

$$f(\xi) = \frac{1}{\sqrt{\pi}} \int_C \frac{e^{i\xi\tau}}{w(\tau)} d\tau; \qquad (1.67)$$

$$g(\xi) = \frac{1}{\sqrt{\pi}} \int_C \frac{e^{i\xi\tau}}{w'(\tau)} d\tau. \qquad (1.68)$$

The duct/contour of integration C is formed by two line segments on the plane of complex variable z=x+iy:

$$\arg z = \frac{2\pi}{3} \text{ при } x < 0,$$
$$\arg z = 0 \text{ при } x > 0.$$

Key: (1). with.

With $\xi < 0$ for calculating the values $H_t$ and $H_s$ according to formulas (1.65), (1.66) it is convenient to use functions $F(\xi)$ and by $G(\xi)$, connected with $f(\xi)$ and $g(\xi)$ with the relationships/ratios:

$$F(\xi) = e^{i\frac{\xi^3}{3}} f(\xi);$$
$$G(\xi) = e^{i\frac{\xi^3}{3}} g(\xi).$$

Functions $F(\xi)$, $G(\xi)$ are slowly changing with $\xi < 0$ (shadow zone). With $\xi > 0$ (region of light/world) slowly are changed functions $g(\xi)$ and $f(\xi)$.

Thus, if antenna is located directly on the surface of the convex conductive body, formula (1.65), (1.66) together with the reciprocity theorem [expression (1.6)] they make it possible to calculate the antenna radiation patterns. Examples of this calculation are given in chapter 6 and 7.

Together with the methods of the solution of the problems examined about the surface emitters wide application find the approximation methods of the physical theory of diffraction [26]. In chapter 7 is given an example of the calculation of the radiation patterns of surface antenna in the approximation/approach of the physical theory of diffraction.

Page 34.


With the development of computational technology ever more
effective use find the numerical methods of the solution of
diffraction problems. With the aid of the contemporary computational
means it is possible to investigate the problem of diffraction on
arbitrary axially symmetrical body [27]. Are developed the numerical
methods of the solution of the incorrectly stated diffraction
problems [28]. The series of problems of diffraction on the tolites,
limited by coordinate surfaces, is solved with the aid of the "method
of join" [29].


In conclusion it should be noted that, if the examined
approximate methods of the theory of the diffraction are applicable
during the calculation of the fields, which diffract on the bodies
with the sizes/dimensions, greater in comparison with the wavelength,
the numerical analyses of diffraction problems are virtually realized
and therefore they are advisable, if sizes/dimensions body are
compared with the wavelength. Thus, the methods indicated supplement
each other and make it possible to investigate the problems about the
emitters, which are located on the bodies which have fairly
complicated layout and virtually arbitrary sizes/dimensions.

2.


TRAVELING-WAVE ANTENNAS IN FREE SPACE.


Among the surface antennas important place occupy the
traveling-wave antennas, which is connected with the possibility of
formation with such antennas of diagrams with the sufficiently high
directivity with the retention/preservation/maintaining of form and,
consequently, also the aerodynamic properties of flight vehicle.
Before beginning the study of surface antennas, let us examine the
radiation characteristics of traveling-wave antennas, which are found
in the free space. This is necessary in order to rate/estimate
subsequently, as affects the surface of object the radiation
characteristics of antenna.


Page 35.


The study of traveling-wave antennas, as any antennas, it can be
broken into two stages, the connected with the solution internal and
external electrodynamic problems. The solution of internal problem
sets as its goal the determination of amplitude-phase field
distribution in antenna aperture. During the solution of exterior
problem is designed antenna radiation, which corresponds to obtained

field distribution in the aperture. Strictly speaking, the exact
solution of the problem about antenna radiation can be obtained only
via the join of the solutions of internal and exterior problems on
the surface of aperture. However, in practice, as a rule,
successfully is utilized the approximate method of the separate
solution of these problems [30].

In the antenna to technology are encountered different varieties
of traveling-wave antennas, based on the use/application of slotted
[31], dielectric [33], flanged [54] and other structures. In present
chapter are investigated the general/common/total properties of
traveling-wave antennas irrespectively of the methods of their
design. Are examined only line-source antennas with continuous field
distribution in the aperture.
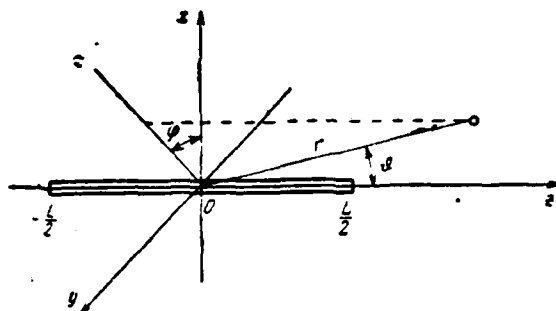
Fig. 2.1. Line-source antenna. Coordinate system.


Page 36.


2.1. Radiation patterns and the directive gain of line-source
antennas.


Diagamma of the directivity of linear traveling-wave antenna
with a length of L (Fig. 2.1) with field distribution in the aperture

$$a(z)e^{i\beta z} \qquad (2.1)$$

is determined by the expression

$$F(\vartheta, \varphi) = F(\vartheta) = \int_{-L/2}^{L/2} a(z)e^{i(\beta - x\cos\vartheta)z}\,dz. \qquad (2.2)$$

Introducing the standardized/normalized coordinate $\xi = 2z/L$ and the
generalized variable/alternating

$$t = \frac{\kappa L}{2}(\Delta - \cos\vartheta), \qquad (2.3)$$

$$\left(\Delta = \frac{t}{\kappa}\right)$$

it is possible to represent diagram (2.2) in the universal form

$$\dot{F}(t) = \frac{L}{2}\int_{-1}^{1} a(\xi)\,e^{it\xi}\,d\xi. \qquad (2.4)$$

Radiation pattern by the power

$$p(t) = \left(\frac{L}{2}\right)^2 \int_{-1}^{1}\int_{-1}^{1} a(\xi)\,a(\xi_1)\,e^{it(\xi-\xi_1)}\,d\xi_1\,d\xi \qquad (2.5)$$

characterizes the dependence of the amounts of the emitted power from

the direction of radiation/emission. During the analysis of

dependence p(∂) on the angular coordinate should be used the formula

$$\vartheta = \arccos\left(\Delta - \frac{2t}{\kappa L}\right). \qquad (2.6)$$

The exemplary/approximate form of diagram (2.5) is depicted in Fig.

2.2. The region of angles 0≪∂≪π, within limits of which is

arranged/located the real antenna radiation pattern, corresponds to

change by the variable/alternating t within limits of t.≪t≪t.+kL,

where

$$t_0 = \frac{\kappa L}{2}(\Delta - 1). \qquad (2.7)$$

Page 37.


In Fig. 2.2 are noted the limits of changes t, which correspond to

real diagrams for three values of the parameter Δ: t'. corresponds to

the case $\Delta<1$, $t_* =0-\Delta=1$ and $t"$ $_*-\Delta>1$. In the first two cases the maximum of radiation pattern occurs with $t=0$, i.e., $\vartheta_{max}=\arccos\Delta$. In third case ($\Delta>1$), when the excitation of antenna is conducted by the deferred-action wave, radiation pattern reaches maximum with $t=t_*$. Further increase in the parameter $\Delta$ can lead to the fact that $t_*$ will exceed the limits of major lobe of diagram (2.5); however, this case will not be examined. Thus, the standardized/normalized radiation pattern (2.5) in entire interesting us range of a change in the parameter $\Delta$ takes the form

$$p_*(t)=\frac{p(t)}{p(t_{max})},\qquad (2.8)$$

where

$$t_{max}=\begin{cases} 0 & \text{при} \quad \Delta<1, \\ t_* & \text{при} \quad \Delta>1. \end{cases}$$

Key: (1). with.

The value of phase wave velocity, which excites aperture, is conveniently characterized by the parameter

$$\sigma=\frac{2t_0}{\pi}=\frac{\varkappa L}{\pi}(\Delta-1),\qquad (2.9)$$

which we will call supplementary phase change.
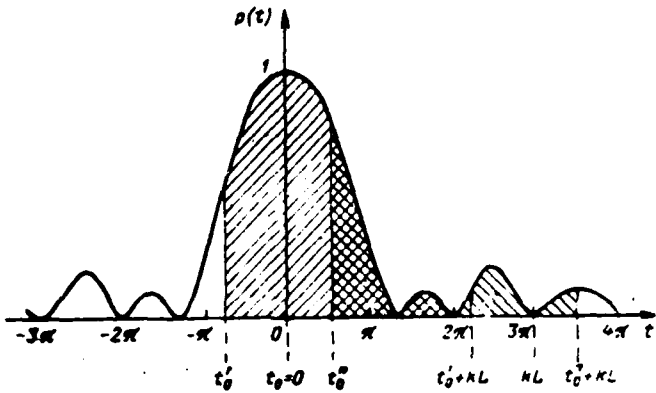
Fig. 2.2. Radiation pattern of line-source antenna.

Page 38.

Actually/really, for the deferred-action waves $\sigma$ it is equal to the value expressed in the portions $\pi$ of supplementary (with respect to the electrical length of aperture) phase change of the wave, which excites aperture. For the antennas with the deflected from the axis ray/beam the parameter $\sigma < 0$.

The directed properties of antenna it is accepted to characterize [35] by the directive gain (derictive gain), equal to

$$K = \frac{4\pi p(\theta, \varphi)}{P_\Sigma},\qquad (2.10)$$

where

$$P_\Sigma = \int_{4\pi} p(\theta, \varphi)\, d\Omega - \qquad (2.11)$$

total power emitted by antenna. Taking into account the axial

symmetry of the linear system of isotropic emitters

$$P_{\Sigma} = \frac{4\pi}{\kappa L} \int\limits_{t_0}^{t_0 + \kappa L} p(t)\, dt =$$

$$= \frac{4\pi}{\kappa L} [I(t_0) - I(t_0 + \kappa L)]. \qquad (2.12)$$

where     $\Pi(\tau) = \int\limits_{\tau}^{\infty} p(t)\, dt.$

Substituting in (2.11) the expression for the diagamma of directivity (2.5), it is possible to obtain under the assumption of smallness of change of the amplitude function a($\xi$) in the interval $\xi \sim -\lambda/L$ the relationship/ratio, which connects $P_{\Sigma}$ with amplitude and phase field distribution in the aperture

$$\frac{P_{\Sigma}}{2\pi\lambda} = Lj = \frac{L}{2} \int\limits_{-1}^{1} a^2(\xi)\, J(\xi, \Delta)\, d\xi, \qquad (2.13)$$

where

$$J(\xi, \Delta) = \frac{1}{2\pi} \left\{ \mathrm{Si}\left[\frac{v}{2}(1+\xi)\right] + \mathrm{Si}\left[\frac{v}{2}(1-\xi)\right] - \right.$$
$$\left. - \mathrm{Si}\left[\frac{u}{2}(1+\xi)\right] - \mathrm{Si}\left[\frac{u}{2}(1-\xi)\right] \right\}; \qquad (2.14)$$
$$u = kL(\Delta - 1) = \pi\sigma; \quad v = \kappa L(\Delta + 1) = \pi\sigma + 2\kappa L.$$

Page 39.

For kL>>1 with $\sigma<0$, which corresponds to the ray/beam deflected from the axis, expression (2.13) substantially is simplified

$$\frac{P_{\Sigma}(\alpha)}{2\pi\lambda} = \frac{L}{2} \int\limits_{-1}^{1} a^2(\xi)\, d\xi. \qquad (2.15)$$

For the uniform amplitude distribution a($\xi$)=1 function j in (2.13) is

numerically equal to relation $P_z(\kappa L)/P_z'(\infty)$. The graph/diagram of dependence of j on $\Delta$ and l=L/$\lambda$ is depicted for this case in Fig. 2.3. Thus, values $p(t_{max})$ and $P_z$, and, consequently, directive gains (2.10) are the functions of phase velocity. With the increase/growth $\Delta$ from 0 to 1 directive gain value K increases approximately/exemplarily doubly. With further increase $\Delta$ the directive gain at first grows/rises, while with the value of the parameter $\Delta$, that exceeds certain optimum value $\Delta_{ont}$, sharply it decreases.

From (2.13) it is evident that the directive gain of antenna with the uniform amplitude distribution with $\sigma$=0 and kL>>1 is equal to

$$K = K_0 = \frac{2}{\pi}\kappa L. \qquad (2.16)$$
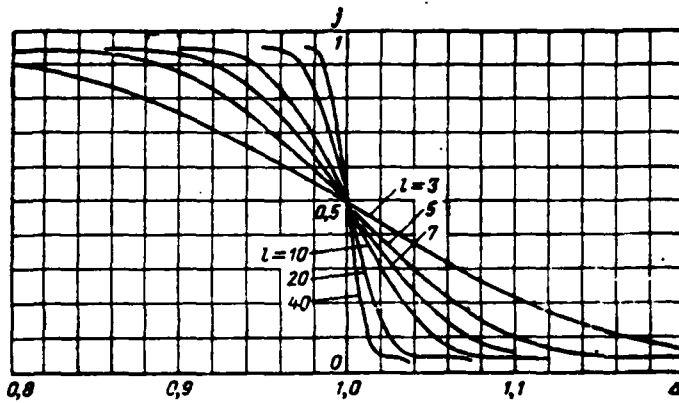
Fig. 2.3. Graph/diagram of dependence j(Δ) for the different values of l=L/λ.

Page 40.

Subsequently we will examine the standardized/normalized values of the directive gain.

$$k = \frac{K}{K_0} = \frac{p(l_{max})}{2L^2 j}. \qquad (2.17)$$

For sufficiently long antennas kL>>1 and σ<0

$$k = \frac{1}{4} \frac{\left|\int_{-1}^{1} a(\xi)\, d\xi\right|^2}{\int_{-1}^{1} a^2(\xi)\, d\xi}. \qquad (2.18)$$

For the antennas of finite length, which radiate along axis (σ⩾0), we obtain approximation for the directive gain, after dropping/omitting in (2.12) the component/term/addend of I(t₊+kL):

$$k = \frac{\pi}{2} \frac{p(l_{max})}{l(l_0)}. \qquad (2.19)$$

This is relationship/ratio by conveniently its universality, since k, actually, depends only on the parameter $\sigma$ and the form of amplitude function.

Together with the directive gain subsequently will be investigated other characteristics of the antenna:

- efficiency [30]

$$\eta = \frac{P_\Sigma}{P_0},\qquad\qquad (2.20)$$

where $P_0$ - total applied to antenna power;

- factor of amplification G and relative factor of amplification g [30]

$$G = K\eta;\ g = k\eta,\qquad\qquad (2.21)$$

the integral characteristic of the lateral radiation of antenna - coefficient of scattering $\rho$ [34]:

$$\rho = \frac{P_{\Sigma\delta\ell}}{P_\Sigma} = 1 - \frac{P_{\Sigma\eta\pi}}{P_\Sigma},\qquad\qquad (2.22)$$

where $P_{\Sigma\eta\pi}$ — portion power $P_\Sigma$, emitted in major lobe; $P_{\Sigma\delta\ell} = P_\Sigma - P_{\Sigma\eta\pi}$.
Omitting in (2.12) with $\sigma \geqslant 0$ the component/term/addend of $I(t_0 + kL)$, we obtain the universal relationship/ratio

$$\rho = \frac{I(t_{min})}{I(t_0)},\qquad\qquad (2.23)$$

where $t_{min}$ — coordinate of the first minimum of diagram.

Page 41.


If is examined the two-dimensional problem (sɘe for example,
[32]), the directed properties of antenna it is possible to
characterize "flat/plane" by directive gain $K_1$ and by amplification
$G_1$, which are connected with (2.10) and (2.21) the
relationships/ratios

$$K_1 = \pi K,$$
$$G_1 = \pi G. \qquad (2.24)$$

Approximation for the width of radiation pattern on the angular scale
can be obtained, expanding in series/row formula (2.6). The width of
radiation pattern on zero and level of the half power of the
line-source antenna with the even distribution, which radiates along
axis ($\sigma=0$), is equal to

$$\Delta\vartheta_0 \approx 2\sqrt{2}\sqrt{\frac{\lambda}{L}} \qquad (2.25a)$$

and

$$\Delta\vartheta_{0.5} \approx \frac{\Delta\vartheta_0}{1,5}. \qquad (2.25b)$$

Calibrated to $\Delta\vartheta_0$ the width of radiation pattern on certain level
$p(t_1)$ for the diagrams with the maximum, oriented in the direction
$t=0$, is equal to

$$\gamma_o = \frac{\Delta \theta}{\Delta \theta_o} \simeq \begin{cases} \sqrt{\frac{t_1 - t_o}{\pi}} \text{ при } -t_1 < t_o, \\ \frac{1}{2} \sqrt{\frac{t_1 - t_o}{\pi}} - \frac{1}{2} \sqrt{\frac{-t_1 - t_o}{\pi}} \text{ при } t_o < -t_1; \end{cases}$$

$$(2.26)$$

Key: (1). with.

where coordinate $t_1$ is the direction, which corresponds to the assigned level of diagram.

Page 42.


2.2. Line-source antennas with symmetrically collapsible/dropped
amplitude distribution.


Let us assign amplitude-phase distribution in antenna aperture
in the form

$$a(z)\,e^{i\beta z} = \left(1 + q\cos\frac{2\pi z}{L}\right)\exp\left[ik\left(1 + \frac{\theta}{2L/\lambda}\right)z\right]. \quad (2.27)$$

The selection of distribution (2.27) is justified by its simplicity
and broad class of the distributions, approximated by it, which are
encountered in practice.


The standardized/normalized to p(0) radiation pattern (2.8) of
antenna with selected field distribution takes the form

$$p_1(t) = \left(\frac{\sin t}{t}\right)^2\left(1 - q\frac{t^2}{t^2 - \pi^2}\right)^2. \quad (2.28)$$

By the selection of the corresponding value of parameter q the
minor lobes of diagram (2.28) can be made sufficiently small.
Therefore the delay/retarding/deceleration of the wave exciting
aperture proves to be in this case more effective than in antennas
with uniform distribution.

According to formula (2.19) for the radiation pattern (2.28) was produced the calculation of directive gain k. Dependence of k on the parameters $\sigma$, q is represented by the lines of constant value $k(\sigma,$ q)=const in Fig. 2.4. Limits of a change in the parameters:

$$-0.2 < q < 1,$$
$$0 < \sigma < 4.$$

The investigation of dependence $k(\sigma)$ for q=0 is carried out in works [37, 38]. The maximum value k=1.8 derictive gain of uniform grating it reaches with $\sigma \approx 0.94$ [37].

The drop of amplitude to the edges in the absence of supplementary phase raids ($\sigma=0$) leads to the decrease derictive gain to value k=0.67 with q=1. Selecting values of q and $\sigma$, it is possible to considerably increase antenna directivity.

Page 43.

With $\sigma=3.3$ and q=0.92 the derictive gain of line-source antenna it reaches maximum value and 4.4 times exceeds derictive gain $K_{\bullet}$ of uniform line-source antenna with the axial radiation/emission with $\sigma=0$. In Fig. 2.4 dotted line plotted/applied curve $q(\sigma)$, on which the derictive gain reaches maximum at the assigned value of phase change. An increase in the relative side-lobe level of diagram with an increase in phase change $\sigma$ is illustrated by Fig. 2.5, where on the

plane $\sigma$, q are shown the lines $\delta(q, \sigma)$=const of relative level of maximum minor lobe. Comparing Fig. 2.4 and 2.5, it is possible to select parametric domain $\sigma$, q with sufficiently high k and permissible sidelobe level.

The standardized/normalized width of diagram on zero for the range of values $t_0 > t_1$ is determined by formula (2.26), where $t_1 = \pi / \sqrt{1-q}$ with q<0.75 and $t_1 = 2\pi$ with q>0.75, and $t_0 = \pi \sigma / 2$.
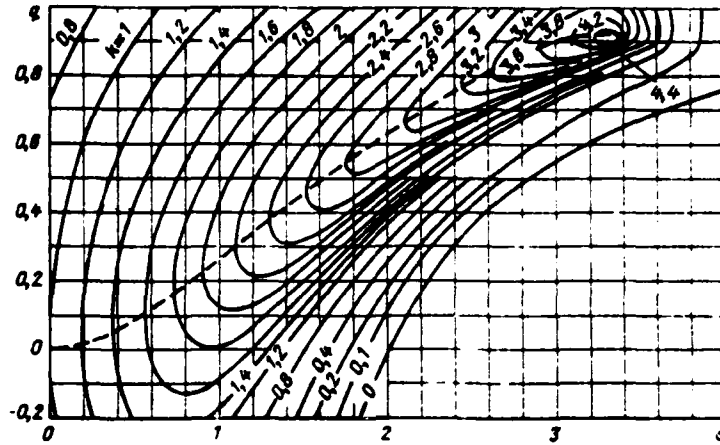
Fig. 2.4. Lines of level the relative derictive gain k=const on the plane of parameters q, σ.


Page 44.


The standardized/normalized width of diagram on the level of the half power

$$\chi_{0.5} = 1.5 \chi_0 = \frac{\Delta\vartheta_{0.5}(q,\ \sigma)}{\Delta\vartheta_{0.5}(0,\ 0)}$$

for $t_0 > -t_1$ is depicted in Fig. 2.6 as lines of equal level on plane q, σ. In the right side of the figure in the region where the regions, where the minor lobe exceeds basis, curves are not plotted/applied. Curves of Fig. 2.6 can be utilized for calculating the width of diagram and in the case of the rays/beams deflected from the axis when $t_0 < -t_1$, after assuming in formula (2.26)

$$t_1 = \frac{\pi}{2.25} \chi_{0.5}^2 \ (\sigma = 0).$$
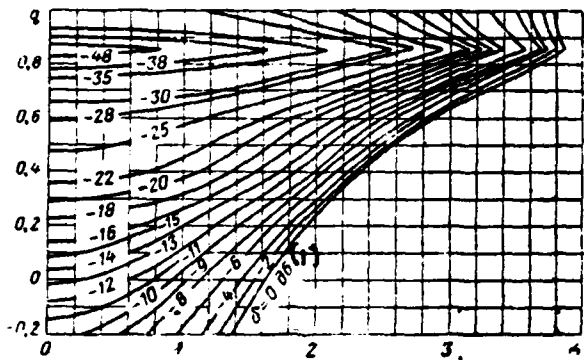
Fig. 2.5. Lines of level of relative value of maximum minor lobe δ(q, σ)=const.

Key: (1). dB.
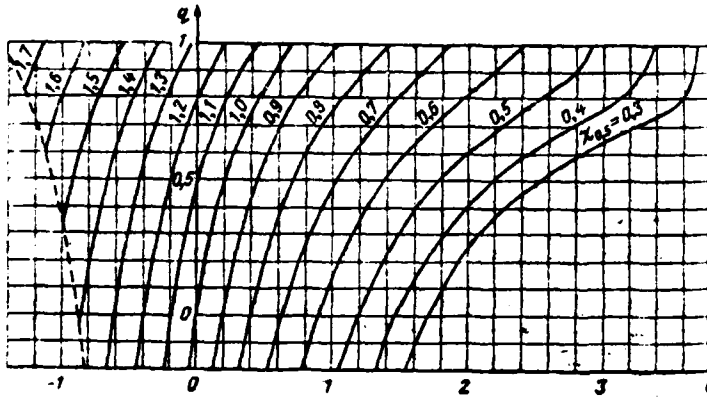


Fig. 2.6. Lines of level $\varkappa_{0.5}$ (q, σ)=const of relative width of diagram on level $0.5\rho_{max}$.

Page 45.

Fig. 2.7 gives the results of calculation according to formula
(2.23) of the lines of level of coefficient of scattering $\rho(\sigma,$
q)=const. For the constant amplitude of field in antenna aperture
($\sigma$=0) the coefficient of scattering composes 10o/o. With the
increase/growth $\sigma$ value $\rho$ sharply grows/rises due to an increase in
the side-lobe level. With a decrease in field level at the edges of
antenna the coefficient $\rho$ decreases.
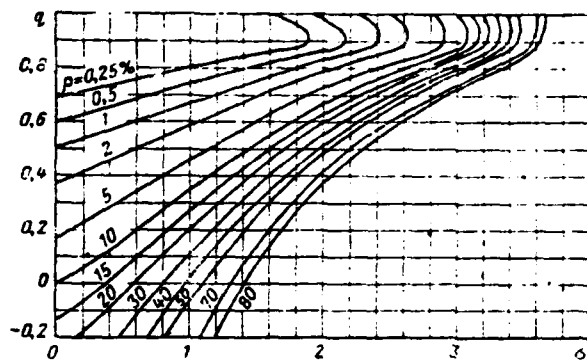
Fig. 2.7. Lines of level of coefficient of scattering $\rho$=const on the plane of parameters q, $\sigma$.
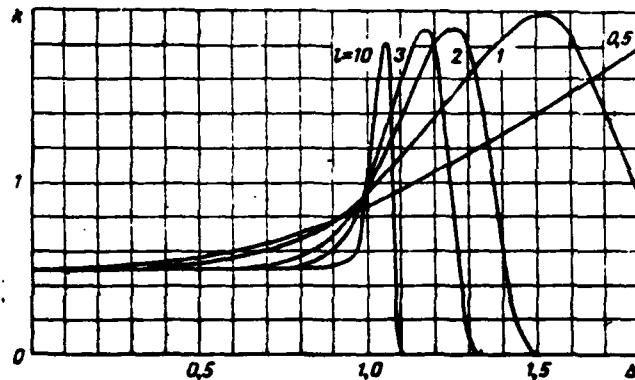


Fig. 2.8. Graph/diagram of dependence derictive gain on phase distribution in aperture (q=0).


Page 46.


Analogous calculations for the fixed values of the length of antenna with the even distribution in the aperture are given in works [30, 35

and 38].

Universal character investigated is above parameters k and $\rho$ is
obtained on the assumption that the size/dimension of antenna is
sufficiently great. In order to quantitatively rate/estimate error
introduced by this assumption, Fig. 2.8 depicts dependences k=f($\Delta$)
for the series/row of the values of the length of antenna with the
uniform amplitude distribution. Fig. 2.9 shows the dependence of
relation $k_\infty/k$ on $\sigma$, where $k_\infty$ is determined from formula (2.19). From
these graphs/curves it follows that already with $l=L/\lambda \geq 3$ for $\sigma=0$
approximate values derictive gain in practice do not differ from
precise ones. With an increase in phase change $\sigma$ an error in the
computation derictive gain as a result of a relative increase in the
minor lobes somewhat increases. With the drop of the amplitude of
field the error sharply descends, which is caused by the decrease of
the value of minor lobes.

2.3. Line-source antennas with the exponential amplitude
distribution.

Exponential amplitude distribution $e^{-\delta(x+L/2)}$ is simplest and
easily realized in practice.
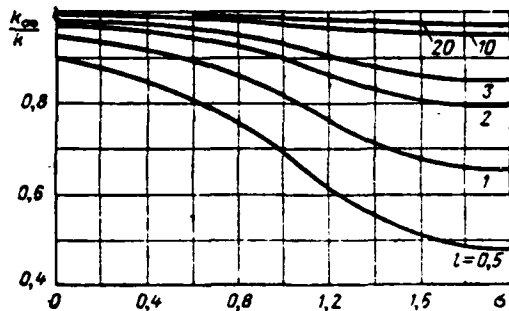
Fig. 2.9. Graph/diagrams of the dependence of relation $\frac{k_\infty}{k}$ on phase change $\sigma$ with q=0.

Page 47.

This distribution is observed in the simplest traveling-wave antennas, which consist of the identical emitters with the series excitation. With this is connected the wide application of such antennas [30, 38, 40]. Most fully the properties of antennas with exponential field distribution in the aperture are investigated in work [38].

Let us assign amplitude-phase distribution in antenna aperture

$$a(z)\,e^{i\mu} = \exp\left[-s\left(1 + \frac{2z}{L}\right)\right] \exp\left[ik\left(1 + \frac{\sigma}{2L\,\lambda}\right) z\right].$$

(2.29)

Parameter s=δL/2 determines the degree of the drop of the amplitude of field to the edge of antenna. The

standardized/normalized to value of p(0) radiation pattern (2.8) in this case takes the form

$$p_1(t) = \frac{s^2}{s^2 + t^2} \cdot \frac{sh^2\, s + \sin^2 t}{sh^2\, s}. \qquad (2.30)$$

The exponential drop of amplitude in the aperture leads to the expansion of diagram, to "floating" of zeros and to the increase of side-lobe level. With s>1.1 the diagram becomes mohotonically decreasing function t. Relative directive gain was designed from formula (2.19) taking into account (2.30). The results of calculation are given in Fig. 2.10 in the form of the lines of level k($\sigma$, s)=const. At the low values of s lines k=const are parallel to axis s. This means that a change in the level of lighting the edge of antenna over wide limits (0-5 dB) weakly affects its directive gain. With an increase $\sigma$ in the derictive gain at first it increases, and then rapidly drops. In contrast to the case of the symmetrically collapsible/dropped distributions, the maximum directive gain during the use of supplementary phase change will be with s=0.

Side-lobe level with an increase in value $\sigma$ grows/rises. Dotted line in Fig. 2.10 depicted the lines of the constant value of the level of the first minor lobe (with respect to the power in the principal maximum).

Page 48.

For the antennas with exponential field distribution in the aperture it is not difficult to calculate the power, which enters the load and, consequently, also the efficiency (2.20). Without taking into account losses in antenna itself efficiency it is equal to

$$\eta = 1 - e^{-4s}. \qquad (2.31)$$

Relative factor of amplification $g = \eta k$ characterizes the directed properties of antenna taking into account power losses in the load. The results of calculating the value $g(\sigma, s)$ are shown in Fig. 2.11.
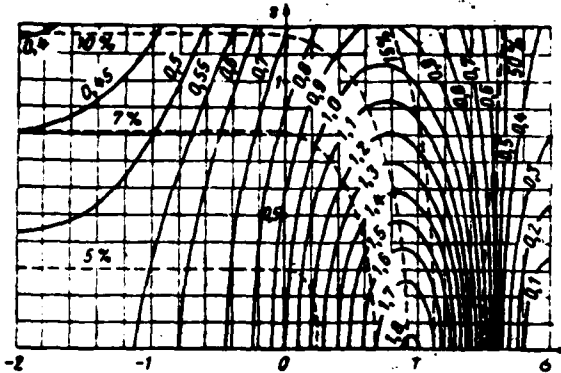
Fig. 2.10. Lines of level derictive gain k=const (continuous) and the first minor lobe δ=const (dotted line) antenna with the exponential distribution.
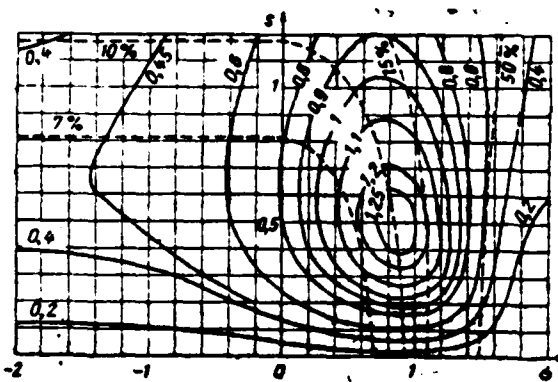


Fig. 2.11. Lines of level of amplification g=const (continuous) and first minor lobe δ=const (dotted line) antenna with exponential distribution.

Page 49.

The value of the optimum phase change is close to $\sigma = 0.9$.
From Fig. 2.11 it is possible to determine the drop of amplitude,
optimum for the assigned value $\sigma$ on the edge of aperture, which makes
it possible to obtain the greatest amplification factor. Maximum
factor of amplification $G \approx 5.11$ is obtained with $\sigma = 0.85$; $s \approx 0.5$.


2.4. Energy calculation of traveling-wave antennas.


The energy method of calculation extensively is used for
determining the fundamental parameters of traveling-wave antennas. In
particular, this method makes it possible to determine amplitude
distribution, if is known the function of the radiating capacity
([36, 39, 41]) and, on the contrary, gives the possibility to
determine the distribution of radiating capacity along the antenna,
the ensuring assigned amplitude distribution ([36, 41-44]). This
method is sufficiently to general/common/total ones and is applicable
to any types of antennas with the series excitation. The energy
method of calculation of traveling-wave antennas is approximation
method. It does not consider interaction of separate emitters or
radiating sections of antenna. Nevertheless for the antennas with a
smooth change in the amplitude distribution and the radiating
capacity according to the aperture this method gives good results.


Let us examine antenna with the phase distribution, which
corresponds to the traveling wave. Each element/cell of antenna
aperture dz emits energy $dW_r$, proportional to radiating capacity $I(z)$
and power of the exciting wave $W(z)$ in section z of antenna (Fig. -
2.12).
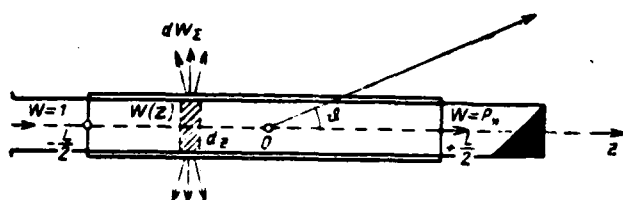
Fig. 2.12. On the calculation of continuous traveling-wave antenna.


Page 50.


Let us assume that the distributed ohmic losses in the antenna are described by function Q(z), and the power absorbed by element/cell dz is equal to $dW_q$. In this case power W(z) in the antenna decreases on element/cell dz to value $dW = dW_x + dW_q$, equal to

$$dW(z) = -[I(z) + Q(z)]W(z)\,dz. \qquad (2.32)$$

We will consider that the matched input of antenna enters the single power

$$W\left(-\frac{L}{2}\right) = 1. \qquad (2.33)$$

The solution of differential equation (2.32) taking into account boundary condition (2.33) is the function

$$W(\xi) = \exp\left\{-\frac{L}{2}\int_{-1}^{\xi}[I(\xi_1) + Q(\xi_1)]\,d\xi_1\right\}, \qquad (2.34)$$

where $\xi = 2z/L$.


The density of distribution of radiated power according to antenna

aperture (i.e. the square of amplitude distribution) is equal to product of $W(\xi)$ times the radiating capacity $I(\xi)$:

$$p(\xi) = a^2(\xi) = I(\xi) W(\xi) =$$

$$= I(\xi) \exp\left\{ -\frac{L}{2} \int\limits_{-1}^{\xi} [I(\xi_1) + Q(\xi_1)] \, d\xi_1 \right\}. \qquad (2.35)$$

The density of distribution of power losses along the antenna can be found from the relationship/ratio

$$p_R(\xi) = Q(\xi) W(\xi) =$$

$$= Q(\xi) \exp\left\{ -\frac{L}{2} \int\limits_{-1}^{\xi} [I(\xi_1) + Q(\xi_1)] \, d\xi_1 \right\}. \qquad (2.36)$$

Page 51.

Complete emitted power $P_\Sigma$ and power of losses in antenna $P_R$ can be found with the integration of functions (2.35) and (2.36) of entire aperture:

$$P_\Sigma = \frac{L}{2} \int\limits_{-1}^{1} p(\xi) \, d\xi; \qquad (2.37)$$

$$P_R = \frac{L}{2} \int\limits_{-1}^{1} p_R(\xi) \, d\xi. \qquad (2.38)$$

It is simple to be convinced of the fact that taking into account the power, which goes into the load

$$P_H = W(1) = \exp\left\{ -\frac{L}{2} \int\limits_{-1}^{1} [I(\xi) + Q(\xi)] \, d\xi \right\}, \qquad (2.39)$$

is made the equation of the energy balance

$$P_\Sigma + P_R + P_H = 1. \qquad (2.40)$$

Function of the radiating capacity to conveniently represent in the form

$$I(\xi) = I_9 g_e(\xi). \qquad (2.41)$$

The amplitude of a change in radiating capacity $I(\xi)$ is determined by the amount of the power, which enters the load, and is equal at the losses $Q(\xi)=$const constant along the length of antenna to value

$$I_\bullet = -\frac{2\gamma + \ln P_H}{\frac{L}{2} \int\limits_{-1}^{1} g_\bullet(\xi)\, d\xi},\qquad (2.42)$$

where

$$\gamma = \frac{L}{2} Q.$$

Let us examine now inverse problem, i.e., let us calculate the distribution of radiating capacity along the traveling-wave antenna, the ensuring assigned amplitude distribution in the aperture. The investigation of the dependence of radiating capacity from field distribution in the aperture is carried out in works [36, 41-44].

Page 52.

For determining the function $I(\xi)$ we will use the equation of energy balance (2.40) and equality to $I(z)W(z)=p(z)$, where $p(z)$ - the density of distribution of the emitted power according to the aperture. Thus we obtain linear differential first-order equation for power $W(\xi)$ in certain section of the antenna

$$W'(\xi) + \frac{L}{2} Q(\xi) W(\xi) = -\frac{L}{2} p(\xi). \qquad (2.43)$$

The solution of this equation taking into account the boundary

condition $W(-1)=1$ for the uniform loss function $Q=2\gamma/L$ takes the form

$$W(\xi) = e^{-\tau(1+\xi)} \left[ 1 - \frac{L}{2} \int\limits_{-1}^{\xi} p(\xi) e^{\tau(1+\xi)} d\xi \right]. \quad (2.44)$$

As a result we obtain for the radiating capacity the following relationship/ratio:

$$I(\xi) = \frac{p(\xi)}{W(\xi)} =$$

$$= \frac{p(\xi) e^{\tau(1+\xi)}}{\dfrac{1}{\eta} \dfrac{L}{2} \int\limits_{-1}^{1} p(\xi_1) d\xi_1 - \dfrac{L}{2} \int\limits_{-1}^{\xi} p(\xi_1) e^{\tau(1+\xi_1)} d\xi_1}. \quad (2.45)$$

In this expression is used equality $P_{\Sigma} = \eta$.

Function $I(\xi)$ does not depend on the absolute value of the function of the distribution of power in aperture $p(\xi)$. The efficiency of antenna in the presence of losses in it is connected with the power, which enters the load, by the relationship/ratio

$$\eta = (1 - P_H e^{2\gamma}) \frac{\dfrac{L}{2} \int\limits_{-1}^{1} p(\xi) d\xi}{\dfrac{L}{2} \int\limits_{-1}^{1} p(\xi) e^{\tau(1+\xi)} d\xi}, \quad (2.46)$$

which is obtained from equality $P_{\Sigma} = \eta$ and $W(1) = P_H$ [see (2.44)].

Page 53.

To constant amplitude distribution in the aperture in the absence of losses in the antenna corresponds the radiating capacity

$$I(\xi) = \frac{2}{L} \cdot \frac{1}{\dfrac{2}{\eta} - (1+\xi)}. \quad (2.47)$$

Dependence L/2 I($\xi$) for this case is shown in Fig. 2.13 for several values of $\eta = 1 - P_H$.

2.5. Antennas with the symmetrical law of a change in the radiating capacity.

As an example of the use of relationships/ratios, obtained in the preceding/previous paragraph, will examine the traveling-wave antennas with the symmetrical distribution of the function of radiating capacity, assuming/setting by the I($\xi$) even function. Such antennas possess the complete symmetry of radiation characteristics with a change in the direction of propagation of the wave, which excites aperture, to the opposite. Antennas with the symmetrical functions of radiating capacity extensively are used in the technology and are examined in the series/row of the works (for example, see [45-47], etc.).
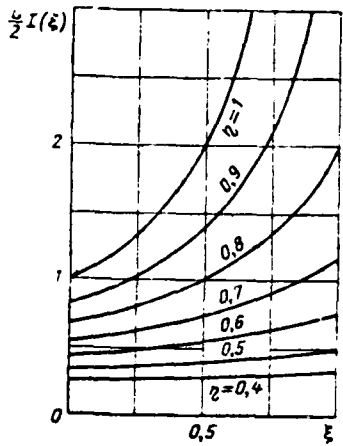
Fig. 2.13. Function the $I(\xi)$, which ensures uniform amplitude distribution in the aperture.


Page 54.


The simplest case of the symmetrical distribution of radiating capacity is $I(\xi)$=const. Amplitude distribution in this case is the exponential function

$$a(\xi) = \sqrt{I_0}\, e^{-\alpha(1+\xi)}, \qquad (2.48)$$

where

$$\alpha = \frac{L}{4} I_0,$$

coinciding with distribution (2.29), examined in S2.3. In certain cases the decrease of the function of radiating capacity $g_0(\xi)$ of the edges of aperture can lead with the constant/invariable $\alpha$ to the increase derictive gain due to an increase in even component of

distribution $a^2(\xi)$. In order to rate/estimate the effect of the law of a change in radiating capacity (2.41) to the radiation characteristics of traveling-wave antenna, let us examine the function

$$g_e(\xi) = 1 - b_s^2 \xi^2. \qquad (2.49)$$
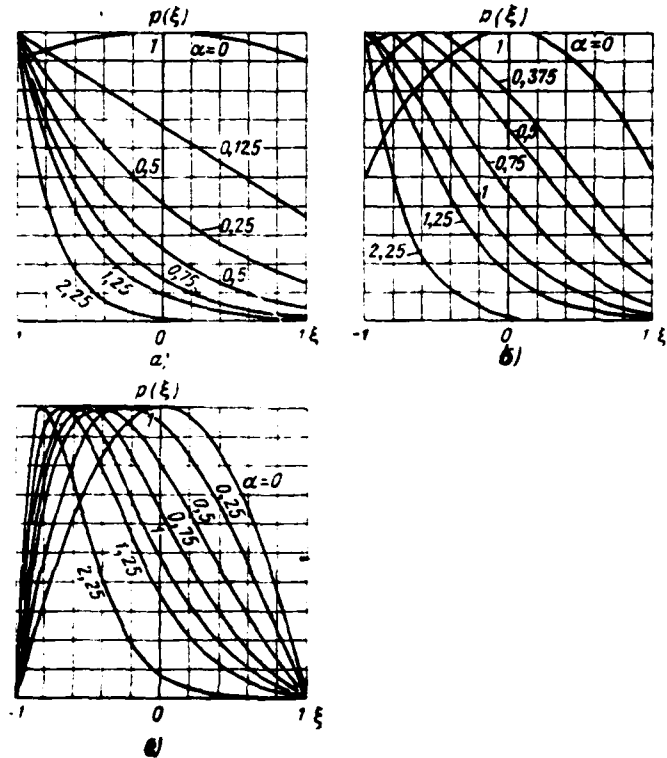
Fig. 2.14. Amplitude distribution in the aperture with the symmetrical function of radiating capacity $g_0(\xi)=1-b\xi^2$: a) b=0.1; b) b=0.5; c) b=1.

Page 55.

The standardized/normalized distribution $p(\xi)=a^2(\xi)$ in antenna aperture with the law of a change in radiating capacity (2.49) with $\gamma=0$ is shown in Fig. 2.14 for the series/row of values b and $\alpha$. Fig. 2.15 gives the values of the relative derictive gain $k=f(\alpha)$,

calculated under the assumption kL>>1, Δ<1 for several values of parameter b. The dependence of amplification g of this antenna on parameters b and α is depicted in Fig. 2.16. As can be seen from figure, the parameter α affects the value of amplification more strongly than b.
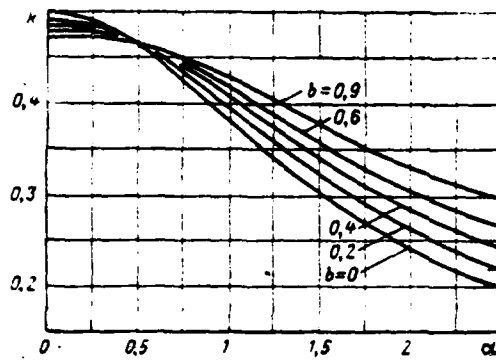
Fig. 2.15. Graph/diagrams of the dependence derictive gain k of antenna with radiating capacity $I(\xi)=I_o(1-b\xi^2)$ on $\alpha$.
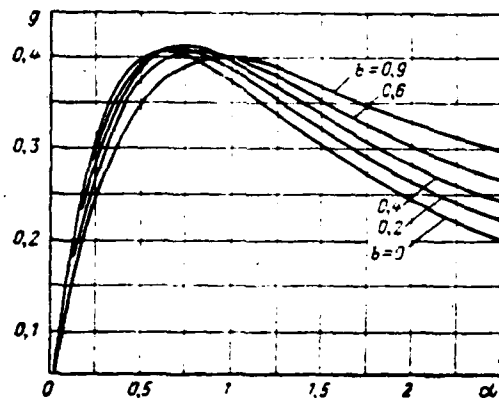


Fig. 2.16. Graph/diagrams of dependence of amplification g of antenna with radiating capacity $I(\xi)=I_o(1-b\xi^2)$ on $\alpha$.

Page 57.

The optimum value $g\approx0.4$ amplification reaches with $\alpha=0.55-0.85$.

In order to rate/estimate the effect of the form of the function
$g_0(\xi)$ on the radiation characteristics of antenna, let us compare
derictive gain and relative antenna gains in three cases (Fig. 2.17).
From the examination of Fig. 2.17 it follows that the fundamental
characteristics of antenna (derictive gain and amplification) weakly
depend on the form of the function $g_0(\xi)$, of the characterizing the law
of change radiating capacity from the center of antenna of its edges.
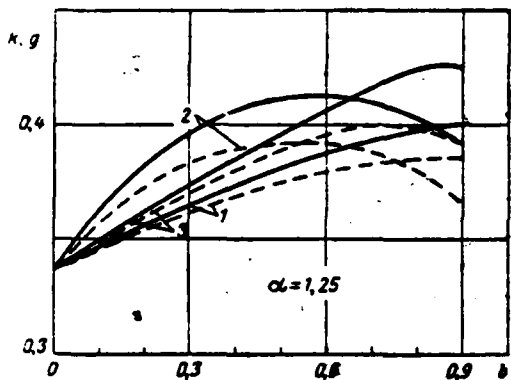


Fig. 2.17. Graph/diagrams of the dependence derictive gain k
(continuous) and amplification g (dotted line) on parameter b for
different functions $g_0(\xi)$:

1) $g_0(\xi) = 1 - b\xi^2$; 2) $g_0(\xi) = \dfrac{1 + b \cos \pi\xi}{1 + b}$; 3) $g_0(\xi) = 1 - b|\xi|$.

3.

RADIATION CHARACTERISTICS OF ANTENNAS LOCATED ON THE SURFACE OF A
HALF-PLANE.

In present chapter is examined the effect of the edge of
flat/plane screen on the radiation pattern of surface antenna. The
analysis of the characteristics of emitters, which are located on the
half-plane, has great practical value for calculating the antennas,
arranged/located on different aerodynamic objects.

Page 57.

The solution of the problem about the radiation/emission from the
half-plane, as it will be shown, serves as a good
approximation/approach for calculating the antennas, which are
located on the surfaces of more complex form (key, to band, to
plate). A strict solution of the problem in question is important
also for the quantitative evaluation/estimate of the suitability of
different approximate methods of calculating the surface antennas.

For the first time the problem about radiation of surface
antenna from the half-plane for the case of perpendicular
polarization is solved in [6]. In [36] is presented an approximate
solution of this problem for parallel polarization which, however,
does not provide the possibility to rate/estimate radiation

level of surface antenna along its axis. The series/row of the
results of particular character is obtained in work [4]. At the same
time in the literature is absent detailed analysis of the radiation
characteristics of the surface traveling-wave antennas, located near
the edge of half-plane. In connection with this are in detail
investigated below the fundamental characteristics of the radiation
pattern (width, the direction of principal maximum, directive gain)
of antenna, which is located on the half-plane, is substantiated the
approximate method of calculating the radiation pattern. The analysis
of radiation characteristics is carried out for two fundamental
polarizations and different amplitude-phase field distributions in
the aperture of surface antenna.

3.1. Derivation of fundamental formulas.

Let in certain section of the flat/plane ideally conducting
semi-infinite screen (Fig. 3.1) be is assigned the tangential
electric field

$$\vec{E}_{\tau} = \vec{e}_{x,y} E(x); \quad \Gamma < x < \Gamma + L. \qquad (3.1)$$
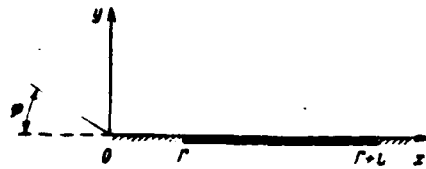
Fig. 3.1. Radiating aperture on the half-plane.


Page 58.


We will examine field distributions in antenna aperture, which correspond to the traveling wave:

$$E_{x,z} = A(x)e^{-i\beta x}, \qquad (3.2)$$

where A(x) - amplitude distribution, and $\beta x$ - phase of field along the antenna. For further analysis let us select the amplitude distributions of two types - symmetrically and exponentially collapsible/dropped to the edge antennas widely utilized in practice:

$$A(x) = 1 - q\cos\frac{2\pi(x-\Gamma)}{L}, \qquad (3.3)$$

$$A(x) = e^{-\beta(\Gamma+L-x)}. \qquad (3.4)$$

After using relationships/ratios (1.6), (1.35) and (1.38) and omitting unessential factors, we obtain the following expressions for the radiation patterns:

$$\Phi_{\perp,q}(t) = \int_{\zeta}^{\zeta+1} [1 - q\cos 2\pi(\xi-\zeta)]\exp[-i\pi(\sigma +$$

$$+ t^2)\xi][1 + \sqrt{2}\,e^{-i\frac{\pi}{4}}F_1(t\sqrt{2\xi})]\,d\xi, \qquad (3.5)$$

$$\Phi_{\perp,s}(t) = \int_{\zeta}^{\zeta+1}\exp[-2s(1+\zeta-\xi) -$$

$$- i\pi(\sigma+t^2)\xi][1 + \sqrt{2}\,e^{-i\frac{\pi}{4}}F_1(t\sqrt{2\xi})]\,d\xi, \qquad (3.6)$$

$$\Phi'_{\|,q}(t) = \cos\frac{\varphi}{2}\int_{\zeta}^{\zeta+1} [1 - q\cos 2\pi(\xi -$$

$$- \zeta)]\exp[-i\pi(\sigma+t^2)\xi]\left\{-2i\pi t\left[1 + \sqrt{2}e^{-i\frac{\pi}{4}}F_1(t\sqrt{2\xi})\right] +$$

$$+ \exp\left[-i\pi\left(\frac{1}{4}-\xi t^2\right)\right]\frac{2}{\sqrt{\xi}}\right\}d\xi. \qquad (3.7)$$

In expressions (3.5)-(3.7) are introduced the designations:

$$\frac{x}{L}=\xi;\ \frac{\Gamma}{L}=\zeta;\ \frac{!L(\beta-k)}{\pi}=\sigma, \qquad (3.8)$$

$$2\sqrt{\frac{L}{\lambda}}\sin\frac{\varphi}{2}=t, \qquad (3.9)$$

$$s=\delta L/2. \qquad (3.10)$$

Page 59.


The parameter $\zeta$ characterizes the relative (in portions L) removal/distance of antenna from the edge/fin of half-plane. Value $\sigma$ determines supplementary phase change, expressed in the portions $\pi$ at the length of antenna, which appears as a result of a difference in phase wave velocity, which excites antenna aperture, from the speed of light. The degree of the drop of the amplitude of field to the edges of antenna aperture characterize parameters q and s.

The examination of expressions (3.5)-(3.7) shows that during the parallel polarization in contrast to the perpendicular it is impossible to avoid parameters t, $\varsigma$, $\sigma$. However, for the antennas whose length $L \geqslant 5\lambda$ within the limits of the major and several first minor lobes $\cos(\varphi/2) \simeq 1$   and therefore we will investigate the function

$$\Phi_{\parallel}(t) = \frac{\Phi'_{\parallel}(t)}{\cos\frac{\varphi}{2}}, \qquad (3.11)$$

depending only on t, $\varsigma$ and $\sigma$. In expressions (3.5) and (3.7) it is possible to fulfill integration, as a result of which we obtain:

$$\Phi_{\perp,q}(t) = \left\{ \left( \frac{1}{v} - q\frac{v}{v^2-4} \right) \times \right.$$

$$\times \left[ \frac{e^{i\frac{\pi}{4}(1-t)}}{\sqrt{\pi}} \int_0^{v\pi\varsigma} e^{iz}\frac{dz}{\sqrt{z}} - \right.$$

$$\left. - e^{-i\pi v\varsigma} \right]_{\varsigma}^{\varsigma+1} - t e^{i\frac{\pi}{4}} \left[ A_0 \frac{1}{v\sqrt{2}} - \frac{q}{2}\left( \frac{A_{-2}}{v-2} + \frac{A_2}{v+2} \right) \right] \right\}.$$

$$(3.12)$$

$$\Phi'_{\parallel,q}(t) = \cos\frac{\varphi}{2} \cdot \sqrt{\frac{\lambda}{L}} \left\{ -it\Phi_{\perp,q}(t) + \right.$$

$$\left. + e^{-i\frac{\pi}{4}} \left[ A_0 - \frac{q}{2}(A_2 + A_{-2}) \right] \right\}, \qquad (3.13)$$

where

$$v = \sigma + t^2; \qquad (3.14)$$

$$A_n = e^{i\pi n\varsigma} \int_{\varsigma}^{\varsigma+1} e^{-i\pi(\sigma+n)z}\frac{dz}{\sqrt{z}} \qquad (3.15)$$

Page 60.

It is not difficult to ascertain that $A_n$ is expressed as

Fresnel's integrals.


In expression (3.6) the integration cannot be completely
fulfilled. If we designate

$$2\int_{\zeta}^{\zeta+1} p^{-s}\, e^{-i s\tau}\, d\tau = J, \quad p = e^{-2s},\qquad (3.16)$$

radiation pattern for the antenna with the exponential amplitude
distribution can be represented in the following form:

$$\Phi_{\perp,s}(t) = \frac{\kappa L}{\left(\frac{v}{\pi}\right)^2 + 4s^2}\left\{ i\left(\frac{v}{\pi} + 2s\right)\times\right.$$

$$\times\left[e^{i\frac{v}{\pi}(\zeta+1)} - e^{-2s - i\frac{v}{\pi}\zeta}\right] + \left[\left(\frac{v}{\pi} + 2s\right) + \right.$$

$$\left. + i\left(\frac{v}{\pi} - 2s\right)\right]\left[F_1(t\sqrt{2(\zeta+1)}) - \right.$$

$$- e^{-2s - i\frac{v}{\pi}\zeta} F_1(t\sqrt{2\zeta})\right] - \left[\left(\frac{v}{\pi} + 2s\right) + \right.$$

$$\left. + i\left(\frac{v}{\pi} - 2s\right)\right]\cdot\frac{e^{-2s(\zeta+1)}}{\sqrt{2}}\, tJ\right\}.\qquad (3.17)$$

The radiation patterns $\Phi^0_{\parallel,\perp}(t_0)$ of the narrow single slots,
parallel to the edge/fin of screen, take the following form:

$$\Phi^0_{\perp}(t_0) = \left[1 + \sqrt{2}\, e^{-i\frac{\pi}{4}} F_1(t_0\sqrt{2})\right] e^{-i\pi t_0^2}.\quad (3.18)$$

$$\Phi^0_{\parallel}(t_0) = \cos\frac{v}{2}\left\{-i\pi t_0\left[1 + \sqrt{2}\, e^{-i\frac{\pi}{4}} F_1(t_0\sqrt{2})\right] + \right.$$

$$\left. + e^{i\pi\left(t_0 - \frac{1}{4}\right)}\right\} e^{-i\pi t_0^2},\qquad (3.19)$$

where

$$t_0 = 2\sqrt{\frac{r}{\lambda}}\sin\frac{\varphi}{2}.$$

Page 61.

AD-A118 960    FOREIGN TECHNOLOGY DIV WRIGHT-PATTERSON AFB OH
               THEORY OF THE RADIATION OF SURFACE ANTENNAS,(U)
               AUG 82   L N ZAKHAR'YEV, A A LEMANSKIY
UNCLASSIFIED   FTD-ID(RS)T-0361-82                                    F/G 9/5

                                                                     NL
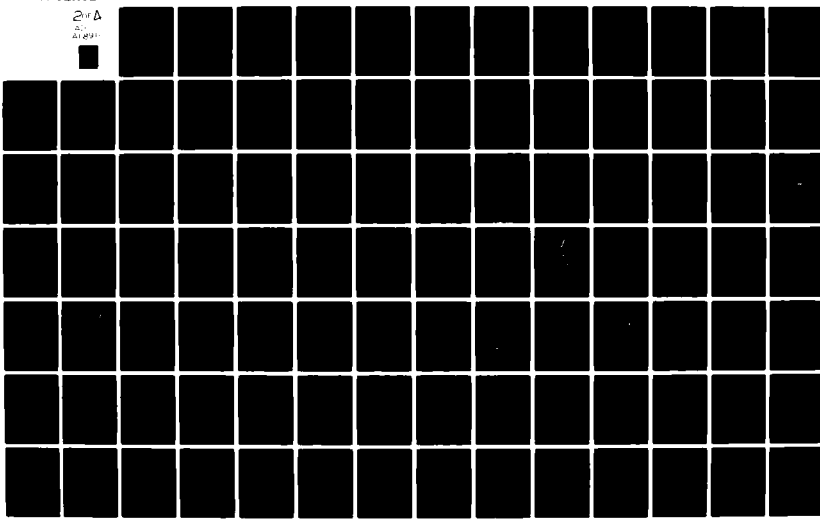
In the case of narrow slot factor $\cos\varphi/2$ in the expression for $\Phi_{\parallel}^0$ plays the significant role in view of the weak directivity of the radiation/emission of slot, and therefore radiation pattern $\Phi_{\parallel}^0(t_\bullet)$ cannot be expressed only through the universal parameter $t_\bullet$.. -

## 3.2. Approximate method of calculating the antenna radiation pattern, which is located on the half-plane.

Together with precise relationships/ratios, which describe the antenna radiation patterns, that are located on the half-plane, can be obtained the approximation formulas, convenient for the practical calculations. Let us show this based on the example of antenna with the perpendicular polarization. Let us examine range of values t, close to t=0, where is approximately correct the relationship/ratio

$$F_1^-(t\sqrt{2\bar{x}}) \simeq t\sqrt{2\bar{x}}. \qquad (3.20)$$

Then radiation pattern (3.5) can be represented by the relationship/ratio

$$\Phi_{\perp, q} \simeq f(q, \sigma, t) + 2t\, e^{-i\frac{\bullet}{4}} \times$$

$$\times \int_{\zeta}^{\zeta+1} \sqrt{\xi}\, A(\xi)\, e^{-i\pi(\sigma+\pi)\xi}\, d\xi, \qquad (3.21)$$

where

$$f(q, \sigma, t) = \int_{\zeta}^{\zeta+1} A(\xi)\, e^{-i\pi(\sigma+\pi)\xi}\, d\xi \qquad (3.22)$$

- antenna radiation pattern in the free space.

Comparing function (3.22) with integral (3.21), it is possible to note that these diagrams are characterized by only factor $\sqrt{\xi}$ in the amplitude distribution.

Page 62.

It is at the same time known that the amplitude distribution affects the antenna radiation pattern more weakly than phase. Taking into account that factor $\sqrt{\xi}$ in the interval $\zeta < \xi < \zeta + 1$ is changed weakly and this change noticeably decreases with the increase/growth $\zeta$, it is possible to consider approximately that

$$\sqrt{\xi} \approx \sqrt{\xi_{cp}} = \sqrt{\zeta + \frac{1}{2}}. \qquad (3.23)$$

Taking into account the aforesaid, we convert formula (3.21) to the following form:

$$\Phi_{\perp, q} = f(q, \sigma, t)\left(1 + \sqrt{2}e^{-i\frac{\pi}{4}}t\sqrt{2\left(\zeta + \frac{1}{2}\right)}\right) \approx$$

$$\approx \left[1 + \sqrt{2}e^{-i\frac{\pi}{4}}F_1\left(t\sqrt{2\left(\zeta + \frac{1}{2}\right)}\right)\right]f(q, \sigma, t). \quad (3.24)$$

Thus, the antenna radiation pattern of the traveling wave, arranged/located on the half-plane, can be approximately represented as the product of the antenna radiation pattern in the free space to the radiation pattern of slot on the half-plane, placed in antenna aperture. Analogous confirmation is correct for the antennas with the

parallel polarization of the exciting field:

$$\Phi_{\parallel.q} \simeq f(q,\ \sigma,\ t) \cdot \Phi_{\parallel}^{0}(t_0,\ \varphi). \qquad (3.25)$$

Approximations (3.24), (3.25) are obtained under the assumption of
the smallness of parameter t both for the region of light/world and
for the shadow zone. As is shown calculation, the field of
application of the obtained relationships/ratios is considerably
wider. In Fig. 3.2 is conducted the comparison of the radiation
patterns

$$P_{\perp} = |\Phi_{\perp}(t)/\Phi_{\perp\ max}(t)|^2,$$

of calculated by precise and approximation formulas for L=5$\lambda$, $\sigma$=0,
q=0 and $\zeta$=0; 0.3. From the figure one can see that with $\zeta$=0 the
difference between the diagrams is noticeable, but already with $\zeta$=0.3
curves barely differ from each other. For the amplitude distribution
collapsible/dropped to the edges of antenna the coincidence
noticeably is improved.

Page 63.


The obtained approximation formulas allow rap.dly and with a
good accuracy to design the antenna radiation patterns of the
traveling wave, arranged/located on the half-plane. Furthermore,
these formulas make more demonstrative the character of the effect of
the edge of flat/plane screen on the radiation pattern of surface
antenna.


3.3. Antenna radiation pattern, arranged/located on the half-plane.


According to precise formulas (3.12), (3.13) and (3.17) in the
electronic computer were designed the radiation patterns of surface
antennas for the different values of the parameters $\sigma$ and $\zeta$, which
lie within the limits

$$0 < \zeta < 2,$$
$$-2 < \sigma < 2.$$

Calculations were performed for two symmetrical amplitude
distributions - uniform to (q=0) and collapsing to the edges of
antenna to 10o/o according to power (q=0.52), and also for the
exponential distribution with

$$0 < s < 1, 2.$$

We will examine the standardized/normalized radiation patterns according to the power, designed depending on the universal parameter t (3.9). The examination of diagrams depending on t will make it possible to utilize results calculations for the antennas of any length.
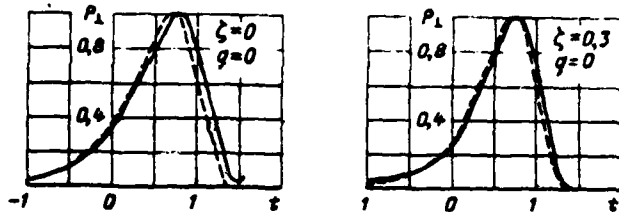
Fig. 3.2. Comparison of the radiation patterns, designed by the approximate (dotted curves) and strict (solid curves) methods.


Page 64.


Nevertheless we will assume that

$$L \geqslant 2\lambda,$$

$$\sigma \geqslant -2$$

(3.26)

so that in the limits of the major lobe/lug of radiation pattern it would be possible to assume

$$t \approx \varphi \sqrt{\frac{L}{\lambda}}.$$

This simplification makes it possible to introduce the concepts of the universal width of the radiation pattern ($\Delta t$) and universal directive gain (K), which with satisfaction of conditions (3.26) are connected with the true values of angular width and derictive gain with the relationships/ratios:

$$\Delta \varphi = \frac{\Delta t}{\sqrt{L/\lambda}},$$

(3.27)

$$K_{\varphi_i} = \sqrt{L/\lambda} K.$$

(3.28)


Let us first examine the general character of the antenna

radiation patterns, arranged/located on the edge of half-plane, and in the following paragraphs in more detail let us pause at the fundamental parameters, which characterize directivity of antenna (directive gain, the width of diagram, the direction of principal maximum).

The antenna radiation patterns of the traveling wave, arranged/located on the metallic half-plane near its edge, have a series/row of characteristic features, which depend on the parameters $\sigma$ and $\zeta$ (Fig. 3.3 and 3.4). The effect of the relative removal/distance of antenna from the edge/fin $\zeta$ we investigate with $\sigma=0$. General/common/total for the diagrams, shown in Fig. 3.3 and 3.4, is the divergence of the principal maximum of radiation/emission from the axis of antenna and the monotone drop of diagram in the shadow zone.

For the perpendicular polarization (Fig. 3.3) is characteristic sufficiently high radiation level in the direction of the axis of antenna (t=0)whose value slowly decreases with the increase/growth $\zeta$ and it approaches value 0.178 from the maximum. Slope of radiation pattern, nearest to t=0, always flat.

Page 65.

The slope of major lobe of diagram with $t > t_{max}$ the steeper/more abrupt and with $\zeta > 1$ at it appear the oscillations, caused by the effect of the edge of half-plane. Should be noted higher side-lobe level in the antennas, arranged/located on the half-plane, in comparison with the same antennas, arranged/located in the free space or on the infinite plane. So usually it is when the maximum of the "factor of grating" (i.e. the antenna radiation pattern in the free space) does not coincide with the maximum of the radiation pattern of elementary source (i.e. slot on the half-plane). True, in our case there is a grating of different emitters, since their diagram depends from the distance to the edge of half-plane, but this does not change the physical content of phenomenon. During the removal/distance of antenna from the edge of screen the maximum of radiation pattern approaches an axis of antenna ($t = 0$), the width of diagram decreases, and the level of lobes/lugs falls. The form of amplitude distribution affects in essence the side-lobe level and the width of radiation pattern.
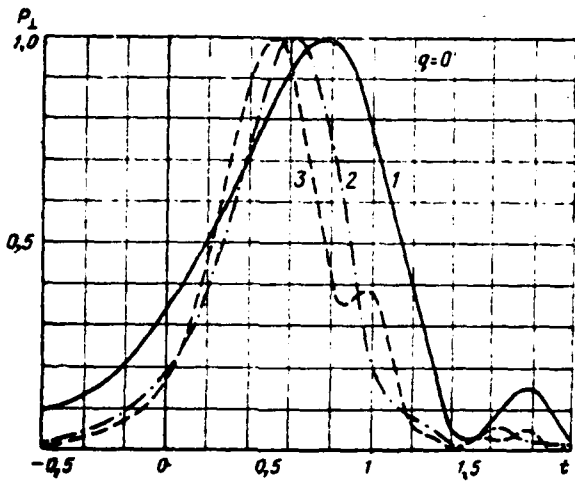
Fig. 3.3. Dependence of the form of radiation pattern on the parameter ς (perpendicular polarization) at q=0; σ=0: 1) ς=0; 2) ς=1; 3) ς=2.


Page 66.


The antenna radiation patterns with the parallel polarization (Fig. 3.4) differ from the case examined in terms of lower radiation level along the axis of antenna, moreover this level vanishes with ς→∞. With an increase in value ς major lobe always remains flat (in contrast to the case of perpendicular polarization), which is directly connected with the form of the radiation pattern of single slot, which is located on the half-plane. The side-lobe level of diagram during the parallel polarization is always higher than for

the perpendicular. Furthermore, in the antennas with the perpendicular polarization with a change in the parameter $\zeta$ is changed in essence the slope of diagram when $t > t_{max}$, and in the antennas with the parallel polarization when $t < t_{max}$.

Let us examine now, assuming/setting $\zeta = 0$, the dependence of the form of radiation pattern on the phase distribution along the antenna, characterized by the parameter $\sigma$ (Fig. 3.5 and 3.6). With $\sigma = 0$ phase wave velocity, which excites antenna, is equal to the speed of light.
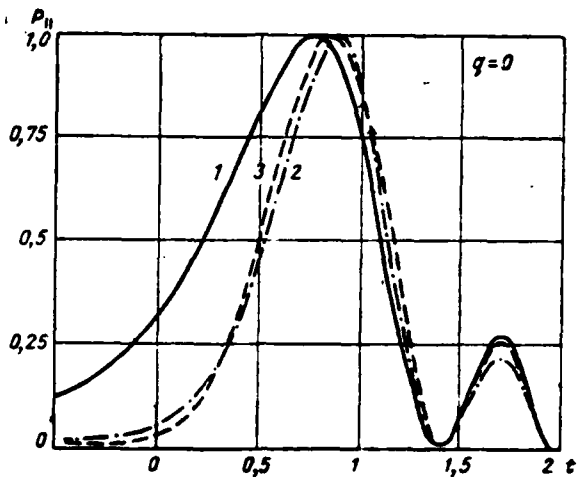
Fig. 3.4. Dependence of the form of radiation pattern on the parameter $\zeta$ (parallel polarization) at q=0; $\sigma$=0: 1)$\zeta$=0; 2) $\zeta$=1; 3) $\zeta$=2.

Page 67.

With $\sigma$=+-1 supplementary phase change along the antenna is equal to +-$\pi$. With an increase in value $\sigma$ the maximum of radiation pattern approaches an axis of antenna (t=0), grow/rise minor lobes. During the parallel polarization minor lobes grow/rise more strongly than with the perpendicular; for the uniform amplitude distribution their level is higher than for that collapsing. The characteristic features of the antenna radiation patterns of the traveling wave, arranged/located on the half-plane, are retained also in the presence

of attenuation along the antenna. Let us examine Fig. 3.7a, in which

for two values of parameter s are constructed the radiation patterns

at the different values $\sigma$ and $\zeta=0$. As in the case of even

distribution, with an increase in phase change along the aperture the

maximum of diagram approaches an axis of antenna, however, beginning

from certain values $\sigma>0$, maximum gradually it differs from axis, in

this case the level of lobes/lugs does not exceed 35o/o.
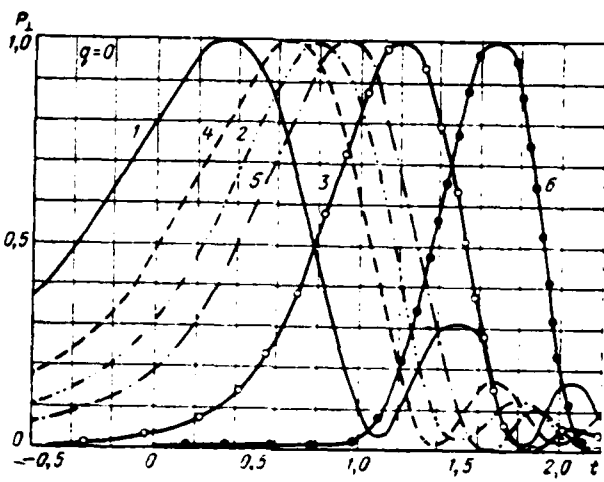
Fig. 3.5. Dependence of the form of the antenna radiation pattern on the phase distribution (perpendicular polarization) with q=0; $\varsigma$=0: 1) $\sigma$=1.2; 2) $\sigma$=0; 3) $\sigma$=-1.36; 4) $\sigma$=0.4; 5) $\sigma$=-0.49; 6) $\sigma$=-2.66.

Page 68.

With s=0 with an increase $\sigma$ the side-lobe level increases very rapidly and with $\sigma$=1.5 it reaches 100o/o, and the position of the maximum of diagram with $\sigma$=1.5 is changed abruptly. Let us note also that the effect of the parameter $\sigma$ on the radiation pattern decreases with an increase in value s. This becomes especially noticeable for large s, when the part of the antenna is excited with a small amplitude.

In Fig. 3.7b for two phase distributions ($\sigma=0$ and $\sigma=1$) are constructed the diagrams of antenna with different amplitude distributions. For $\sigma=0$ the dependence of the form of radiation pattern on s is sufficiently weak. Apparently, this is connected with the fact that the section of antenna, close to the edge/fin of the half-plane where the amplitude of electric field is small, it is located into the radiation field of the remaining sections of antenna and is strongly excited; moreover with the phase, which corresponds $\sigma=0$. The strong amplitude reduction at the end/lead of the antenna is equivalent to some degree to its shortening and, therefore, must lead to the expansion of radiation pattern (for the antenna in the free space radiation pattern with increase of s actually/really it is expanded).
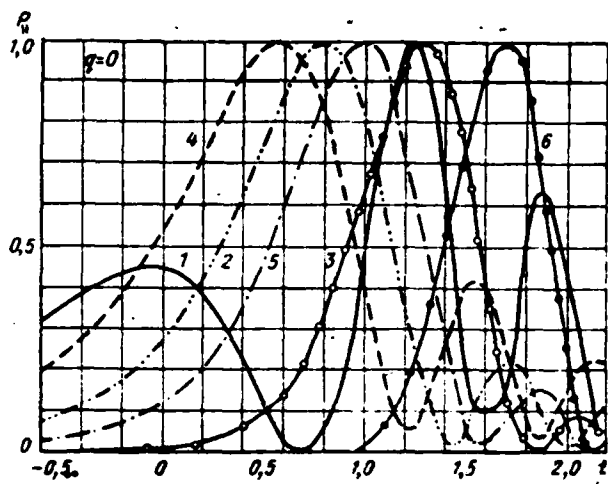
Fig. 3.6. Dependence of the form of the antenna radiation pattern on the phase distribution (parallel polarization) with q=0; $\zeta$=0: 1) $\sigma$=1.2; 2) $\sigma$=0; 3) $\sigma$=-1.36; 4) $\sigma$=0.4; 5) $\sigma$=-0.48; 6) $\sigma$=-2.66.

Page 69.

Together with this the antenna seemingly is driven out from the edge/fin, which affects the width of radiation pattern oppositely. As are shown to Fig. 3.7b, the width of radiation pattern decreases, i.e., predominant proves to be the action of the equivalent removal/distance of antenna from the edge/fin.
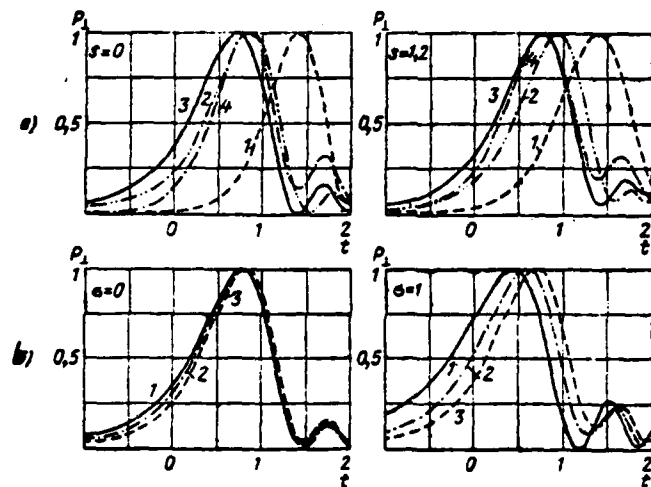
Fig. 3.7. The dependence of the antenna radiation pattern with exponential field distribution in aperture ($\varsigma=0$) on the parameter $\sigma$ and parameter s: a) 1-$\sigma=-2$; 2 - $\sigma=-0.3$; 3 - $\sigma=0.3$; 4 - $\sigma-2$; b) 1 - s=0; 2 - s=0.6; 3 - s=1.2.

## 3.4. Divergence of maximum of radiation pattern from the axis of antenna.

Traveling-wave antennas are utilized for the creation of intense radiation/emission in the axial direction t=0. However, if this antenna is located near the edge of flat/plane metallic surface, the maximum of radiation pattern is always deflected from the axis of antenna to certain angle. Therefore the study of the dependence of the position of the principal maximum of radiation pattern on the

parameters of antenna has great practical value.

Page 70.

The direction of maximum antenna radiation is determined by the value of parameter $t_m$, which is connected with the angular deflection by the relationship/ratio

$$t_m = 2\sqrt{\frac{L}{\lambda}}\sin\frac{\varphi_m}{2}. \qquad (3.29)$$

In Fig. 3.8 are plotted the lines of level

$$t_m = \text{const}$$

on the plane $\sigma$, $\zeta$ for two symmetrical amplitude distributions ($q=0$, $q=0.52$) and two polarizations. Numerals on lines $t_m = \text{const}$ designate value $t_m$.

Let us examine first perpendicular polarization. Fig. 3.8 shows that the divergence of the maximum of the radiation pattern weakly depends on amplitude distribution in antenna aperture, since the position of maximum is determined in essence by phase distribution of field in the aperture. With an increase in phase change along the antenna the ray/beam approaches an axis. For small ones $\zeta$ the position of maximum of diagram is changed smoothly with the change $\sigma$; for $\zeta > 1/2$ at certain value of $\sigma_*(\zeta) > 0$ it occurs an abrupt change in the position of the maximum.
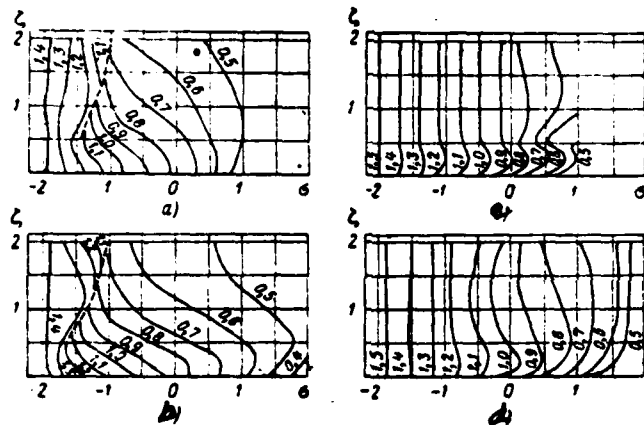
Fig. 3.8. Lines of constant value $t_m$ on the plane $\sigma$, $\zeta$;

a) $E_\perp$, $q=0$; b) $E_\perp$; $q=0.52$; c) $E_\parallel$, $q=0$; d) $E_\parallel$; $q=0.52$.

Page 71.

For $\sigma<\sigma_e$ the direction of the maximum of diagram is determined, mainly, by its own diagram of antenna (on the infinite plane). Along other side of line of discontinuity $\sigma>\sigma_e$ the principal maximum of radiation/emission is formed/shaped under the strong influence of the edge of the screen. In the region, which is adjacent to the line of discontinuity $\sigma=\sigma_e(\zeta)$, the radiation pattern has two maximums. This case of the appearance of two maximums should be differed from that, when the second maximum appears as a result of the strongly increased minor lobe with $\sigma\approx1.5$. The effect of the parameter $\zeta$ begins to be manifested with $\sigma>-2$. For smaller $\sigma$ the effect of the edge of screen is very insignificant, and therefore with $\sigma\leqslant-2$ it is possible to

design the antenna radiation patterns, considering it their arranged/located on the infinite plane. If we exclude the region of disruption $l_m$, and also the region of small ones $\varsigma$ with $\sigma > 0$, it is possible to assert that with the removal/distance of antenna from the edge/fin the maximum of diagram it approaches an axis of antenna. In the region of small ones $\varsigma$ and $\sigma > 0$ the direction of the maximum of radiation pattern very insignificantly depends on $\varsigma$.

For the parallel polarization the effect of the edge of screen is manifested considerably weaker considering that during this polarization even in the case of the infinite plane of maximum of radiation pattern it is deflected from the axis of antenna. The effect of the parameter $\varsigma$ on the position of principal maximum substantially is manifested with $\sigma > -1$ and only for small ones $\varsigma$; dependence $l_m$ on $\sigma$ approximately the same, as in the case of infinite plane.

The position of the maximum of radiation pattern for the antennas with exponential field distribution in the aperture weakly depends on parameter s, as this follows from the examination of Fig. 3.9, during which are given the lines of level $l_m = \text{const}$ on plane s, $\sigma$ with $\varsigma = 0$. For $\sigma < 0.5$ the level line they go virtually in parallel, slightly diverging with an increase s. This disagreement is caused by the fact that for the antennas with the strong drop of amplitude

operating supplementary phase change is less than during the even
distribution. For small s with $\sigma \approx 1,5$ the position of maximum is
changed by jump. This occurs at the point where the first minor lobe
of diagram becomes equal to fundamental. With s>0.4 minor lobe does
not reach the value of basis and the position of the maximum changes
continuously.

Page 72.

It should be noted that with the assigned drop of the amplitude of
field in antenna s there is certain limiting value $f'_m$ being
determining the minimally attainable angle of pressing the maximum of
radiation pattern against the axis of antenna. The effect of the
parameter $\varsigma$ on the position of the principal maximum of antenna
radiation with exponential field distribution is insignificant.
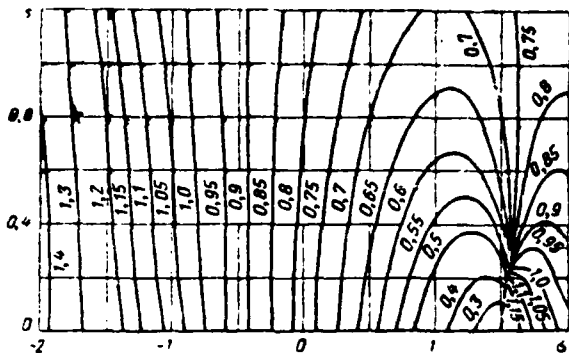
Fig. 3.9. Lines of constant value $t_m$ on the plane $\sigma$, s, $(\zeta=0)$.

## 3.5. Width of radiation pattern.

We examine the radiation patterns, designed depending on the universal parameter $t$ (3.9). Therefore, if the standardized/normalized radiation patterns according to power p=0.5 with $t=t_1$, $t_2$, then the width of diagram at the level of half power for the perpendicular and parallel polarization is equal to

$$\Delta\varphi = 2\arcsin\frac{t_2}{2\sqrt{\frac{L}{\lambda}}} - 2\arcsin\frac{t_1}{2\sqrt{\frac{L}{\lambda}}}. \quad (3.30)$$

For the precision determination of values $\Delta\varphi$ it is necessary to have the detailed data about values of $t_1$ and $t_2$. However, with satisfaction of conditions (3.26) it is possible to be bridged with one value - the universal width of radiation pattern $\Delta t$ (3.27).

Page 73.

Fig. 3.10 shows the lines of level Δt=const on the plane of the parameters σ, ζ for two symmetrical amplitude distributions (q=0 and 0.52) and two polarizations. Numerals in the curves designate value Δt.

Let us examine the first perpendicular polarization (Fig. 3.10a, b). At the negative values σ(σ≤-2) high in the absolute value value Δt barely depends on ζ. This means that the diagram is so deflected from the axis that fringe effect of screen virtually is not manifested. For the positive values σ of the level line they go almost in parallel to the axis of abscissas with the small positive inclination/slope, which corresponds to the slow expansion of diagram with an increase in phase change along the antenna. This is in apparent contradiction with the results, given in Chapter 2 for traveling-wave antennas in the free space, whose supplementary phase change leads to the contraction of radiation pattern. The physical sense of this phenomenon becomes clear, if we examine approximation (3.24) for the radiation pattern.

At the positive values σ the width of radiation pattern strongly depends on the removal/distance of antenna on the edge monotonically decreasing to a definite limit with the increase/growth ζ.
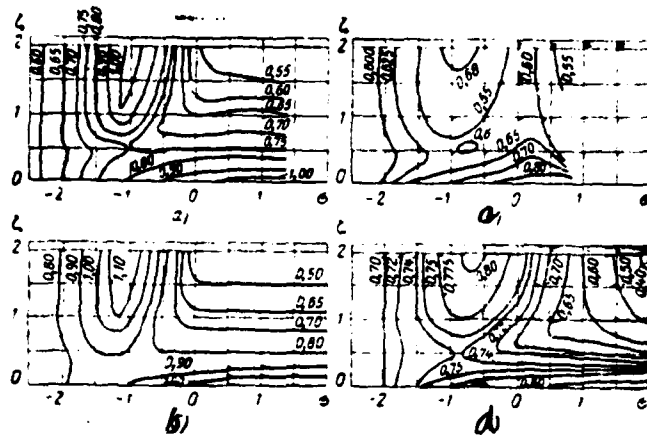
Fig. 3.10. Lines of fixed level Δt=const on the plane of the parameters σ, ζ:

a) $E_\perp$, $q = 0$; b) $E_\perp$, $q = 0.52$; в) $E_{\|}$, $q = 0$; d) $E_{\|}$, $q = 0.52$.

Page 74.

It should be noted that on the infinite plane the antenna σ=0 has a width of diagram approximately the same as the antenna, arranged/located on the half-plane with σ=ζ=0. The region of negative ones σ from 0 to -1.5 is transient from the lines, parallel to the axis of abscissas (with σ>0), to the lines, parallel to the axis of ordinates (with σ<-2). The level lines in this region have complicated character. Comparing graphs for different amplitude distributions, it is possible to ascertain that the shape of the curve Δt=const is similar, but numerical values noticeably depend on parameter q. With q=0 the width of radiation pattern always somewhat

less. For the uniform amplitude distribution the curves are
constructed only to $\sigma=1.2$, since approximately at this value of the
parameter $\sigma$ the minor lobe of diagram becomes more than basis and the
concept of the width of radiation pattern becomes meaningless.

Let us examine briefly the case of parallel polarization. On the
graphs/curves Fig. 3.10a, b, c, d it is not difficult to note the
considerable difference between the lines $\Delta t=$const for the
perpendicular and parallel polarizations. Dependence $\Delta t$, from $\sigma$, $\zeta$
during the parallel polarization proves to be weaker, especially this
is noticeable for the uniform amplitude distribution. With $\sigma>0$ the
line of level $\Delta t=$const during the parallel polarization no longer
they are parallel to axis $\sigma$. On the contrary, for $\zeta>1$ them more often
it is possible to consider parallel to axis $\zeta$. This means that during
the parallel polarization the approximation/approach to an infinite
plane begins much earlier (with $\zeta \gtrsim 1$), man with the perpendicular.
At the same time curves $\Delta t=$const, shown in Fig. 3.10, have certain
resemblance, especially in the transition region where $0>\sigma>-0.5$. In
contrast to the perpendicular, for the parallel polarization the
width of radiation pattern with the increase/growth $\zeta$ with $\sigma>0$ first
decreases, and then it begins to grow/rise. In Fig. 3.11 and 3.12 are
constructed the lines of level $\Delta t=$const on plane s, $\sigma$ for the
antennas with the exponential amplitude distribution with $\zeta=0$ and
0.5. Let us examine the first first case. The decrease of phase wave

velocity, which excites antenna, leads to the monotone expansion of diagram everywhere, with exception of region $\sigma>1.3$. With $s<0.6$ and $\sigma=1.3$ (in the shaded region) the concept of the width of radiation pattern becomes meaningless because of the fact that the minor lobe exceeds level $0.5p_{max}$.

Page 75.

The effect of amplitude distribution on the width of radiation pattern is manifested differently depending on the value of phase change $\sigma$. With $\sigma<-0.6$ an increase in parameter $s$ leads to the expansion of radiation pattern, while at higher values of $\sigma$ the reduction of amplitude (up to $s=1.2$).
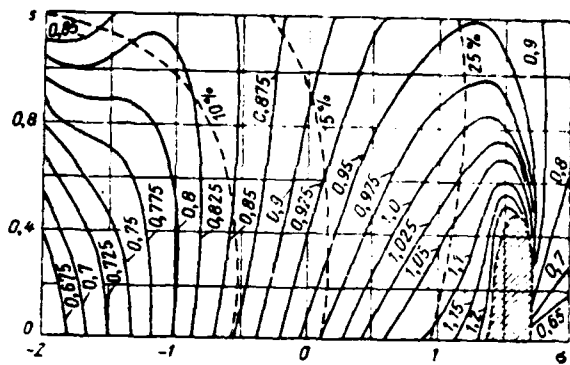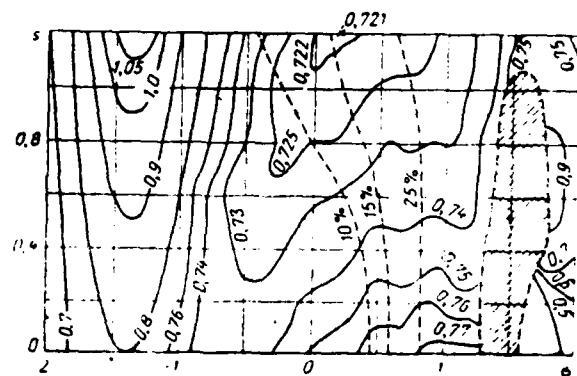
Fig. 3.11.                              Fig. 3.12.

Fig. 3.11. Lines of fixed level Δt=const on plane of parameters σ, s (ζ=0). Dotted line plotted/applied the level of the first minor lobe.

Fig. 3.12. Lines of fixed level Δt=const on plane of parameters σ, s(ζ=0.5).      Dotted line plotted/applied the level of the first minor lobe.

Page 76.

This makes it possible to utilize in the antennas the energetically advantageous collapsible/dropped distributions. Removal/distance of antenna from the edge/fin gives, as is shown Fig. 3.11 and 3.12, noticeable contraction of radiation pattern. The character of curves Δt=const with ζ=0 and ζ=0.5 is substantially various. In the interval

-0.8≤σ≤1 the width of radiation pattern for ζ=0.5 changes insignificantly.

In Fig. 3.11 and 3.12, besides the lines of the constant values of the width of radiation pattern, are constructed with dotted line the lines of level of the first minor lobe. It is known that the antennas with the exponential amplitude distribution even in the free space have large minor lobes. During the placement of antenna on the half-plane the level of lobes/lugs, as a rule, increases. Therefore antennas with the exponential amplitude distribution can be used only for the not too stringent requirements for the side-lobe level.

3.6. Directive gain.

with respect to

If the standardized/normalized radiation pattern $\wedge$ power is described by function p(t) and parameter t is connected with the angle φ with relationship/ratio (3.9) it is possible to introduce the integral characteristic of the diagram

$$K_i^r(t_o) = \frac{2\pi p(t_o)}{\int\limits_{-t_i}^{t_i} p(t)\, dt},\qquad (3.31)$$

which is universal directive gain. Value $t_o$ characterizes the direction in which it is examined by directive gain, and integration limits in (3.31) are selected sufficiently large[1].

FOOTNOTE [1]. During calculations $t_1$ it took as the equal to 3.2.
ENDFOOTNOTE.


The directive gain, by specific relationship (3.31), characterizes
the directed properties of antenna in plane $xy$ (Fig. 3.1) and with
satisfaction of conditions (3.26) is connected with the usual
directive gain with relationship/ratio (3.28).


Page 77.


Let us examine the directive gain of antenna, which is located
on the half-plane, in the direction of the maximum of
radiation/emission $K(t_m)$, and in the axial direction $K(0)$. For the
antennas with exponential amplitude distribution of field in the
aperture we will examine also the value of the amplification [see
formulas (2.21) and (2.31)].


Directive gains in the direction of maximum.


In Fig. 3.13 on the plane of the parameters $\sigma$, $\zeta$ are constructed
the lines of level

$$K(t_m) = \text{const}$$

for both of polarizations and two symmetrical amplitude
distributions, which correspond $q=0$ and $q=0.52$. During the

perpendicular polarization the curves resemble the appropriate curves
for the width of radiation pattern. It is distinctly evident that the
directive gain gradually falls from an increase in the phase change
along the antenna (with $\sigma>0$). This is a characteristic difference in
the antennas, arranged/located on the half-plane, from the antennas
in the free space or on the infinite plane. It is interesting to
compare values $K(t_m)$ for that collapsing and uniform amplitude
distributions.
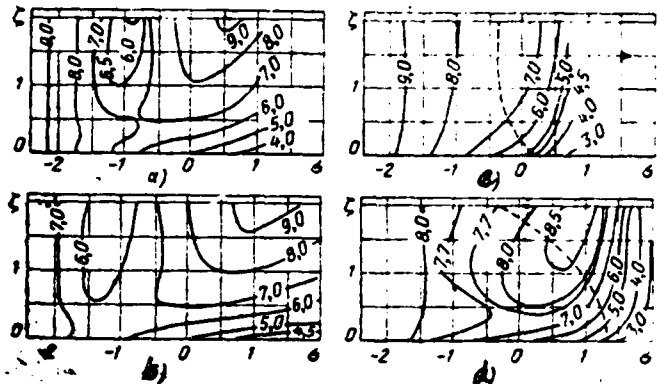
Fig. 3.13. Lines $K(t_m) = \text{const}$ on the plane of the parameters $\sigma$, $\zeta$:

a) $E_\perp$. $q = 0$; b) $E_\perp$. $q = 0.52$; c) $E_\parallel$. $q = 0$; d) $E_\parallel$. $q = 0.52$.

Page 78.

For the negative $\sigma$, when fringe effect of screen is weaker, directive gain during the even distribution are more. However, that, where the effect of the edge of half-plane is manifested more strongly (with $\sigma > 0$), derictive gain are more in antenna with the collapsible/dropped distribution. During the parallel polarization the advantage of the collapsible/dropped distribution is still more noticeable. For this distribution the character of dependence $K(t_m)$ on $\sigma$ and $\zeta$ remains the same as during the perpendicular polarization, the difference consists only of the sharper decrease of directive gain with the increase/growth $\sigma$ with $\sigma > 0$.
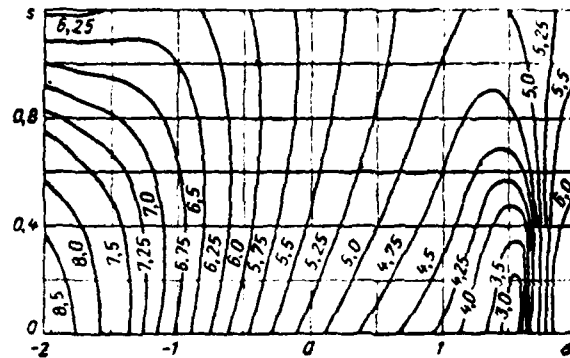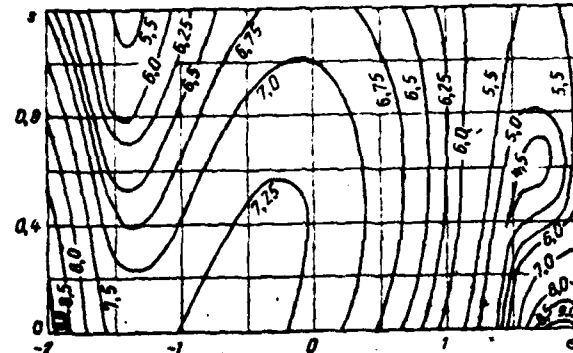
Fig. 3.14.                              Fig. 3.15.

Fig. 3.14. Lines $K(t_m) = \text{const}$ on plane of parameters $\sigma$, s ($\zeta = 0$).

Fig. 3.15. Lines $K(t_m) = \text{const}$ on plane of parameters $\sigma$, s ($\zeta = 0.5$).

Page 79.

Each of Fig. 3.13c, d is divided by dotted line into two parts. To the left of this line directive gain of antenna with the parallel polarization it is more than with the perpendicular, to the right — it is less. In the case of the collapsible/dropped distribution this line considerably is displaced into the region of the positive values of the parameter $\sigma$.

In Fig. 3.14 and 3.15 are plotted the lines of level $K(t_m) = \text{const}$

←—on the plane $\sigma$, s for the antennas with exponential field
distribution in the aperture with $\zeta=0$; 0.5. analogous curves (Fig.
3.16 and 3.17) are constructed for the factor of amplification $G(t_m)$.
Dependences K and G on the amplitude distribution strongly differ
from each other. Value K weakly depends on s, moreover with $\sigma<-1$ and
$\zeta=0$, when the effect of edge/fin is small, an increase in parameter s
leads to the decrease of directive gain. On the contrary, with the
strong effect of edge/fin ($\sigma>-1$) it is profitable to utilize the
collapsible/dropped distribution. With $\zeta=0.5$ (Fig. 3.17) to
accurately indicate this boundary ($\sigma=-1$ with $\zeta=0$) is impossible; the
advantage of the collapsible/dropped distributions becomes noticeable
only in the region of positive values $\sigma$.

Let us examine now the dependence of amplification G on
parameter s. It is obvious that the greater the drop of amplitude,
the more completely is utilized the power applied to the antenna and
the less part of it goes into the load.
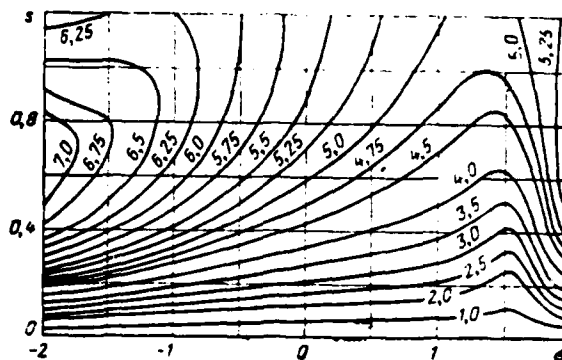
Fig. 3.16. Lines of constant value $G(t_m) = \mathrm{const}$ on the plane of the parameters $\sigma$, $s$ ($\zeta = 0$).


Page 80.


On the other hand, at sufficiently high values of s the directed properties of antenna noticeably deteriorate as a result of the decrease of its effective length. Therefore must exist the optimum value s, at which the antenna gain is maximal. With $\zeta = 0$ (Fig. 3.16) this optimum is noticeable only for $\sigma < -0.6$. At the high values of supplementary phase change $\sigma$ the optimum value s is located beyond the limits of the figure (s>1.2). This means that for obtaining the larger amplification it is profitable to utilize the strongly collapsible/dropped distributions. However, in practice to select s>1 is inexpedient, since the gain in amplification in this case is insignificant, and the series/row of other parameters of the antenna

are worsened. With $\varsigma=0.5$ the optimum value s pronounced for all
values $\sigma<1$ comprises $s_{opt}\approx0.9$, which corresponds to the distribution,
which collapses toward the end of the antenna to 3o/o according to
the power.
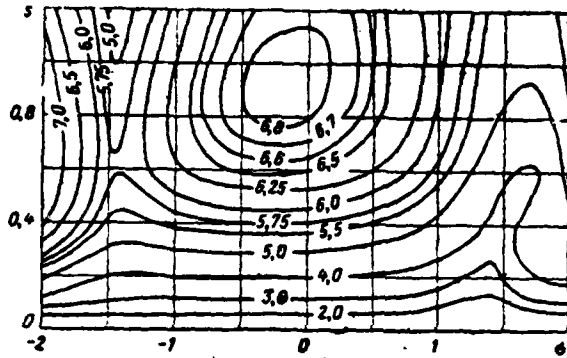
Fig. 3.17. Lines of constant value $G(t_m) = \text{const}$ on the plane of the parameters $\sigma$, s ($\zeta = 0.5$).

Directive gains in the direction of the axis of antenna.

In a number of cases it is necessary to ensure the largest possible signal level in the axial direction t=0. Since the maximum of radiation of the antenna, arranged/located on the half-plane, is deflected from the axis, it is of interest to determine, at what values of the parameters $\sigma$ and $\zeta$ the directive gain in the axial direction will be greatest.

Page 81.

For the perpendicular polarization the amplitude of the field, emitted in the axial direction t=0, during any amplitude-phase

distribution in antenna aperture does not depend on the parameter $\zeta$.
Of this it is not difficult to be convinced, assuming/setting in
expressions (3.5) and (3.6) t=0. At the same time, if amplitude-phase
distribution in antenna aperture is assigned, proves to be
fixed/recorded the *power*, emitted by antenna and, consequently, also
the directive gain (amplification) of antenna in the axial direction.
The dependence derictive gain on the phase change along the antenna
for two symmetrical amplitude field distributions in antenna aperture
they are shown in Fig. 3.18.
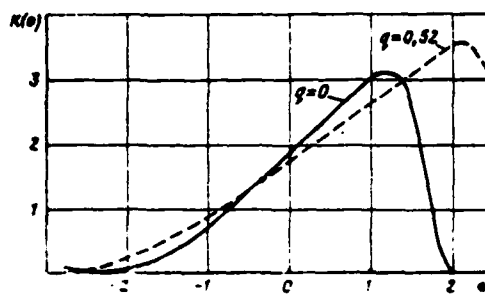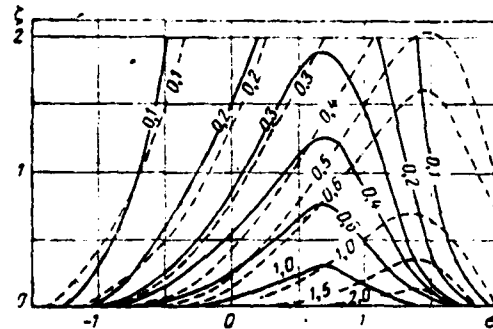
Fig. 3.18.



Fig. 3.19.

Fig. 3.18. Dependence of directive gain K(0) on phase change along antenna during perpendicular polarization.

Fig. 3.19. Lines K(0) =const on plane of parameters $\sigma$, $\zeta$ at parallel polarization; continuous - q=0; dotted line - q=0.52.

Page 82.

It is characteristic that the curve, which corresponds to even distribution, reaches maximum with $\sigma \approx 1.2$, and collapsing - with $\sigma \approx 2$. This is located in accordance with the results, led in Chapter 2. Thus, if directive gain in the direction of the maximum of radiation/emission falls from the increase/growth $\sigma$, then in the axial direction it increases and it reaches maximum at the specific value of this parameter.

In Fig. 3.19 on the plane of the parameters $\sigma$, $\varsigma$ are constructed the lines of level $K(0)$=const for the parallel polarization and two symmetrical field distributions. The numerals, plotted/applied to the curves, show that the directive gain in the axial direction for this polarization is very small, but also it increases with the increase/growth $\sigma$ and it reaches maximum with $\sigma \approx 0.7$ for q=0 and with $\sigma$=1.4 for q=0.52. From the increase/growth $\varsigma$ value $K(0)$, naturally, rapidly falls.

In Fig. 3.20 and 3.21 are constructed values $K(0)$=const and $G(0)$=const on the plane of the parameters $\sigma$ and s for the antennas with the exponential amplitude distribution. These curves are close in the character to the curves, which correspond by the surface of antennas, which is located on the plane (see S2.3). However, it should be noted that in S2.3 are examined the three-dimensional/space directive gains and antenna gain, connected with "flat/plane" relationships/ratios (2.25). As is shown calculation, directive gain $K(0)$ is maximum with s=0 and $\sigma$=1.2. During the removal/distance from this point in any direction on the plane $(\sigma, \sigma)$ directive gain $K(0)$ monotonically it decreases.
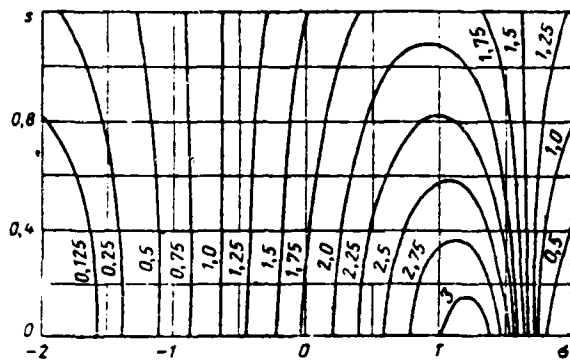
Fig. 3.20. Lines K(0)=const on the plane $\sigma$, s ($\zeta$=0).

Page 83.

With an increase in the drop of amplitude optimum phase change along the antenna somewhat decreases. Fig. 3.21 shows that the factor of amplification G(0) is maximum with s=0.6, $\sigma$=1.05. An increase in the drop of amplitude in comparison with the optimum leads to the insignificant decrease of G(0). During more uniform amplitude distributions amplification G(0) sharply decreases.
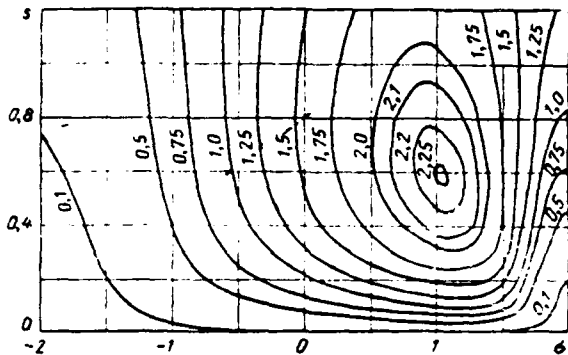
Fig. 3.21. Lines G(0)=const on the plane σ, s (ς=0).


4. Antenna radiation patterns, ██████████ located on the surface of key.


The radiation patterns of the arbitrary sources of field, which are located near the surface of key or it is direct on it, they can be designed with the aid of formulas (1.4) and (1.41)-(1.46). However, in the case in question calculation according to precise formulas is considerably more complicated than in the case of half-plane. In connection with this numerical calculations according to precise formulas were conducted in the limited space and they will be used in order on one hand, to trace based on specific example, as varies the radiation pattern of surface antenna with a change in the internal wedge angle from 0° to 180°, and on the other hand, to establish/install, when is possible the replacement of key by

half-plane during the calculation of the radiation pattern of the surface antenna.

Page 84.

4.1. Fundamental calculated relationships/ratios.

Let on the face $\varphi'=0$ (Fig. 4.1) the ideally conducting key up to distances $\Gamma$ from the edge/fin be arranged/located the antenna of length L. As in the preceding/previous chapter, we will describe amplitude-phase field distribution in antenna aperture by the function

$$a(x) = \left[1 - q\cos\frac{2\pi}{L}(x-\Gamma)\right]e^{-i\beta x}. \qquad (4.1)$$

After using expressions (1.41)-(1.46) together with (1.6), we will obtain the following expressions for the radiation patterns of the antenna in question:

during the parallel polarization

$$F_{\parallel}(\varphi, l, \zeta, \sigma, q, \alpha) =$$

$$= \int_0^1 \left\{ \exp[-i\pi(\sigma+2l)(x+\zeta)] \frac{1-q\cos 2\pi x}{x+\zeta} \times \right.$$

$$\left. \times \sum_{n=1}^{\infty} n \exp\left(-\frac{ln\pi^2}{2\alpha}\right) J_{\frac{n\pi}{\alpha}} [2\pi l(x+\zeta)] \sin\frac{n\pi}{\alpha}\varphi \right\} dx; \qquad (4.2)$$

during the perpendicular polarization

$$F_{\perp}(\varphi, l, \zeta, \sigma, q, \alpha) = \int_0^1 \left\{ \exp[-i\pi(\sigma+2l)(x+\zeta)] \times \right.$$

$$\times (1-q\cos 2\pi x) \sum_{n=0}^{\infty} \varepsilon_n \exp\left(-\frac{ln\pi^2}{2\alpha}\right) \times$$

$$\left. \times J_{\frac{n\pi}{\alpha}} [2\pi l(x+\zeta)] \cos\frac{n\pi}{\alpha}\varphi \right\} dx. \qquad (4.3)$$

Fig. 4.1. On the calculation of surface antenna, which is located on the key.

Page 85.

In expressions (4.2) and (4.3) are introduced the following designations:

l=L/λ - electrical length of antenna;

$\zeta = \dfrac{\Gamma}{L}$ - relative removal/distance of antenna from the edge of key;

$\sigma = \dfrac{l-\zeta}{\pi} L$ - supplementary phase change at the length of antenna, measured in the portions $\pi$.

According to formulas (4.2) and (4.3) can be designed the radiation patterns $F_{\parallel}(\varphi)$ and $F_{\perp}(\varphi)$ for any values of parameters 1, $\zeta$, $\sigma$, q, $\alpha$, which completely describe the character of excitation and the location of surface antenna.

4.2. Analysis of the results of the numerical calculation of radiation patterns.

With the aid of relationships/ratios (4.2) and (4.3) for both forms of polarization were designed the standardized/normalized radiation patterns according to the power

$$P(\varphi) = \left| \frac{F(\varphi)}{F(\varphi_m)} \right|^2$$

and the phase diagrams

$$\Phi(\varphi) = \arg F(\varphi)$$

of antenna, which is located on the key.

Page 86.


The calculation of radiation pattern is carried out for the interval of values $\varphi$, the including the main thing and first minor lobes, and also shadow zone $\pi \leqslant \varphi \leqslant \alpha$. Let us examine how depend radiation patterns $P(\varphi)$ on parameters $l$, $\zeta$, $\sigma$, q, $\alpha$.


In the expressions for the antenna radiation patterns, which is located on the half-plane, it is possible to introduce the parameter (see Chapter 3):

$$t = 2\sqrt{l}\sin\frac{\varphi}{2} \simeq \sqrt{l}\varphi,$$

thanks to which can be designed universal radiation pattern and is excluded parameter $l$. Knowing universal diagram, it is not difficult to calculate the radiation pattern, which corresponds to the concrete/specific/actual value $l$. The character universal with respect to $l$ of the antenna radiation patterns on the half-plane (and plane) is physically explained by the fact that the currents, induced by the field of antenna on the surface of screen, are located in one plane. In the case of the antenna, arranged/located on the key, does

not succeed in introducing the universal parameter in the expressions
for F($\varphi$). However, one should expect that in the specific sector of
the values of angle $\varphi(\varphi<\pi)$, where the effect of the current, which
flows in to the shadow face of key, is insignificant, diagrams F($\varphi$)
are universal relative to parameter $l$.
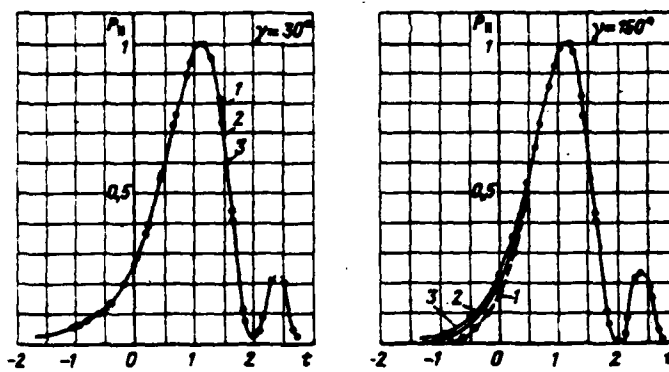


Fig. 4.2. Radiation patterns $p_{||}(t)$ at wedge angle of $\gamma=30°$ and $150°$:
1) $l=2$; 2) $l=5$; 3) $l=10$.


Page 87.


It is obvious that the boundaries of this sector depend on angle
$\gamma=2\pi-\alpha$ between the faces of key (Fig. 4.1), size/dimension and
removal/distance of antenna from the edge of key, and to a lesser
degree from the form of amplitude-phase distribution in antenna
aperture.

The antenna radiation pattern during the parallel polarization will be universal in considerably the wider sector than with the perpendicular in view of the less intense flowing in of current to the shadow face of key during the parallel polarization. The given considerations are confirmed by the results of calculation according to precise formulas. In Fig. 4.2 and 4.3 are constructed the antenna radiation patterns on the key. Diagrams P(t) correspond to the antennas, located near the edge/fin of key ($\zeta=0$) and excited by the wave, which is propagated with the speed of light ($\sigma=0$). At the wedge angle, equal to 30°, the radiation patterns $P_\perp(t)$ virtually coincide; calculation shows that at $\gamma=90°$ appears the small difference between the diagrams, which correspond to perpendicular polarization. In the case of the dull key ($\gamma=150°$ and more) this difference becomes more essential, moreover most considerably radiation patterns differ in the shadow zone where strongly is manifested the effect of the flowing in currents.
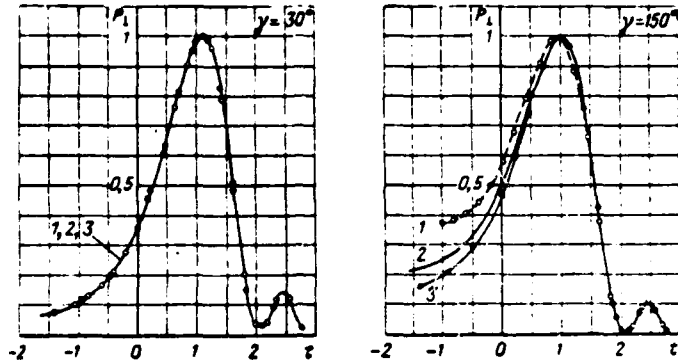
Fig. 4.3. Radiation patterns $P_\perp(t)$ at wedge angle of $\gamma$=30° and 150°:
1) $l$=2; 2) $l$=5; 3) $l$=10.

Page 88.

In illuminated region ($\varphi$<180°) the radiation patterns P(t) virtually coincide even at angle of $\gamma$=150°. In view of the fact that there is fundamental practical interest in the case of narrow wedge, and at $\gamma$<90° dependence of the antenna radiation pattern on its length carries trivial character, we will examine subsequently of the antenna of the fixed/recorded length $l$=5.

Antenna with this size/dimension possesses sufficient directivity so that calculation data, obtained for the infinite key, would be suitable for the real key of finite dimensions. At the same time the length of antenna l=5 is still sufficiently small, which

substantially facilitates calculation according to precise formulas
(4.2), (4.3). Finally, the effect of the shadow face of key on the
radiation pattern of surface antenna begins to be manifested at the
angles $\gamma$, larger, the greater is $l$, so that if for the antenna with a
length of $l=5$ proves to be possible during the practical calculations
key to replace with half-plane, this will be all the more correctly
for the antennas of great length.

In order to shorten calculation according to precise formulas
(4.2), (4.3) and to make its results demonstrative, let us conduct
the study of the dependence of the antenna radiation pattern of the
traveling wave on the apex angle of key as follows. Let us select as
the basic version the arranged/located at the edge of key ($\varsigma=0$)
antenna with a length of $l=5$ with uniform amplitude distribution
($q=0$), phase response, which corresponds $\sigma=0$ ($\beta=k$), and let us
examine how change the radiation patterns $P(\varphi)$ of this antenna for
both forms of polarization with a change in the wedge angle $\gamma$. Then,
changing alternately one of parameters $\varsigma$, $\sigma$, q and comparing these
versions with the basis, we will succeed in composing a comparatively
complete representation about the character of the dependence being
investigated. Fig. 4.4 shows the radiation patterns $P(\varphi)$ of the basic
version, designed for several values of wedge angle $\gamma$. The
examination of Fig. 4.4 shows that during the parallel polarization
the effect of wedge angle in sector of $130°\leqslant\varphi\leqslant210°$ becomes noticeable

only at $\gamma > 90°$. Further increase in the angle $\gamma$ leads to the fact that the level of diagram $P_{\parallel}(\varphi)$ in the shadow region decreases, approaching $P_{\parallel}(\pi) = 0$ with $\gamma = \pi$.

Page 89.

The maximum of diagram $P_{\parallel}(\varphi)$, its right slope and side lobes with the change $\gamma$ remain virtually without the changes. During the perpendicular polarization the effect of angle $\gamma$ on diagram $P_{\perp}(\varphi)$ in the sector of values $\varphi$ in question begins to be manifested already at $\gamma = 60°$, and with further increase/growth $\gamma$ grows/rises antenna radiation in the shadow zone, decreases the level of the first minor lobe, and entire/all diagram is displaced to the soy-bean of antenna, approaching its limiting value with $\gamma = \pi$.
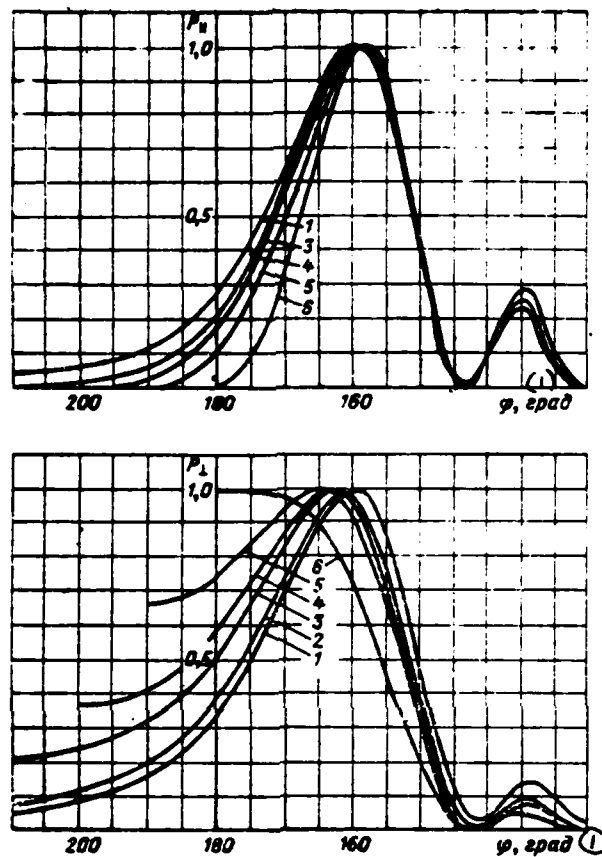
Fig. 4.4. Radiation patterns P($\varphi$) of basic version (l=5, $\zeta=\sigma-q=0$) with different ones $\gamma$: 1) $\gamma=0-30°$; 2) $\gamma=90°$; 3) $\gamma=150°$; 4) $\gamma=160°$; 5) $\gamma=170°$; 6) $\gamma=180°$.

Key: (1). deg.

Page 90.

Radiation pattern $P_{\parallel}(\varphi)$ in region $\varphi < \varphi_{m\parallel}$ ($\varphi_{m\parallel}$ — the direction of principal maximum) virtually is not changed with a change in the

angle $\gamma$ from $\gamma=0$ to $\gamma\simeq\pi$, since the maximum of the antenna radiation pattern, which is located on the plane, is deflected from the metallic surface, and therefore upon transfer from the plane to the half-plane edge affects in essence only the shadow slope of diagram $P_{\parallel}(\varphi)$. On the contrary, during the perpendicular polarization the maximum of radiation of antenna, which is located on the plane, with $\sigma\geqslant 0$ is directed along the metal, and therefore transition/junction from the plane to the half-plane $\pi\geqslant\gamma\geqslant 0$) leads to a substantial change in the entire radiation pattern $P_{\perp}(\varphi)$.

However, both in the case of parallel and in the case perpendicular polarization fundamental changes of the radiation pattern occur with a change of the wedge angle within limits of $150°\leqslant\gamma\leqslant 180°$. For $\gamma\leqslant 90°$ effect of the shadow face of key on the radiation pattern in the sector of the values of angle $\varphi$ in question is virtually unessential.

With an increase in the length of antenna the effect of wedge angle on the radiation pattern begins to be manifested at large values of $\gamma$ and, therefore, transition/junction from the diagram, which corresponds to radiation/emission from the half-plane, to the diagram of antenna, which is located on the plane, occurs more sharply, in the smaller interval of the variation in the angle $\gamma$, which adjoins limiting value of $\gamma=180°$.

Similar phenomenon is observed with increase of parameter $\zeta$ (Fig. 4.5).

It should be noted that an increase in the size/dimension of
antenna and its removal/distance from the edge/fin of key affect the
dependence of radiation pattern on the wedge angle not completely
equally. With the increase/growth $\zeta$ the antenna radiation pattern,
arranged/located on the key, strives, although slowly (is
proportional $1/\sqrt{\zeta}$). to the diagram of antenna on the plane, so that in
the limit with $\zeta \to \infty$ the diagram of antenna generally ceases to depend
on wedge angle.

Page 91.

On the other hand, with an increase in the length of antenna its
radiation pattern, examined/considered in the dependence on universal
by the variable/alternating t, does not change and dependence $P(\varphi)$ on
the angle $\gamma$ is retained with any $l$. The difference indicated is
connected with the fact that during the removal/distance of antenna
from the edge/fin of key its effect on the radiation pattern
decreases, whereas with an increase in the length of antenna the
edge/fin of key always is located in the near zone of antenna, in
consequence of which is retained the dependence of radiation pattern
on the wedge angle. If in contrast to the basic version antenna is
excited by the deferred-action wave ($\beta > k$, $\sigma > 0$), the edge/fin of key

is irradiated more intensely and the dependence of radiation patterns $P(\varphi)$ on the angle $\gamma$ it is amplified (Fig. 4.6).
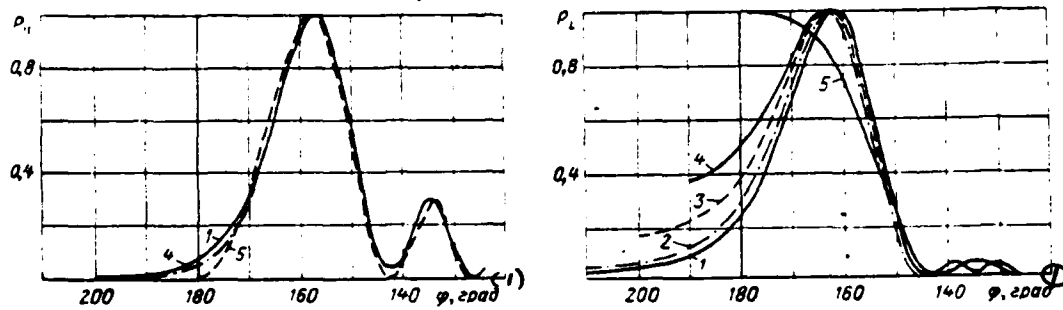


Fig. 4.5. Radiation patterns $P(\varphi)$ for parallel and perpendicular polarization at different angles $\gamma$ for $L=5$, $\sigma=0$, $q=0$, $\zeta=0.5$: 1) $\gamma=0-60°$; 2) $\gamma=120°$; 3) $\gamma=160°$; 4) $\gamma=170°$; 5) $\gamma=180°$.

Key: (1). deg.

Page 92.

On the contrary, with $\beta<k$, when phase wave velocity, which excites antenna, is more than the speed of light, the main lobe of radiation differs from the axis of antenna, edge/fin is irradiated more weakly, which leads to weakening of the effect of wedge angle on the radiation patterns $P(\varphi)$ (Fig. 4.7). The drop of the amplitude of field from the center to the edges of antenna ($q\neq0$) is equivalent simultaneously to certain shortening of antenna and its removal/distance from the edge of key. As is shown calculation (Fig. 4.8), the effect of "removal/distance" proves to be predominant.

Together with the examination of radiation patterns $P(\varphi)$ is of interest the analysis of phase diagrams $\Phi(\varphi)$. Fig. 4.9 shows phase diagrams $\Phi(\varphi)$, corresponding to the values of parameters $l$=5; $\zeta$=0; q=0; by $\gamma$=0° and 170°; $\sigma$=0 and 0.5.
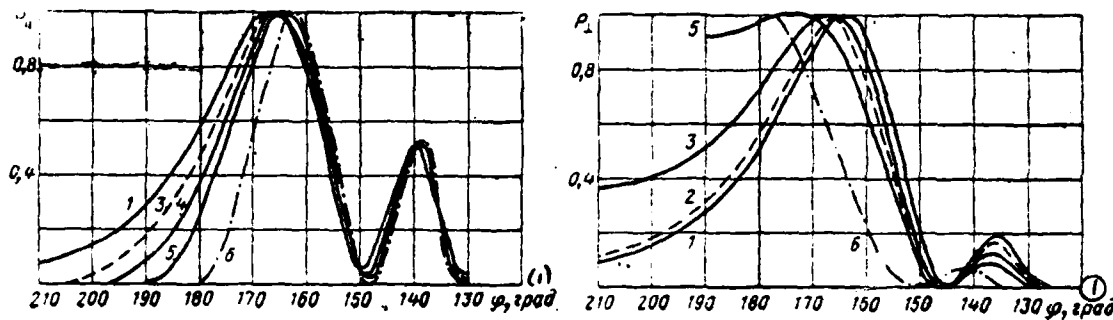


Fig. 4.6. Radiation patterns $P(\varphi)$ for different ones $\gamma$ with l=5, $\zeta$=0, $\sigma$=0.5, q=0: 1) $\gamma$=0-30°; 2) $\gamma$=90°; 3) $\gamma$=150°; 4) $\gamma$=160°; $\gamma$=170°; 6) $\gamma$=180°.

Key: (1). deg.

Page 93.

Phase diagrams $\Phi(\varphi)$ insignificantly depend on wedge angle $\gamma$. In the shadow zone phase diagrams $\Phi(\varphi)$ approach constant limit with $\varphi \to 2\pi$. Since the reading of the phase of diagrams $F(\varphi)$ is conducted relative to the edge/fin of key, then this means that in the shadow zone the phase center of antenna is located on the edge of key. Since in the

region of light/world- the dominant role plays the intrinsic emission of antenna, one should expect that with $\varphi<\pi$ the phase center must be located near the center of its aperture.
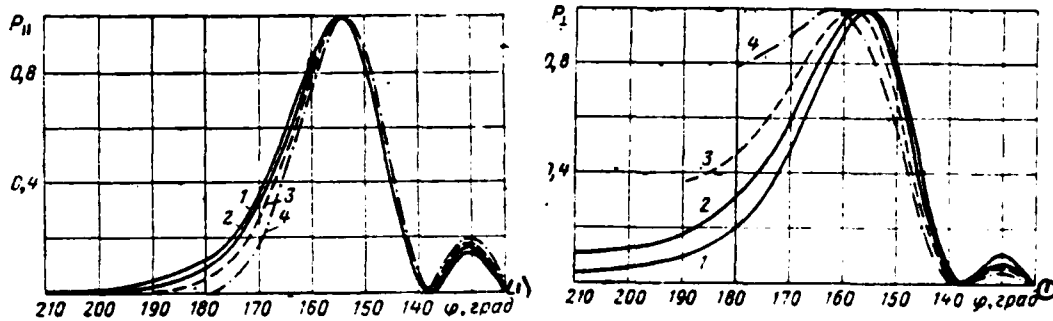


Fig. 4.7. Radiation patterns $P(\varphi)$ for different ones $\gamma$ with l=5, $\varsigma$=0, $\sigma$=-0.5, q=0: 1) $\gamma$=0-90°; 2) $\gamma$=150°; 3) $\gamma$=170°; 4) $\gamma$=180°.

Key: (1). deg.

Page 94.

This confirms the examination of the phase diagrams

$$\Phi'(\varphi) = \Phi(\varphi) - \kappa\left(\Gamma + \frac{L}{2}\right)\cos\varphi,$$

corresponding to the basic version and calculated relative to the center of aperture (Fig. 4.9). In the case of perpendicular polarization in the limits of major lobe of diagram $P(\varphi)$ phase diagram $\Phi'(\varphi) \approx const.$ i.e. phase center in the region of major lobe virtually coincides with the center of aperture.
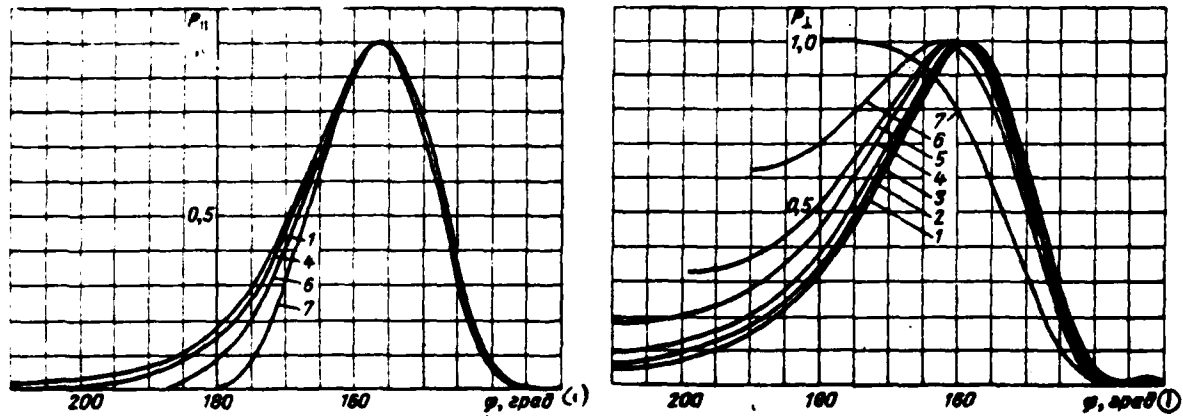
Fig. 4.8. Radiation patterns P($\varphi$) for different ones $\gamma$ with $l$=5, q=0.52, $\zeta$=0, $\sigma$=0: 1) $\gamma$=0~30°; 2) $\gamma$=90°; 3) $\gamma$=120°; 4) $\gamma$=150°; 5) $\gamma$=160°; 6) $\gamma$=170°; 7) $\gamma$=180°.

Key: (1). deg.

Page 95.

During the parallel polarization phase diagram $\Phi'_{\parallel}(\varphi)$ is almost linear in the region in question. It is not difficult to be convinced with the aid of Fig. 4.9 that the phase center of antenna during the parallel polarization is located at point with the coordinates

$$x = 0.15l\,(2l + 1),$$
$$y = -0.12l\,(2l + 1).$$
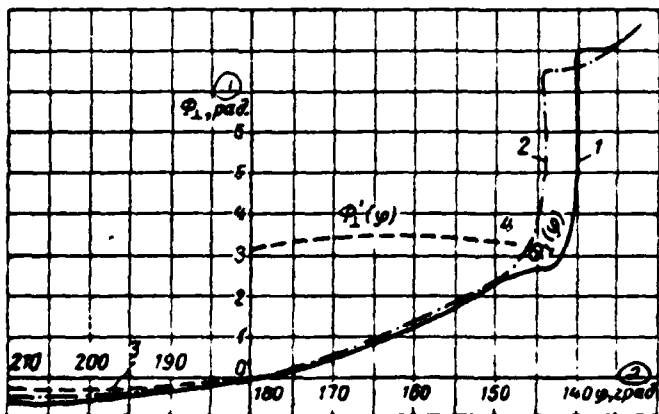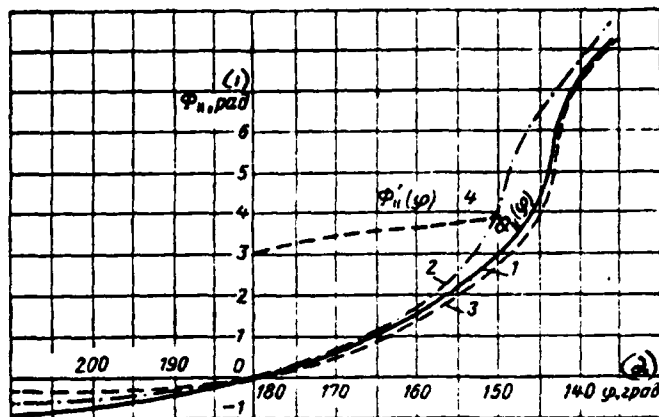
Fig. 4.9. Phase diagrams of antennas, arranged/located on key: 1) γ=0; **l**=5; ς=0; σ=0; q=0; 2) γ=0; **l**=5; ς=0; σ=0.5; q=0; 3) by γ=150°; **l**=5; ς=0; σ-0; q=0; 4) Φ'(φ).

Key: (1). rad. (2). deg.

Page 96.


The analysis of the results of the numerical calculations of radiation patterns $F(\varphi)$ makes it possible to make a following conclusion. A change in the wedge angle leads to substantial changes in the radiation patterns $(130° \leqslant \varphi \leqslant 210°)$ only at $\gamma \gtrsim 150°$ in the case of parallel and at $\gamma \lesssim 90°$ in the case of perpendicular polarization, if $L \gtrsim 5\lambda$. Therefore during the solution of the series/row of the practical problems, connected with the calculation of antennas, which are located on the surface of wedge shape, the surface of key with the sufficient degree of accuracy can be replaced by half-plane, which substantially facilitates the calculation of antenna.


4.3. Approximate methods of calculating the antenna radiation pattern, which is located on the surface of key.


In the preceding/previous chapter it is shown that the radiation pattern of surface antenna, which is located on the half-plane, can be represented in the form of product (3.24) or (3.25). The analogous approximate representation is correct for the antenna, arranged/located on the key. In connection with this there is special interest in the description of the radiation pattern of elementary slotted emitter on the key. Fig. 4.10 shows radiation patterns $|u(\varphi)|^2$ slot, which is located on the key, designed according to

precise formula (4.3) for the series/row of the values of angle $\gamma$ and distance $\Gamma=2\lambda$ from the slot to the edge of key. At $\gamma\lesssim 90°$ diagram $|u_\perp(\varphi)|^2$ insignificantly differs from the radiation pattern of slot by half-plane. Therefore at $\gamma\lesssim 90°$ antenna radiation pattern, which radiates from the surface of key, they can be approximately calculated by formulas of S 3.2. Together with the approximate method of describing the radiation pattern of slot indicated on the key with the apex angle of $\gamma\lesssim 90°$, it is expedient to obtain approximate expressions for pattern $u(\varphi)$, valid at any values of angle $\gamma$.

Page 97.

For this purpose in appendix I are determined asymptotic expressions for the radiation patterns $u(\varphi)$, which correspond to condition $\kappa\Gamma\gg 1$.

Asymptotic formulas (I.12) obtained in application/appendix I[1], (I.13) can be used for the approximate computation of the antenna radiation patterns, which are located on the surface of key, according to the method, described in S 3.2.

FOOTNOTE [1]. All appendices are given at the end of the book. ENDFOOTNOTE.

These formulas, furthermore, it is possible directly to utilize for calculating the surface antennas according to the reciprocity theorem. It is necessary to note that to the construction of the asymptotic behavior of the field, which diffracts on the key, are dedicated the works of Pauli [49] and Oberhettinger [50]. Asymptotic formulas (I.12), (I.13) are the first terms of the asymptotic series/rows, obtained by Oberhettinger [50] in another manner.

For the evaluation/estimate of the limits of the applicability of asymptotic expressions (I.12) and (I.13) was produced the calculation according to formulas (4.2), (4.3) and (I.12), (I.13) the radiation patterns of slot, which is located on the surface of key (Fig. 4.11). The comparison of the results of the approximate and precise calculations makes it possible to assert that asymptotic formulas (I.12) and (I.13) give the results satisfactory for practical purposes (with the accuracy not worse than $10^{-2}-10^{-3}$), if $\Gamma \geq \lambda$.
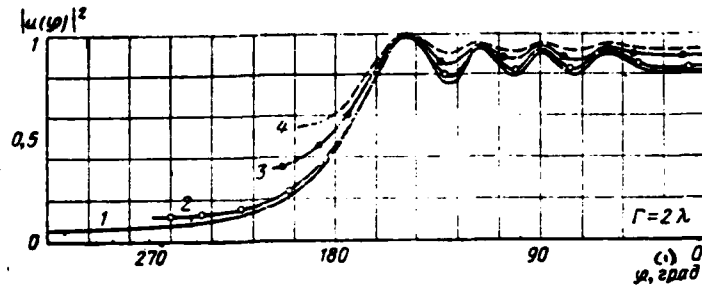
Fig. 4.10. Radiation pattern of slot, which is located on key, when $\Gamma=2\lambda$: 1) $\gamma=0°$; 2) $\gamma=90°$; 3) $\gamma=150°$; 4) $\gamma=165°$.

Key: (1). deg.

Page 98.

According to formulas (I.12) and (I.13) was produced supplementary performance calculation of the radiation/emission of slot. Fig. 4.12 gives power coefficients, emitted by slot in the direction of the boundary of shadow ($\varphi=\pi$), and also power coefficients of radiation/emission on the shadow face of the key:

$$|u_\perp(\varphi = \pi)|^2 = \Big| 1 + \exp[-i2\kappa\Gamma(\alpha - \pi)^2] \times$$

$$\times \Big\{ 1 - \sqrt{2}\, e^{-i\frac{\pi}{4}} F_1 \Big[ 2\sqrt{\frac{\kappa\Gamma}{\pi}}\,(\alpha - \pi) \Big] \Big\} -$$

$$- \frac{1}{2}\, e^{i\frac{\pi}{4}} \Big\{ \frac{1}{\alpha} \operatorname{ctg} \frac{\pi^2}{\alpha} + \frac{1}{\pi(\alpha - \pi)} \Big\} \sqrt{\frac{2\pi}{\kappa\Gamma}} \Big|^2, \qquad (4.4)$$

$$|u_\perp(\varphi = \alpha)|^2 = \Big| 2 e^{-i\frac{\pi}{4}} e^{-i\kappa\Gamma(\alpha - \pi)^2} \times$$

$$\times \Big\{ 1 - \sqrt{2}\, e^{-i\frac{\pi}{4}} F_1 \Big[ \sqrt{\frac{\kappa\Gamma}{\pi}}\,(\alpha - \pi) \Big] \Big\} + \sqrt{\frac{2\pi}{\kappa\Gamma}} \operatorname{tg} \frac{\pi^2}{2\alpha} \Big|^2.$$

$$(4.5)$$

Calculation is carried out for the perpendicular polarization depending on wedge angle $\gamma$ for the series/row of values $\Gamma$. The curves, shown in Fig. 4.12, virtually coincide in the considerable range of values of wedge angle, that is adjacent to $\gamma = 0$. The *coincidence of curves for different ones* $\Gamma$ in the region indicated shows that at $\gamma \leq 60°$ radiation pattern of slot $u_\perp(\varphi)$ is universal relative to the removal/distance of slot $\Gamma$ from the edge/fin of key, i.e., it depends only on the universal parameter t.
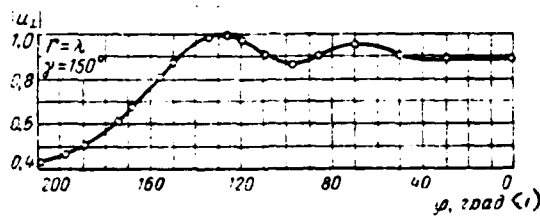
Fig. 4.11. Comparison of results of precise and approximate computations of radiation patterns of slot at $\Gamma=\lambda$ and $\gamma=150°$. Circles designated the asymptotic values of diagram.

Key: (1). deg.

Page 99.
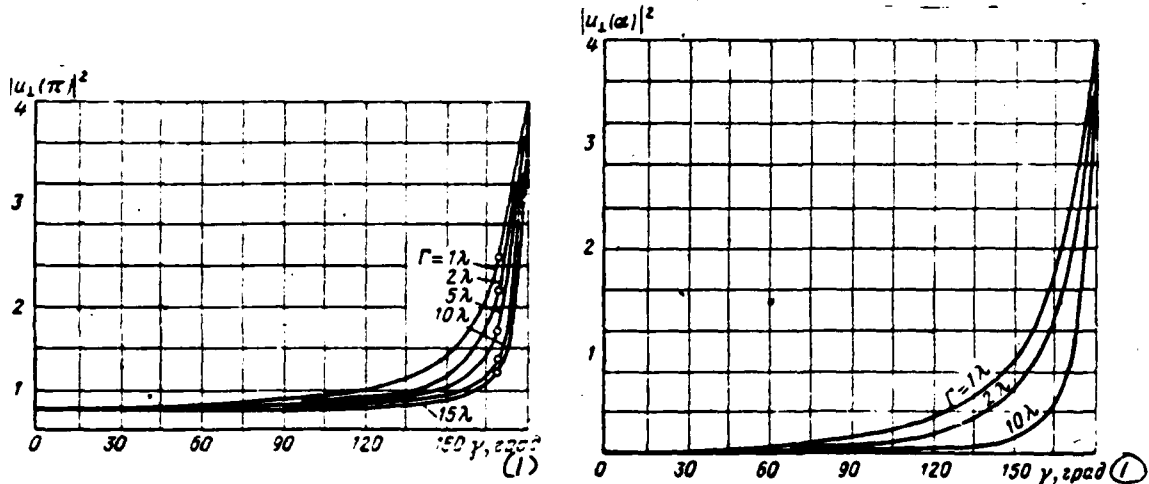


Fig. 4.12. Values $|u_\perp(\pi)|^2$ and $|u_\perp(\alpha)|^2$ with different ones $\gamma$ and $\Gamma$.

Key: (1). deg.

Page 100.

At $\gamma > 60°$ curves $|u_\perp (\varphi = \pi)|^2$ $|u_\perp (\varphi = \alpha)|^2$ begin to diverge, and diagram $u_\perp(\varphi)$, constructed depending on the universal parameter $t_\bullet$, they will more noticeably differ from each other, the stronger the dependence $|u_\perp (\varphi = \pi)|^2$ on $\Gamma$, as measure of which can serve the function

$$
K(\gamma,\ \kappa\Gamma) = \frac{\partial u_\perp}{\partial (\kappa\Gamma)}\Big|_{\varphi = \pi} =
$$
$$
= e^{i\pi\Gamma}\Big\{ -4\pi i\,(\alpha - \pi)^2 \exp\left[-i2\kappa\Gamma(\alpha - \pi)^2\right] \times
$$
$$
\times \Big(1 - \sqrt{2}e^{-i\frac{\pi}{4}}F_1\Big[2\sqrt{\tfrac{\kappa\Gamma}{\pi}}\,(\alpha - \pi)\Big]\Big) -
$$
$$
- 2e^{-i\frac{\pi}{4}}\sqrt{\tfrac{2\pi}{\kappa\Gamma}}\,(\alpha - \pi) +
$$
$$
+ \tfrac{1}{4}e^{-i\frac{\pi}{4}}\Big(\sqrt{\tfrac{2\pi}{\kappa\Gamma}}\Big)^3 \Big[\tfrac{1}{\alpha}\operatorname{ctg}\tfrac{\pi^2}{\alpha} + \tfrac{1}{\pi(\alpha - \pi)}\Big]\Big\}. \quad (4.6)
$$

Curves $|K(\gamma, \kappa\Gamma)|^2$ (Fig. 4.13) clearly show that the radiation pattern of slot is universal in the sufficiently wide range of values of wedge angles, that is adjacent to $\gamma = 0$, and also in a small interval of values $\gamma$ near $\gamma = \pi$. Function $|K(\gamma, \kappa\Gamma)|^2$ reaches maximum at $\gamma = 150° - 170°$; the position of maximum depends on distance $\Gamma$, and its value sharply decreases in proportion to the removal/distance of slot from the edge/fin of key. The given results, based on the analysis of asymptotic formulas (I.12) and (I.13), relate not only to the thin slots, but also to the directional antennas, arranged/located on the key.
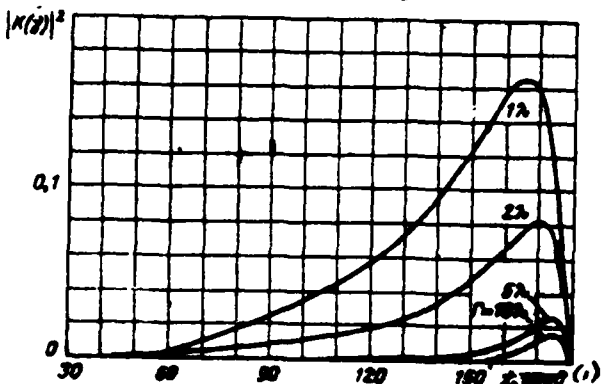
Fig. 4.13. Function $|K(\gamma, k\Gamma)|^2$ with different ones $\gamma$ and $\Gamma$...

Key: (1). deg.

Page 101.

## 4.4. Radiation patterns of "two-way" antenna on the key.

As the illustration of the approximate computation of antennas, which are located on the key, let us calculate the radiation patterns of "bilateral" antenna on the key (Fig. 4.14). It is known that for accomplishment of the survey/coverage of space in the sector $-\vartheta_0 \leqslant \vartheta \leqslant \vartheta_0$ (Fig. 4.14) necessary to utilize two antennas, arranged/located on the faces of key. Survey/coverage in the sector of the angles, distant from the direction $\vartheta = 0$, is realized with the aid of one of the antennas, by changing the phase of field distribution in its

aperture. The oscillation of diagram in the sector, which is adjacent to $\vartheta=0$, is provided by the selection of the corresponding relationship/ratio between the amplitudes and by the phases of the excitation coefficients of both antennas.

In order to calculate "two-way" antenna, we will use the fact that at the small wedge angles $\gamma$ the radiation pattern of the surface antenna, arranged/located on the key, differs little from the diagram of antenna on the half-plane. In turn, for calculating the antenna radiation pattern the traveling wave, arranged/located on the half-plane, we will use in an approximate manner, described into 3.2.
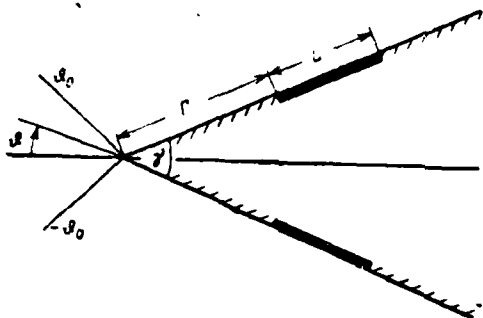
Fig. 4.14. On calculation of "bilateral" antenna, which is located on key.


Page 102.


Noting by marks "+" and "-" the values, which relate respectively to the upper and lower bounds of key, let us record as follows the radiation patterns of both antennas during the perpendicular polarization:

$$\Phi_\perp^{(+)} = \{1 + \sqrt{2}e^{-i\frac{\pi}{4}}F_1(t^{(+)}\sqrt{2\zeta+1})\}f(\sigma, q, t^{(+)}),$$

$$\Phi_\perp^{(-)} = -\{1 - \sqrt{2}e^{-i\frac{\pi}{4}}F_1(t^{(-)}\sqrt{2\zeta+1})\}f(\sigma, q, t^{(-)}), \quad (4.l)$$

where

$$t^{(\pm)} = 2\sqrt{l}\sin\frac{\vartheta \pm 0.5\gamma}{2};$$

$$f(\sigma, q, t^{(\pm)}) = \sin u^{(\pm)}\frac{[u^{(\pm)}]^2(1-q)-\pi^2}{u^{(\pm)}\{[u^{(\pm)}]^2-\pi^2\}};$$

$$u^{(\pm)} = \frac{\pi}{2}[\sigma + (t^{(\pm)})^2].$$

According to the principle of superposition total diagram (diagram of

"bilateral" antenna) can be represented as follows:

$$\Phi_\perp = \Psi_\perp^{(+)}(t^{(+)}) + Be^{jb}\Phi_\perp^{(-)}(t^{(-)}). \qquad (4.8)$$

Writing/recording the radiation pattern of "bilateral" antenna in the form of the superposition of diagrams $\Phi^{(+)}$ and $\Phi^{(-)}$, we it is disregarded by interaction between these antennas. Interaction it would be possible to consider, if to use Green's functions for the key and reciprocity theorem. However, we will be restricted to the approximate computation of "bilateral" antenna. Fig. 4.15 gives the standardized/normalized radiation patterns $|\Phi_\perp(\theta)|^2$, designed for the different values $\gamma$ when $B=1$; $\psi=\pi$, $\sigma=0$; $q=0$; $\Gamma=0$; $L=10\lambda$. The examination of figure shows that, as one would expect, with an increase in the wedge angle major lobe of diagram becomes narrow, and side-lobe level increases. Fig. 4.16 shows diagrams $|\Phi_\perp(\theta)|^2$, designed for the series/row of values B when $\gamma=12°$, $\psi=\pi$, $q=0.52$ (power level of field on the edge of aperture it composes 10o/o), $\Gamma=0$, $L=30\lambda$, $\sigma=0$. The results of calculations, given in Fig. 4.15 and 4.16, make it possible to rate/estimate the distortion of the radiation pattern of the antenna in question.
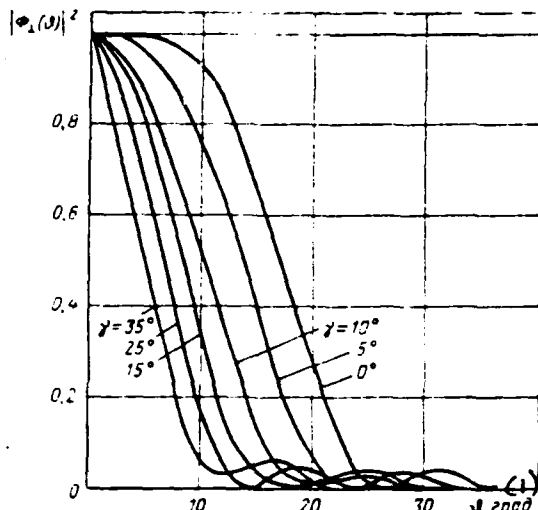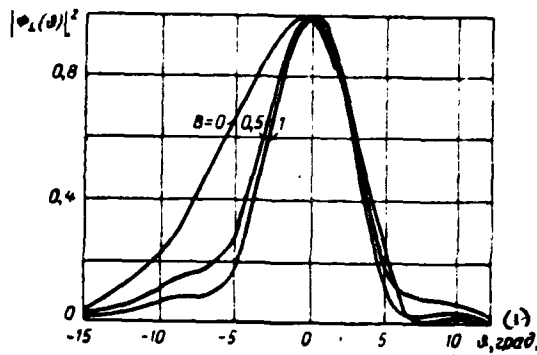
Fig. 4.15.                    Fig. 4.16.

Fig. 4.15. Radiation patterns of "bilateral" antenna with different $\gamma$.

Key: (1). deg.

Fig. 4.16. Radiation patterns of "bilateral" antenna for different values of parameter B.

Key: (1). deg.

Page 104.

4.5. Comparison of the results of calculation with the experimental data.

Since the calculations of the radiation patterns of surface antennas, which are located on the key, were conducted, mainly, according to precise formulas, experimental results are given for the purpose of the evaluation of the effect of the divergence of the real body of wedge shape from the infinite key.

The measurements of radiation patterns were made in the mock-up, shown in Fig. 4.17. Mock-up was the angled $30^o$ metallic sheet, on one of faces of which could freely be moved slotted waveguide traveling-wave antenna. Slots in the waveguide were gashed in parallel to the edge/fin of key, which corresponds to perpendicular polarization. Phase distribution was selected so that the velocity of propagation of the exciting wave would be the order or somewhat less than the speed of light. Amplitude field distribution in the antenna was almost symmetrical, that collapses to the edges on 10 dB. Fig. 4.18 compares the calculated and experimental radiation patterns of surface antenna. The comparison of calculated and experimental diagrams shows that the theory makes it possible to sufficiently accurately determine the antenna radiation patterns, which is located on the key.
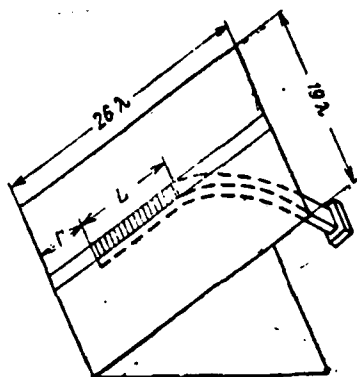
Fig. 4.17. Form of experimental mock-up.

Page 105.

Finite dimensions and roundedness of the edge of real wedge-shaped body insignificantly affect radiation pattern. Some differences in the calculated and experimental curves are caused by the divergences of real field distributions in the antenna from field distribution (4.1), accepted during the calculation.
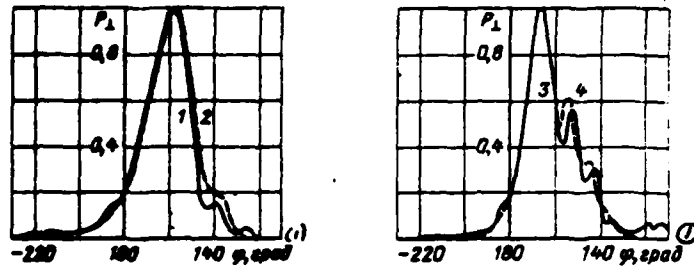
Fig. 4.18. Comparison of results of calculation and experiment: 1 - experimental curve ($l$=3.07, $\zeta$=1, $\sigma$=0, q=0.52); 2 - calculated curve ($l$=3, $\zeta$=1, $\sigma$=0, q=0.52); 3 - experimental curve ($l$=3.07, $\zeta$=3, $\sigma$=0, q=0.52); 4 - calculated curve ($l$=3, $\zeta$=3, $\sigma$=0 q=0.52).

Key: (1). deg.

5. Radiation patterns of slots, which are located on the plane and the half-plane with surface impedance.

Together with the analysis of the dependence of the radiation pattern of surface antenna on the form of the ideally conducting object, is of interest the evaluation of the effect of impedance of surface on the radiation characteristics of antennas of the type in question. The knowledge of the dependence of radiation pattern on the value of surface impedance makes it possible, in particular, to determine the effect of sealing coats on the radiation/emission of slot antennas, to rate/estimate the effect of the final conductivity of metal on the radiation patterns of surface antennas.

Page 106.

The solution of the problem indicated, furthermore, it is of independent interest and can be used for the determination of the value of the surface impedance, necessary for the formation of the required radiation pattern.

In this chapter will be examined the radiation patterns of the thin slots, which are located on the impedance plane and the

impedance half-plane. In the case of impedance plane the radiation
pattern of slot it is not difficult to calculate, using reciprocity
theorem.

A precise calculation of the radiation/emission of slot, which
is located on the impedance half-plane, can be produced on the basis
of the results of work [51]. However, exact expressions for the
radiation patterns, obtained thus, are bulky and complicated for the
practical use. In order to entreat numerical calculations, and to
also give simplicity and clarity to the expressions, which describe
the radiation pattern of slot on the impedance half-plane, we will
use the approximation method of Kirchhoff. In accordance with the
approximation/approach of Kirchhoff we will consider that the field,
created by slot on the surface of impedance half-plane, coincides
with the field of slot in the section of impedance plane. The problem
about the excitation of impedance plane by slotted emitter is in
detail examined in appendix II.

5.1. Calculation of the radiation pattern of slot, which is located
on the impedance plane.

The radiation pattern of slot in the impedance plane is the
superposition of the radiation field of slot and fields, created by
the ground waves, which are excited on the impedance surface in

question.


The radiation field of slot in the remote zone can be determined
as follows. Let on the impedance plane fall at angle α the plane wave
(Fig. 5.1)

$$\vec{H}_i = e^{isr\cos(\vartheta-\alpha)}\vec{e}_y$$

Page 107.


On the geometric optic/optics complete field at point $(r, \vartheta)$ has the
following value:

$$\vec{H} = \{e^{isr\cos(\vartheta-\alpha)} + \Gamma_0 e^{isr\cos(\vartheta+\alpha)}\}\vec{e}_y, \qquad (5.1)$$

where $\Gamma_0 -$ reflection coefficient from the impedance plane. If the
surface impedance Z of plane is purely reactive/jet, field $\vec{H}$
satisfies the boundary condition

$$\frac{1}{H}\frac{\partial H}{\partial y}\bigg|_{x=0} = -\kappa\eta, \qquad (5.2)$$

where $\eta = -iZ/Z_0 -$ real value;


$Z_0 = \sqrt{\mu_0/\epsilon_0} = 120\pi \,(o.m) -$ the impedance of free space [1].


FOOTNOTE [1]. Values $\eta$, corresponding to different impedance
structures, are given in works [12, 31]. ENDFOOTNOTE.


Substituting complete field (5.1) in equation (5.2), we find the

value of the coefficient of reflection

$$\Gamma_\bullet = \frac{\sin \alpha - i\eta}{\sin \alpha + i\eta}.$$

Thus,

$$H_\nu = e^{i\kappa r \cos(\theta - \alpha)} + \frac{\sin \alpha - i\eta}{\sin \alpha + i\eta} e^{i\kappa r \cos(\theta + \alpha)}. \qquad (5.3)$$

Utilizing (5.3) and a reciprocity theorem (1.5), we will obtain following field expression of the radiation/emission of slot in the remote zone:

$$H(\theta) = \frac{\omega \epsilon}{2} \cdot \frac{\sin \theta}{\sin \theta + i\eta}. \qquad (5.4)$$

For calculating the amplitudes of the excitation of ground waves and field, created by them, can be also used the reciprocity theorem.

The idea of the use/application of a reciprocity theorem for calculating the amplitudes of the ground waves, which are propagated along the interface of two media, belongs to Goubau [53] and is presented in works [36] and [12]. Let the infinite thin slot in the impedance plane x=0 (Fig. 5.1) be excited by the field

$$\vec{E}_\mathbf{m} = \delta(z) \vec{e}_z. \qquad (5.5)$$

Page 108.

Let us designate $\vec{E}_T, \vec{H}_T$ — the complete field of slot; $\vec{E}_s, \vec{H}_s$ — the ground waves of single amplitude; $\vec{E}_R, \vec{H}_R$ — radiation field. Noting by

index "1" the field of the ground wave, which runs in direction z>0, and by index "2" - the field of the wave, which runs in direction z<0, can be written:

$$\vec{E}_T = -a_1\vec{E}_{n1} + \vec{E}_R; \quad \vec{H}_T = a_1\vec{H}_{n1} + \vec{H}_R \text{ (for } z>0) \qquad (5.6)$$

and

$$\vec{E}_T = a_1\vec{E}_{n2} + \vec{E}_R; \quad \vec{H}_T = a_1\vec{H}_{n2} + \vec{H}_R \text{ (for } z<0),$$

where $a_{1,2}$ — unknown amplitudes of ground waves.

Taking into account the polarization of the exciting field it is obvious that:

$$\vec{H}_{n1} = e^{-\Gamma x}e^{i\beta z}\vec{e}_y;$$

$$\vec{E}_{n1} = -\frac{i\gamma}{\omega\varepsilon}H_{n1}\vec{e}_x - \frac{\beta}{\omega\varepsilon}H_{n1}\vec{e}_z; \qquad (5.7)$$

$$\vec{H}_{n2} = e^{-\Gamma x}e^{-i\beta z}\vec{e}_y;$$

$$\vec{E}_{n2} = -\frac{i\gamma}{\omega\varepsilon}H_{n2}\vec{e}_x + \frac{\beta}{\omega\varepsilon}H_{n2}\vec{e}_z$$
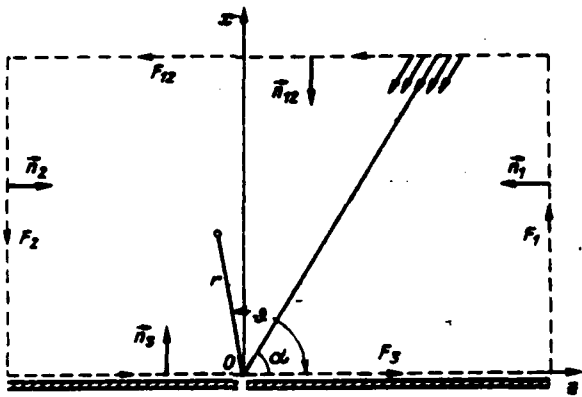
Fig. 5.1. On calculation of radiation pattern of slot in impedance plane.


Page 109.


In view of boundary condition, which must satisfy the ground waves:

$$\frac{E_{\text{п1, з}}}{H_{y1, з}} = \frac{-\Upsilon\frac{1}{\omega\varepsilon}|\vec{H}_{\text{п1, з}}|}{|\vec{H}_{\text{п1, з}}|} = -i\eta Z_\bullet$$

and therefore

$$\begin{aligned} \Upsilon &= \psi\kappa; \\ \beta &= \kappa\sqrt{1+\eta^2}. \end{aligned} \qquad (5.8)$$

The total field of slot $\vec{E}_\text{т}$ and $\vec{H}_\text{т}$ and ground waves $\vec{E}_{\text{п1, з}}, \vec{H}_{\text{п1, з}}$ satisfy reciprocal relation:

$$\oint_{F} \{[\vec{E}_\text{т}, \vec{H}_{\text{п1, з}}] - [\vec{E}_{\text{п1, з}}, \vec{H}_\text{т}]\} \, \vec{n}_\varepsilon df = 0, \qquad (5.9)$$

where $\vec{n}_e$ — the standard/normal, external with respect to the space, limited by surface of F, which consists of the flat/plane sections $F_1$, $F_{1.2}$, $F_2$ and $F_3$ (Fig. 5.1). Since the field of ground waves rapidly decreases in proportion to removal/distance from plane x=0,

$$J_{1,2} = \int_{F_{1,2}} \{[\vec{E}_T, \vec{H}_{n1,2}] - [\vec{E}_{n1,2}, \vec{H}_T]\} \vec{n}_e df = 0. \quad (5.10)$$

Integrals on surfaces of $F_1$ and $F_2$ in view of the orthogonality of the radiation fields and ground waves [36] are equal to

$$J_1 + J_2 = \left\{ \int_{F_1} + \int_{F_2} \right\} \{[\vec{E}_T, \vec{H}_{n1,2}] -$$

$$- [\vec{E}_{n1,2}, \vec{H}_T]\} \vec{n} df = 2a_{1,2} \int_0^\infty [\vec{A}, \vec{B}] \vec{e}_z dx_1 \quad (5.11)$$

respectively for the waves, which are propagated in directions z>0 and z<0. In expression (5.11) are introduced the designations

$$\vec{A} = -\frac{1}{\omega\varepsilon} e^{-\gamma x} \vec{e}_x; \quad \vec{B} = -e^{-\gamma x} \vec{e}_y. \quad (5.12)$$

Page 110.

Let us now calculate integral (5.9) in section $F_3$ of surface F:

$$J_3 = \int_{F_1} \{ [\vec{E}_T, \vec{H}_{s1,2}] - [\vec{E}_{s1,2}, \vec{H}_T] \} \, \vec{n}_s df. \qquad (5.13)$$

On surface of $F_3$, which coincides with the impedance plane,

$$|\vec{E}_T^{\tau}|_{x=0} + \eta Z_\bullet |\vec{H}_T^{\tau}|_{x=0} = \delta(z),$$

$$|\vec{E}_{s1,2}^{\tau}|_{x=0} = -\eta Z_\bullet |\vec{H}_{s1,2}^{\tau}|_{x=0}. \qquad (5.14)$$

Therefore

$$J_3 = \int_{-\infty}^{\infty} \{ [\vec{e}_x \vec{e}_y] |\delta(z) - \eta Z_\bullet |\vec{H}_T^{\tau}| ] |\vec{H}_{s1,2}^{\tau}| +$$

$$+ \eta Z_\bullet |\vec{H}_{s1,2}^{\tau}| |\vec{H}_T^{\tau}| [\vec{e}_x, \vec{e}_y] \} \, \vec{e}_x dz =$$

$$= -\int_{-\infty}^{\infty} |\vec{H}_{s1,2}^{\tau}| \delta(z) \, dz = -1. \qquad (5.15)$$

Substituting the value (5.10), (5.11), (5.15) integrals $J_{1,2}$, $J_1$, $J_2$, $J_3$ in relationship/ratio (5.9), we obtain

$$a_{1,2} = \frac{1}{2 \int_{0}^{\infty} [\vec{A}, \vec{B}] \vec{e}_x dx}. \qquad (5.16)$$

In accordance with expressions (5.12) and (5.16) the amplitudes of excitation $a_{1,2}$ of ground waves take the following form:

$$a_{1,2} = \omega s \frac{\eta}{\sqrt{1+\eta^2}}. \qquad (5.17)$$

Therefore according to expressions (5.7), (5.8) and (5.17) the
magnetic intensity of ground waves on the impedance plane

$$a_{1,2}\vec{H}_{s1,2} = \omega\epsilon \frac{\eta}{\sqrt{1+\eta^2}} \exp[i\kappa\sqrt{1+\eta^2}|z'|]\vec{e}_y. \quad (5.18)$$

Page 111.

Using expression (5.18), it is not difficult to determine the
contribution, introduced by ground waves into the radiation pattern
of the slot

$$H_s(\vartheta) = -\frac{\omega\epsilon}{2} \cdot \frac{2\eta^2}{\eta^2 + \sin^2\vartheta}. \quad (5.19)$$

Uniting relationships/ratios (5.4) and (5.19), we obtain the
following expression for the radiation pattern of the slot:

$$H = \frac{\omega\epsilon}{2}\left(\frac{\sin\vartheta}{\sin\vartheta + i\eta} - \frac{2\eta^2}{\eta^2 + \sin^2\vartheta}\right). \quad (5.20)$$

Analogous result can be obtained by another method. In appendix the
II method of solution of integral equation found magnetic field
(II.21), created by slot on the surface of impedance plane. Using
expression (II.21), it is possible to calculate magnetic field H(x,
z) at any point of space above impedance plane (x⩾0). Calculation
shows that

$$H(x, z) = \frac{\omega e}{2} \left\{ H_0^{(1)}[\kappa \sqrt{x^2 + (z - \Gamma)^2}] - \right.$$

$$- \frac{\kappa \eta}{\pi} \int_{-\infty}^{\infty} H_0^{(1)}[\kappa \sqrt{x^2 + (z - z')^2}] \left[ \int_1^{1+i\infty} \frac{\exp[i\kappa t | z' - \Gamma|]}{t^2 - 1 - \eta^2} \times \right.$$

$$\times \sqrt{t^2 - 1} \, dt \Big] dz' + \frac{i\kappa \eta^2}{\sqrt{1 + \eta^2}} \times$$

$$\left. \times \int_{-\infty}^{\infty} e^{i\beta | z' - \Gamma|} H_0^{(1)}[\kappa \sqrt{x^2 + (z - z')^2}] \, dz' \right\}. \quad (5.21)$$

In order to determine the radiation pattern of slot, let us introduce the cylindrical coordinates

$$x = r \sin \vartheta, \qquad y = y, \qquad z = r \cos \vartheta$$

and let us pass to the limit with r→∞ in expression (5.21). After the replacement of the Hankel functions in (5.21) them asymptotic expressions it will seem that

$$H(r, \vartheta) = \frac{\omega e}{2} \sqrt{\frac{2}{\pi \kappa r}} e^{i\left(\kappa r - \frac{\pi}{4}\right)} \times$$

$$\times \left\{ 1 - \frac{2i\eta}{\pi} \int_1^{1+i\infty} \frac{t \sqrt{t^2 - 1} \, dt}{(t^2 - 1 - \eta^2)(t^2 - \cos^2 \vartheta)} - \frac{2\eta^2}{\eta^2 - \sin^2 \vartheta} \right\}.$$

Page 112.

Passing to variable/alternating $t = \sqrt{\eta^2 + 1}$ in the latter/last integral, and then dividing/marking off integrand into the common fractions, we obtain

$$\int_1^{1+i\infty} \frac{t \sqrt{t^2 - 1} \, dt}{(t^2 - 1 - \eta^2)(t^2 - \cos^2 \vartheta)} = \frac{\pi}{2} \frac{1}{\sin \vartheta + i\eta}.$$

Thus, finally expression for the radiation pattern takes the following form:

$$H(r, \vartheta) = \frac{\omega e}{2} \sqrt{\frac{2}{\pi \kappa r}} e^{i\left(\kappa r - \frac{\pi}{4}\right)} \left\{ \frac{\sin \vartheta}{\sin \vartheta + i\eta} - \frac{2\eta^2}{\eta^2 + \sin^2 \vartheta} \right\}.$$

$$(5.22)$$

Comparing expressions (5.22) and (5.20), we are convinced of the complete identity of the radiation patterns of slot on the impedance plane, designed by different methods.

5.2. Dependence of the form of the radiation pattern of slot on the impedance plane on the value of impedance.

Fig. 5.2 gives the results of calculating the standardized/normalized radiation pattern of slot, which is located on the impedance plane.
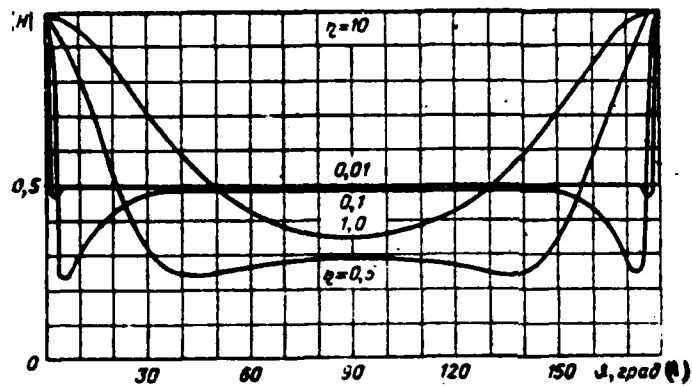
Fig. 5.2. Radiation pattern of slot, which is located on the impedance plane.

Key: (1). deg.

Page 113.

Radiation patterns are calculated with the aid of expression (5.22) for the series/row of the values of parameter $\eta$. When $\eta=0$. which corresponds of the ideally conducting planes, the radiation pattern of slot is uniform. At small values $\eta$ the diagram of slot is virtually uniform with exception of regions near $\vartheta=0°$ and $180°$, where there are two sharp lobes/lugs, the caused by radiation/emission ground waves, which spread from the slot. With increase/growth $\eta$ the contribution of ground waves to the radiation pattern increases, and radiation field - it decreases, which is clearly confirmed of the

curves of Fig. 5.2. It is possible to show that the power, emitted by ground waves, changes in the dependence on the impedance as $\eta^2/(1+\eta^2)$ and the power of radiation field - as $1/(1+\eta^2)$. Therefore when $\eta \rightarrow 0$ the radiation pattern of slot becomes uniform as a result of the decrease of the power, emitted by ground waves. However, when $\eta \rightarrow \infty$ the power of radiation field decreases also with sufficiently large ones $\eta$ (for example, $\eta=10$) radiation pattern also becomes uniform. In this case almost entire/all energy is emitted by the ground waves each of which as a result of the strong delay/retarding/deceleration creates wide radiation pattern, so that as a result of the superposition of the fields of ground waves the total field of slot again becomes uniform.

Interesting results according to the calculation of the radiation patterns of single horizontal wire and vertical dipole above the impedance plane are given in works [55, 56]. In the works indicated the impedance surface properties are caused by the dielectric coating of the ideally conducting screen. Some results of works [55, 56] can be found in book [36].

5.3. Calculation of the radiation pattern of slot, which is located on the impedance half-plane. In order to calculate in the approximation/approach of Kirchhoff the radiation pattern of slot, which is located on the impedance half-plane, should be used

Kirchhoff's formula (S 1.3) and expression (II.21) of

application/appendix for the field of slot on the surface of

impedance plane.


Page 114.


However, the complicated integral in expression (II.21), which

corresponds to radiation field on the surface of screen, will

considerably hinder/hamper the numerical calculations of the diagram

of slot, which is located on the half-plane. Therefore it is

expedient to approximate the integral indicated by simpler function.


First of all let us examine the dependence of integral in

expression (II.21) of value z' at the different values of parameter

$\eta$. For this was designed the function

$$\Delta H (0, z', \eta) = H_1 (0, z', \eta) - H_1 (0, z', 0) =$$

$$= \frac{i \eta^2 \omega \epsilon}{\pi} \int_1^{1+i\infty} \frac{\exp [i \kappa | z' - \Gamma | t]}{(t^2 - 1)(t^2 - 1 - \eta^2)} \sqrt{t^2 - 1} \, dt, \quad (5.23)$$

which does not have in contrast to $H_1 (0, z', \eta)$ the special

feature/peculiarity at point $z' = \Gamma$. In expression (5.23)

$$H_1 (0, z', \tau) = \frac{i \omega \epsilon}{\pi} \int_1^{1+i\infty} \frac{\exp [i \kappa | z' - \Gamma | t]}{t^2 - 1 - \eta^2} \sqrt{t^2 - 1} \, dt; \quad (5.24)$$

$$H_1 (0, z', 0) = \frac{i \omega \epsilon}{\pi} \int_1^{1+i\infty} \frac{\exp [i \kappa | z' - \Gamma | t]}{\sqrt{t^2 - 1}} \, dt =$$

$$= \frac{\omega \epsilon}{2} H_0^{(1)} (\kappa | z' - \Gamma |) \quad (5.25)$$

of the value of the radiation fields, created by slot on the surfaces

of impedance and ideally conducting of screens respectively.


If one assumes that $\kappa |z' - \Gamma|$ is sufficiently great, it is possible

to obtain in accordance with (5.23) the following asymptotic formula

for function $\Delta H(0, z' \eta)$:

$$\Delta H(0, z', \eta) \approx -\frac{\eta \omega \varepsilon}{2} \exp\left[i\kappa|z'-\Gamma|\left(1+\frac{\eta^2}{2}\right)\right] \times$$

$$\times \left\{1 - \sqrt{2}\, e^{i\frac{\pi}{4}} F_s\left(\sqrt{\frac{\kappa|z'-\Gamma|}{\pi}}\,\eta\right)\right\}, \qquad (5.26)$$

where

$$F_s(v) = \int_0^v e^{-i\frac{\pi}{2}t^2}\, dt.$$

Page 114.


The comparison of the results of precise and approximate computations

shows that when $\eta \lesssim 1$ formula (5.26) sufficiently accurately

approximates expression (5.23) with any $|z'-\Gamma|$. However, when $\eta > 1$

there is a noticeable disagreement between expressions (5.23) and

(5.26) near the slot $(z' = \Gamma)$. It is possible to show, that with $z' = \Gamma$

and small values $\eta$

$$\Delta H(0, \Gamma, \eta) = \frac{i\, \eta \omega \varepsilon}{2\pi \sqrt{1+\eta^2}} \left\{ i\pi + \ln \frac{\sqrt{1+\eta^2}+\eta}{\sqrt{1+\eta^2}-\eta} + \right.$$

$$\left. + \ln \frac{\sqrt{1+\eta^2}-1}{\sqrt{1+\eta^2}-1-2\eta^4} \right\} \approx -\frac{\eta}{2}, \qquad (5.27)$$

which is located in accordance with expression (5.26). However, when

$\eta \gg 1$ and $z' = \Gamma$

$$\Delta H(0, \Gamma, \eta) \approx \frac{\eta \omega \varepsilon}{2\pi} \ln 4\eta^2, \qquad (5.28)$$

i.e., expressions (5.23) and (5.26) actually/really essentially are distinguished when $z' \approx \Gamma$ and $\eta \gg 1$. Nevertheless, since of greatest practical interest are the structures with $\eta < 1$, during calculation of the radiation pattern of slot, which is located on the impedance half-plane, we will approximate field H(0, z', $\eta$) by the following function:

$$H_1(0, z', \eta) \approx$$
$$= \frac{\omega \epsilon}{2} \left\{ H_0^{(1)} (\kappa |z' - \Gamma|) - \eta \exp\left[ i\kappa |z' - \Gamma| \left( 1 + \frac{\eta^2}{2} \right) \right] \times \right.$$
$$\left. \times \left[ 1 - \sqrt{2} e^{i\frac{\pi}{4}} F_s \left( \sqrt{\frac{\kappa |z' - \Gamma|}{\pi}} \, \eta \right) \right] \right\}. \qquad (5.29)$$

It should be noted that, although expression (5.29) when $\eta \gg 1$ noticeably differs from precise when $z' \approx \Gamma$, it it is possible to use for calculating the radiation pattern of slot virtually with any $\eta$, since when $\eta \gg 1$ the dominant role in the formation of pattern play the ground waves (see Fig. 5.2). Furthermore, asymptotic formula (5.29) noticeably differs from precise only when $z' \approx \Gamma$.

Let us now move on to the calculation of the radiation pattern of slot, which is located on the impedance half-plane.

Page 116.

Let on the surface of impedance half-plane be located the ideally thin and infinitely long slot, which excites space in accordance with condition (II.4). In the approximation/approach of

Kirchhoff the slot creates the following distribution of magnetic field on the surface of the semi-infinite screen:

$$H_y = H(0, z', \eta) \approx \frac{\omega \omega}{2} \left\{ H_0^{(1)}(\kappa|z' - \Gamma|) - \right.$$
$$- \eta \exp[i\kappa|z' - \Gamma|(1 + \eta^2/2)]\left[ 1 - \right.$$
$$\left. - \sqrt{2} e^{i\frac{\pi}{4}} F_2\left( \sqrt{\frac{\kappa|z' - \Gamma|}{\pi}} \eta \right)\right] +$$
$$\left. + \frac{2\eta}{\sqrt{1 + \eta^2}} \exp[i\kappa\sqrt{1 + \eta^2}|z' - \Gamma|] \right\} \quad (5.30)$$

при $x = +0$; $0 \leqslant z < \infty$; $-\infty < y < \infty$;
$$H_y = 0 \text{ при } x = -0.$$

Key: (1). with.


For calculating the radiation pattern of slot we will use Kirchhoff's formula (1.62). Value H(0, z') is determined in (5.30), and $\frac{\partial H(x, z)}{\partial x}\Big|_{x=0}$ is expressed as H(0, z') with the aid of condition (II.4).


Assuming that observation point is located in the remote zone, and taking into account of radiation condition, after integration for Kirchhoff's formula we obtain the following expression for the radiation pattern of the thin slot, which is located on the impedance half-plane:

$$H(\vartheta,\gamma,\eta)=1+\frac{\sin\vartheta-i\eta}{2}\left\{\frac{2}{|\sin\vartheta|}-\right.$$

$$-\frac{2\sqrt{2\gamma}}{|v_1|}\left[1-\sqrt{2}\,e^{-i\frac{\pi}{4}}F_1(|v_1|)\right]+$$

$$+\frac{i\eta}{2}\left[\frac{4\pi\gamma}{u}\left(e^{iu}\left[1-\sqrt{2}\,e^{-i\frac{\pi}{4}}F_2(v_2)\right]-\right.\right.$$

$$\left.-1+\sqrt{2}\,e^{i\frac{\pi}{4}}\frac{v_2}{v_1}F_1(|v_2|)\right)+$$

$$\left.\left.+\frac{\frac{i\eta}{|2|\sin\vartheta/2|}-1}{\sin^2\frac{\vartheta}{2}+\frac{\eta^2}{4}}\right]\right\}- \qquad (5.31)$$

$$-\frac{\eta^2}{\sqrt{1+\eta^2}}\left\{\frac{2\pi\gamma}{u_1}\left[-2i\,e^{i\frac{u_1}{2}}\sin\frac{u_1}{2}\left[1+\sqrt{2}\,e^{-i\frac{\pi}{4}}F_1(v_1)\right]-\right.\right.$$

$$-e^{iu_1}\left[1+\sqrt{2}\,e^{-i\frac{\pi}{4}}\frac{v_1}{v_3}F_2(v_3)\right]\right]-\frac{2\pi\gamma}{u_2}\left[1+\right.$$

$$\left.\left.+\sqrt{2}\,e^{-i\frac{\pi}{4}}F_1(v_1)+\frac{v_1}{v_4}e^{iu_2}\left[1-\sqrt{2}\,e^{-i\frac{\pi}{4}}F_1(v_4)\right]\right]\right\}.$$

where

$$v_1=2\sqrt{2\gamma}\cos\frac{\vartheta}{2};\quad v_2=\sqrt{2\gamma}\,\eta;\quad v_3=2\sqrt{(\sqrt{1+\eta^2}-1)\gamma};$$

$$v_4=2\sqrt{(\sqrt{1+\eta^2}+1)\gamma};\quad u=4\pi\gamma\left(\cos^2\frac{\vartheta}{2}+\frac{\eta^2}{4}\right);$$

$$u_1=2\pi\gamma\,(\cos\vartheta+\sqrt{1+\eta^2});\quad u_2=2\pi\gamma\,(\cos\vartheta-\sqrt{1+\eta^2});$$

$\gamma=\Gamma/\lambda$— the distance from the slot to the edge of half-plane, measured in the wavelengths.

Page 117.

Expression (5.31) is the solution of stated problem. With the aid of this expression were designed the radiation patterns of slot

for the series/row of the values of parameters $\eta$ and $\gamma$.

It should be noted that the obtained solution of problem for the slotted emitter can be used for calculating the antenna radiation patterns, arranged/located on the impedance half-plane. If is assigned amplitude-phase field distribution in the aperture of surface antenna, its radiation pattern $U(\vartheta)$ can be expressed as follows:

$$U(\vartheta) = \int_{\gamma}^{\gamma+l} A(\xi) e^{i\Re} H(\vartheta, \eta, \xi) d\xi.$$

Page 118.

5.4. Results of the numerical calculation of the radiation pattern of slot, which is located on the impedance half-plane.

Radiation pattern $|H(\vartheta, \eta)|$ begins to differ from the radiation pattern of slot, which is located on the ideally conducting half-plane, at the value of parameter $\eta$, equal to already 0.01. With an increase in the surface impedance this difference becomes ever more noticeable (Fig. 5.3). If value $\eta$ grows/rises from 0 to 0.1, the principal maximum of radiation pattern $|H(\vartheta, \eta)|$ decreases, falls the radiation/emission of slot in the shadow zone and in the penumbra. This is explained by the fact that for the values $\eta$ indicated the fundamental contribution to the diagram gives the radiation field of slot, which changes with increase/growth $\eta$, as shown in Fig. 5.4.
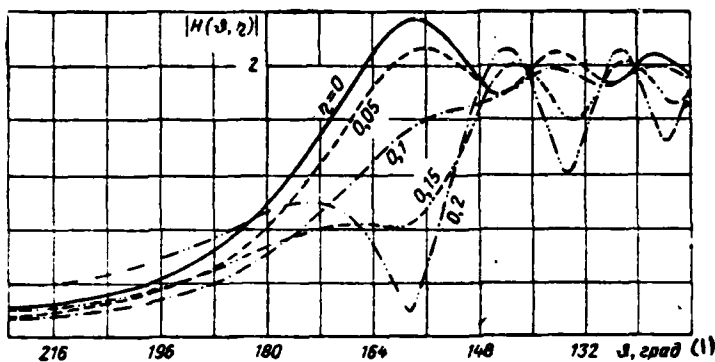
Fig. 5.3. Radiation patterns of slot $|H(\vartheta, \eta)|$, which correspond $\gamma=5$ and to different values $\eta$.
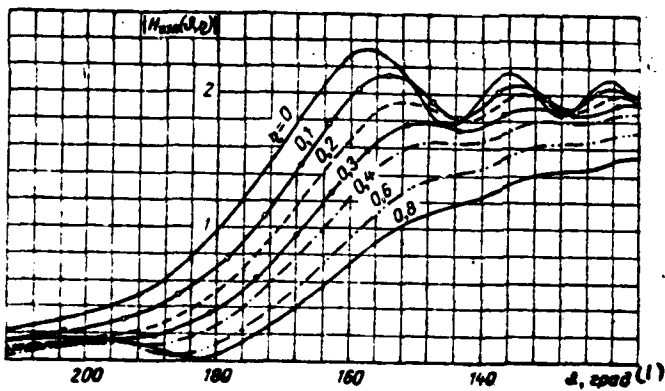
Key: (1). deg.



Fig. 5.4. Radiation field of slot $H_{max}(\vartheta, \eta)$.

Key: (1). deg.

Page 119.

The role of ground waves in the sector of angles $(110°\leqslant\vartheta\leqslant240°)$ when $\eta=0.01-0.1$ and $\gamma=5$ is small, since the value of the maximum of the radiation/emission of the ground wave, which encounters to the edge of half-plane, is proportional to $\eta^2\gamma$, and the radiation/emission of the ground wave, which is propagated in direction $\dot{z}>0$, when $\eta=0.01\div0.1$ is concentrated near $\vartheta=0°$. With an increase in parameter $\eta$ from 0.1 to 0.2 at $\gamma=5$ (Fig. 5.3) grows/rises the radiation/emission of slot in the shadow region, appears the new maximum of diagram near the geometric boundary of shadow. These changes in the radiation pattern are caused by the radiation/emission of the ground wave, which is propagated in direction $\dot{z}<0$. Further increase in the surface impedance leads to a considerable increase in the maximum of diagram, caused by the radiation/emission of ground wave (Fig. 5.5).
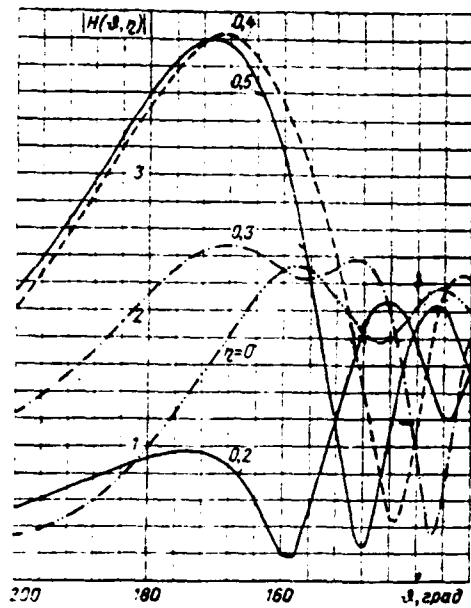
Fig. 5.5. Radiation patterns $|H(\vartheta, \eta)|$, which correspond $\gamma=5$ and to different values

Key: (1). deg.

Page 120.

At comparatively small values $\eta\,(\eta\leqslant 0.2)$, when the radiation/emission of the ground wave, which is propagated in direction $z'>0$, in region $(90°\leqslant\vartheta\leqslant240°)$ in question is small, the radiation pattern of ground waves (Fig. 5.6) virtually coincides with the diagram of traveling-wave antenna, located near the edge/fin of the ideally

conducting half-plane and which has the constant amplitude and linear phase response with phase change to the ends/leads of the antenna

$$\sigma = \frac{\xi - k}{\pi} \Gamma,$$

where $\Gamma$ — length of antenna, equal to distance from the slot to the edge/fin of impedance half-plane. At large values of $\eta$ the radiation pattern of ground waves differs in the region of the first minor lobes from the diagram of traveling-wave antenna as a result of the increase from the examined region of radiating/emitting the ground wave, which is propagated in direction $z > 0$.

At the sufficiently high values of surface impedance $[\eta > \eta_1 = \eta(\gamma)]$ for the radiation pattern of slot is characteristic the decrease of the absolute value of the main thing the maximum of diagram.
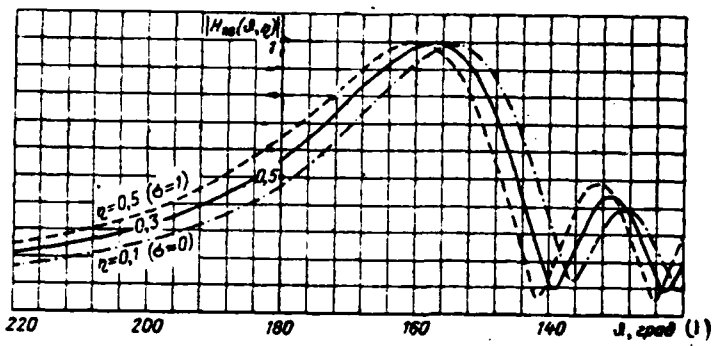
Fig. 5.6. Standardized/normalized radiation patterns of ground waves $|H_{ss}(\vartheta, \eta)|$ for the case $\gamma=5$ and different values $\eta$.

Key: (1). deg.

Page 121.

Value $\eta_1(\gamma)$, with which principal maximum reaches the greatest value, corresponds $\sigma=1$ for the ground wave, which encounters to the edge of half-plane. When $\eta \geqslant \eta_1$ the absolute maximum of the radiation pattern of slot is displaced into the region of the complex angles (see Chapter 2). The radiation patterns of slot, which correspond to large phase changes $\sigma$, they are shown in Fig. 5.7. For $\gamma=5$ the principal maximum of the radiation pattern of slot reaches the greatest value when $\eta_1=0.45$, while for $\gamma=10$ - when $\eta_1=0.32$. For the values $\eta_1$ and $\gamma$ indicated supplementary phase change $\sigma=1$.
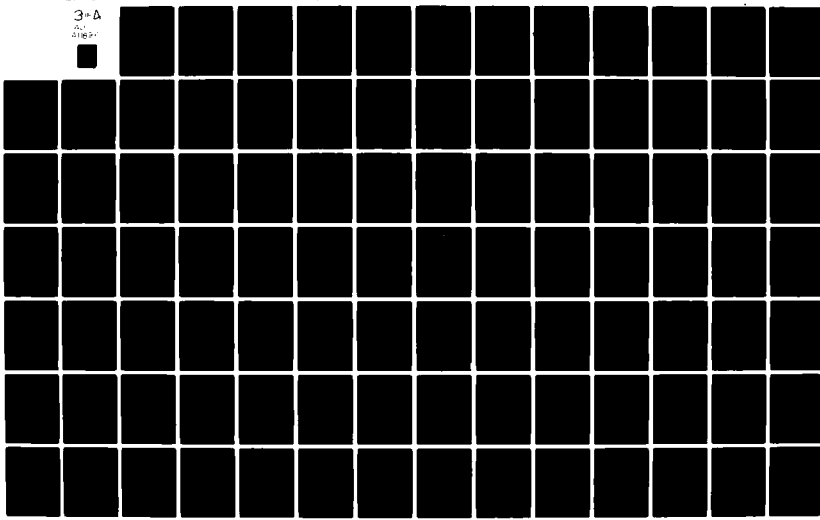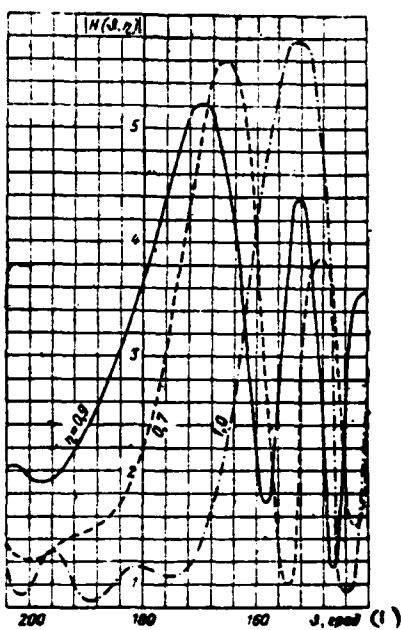
Fig. 5.7. Radiation patterns of slot $|H(\Phi, \eta)|$, which correspond $\gamma=10$ and to different values $\eta$.

Key: (1). deg.

Page 122.

Since at sufficiently high values $\eta$ (Fig. 5.5 and 5.7) the absolute value of minor lobes virtually does not depend on $\eta$, relative side-lobe level sharply grows/rises when $\eta \geqslant \eta_1$. About the speed of the increase of relative side-lobe level testify the curves, shown in Fig. 5.8. Curves have maximums when $\eta = \eta_1(\gamma)$  ($\gamma = 10$, $\eta_1 = 0{,}32$         and

$\gamma = 5$, $\eta_1 = 0.45$), moreover the values of these maximums are virtually identical. The equality of the maximums of curves in Fig. 5.8 is not by chance, since at the identical values $\sigma$ of the radiation pattern of slots, distant up to different distances $\gamma$ from the edge of half-plane, have the identical values of principal maximums, since with that fixed/recorded $\sigma$ the value of maximum is proportional $\eta^2 \gamma$, and $\eta^2 \gamma \approx \sigma = const.$

When $\eta \gtrsim 1/2\sqrt{\gamma}$, the position of principal maximum, the width of radiation pattern at the level of half power, radiation level of slot in the direction of the geometric boundary of shadow, i.e., that part of the diagram where the dominant role plays the radiation/emission of the ground wave, which encounters to the edge of half-plane, can be designed with the sufficient degree of accuracy on the base of the results of the study of traveling-wave antenna, led in Chapter 3.
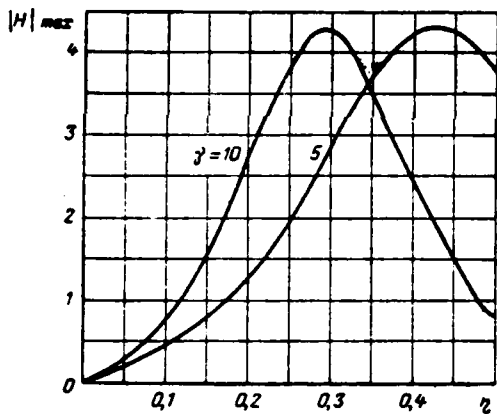
Fig. 5.8. Values of the principal maximums of the radiation/emission of slot, which correspond $\gamma=5$ and 10 and to different values $\eta$.

Page 123.

In the shadow zone the radiation/emission of slot monotonically decreases in proportion to removal/distance from the boundary of shadow, if the value of surface impedance is comparatively small. At sufficiently high values $\eta$ curves $H(\vartheta, \eta)$ (Fig. 5.7) become cut in the shadow zone as a result of the interference of the diffraction fields, which correspond to ground wave and radiation field of slot.

5.5. Evaluation/estimate of the accuracy of the approximation/approach of Kirchhoff.

The estimation of error in the approximation/approach of Kirchhoff will be carried out for two cases, when obtaining the accurate results, necessary for the comparison, does not present difficulties. Let us at first compare the radiation patterns of sharpened slot, which is located on the ideally conducting half-plane, calculated in the approximation/approach of Kirchhoff and by precise formula (3.18). The second example will make it possible to rate/estimate, as affects the value of the impedance of surface the accuracy of the results, obtained with the aid of the approximation/approach of Kirchhoff. For this let us calculate in the approximation/approach of Kirchhoff the radiation/emission of the ground wave, which encounters to the edge/fin of impedance half-plane. A strict solution of the problem indicated is obtained in work [52]. Approximate solution of the problem for the slot on the ideally conducting half-plane is not difficult to determine from expression (5.31). After assuming $\eta=0$ in formula (5.31), we will obtain the following approximation for the radiation pattern of the slot:

$$H(x, z)\big|_{\eta=0} = H(\vartheta, \gamma, 0) = 1 + \text{sign}(\sin\vartheta) -$$

$$- \sin\frac{\vartheta}{2}\,\text{sign}\left(\cos\frac{\vartheta}{2}\right)\left[1 - \sqrt{2}\,e^{-i\frac{\pi}{4}}\,F_1\left(2\sqrt{2\gamma}\cos\frac{\vartheta}{2}\right)\right].$$
$$(5.32)$$

With the aid of expression (5.32) were designed the radiation patterns of slot for $\gamma=2$ (curve 1 in Fig. 5.9). The same figure gives precise values of the radiation pattern $H(\vartheta, 0, \gamma)$, designed

according to expression (3.18) (curve 2). The comparison of the
results of the approximate and precise calculations shows that
Kirchhoff's method satisfactorily describes the radiation pattern of
slot in the region of major lobe, first minor lobes and in the
monotonically decreasing section of radiation pattern in the region
of the penumbra where the dominant role plays the radiation/emission
of the current wave, half-plane incoming to the edge.

Page 124.

In the remote minor lobes and in the shadow zone far from $\vartheta = 180°$
method gives noticeable errors as a result of the fact that the
approximation/approach of Kirchhoff does not consider currents,
reflected from the edge of half-plane and flowing in to the shadow
side of screen. In proportion to the removal/distance of slot from
the edge of half-plane the sector of angles in which Kirchhoff's
method gives satisfactory results, is expanded, since decreases the
strength of current, which encounters to the edge of half-plane.

Let us now examine the ground wave

$$H_y = e^{-\gamma k z} e^{-i k \sqrt{1+\gamma^2}\, x},$$

$$E_z = -i \frac{\gamma k}{\omega \varepsilon} e^{-\gamma k z} e^{-i k \sqrt{1+\gamma^2}\, x}; \qquad (5.33)$$

encountering from infinity to the edge/fin of impedance half-plane.
The standardized/normalized radiation pattern of this system is

determined by expression [52]

$$f(\varphi) = \frac{\eta^2 \sin^2 \frac{\varphi}{2}}{\eta^2 + \sin^2 \varphi}. \qquad (5.34)$$
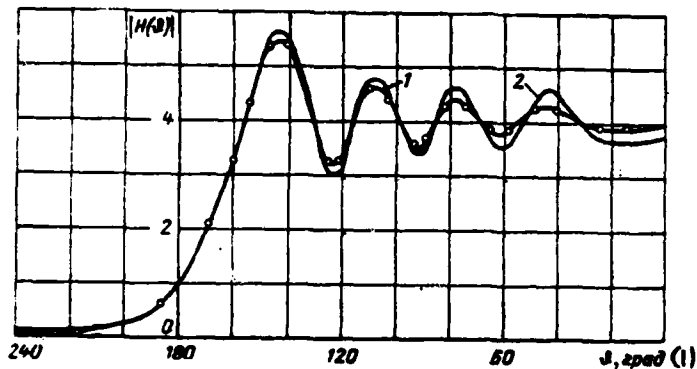
Fig. 5.9. To evaluation/estimate of the accuracy of the approximation/approach of Kirchhoff $(\eta = 0)$.

Key: (1). deg.

Page 125.

Formula (5.34) shows that diagram $f(\varphi)$ is symmetrical relative to direction $\varphi = \pi$ and has a maximum in the direction of propagation of ground wave. With $\varphi = 0$ the radiation pattern is always equal to zero.

Using expressions (5.33) and (1.62), it is not difficult to calculate the radiation pattern of ground wave in the approximation/approach of Kirchhoff:

$$f'(\varphi) = \frac{(\sqrt{1+\eta^2}-1)^2}{\eta^2} \cdot \frac{\eta^2 + \sin^2\varphi}{(\sqrt{1+\eta^2}+\cos\varphi)^2}. \qquad (5.35)$$

Expression (5.35) also symmetrically and has a maximum in the direction $\varphi = \pi$. However, with $\varphi = 0$ diagram is not turned into zero when $\eta \neq 0$. For the quantitative evaluation/estimate of the approximation/approach of Kirchhoff Fig. 5.10 gives the results of calculation according to precise (5.34) and that approximated (5.35) to formulas for several values $\eta$. The comparison of results shows that precise and approximated diagrams are substantially distinguished only in the sector of angles, close to $\varphi = 0$. Thus, it is possible to conclude that Kirchhoff's method is suitable for performance calculation of the radiation/emission of the sources, arranged/located on the impedance half-plane.
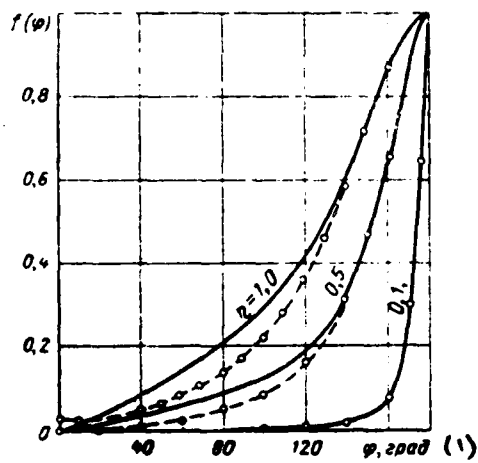
Fig. 5.10. To evaluation/estimate of the accuracy of the approximation/approach of Kirchoff small circles showed approximate values.

Key: (1). deg.

Page 126.

6. Radiation characteristics of antennas, which are located on the bodies with the constant and weakly changing curvature.

Bodies from the constant or weakly changing by surface curvature relate to the important and very vast class of aerodynamic objects. To the analysis of radiation of antennas, which are located on the bodies of the form indicated, are dedicated the investigations of a number of the Soviet and foreign authors. In the work of Pistol'kors [2], [3] is solved the problem about the radiation/emission of the slots, arranged/located on the surface of cylinder. Belkina and Weinstein [23] in detail investigated the characteristics of elementary sources, which are located on the sphere. White [57, 58] obtained a number of interesting results, which relate to radiation of the antennas, arranged/located on the cylinder.

Detailed bibliography on the question in question the reader can find in works [4, 59].

In present chapter, in contrast to the cited works, primary attention is given to the analysis of the radiation characteristics of the antennas, which possess sufficiently high directivity. The

obtained results make it possible to rate/estimate, as they affect constant, slowly changing to rate/estimate, as affect the constant, slowly changing and dual surface curvature shaping of the antenna radiation pattern.

6.1. Radiation patterns of the thin slots, arranged/located on the cylinder.

Let us examine the characteristics of elementary slotted emitters, which are located on the surface of the ideally conduct circular cylinder.

For calculating the radiation patterns $G(\varphi)$ of the thin slots, which are located at point O (Fig. 6.1), we will use relationships/ratios (1.6) and (1.59), (1.60).

Page 127.

After simple conversions we will obtain

$$G_{\shortparallel}(\eta) = \frac{2}{\pi \varkappa a} \sum_{0}^{\infty} \varepsilon_n \frac{e^{-i\frac{n\pi}{2}}}{H_n^{(1)}(\varkappa a)} \cos n\varphi \qquad (6.1)$$

for the parallel and

$$G_{\perp}(\varphi) = \frac{2}{\pi \varkappa a} \sum_{0}^{\infty} \varepsilon_n \frac{e^{-i\frac{n\pi}{2}}}{H_n^{(1)'}(\varkappa a)} \cos n\varphi \qquad (6.2)$$

for the perpendicular polarization.

If tangential electric field $E_z(\varphi)$ or $E_\varphi(\varphi)$ is assigned in the section of the surface of cylinder with $\varphi_1 \leqslant \varphi \leqslant \varphi_2$, then the corresponding radiation patterns can be expressed through $G(\varphi)$ with the aid of the relationships/ratios

$$f_\parallel(\varphi) = \int_{\varphi_1}^{\varphi_2} E_z(\varphi + \psi) G_\parallel(\psi) d\psi, \qquad (6.3)$$

$$f_\perp(\varphi) = \int_{\varphi_1}^{\varphi_2} E_\varphi(\varphi + \psi) G_\perp(\psi) d\psi. \qquad (6.4)$$
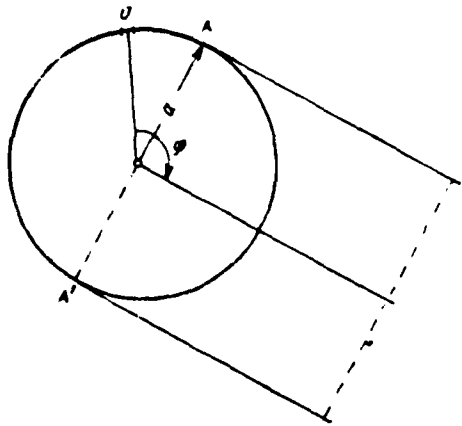
Fig. 6.1. On the calculation of the radiation pattern of slot in the surface of circular cylinder.


Page 128.


According to formulas (6.1), (6.2) was carried out numerical calculation for the series/row of the values of parameter ka. Since us interest mainly the radiation patterns, subsequently will be examined functions $G(\varphi)$, in reference to the maximum values. Fig. 6.2 and 6.3 give the amplitude and phase radiation patterns, constructed depending on angular coordinate $\varphi$, for several values of parameter ka.
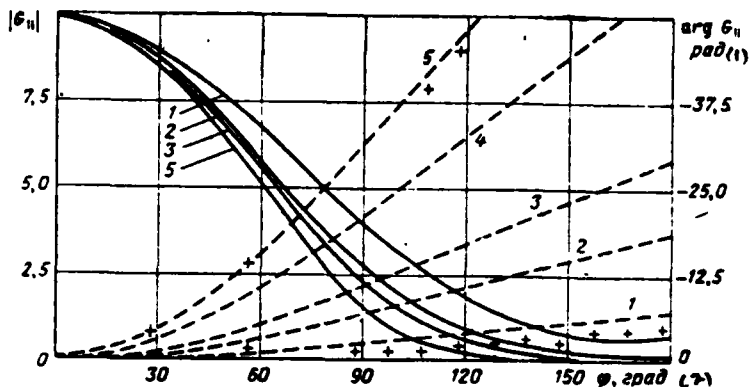
Fig. 6.2. Dependences $|G_\parallel(\varphi)|$ (solid lines) and $\arg G_\parallel(\varphi)$ (dotted lines):

1) $\kappa a = 2$; 2) $\kappa a = 6$; 3) $\kappa a = 10$; 4) $\kappa a = 20$; 5) $\kappa a = 30$.
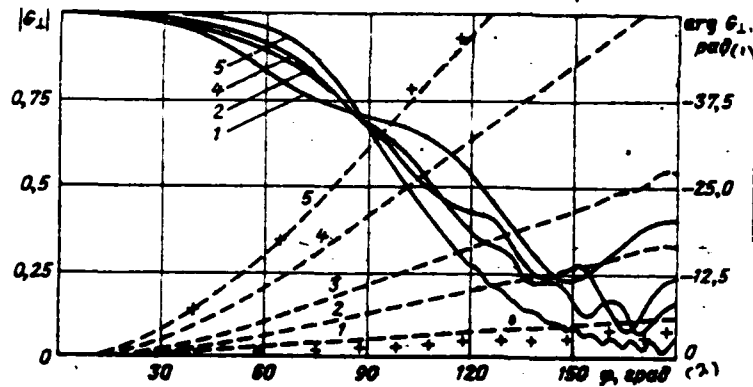
Key: (1). rad. (2). deg.



Fig. 6.3. Dependences $|G_\perp(\varphi)|$ (solid lines) and $\arg G_\perp(\varphi)$ (dotted lines):

1) $\kappa a = 2$; 2) $\kappa a = 6$; 3) $\kappa a = 10$; 4) $\kappa a = 20$; 5) $\kappa a = 30$.

Key: (1). rad. (2). deg.

Page 130.


If slot is located with $\varphi=0$, then the maximum of its radiation
pattern is always oriented in the direction $\varphi=0$. With an increase in
the angle $\varphi$ of function $|G(\varphi)|$ for the parallel and perpendicular
polarization monotonically they drop, and in the shadow zone diagrams
become cut as a result of interaction of two radiating points A, A'
(Fig. 6.1). In direction of $\varphi=180°$ fields, emitted by points A and
A', store/add up, and radiation patterns have a maximum. The phase of
the field of slot in far zone with $|\varphi|<\pi/2$ is close to phase $\Phi(O)$ of
point source, arranged/located at point O (Fig. 6.1) in the absence
of cylinder, and in the region $\pi>|\varphi|>\pi/2$ is close to phase $\Phi(OA)$ of
point source, placed at point A (Fig. 6.1) and excited with the time
lag which corresponds to distance of OA, calculated on the circular
arc. Values $\Phi(O)$ and $\Phi(OA)$ for ka=2 and ka=30 are noted in Fig. 6.2
and 6.3 by crosses.


In the case of the polarization, which corresponds to the
transverse slot (Fig. 6.2), function $G_{\parallel}(\varphi)$ monotonically drops with
the increase/growth $\varphi$. Small flash-ups appear only at $\varphi\sim180°$.
Radiation level in the opposite direction monotonically decreases
with increase of ka. During the polarization, which corresponds to
the longitudinal slot, function $G_{\perp}(\varphi)$ more weakly drops with an
increase in the angle $\varphi$. The brokenness of radiation patterns with

φ>π/2 is expressed more sharply, that as the flowing in of currents into the shadow zone in the case of perpendicular polarization considerably stronger. It should be noted that if field level in direction of φ=180° and in this case also monotonically drops with increase of ka, then in direction of φ=90° radiation level of the longitudinal slot is approximately constant and equal to 0.7.

Calculation according to formulas (6.1), (6.2) is suitable for any values parameter ka. However, with increase in ka it becomes very bulky. Therefore it is expedient to examine approximations for functions G(φ), valid at the high values of ka. For this purpose we will use the solution of the problem of diffracting the plane wave on arbitrary convex ideally conductive body [15].

Page 130.

Utilizing this solution [formulas (1.65), (1.66)], and also relationship/ratio (1.6), we obtain the following expressions for the radiation patterns of the thin slots on the cylinder of the large radius:

$$G_{\parallel} = f(\xi)\, e^{-i\pi\alpha(\pi/2-\varphi)}; \qquad (6.5)$$

$$G_{\perp} = g(\xi)\, e^{-i\pi\alpha(\pi/2-\varphi)} \qquad (6.6)$$

during the parallel and perpendicular polarizations respectively. In

expressions (6.5) and (6.6)

$$\xi = \sqrt[3]{\frac{\varkappa a}{2}}\left(\varphi - \frac{\pi}{2}\right). \qquad (6.7)$$

For the comparison of the approximation formulas with precise ones in Fig. 6.4, 6.5 to scale of the universal parameter $\xi$ are constructed precise and approximate values of the amplitude and phase radiation patterns of thin slots. During the construction of phase diagram was excluded the trivial dependence arg G on ka. From the figures we see that already for values of $\varkappa a \approx 6$ the approximate curves satisfactorily coincide with precise ones.
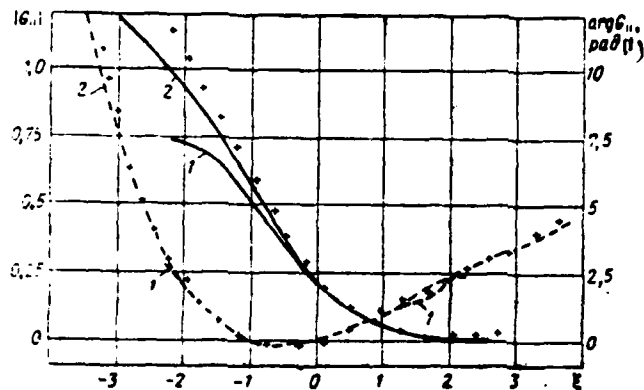
Fig. 6.4. Dependences $|G_{\|}(\xi)|$ (solid lines) and argG($\xi$) (dotted lines): 1) ka=6; 2) ka=30. Crosses designated asymptotic values $|G_{\|}(\xi)|$ and arg$G_{\|}(\xi)$.

Key: (1). rad.

Page 131.

During the perpendicular polarization the coincidence of results of precise and approximate computations in the illuminated region is better than in the shadow zone, since the given approximation formulas do not consider diffraction waves, several times of those bypassed around the cylinder. For another polarization the coincidence is better in the shadow zone and penumbra where precise and approximate curves virtually run together.

On the basis of the analysis Fig. 6.4 and 6.5 it is possible to conclude that for the cylinders whose radius more or is commensurated with the wavelength, it is possible to use approximations (6.5), (6.6) for calculating the functions $G(\varphi)$ (with exception of region $\xi < -1$ during the parallel polarization).

In conclusion let us note that has the capability to obtain a more precise approximation/approach, which considers the repeated run of diffraction waves around cylinder [60]. In this case expressions for Green's functions are represented in the form of the series/row whose members correspond to fundamental and repeatedly bypassed current waves.
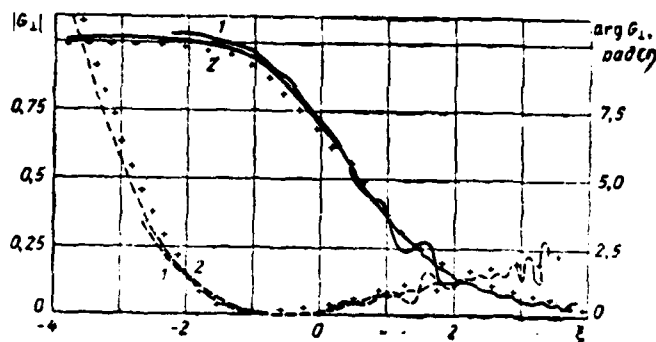
Fig. 6.5. Dependence $|G_\perp(\xi)|$ (solid lines) and $\arg G_\perp(\xi)$ (dotted lines):
1) ka=6; 2) ka=30. Crosses designated asymptotic values $|G_\perp(\xi)|$ and $\arg G_\perp(\xi)$.

Key: (1). rad.

Page 132.

Without carrying out detailed analysis of refined approximate

solution, let us point out only that the more accurate result is

obtained by the value of the insignificant complication of

calculation. The comparison of the results, obtained in a refined

manner (were considered only two members of asymptotic series/row),

with precise ones (Fig. 6.6) shows that even for ka=2 coincidence of

precise and approximate values $G_\perp(\varphi)$ is completely satisfactory.
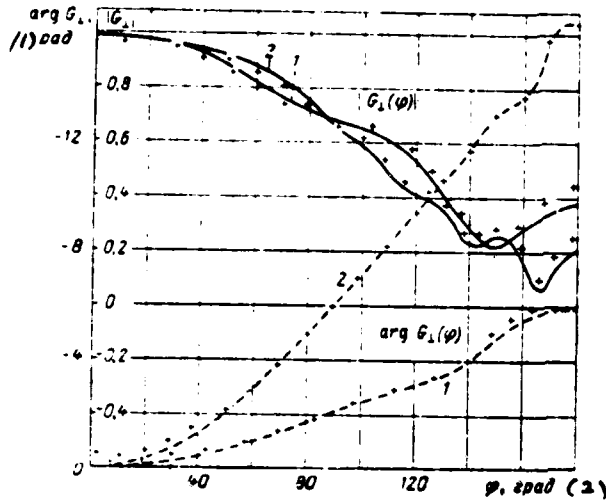
Fig. 6.6. Dependences $|G_\perp(\varphi)|$ (solid lines) and $\arg G_\perp(\varphi)$ (dotted lines): 1) ka=2, 2) ka=6. crosses designated refined asymptotic values $|G_\perp|$ and $G_\perp$.

Key: (1). rad. (2). deg.

## 6.2. Radiation/emission of the sources, arranged/located on the surface of the ideally conducting sphere.

With the solution of the problem about the radiation/emission of the sources of electromagnetic field, arranged/located on the surface of the conducting sphere, it is necessary to solve vector problem. The solution of this problem for the case when plane wave falls on the sphere in the direction of the negative z axis, and vector $\vec{E}$ is

parallel to axis x (Fig. 6.7), it is given in S 1.3.

Page 133.

Let us show how, using this solution, and also reciprocity theorem (1.6), it is possible to obtain the radiation pattern of the arbitrary sources, arranged/located on the sphere.

Let on the sphere at point with the radius-vector $\vec{\rho_0} = \vec{\rho}a\,(|\vec{\rho}| = 1)$ and coordinates $\{a\sin\vartheta_0\cos\varphi_0;\ a\sin\vartheta_0\sin\varphi_0;\ a\cos\vartheta_0\}$ (Fig. 6.7) assign tangential electric field $\vec{E_\tau}(\vartheta_0, \varphi_0)$ and it is necessary to find the radiation/emission of this source in the direction of unit vector $\vec{r} = \{\sin\vartheta\cos\varphi,\ \sin\vartheta\sin\varphi,\ \cos\vartheta\}$. So that it would be more convenient to use the results of Chapter 1, let us introduce the support systems of the coordinates:

$$
\begin{aligned}
\vec{x_1} &= [\vec{y_1}, \vec{z_1}],\ \vec{x_2} = -\vec{y_1}; \\
\vec{y_1} &= \frac{[\vec{r}, \vec{\rho}]}{|[\vec{r}, \vec{\rho}]|},\ \vec{y_2} = \vec{x_1}; \\
\vec{z_1} &= \vec{r},\ \vec{z_2} = \vec{z_1}.
\end{aligned}
\right\} \qquad (6.8)
$$
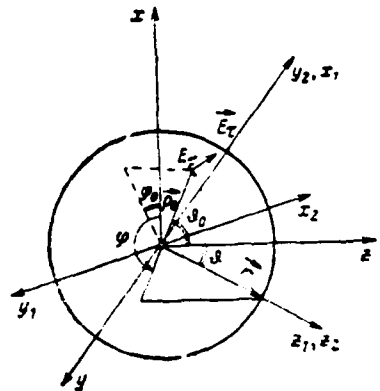
Fig. 6.7. To performance calculation of the radiation/emission of source, arranged/located on the sphere.

Page 134.


It is obvious that in the systems of coordinates (6.8) the components of the radiation field of the source in question, parallel to axes $\vec{x}_1$, $\vec{x}_2$, are excited by the components

$$\vec{E}_{v1} = \vec{E}_v - (\vec{E}_v, \vec{y}_1)\vec{y}_1, \qquad (6.9)$$

$$\vec{E}_{v2} = (\vec{E}_v, \vec{x}_2)\vec{x}_2. \qquad (6.10)$$

Then in accordance with expressions (1.6) and (1.60) the radiation pattern of the emitter in question can be represented as follows:

$$\vec{E} = ([\vec{E}_{v1}, \vec{y}_1|\vec{\rho})\vec{x}_1\Phi'(\theta_1)' + ([\vec{E}_{v2}, [\vec{\rho}, \vec{x}_2]]\vec{\rho})\vec{x}_2\theta(\theta_1). \qquad (6.11)$$

where

$$\cos\theta_1 = \vec{\rho}\,\vec{r}.$$

Components of field $\vec{E}$ along the directions

$$\vec{\varphi} = \frac{[\vec{z}, \vec{r}]}{|[\vec{z}, \vec{r}]|}^{(1)}_{H} \cdot \vec{\vartheta} = [\vec{\varphi}, \vec{r}] \cdot \qquad (6.12)$$

Key: (1) and.


they can be found from the relationships/ratios

$$E_\varphi(\vartheta, \varphi, \vartheta_0, \varphi_0) = \vec{E}\vec{\varphi}; \quad E_\vartheta(\vartheta, \varphi, \vartheta_0, \varphi_0) = \vec{E}\vec{\vartheta}. \qquad (6.13)$$

Let us examine the special case, when by the source of field is the point slot, arranged/located at point with the coordinates $\vec{\rho}_0 = \{$

0, 0, a }, moreover the vector of electric field in the slot is
parallel to axis $x$ $\vec{E}_\tau = \{1, 0, 0\}$ (Fig. 6.7). From formulas (6.11) and
(6.13) it follows that in the plane $\varphi = 0$ the radiation pattern of this
slot takes the form

$$E_\vartheta(\vartheta) = \Phi(\vartheta). \qquad (6.14)$$

since $E_\varphi(\vartheta) = 0$.


In the plane $\varphi = \pi/2$, on the contrary, $E_\vartheta(\vartheta) = 0$, and radiation
pattern

$$E_\varphi(\vartheta) = \Theta(\vartheta). \qquad (6.15)$$

Functions $\Phi$ and $\Theta$ are the complex functions of angle $\vartheta$.


Let us examine amplitude radiation patterns $|\Phi(\vartheta)|$ and $|\Theta(\vartheta)|$ for
several values of parameter $ka$ and let us compare them with the
appropriate diagrams of the slots, gashed in the surface of the
ideally conducting cylinder. In this case, obviously, $|\Phi(\vartheta)|$ one
should compare with function $|G_\perp(\vartheta)|$ (6.2), and $|\Theta(\vartheta)|$ with $|G_\parallel(\vartheta)|$ (6.1).


Fig. 6.8 and 6.9 give computed values of radiation patterns
$|\Psi(\vartheta)|$ and $|G_\perp(\vartheta)|$, $|\Theta(\vartheta)|$ and $|G_\parallel(\vartheta)|$. The values of the radiation
patterns of slot on the sphere are borrowed from work [23]. The
comparison of the curves, which correspond $|\Phi(\vartheta)|$ and $|G_\perp(\vartheta)|$, $|\Theta(\vartheta)|$ and
$|G_\parallel(\vartheta)|$ shows that in the region of light/world and in the penumbra
the radiation patterns of slots on the cylinder and sphere change in

the dependence on the angle $\vartheta$ analogously, moreover the resemblance between the compared diagrams is more noticeable, the greater the parameter ka. However, in the shadow zone even at the high values of product ka remains the difference between the radiation patterns, which correspond to cylinder and sphere. In particular, values $|\dot{\Phi}(\vartheta)|$ and $|\Theta(\vartheta)|$ for the direction $\vartheta=\pi$ coincide.
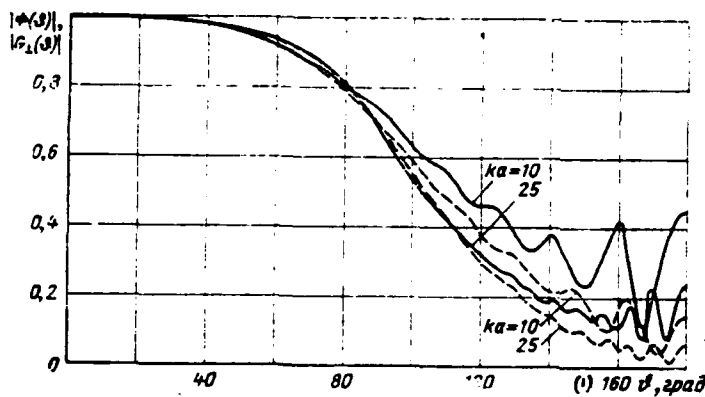
Fig. 6.8. Comparison of the radiation patterns of the elementary sources, arranged/located on the sphere (solid line) and the cylinder (dotted line).


Key: (1). deg.


Page 136.


This physically obvious result escape/ensues, for example, from relationships/ratios (6.14) and (6.13). At the same time for the cylinder the equality of values $G_{\perp}(\pi)$ and $G_{\parallel}(\varphi)$ is not made with any ka. However, with an increase in value ka becomes narrow the angular sector, in which the radiation patterns of the slots, located on the cylinder and the sphere, substantially are distinguished. Thus, the given analysis confirms the conclusion, made in Chapter 1, about the

weak dependence of the main section of the antenna radiation pattern, arranged/located on the convex body, on the surface curvature in the plane, perpendicular to main section.
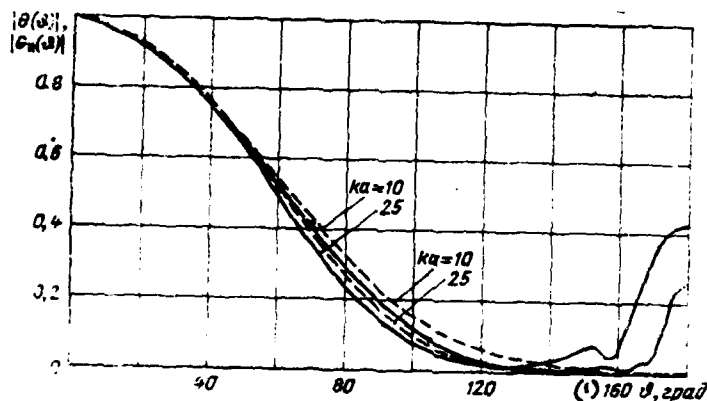
Fig. 6.9. Comparison of the radiation patterns of the elementary sources, arranged/located on the sphere (solid line) and the cylinder (dotted line).

Key: (1). deg.

## 6.3. Optimum field distributions on the cylinder.

Let us examine field distributions on the cylinder, which make it possible to obtain the optimum value of the directive gain of surface antenna. Let on the surface of cylinder be is assigned arbitrary field distribution

$$E_{z, \varphi} = \sum_{n=0}^{\infty} a_n \cos n\varphi. \qquad (6.16)$$

Page 137.

In accordance with expressions (6.1)-(6.4) field distribution (6.16) creates radiation pattern

$$f(\varphi) = \sum_{n=1}^{\infty} a_n c_n \cos n\varphi = \sum_{n=1}^{\infty} d_n \cos n\varphi, \qquad (6.17)$$

where

$$c_n = \frac{e^{-i\frac{n\pi}{2}}}{H_n^{(1)}(\kappa a)}$$

during the parallel polarization and

$$c_n = \frac{e^{-i\frac{n\pi}{2}}}{H_n^{(1)'}(\kappa a)}$$

during perpendicular polarization.

Since the discussion deals with two-dimensional problem, the directive gain of the antenna in question in the direction $\varphi=0$ according to formula (2.18) is equal to

$$K = 2 \frac{(\Sigma \alpha_n)^2 + (\Sigma \beta_n)^2}{\sum \frac{1}{\epsilon_n}(\alpha_n^2 + \beta_n^2)}, \qquad (6.18)$$

where $\alpha_n + i\beta_n = d_n$.

Expression (6.18) is maximal, if

$$\alpha_n = \alpha \epsilon_n, \quad \beta_n = \beta \epsilon_n. \qquad (6.19)$$

Since constants $\alpha$, $\beta$ do not affect value derictive gain, it is possible to consider that $d_n = \epsilon_n(1+i)$ and, therefore, the optimum values of the coefficients

$$a_n = \frac{\epsilon_n}{c_n}. \qquad (6.20)$$

From expressions (6.18), (6.19) it follows that the radiation
pattern, created by "optimum" field distribution, possesses infinite
directive gain (k.n.d.). However, the in actuality attainable value
derictive gain has a limit. This is connected with the fact that it
is not possible to excite on the surface of cylinder the high
harmonics of field with the assigned amplitudes.

Page 138.

From the simple physical considerations it is clear that for the
reproduction of the n harmonic of field on the cylinder it is
required at least 2n slots, moreover adjacent slots must be excited
in the antiphase. At the same time on the cylinder of radius a it is
placed ka waves. Therefore in practice during finding of optimum
distribution it is expedient to be limited to a finite number of
harmonics, assuming that

$$E_z(\varphi) = \sum_{n=0}^{N} a_n e^{i\frac{n\pi}{2}} H_n^{(1)}(\kappa a) \cos n\varphi, \qquad (6.21)$$

$$E_\varphi(\varphi) = \sum_{n=0}^{N} a_n e^{i\frac{n\pi}{2}} H_n^{(1)\prime}(\kappa a) \cos n\varphi, \qquad (6.22)$$

where N=ka.

The optimum standardized/normalized radiation pattern at the
assigned value of N of a number of harmonics takes the form

$$f_N(\varphi) = \frac{\sin\left(\frac{2N+1}{2}\varphi\right)}{(2N+1)\sin\frac{\varphi}{2}}. \qquad (6.23)$$

The corresponding value derictive gain is equal to

$$K_N = 2N + 1. \qquad (6.24)$$

Expression (6.23) for the radiation pattern sufficiently simple and can be investigated in general form. For the analysis of optimum distributions (6.21), (6.22) were carried out detailed numerical calculations.

As one would expect, the amplitude of optimum distribution has a character of the oscillating function. A number of maximums (or the minimums) of amplitude distribution virtually coincides with a number of harmonics N. When a number of harmonics does not exceed a number of wavelengths, which are placed on the perimeter of cylinder, the range of oscillations of amplitude is comparatively small and on average amplitude decreases in proportion to removal/distance from the direction $\varphi = 0$. When $N \gg ka$, the range of oscillations sharply grows/rises, and the average/mean level of amplitude remains in effect constant on the entire circle/circumference of cylinder.

Page 139.

The phase of optimum distribution with an increase in the angle
φ monotonically grows/rises, the flattest sections of curve $\Phi(\varphi)$
corresponding to maximums, and steepest/most abrupt - to minimums in
amplitude distribution. Phase response $\Phi(\varphi)$, corresponding to optimum
field distribution on the cylinder, was compared with phase
distribution

$$\Phi_0 = \kappa a (1 - \cos \varphi), \qquad (6.25)$$

which in the approximation/approach of geometric optic/optics
provides the flat/plane phase front of field near the cylinder. As a
result of comparison it turned out that for N=ka difference

$\Delta\Phi=\Phi-\Phi_0$ differs from constant not more than by +-0.5 rad, i.e.,
actually/really optimum phase distribution creates approximately
flat/plane phase front near the cylinder. For a number of harmonics
N, which differs from ka, difference $\Delta\Phi$ proves to be considerably
greater (Fig. 6.10).
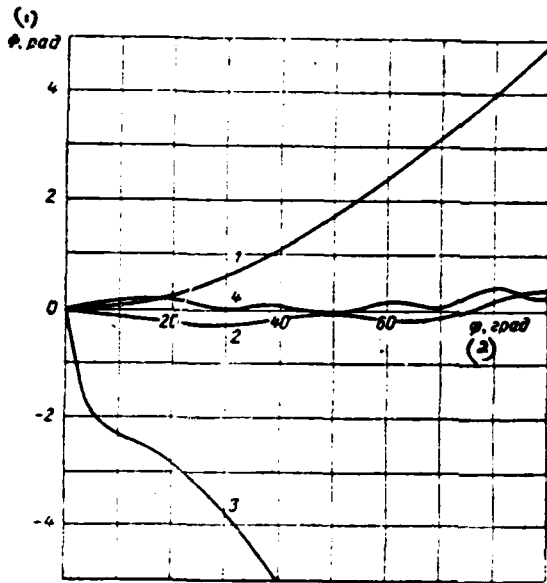
Fig. 6.10. To the analysis of optimum phase distributions on the cylinder during the perpendicular polarization: 1) ka=5, N=2; 2) ka=5, N=5; 3) ka=5, N=9; 4) ka=10, N=10.


Key: (1). rad. (2). deg.


Page 140.


The differences between the optimum distributions for the case of parallel and perpendicular polarizations are insignificant. Fig. 6.11, 6.12 give characteristic optimum amplitude distributions and phases, which correspond to parallel and perpendicular polarizations

and to different values ka. Optimum distributions for different values of N with constant value ka=5 are depicted in Fig. 6.13 and 6.14.

Let us examine the possibility of designing of the radiation patterns, determined by formula (6.23), with the aid of the thin slots, gashed in the surface of cylinder. We will consider that in the case of parallel polarization the width of slot is equal to half of wavelength and corresponding field distribution in it changes on the cosine. In the case of polarization $E_\perp$ the slot infinitely thin and field in it takes the form of delta function. The amplitudes of the excitation of slots let us take as equal to the values of the amplitudes of optimum distributions (6.21) and (6.22) at the points, which coincide with the centers of slots. Radiation patterns f'($\varphi$) the system of slots during both polarizations can be recorded in the following form:

$$f'(\varphi) = \sum_{i=0}^{2\pi a} E^\circ(\psi_i) F(\varphi - \psi_i), \qquad (6.26)$$

where $\psi_i$ - the angular coordinate of the i slot;

F($\varphi$) - the radiation pattern of single slots during the parallel or perpendicular polarization.

$$F_{\parallel}(\varphi) = \int_{-\pi/2\pi a}^{\pi/2\pi a} G_{\parallel}(\varphi - \psi) \cos \varkappa a\psi d\psi,$$
$$F_{\perp}(\varphi) = G_{\perp}(\varphi).$$

Fig. 6.15 depicts radiation pattern $f'_{\parallel}(\varphi)$, appropriate ka=6, diagram for continuous optimum distribution (6.21), and also the diagram, created by six slots, arranged/located on the surface of cylinder with $0 \leqslant \varphi \leqslant \pi/2$.

The examination of Fig. 6.15 shows that the side-lobe level of radiation pattern $f'_{\parallel}(\varphi)$ is 2.5-3 times more than in "ideal" diagram $f_{\parallel}(\varphi)$.

Page 141.
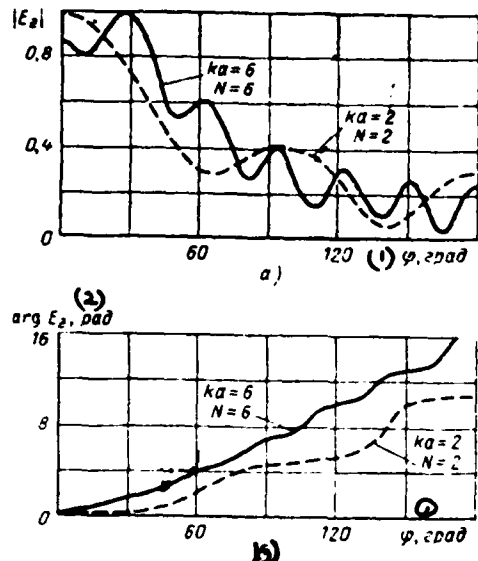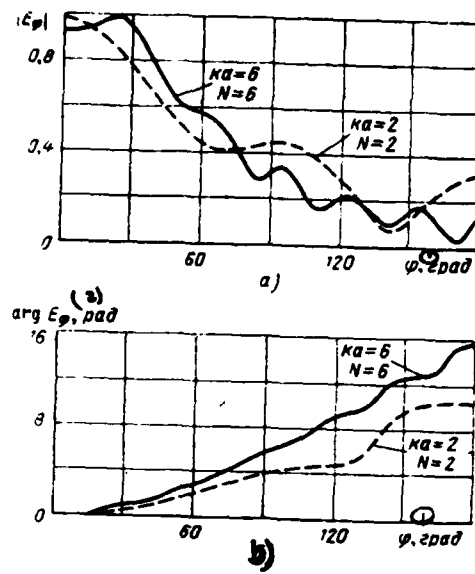


Fig. 6.11.                    Fig. 6.12.


Fig. 6.11. Optimum amplitude distribution (a) and phase (b) on cylinder during parallel polarization.


Key: (1). deg. (2). rad.


Fig. 6.12. Optimum amplitude distribution (a) and phase (b) on cylinder during perpendicular polarization.


Key: (1). deg. (2). rad.

233

Page 142.
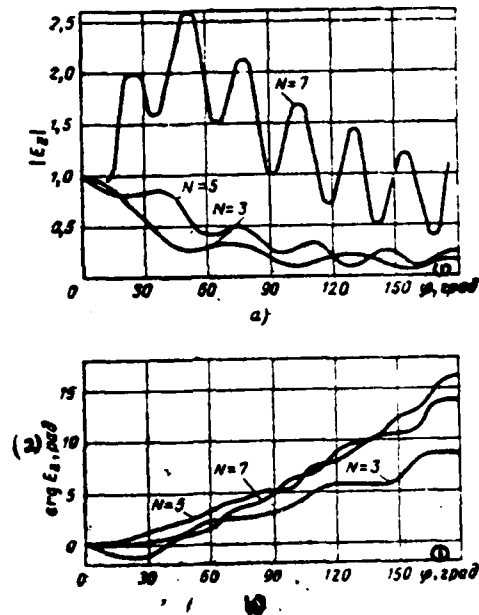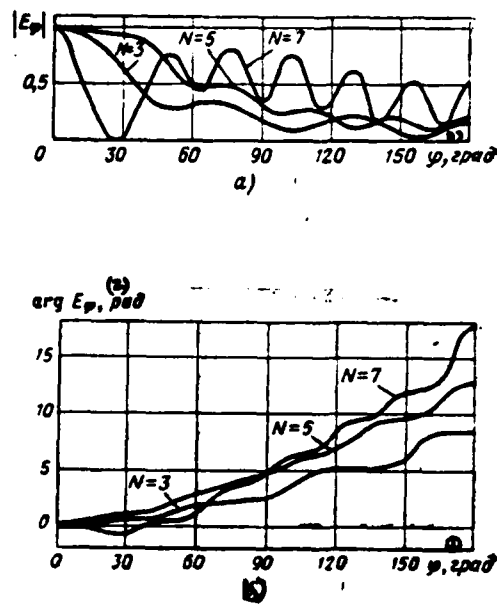


Fig. 6.13

Fig. 6.14

Fig. 6.13. Optimum distributions of amplitude (a) and phase
(b) of a field or a cylinder with parallel polarization for
various values of N and ka=5.

Key: (1). deg. (2). rad.

Fig. 6.14. Optimum distributions of amplitude (a) and phase (b)
of a field or a cylinder with perpendicular polarization for
various values of N and ka=5.

Key: (1). deg. (2). rad.

Page 143.


Derictive gains of the systems of slotted emitters in question
somewhat less than the "ideal" (6.24).


   For the perpendicular polarization, as one would expect, the
radiation patterns of the systems of slots more greatly differ from
"ideal" diagram. In connection with this for the perpendicular
polarization were designed the radiation patterns of the slots,
arranged/located at a distance quarter wavelength from each other. In
this case a difference in the designed diagrams from the ideal is
virtually unessential.
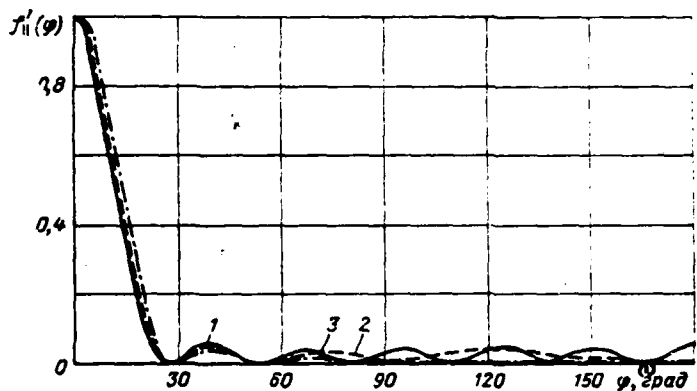
Fig. 6.15. To the evaluation/estimate of the discontinuous distributions of field on the cylinder during the parallel polarization: 1 - radiation pattern $'_{\parallel}(\varphi)$; 2 - the diagram of six slots, arranged/located with $0 \leqslant \varphi \leqslant \pi/2$, 3 - "ideal" radiation pattern.

## 6.4. Traveling-wave antennas on the cylinder.

Let us examine how affects the conducting cylindrical surface to the antenna radiation pattern of the traveling wave. Of practical interest this problem is only when a radius of the cylindrical surface a is great in comparison with the wavelength and the size/dimension of antenna L. Since we will examine the case, which corresponds ka>>1, the results of present paragraph to a determined degree they relate also to the traveling-wave antennas arranged/located on the conducting sphere.

Page 144.


It is possible to show that the directed properties of
traveling-wave antenna are retained, if the length of antenna differs
from the chord length, which connects its ends/leads, not more than
on $\lambda/8$. This condition is satisfied with

$$\frac{R}{\lambda} \geqslant 0.6 \frac{L\sqrt{L}}{\lambda\sqrt{\lambda}}. \qquad (6.27)$$

For the antenna in all in several wavelengths values $R/\lambda$ indicated
become such large that a strict solution of problem is virtually
unsuitable for the investigation due to the complexity of numerical
calculation. However, precisely for the high values of $R/\lambda$ good
results gives approximate theory [15], briefly presented in $\S$ 1.3.


Let us assign amplitude-phase field distribution along the
antenna in the following form:

$$B(s) = A(s)\, e^{i\beta s}, \qquad (6.28)$$

where s - arc length, calculated over the surface of cylinder. In
this case the antenna radiation patterns during the parallel and
perpendicular polarizations can be calculated by the formulas:

$$f_\parallel(\psi) = \int_{-1/2}^{1/2} A(s) e^{i(\beta - \varkappa)s} f(\xi)\, ds; \qquad (6.29)$$

$$f_\perp(\psi) = \int_{-1/2}^{1/2} A_-(s) e^{i(\beta - \varkappa)s} g(\xi)\, ds. \qquad (6.30)$$

where $f(\xi)$ and $g(\xi)$ are determined in S 1.3, and

$$\xi = \sqrt[3]{\frac{\varkappa R}{2}}\left(\psi - \frac{s}{R}\right).$$

For functions $f(\xi)$ and $g(\xi)$ are detailed tables, so that the problem of calculating the radiation patterns $f(\psi)$ is reduced to the numerical integration.

Page 145.

However, if is satisfied condition (6.27), in expressions (6.29), (6.30) it is possible to assume

$$f_\parallel(\psi) = \left| f\left(\sqrt[3]{\frac{\varkappa R}{2}}\,\psi\right) \right| \int_{-1/2}^{1/2} A(s) \exp\left[i(\beta - \varkappa)s + \right.$$
$$\left. + i \arg f(\xi)\right] ds, \qquad (6.31)$$

$$f_\perp(\psi) = \left| g\left(\sqrt[3]{\frac{\varkappa R}{2}}\,\psi\right) \right| \int_{-1/2}^{1/2} A(s) \exp\left[i(\beta - \varkappa)s + \right.$$
$$\left. + i \arg g(\xi)\right] ds. \qquad (6.32)$$
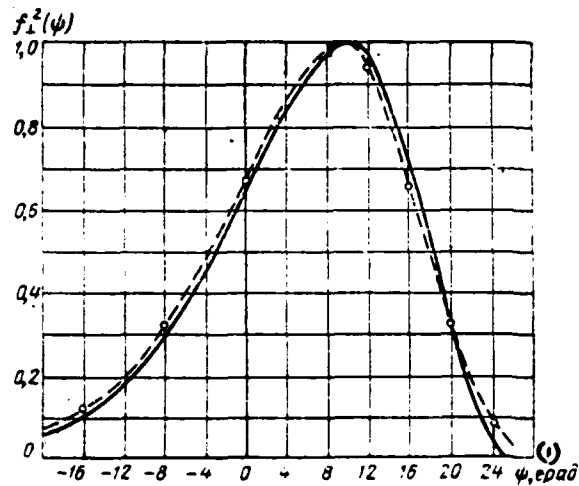
Fig. 6.16. Precise (solid line) and approximated (dotted line) of the antenna radiation pattern of the traveling wave, arranged/located on the cylinder. The length of antenna $L=10\lambda$, a radius of cylinder $31.6\lambda$, i.e., condition (6.27) are made: $A(s)=const$; $\beta=k$.

Key: (1). deg.

Page 146.
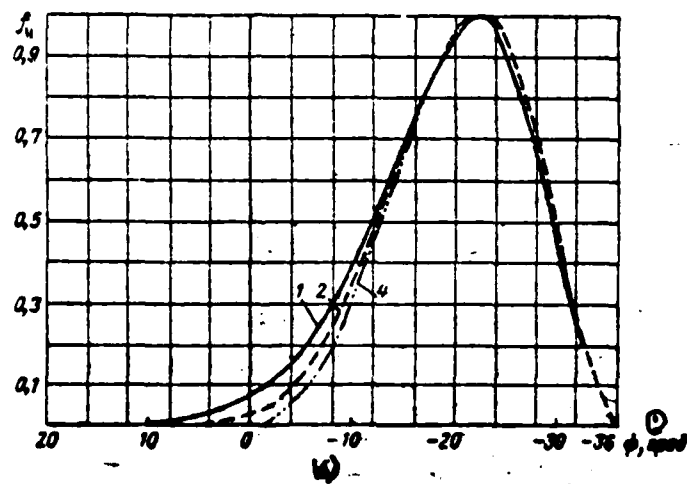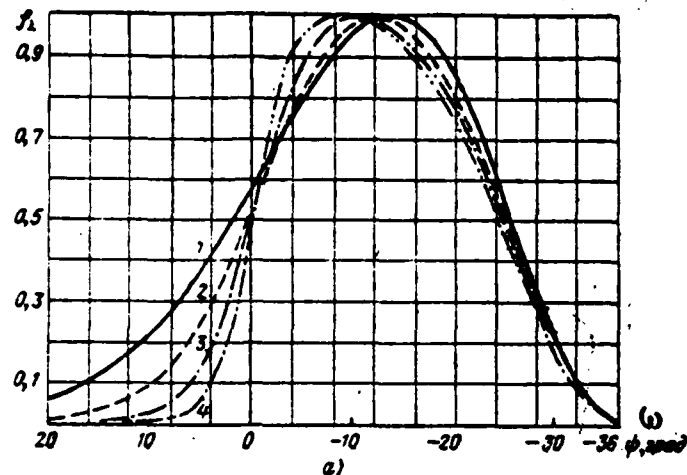


Fig. 6.17. Effect of radius of cylinder on form of radiation pattern during perpendicular (a) and parallel (b) polarizations: 1) R=6.25L; 2) R=25L; 3) R=100L; 4) R=400L.

Key: (1). deg.

Page 147.

In this case for $\psi \leqslant 0$

$$\arg f, \; g \approx -\frac{\xi^3}{3} = \kappa s \frac{\psi^2}{2} \approx \kappa s \, (1 - \cos \psi). \quad (6.33)$$

i.e. in the illuminated region

$$f_\parallel (\psi) \approx f_0 (\psi) \left| f \left( \sqrt[3]{\frac{\kappa R}{2}} \, \psi \right) \right|, \quad (6.34)$$

$$f_\perp (\psi) \approx f_0 (\psi) \left| g \left( \sqrt[3]{\frac{\kappa R}{2}} \, \psi \right) \right|, \quad (6.35)$$

where   $f_0(\psi)$ – antenna radiation pattern in the free space. It is
analogous for angles $\psi > 0$ are approximately valid the following
representations:

$$f_\parallel (\psi) = f_0 (0) \left| f \left( \sqrt[3]{\frac{\kappa R}{2}} \, \psi \right) \right|, \quad (6.36)$$

and $\arg g(\psi)$ $\qquad f_\perp (\psi) = f_0 (0) \left| g \left( \sqrt[3]{\frac{\kappa R}{2}} \, \psi \right) \right|, \quad (6.37)$

since $\arg f(\psi)$ ∧when $\psi > 0$ are close to constant values.


Formulas (6.34)-(6.37) allow simply and with the sufficient
degree of accuracy to design the antenna radiation patterns of the
traveling wave, arranged/located on the cylinder. The results of
calculating the radiation pattern according to formulas (6.34)-(6.37)
and according to precise formulas (6.1), (6.2) virtually coincide
(Fig. 6.16).

In order to trace, as is changed the form of the antenna radiation pattern with a change in the radius of cylinder, let us turn to Fig. 6.17. For both polarizations a change in the radius of cylinder affects mainly the form of the slope of radiation pattern when $\psi > 0$. With an increase in ratio $R/\lambda$ the form of the antenna radiation pattern, arranged/located on the cylinder, gradually emerges by the same as in antenna, which is located on the plane. For the antennas of larger length this transition/junction is completed more rapidly.

6.5. Traveling-wave antennas, arranged/located on the slightly bent/slightly curved surface with variable chamber.

Antennas of the type in question are arranged/located on the surfaces with variable chamber, moreover usually surface curvature is small and changes within small limits, since virtually only in this case antenna can possess high directivity. A slow change in the surface curvature on which is arranged/located the antenna, in the first approximation, can be considered, if to consider that each element/cell of antenna emits in the manner that if it was arranged/located on the surface of the constant curvature, equal to curvature at the point where is located the element/cell in question.

Page 148.


For the illustration of the approximate method indicated let us
conduct the calculation of the antenna radiation pattern of the
traveling wave, arranged/located on the surface of the ideally
conducting parabolic cylinder. The surface of parabolic cylinder is
described by simple equation and at the same time it can approximate
the large class of aerodynamic surfaces. Let on the surface of the
parabolic cylinder

$$y^2 = 2px \qquad (6.38)$$

at a distance of s from the apex/vertex be gashed the thin slot. The
radius of curvature of surface at the point where is arranged/located
slot, is equal to

$$R = \frac{p}{|\sin^3 \varphi_\bullet|}. \qquad (6.39)$$

Angle $\varphi_\bullet$ characterizes the inclination/slope of tangent to the
surface of parabolic cylinder at the point where is located slot, and
it is connected with an arc length s with the relationship/ratio

$$s = -\frac{p}{2}\left(\frac{\cos \varphi_\bullet}{\sin^2 \varphi_\bullet} + \ln\left|\operatorname{ctg} \frac{\varphi_\bullet}{2}\right|\right). \qquad (6.40)$$

In accordance with the approximation/approach accepted the field
of slot in the parabolic cylinder coincides with the
radiation/emission of the slot, gashed in the circular cylinder which
concerns parabolic at the point where is located slot, and has radius

R(6.39). If the center of the cross section of circular cylinder was found in the beginning of coordinates, then the field of slot in the remote zone in the direction $\varphi$ according to (6.5) and (6.6) had a value

$$f^0_{\shortparallel} = e^{i\kappa R(\varphi - \varphi_0)} f\left[\sqrt[3]{\frac{\kappa R}{2}}(\varphi - \varphi_0)\right], \qquad (6.41)$$

$$f^0_{\perp} = e^{i\kappa R(\varphi - \varphi_0)} g\left[\sqrt[3]{\frac{\kappa R}{2}}(\varphi - \varphi_0)\right]. \qquad (6.42)$$

Page 149.

Since in the case in question the axis of circular cylinder runs through the point with the coordinates

$$x_c = p\left(1 + \frac{3}{2\,\mathrm{tg}^2\,\varphi_0}\right), \qquad (6.43)$$

$$y_c = -\frac{p}{\mathrm{tg}^2\,\varphi_0}, \qquad (6.44)$$

the complex radiation patterns of slots take the following form:

$$f_{\shortparallel} = \exp[i\kappa R(\varphi - \varphi_0)] f\left[\sqrt[3]{\frac{\kappa R}{2}}(\varphi - \varphi_0)\right] \times$$
$$\times \exp[-i\kappa(x_c\cos\varphi + y_c\sin\varphi)],$$
$$f_{\perp} = \exp[i\kappa R(\varphi - \varphi_0)] g\left[\sqrt[3]{\frac{\kappa R}{2}}(\varphi - \varphi_0)\right] \times$$
$$\times \exp[-i\kappa(x_c\cos\varphi + y_c\sin\varphi)]. \qquad (6.45)$$

Let us find the antenna radiation pattern of the traveling wave, arranged/located on the surface of parabolic cylinder. Let the antenna have a length L and is located from the vertex of parabola at a distance $\Gamma$. Let us assign amplitude-phase field distribution in antenna aperture in the following form:

$$E(s) = A(s) e^{-i\beta s}. \qquad (6.46)$$

In this case the antenna radiation pattern can be represented as follows:

during the parallel polarization

$$F_\parallel = \int_\Gamma^{\Gamma+L} A(s) \exp[-i\beta s + i\kappa R(\varphi - \varphi_0) -$$
$$- i\kappa(x_c \cos\varphi + y_c \sin\varphi)] f\left[\sqrt[3]{\frac{\kappa R}{2}}(\varphi - \varphi_0)\right] ds, \quad (6.47)$$

during the perpendicular polarization

$$F_\perp = \int_\Gamma^{\Gamma+L} A(s) \exp[-i\beta s + i\kappa R(\varphi - \varphi_0) -$$
$$- i\kappa(x_c \cos\varphi + y_c \sin\varphi)] g\left[\sqrt{\frac{\kappa R}{2}}(\varphi - \varphi_0)\right] ds. \quad (6.48)$$

Calculation according to formulas (6.47), (6.48) is connected with the numerical integration and the solution of equation (6.40). Diagrams (6.47), (6.48) depend on a large number of parameters and therefore the calculation, which claims to the completeness, hardly it is advisable. In connection with this we will be restricted only to a small number of examples.

Page 150.
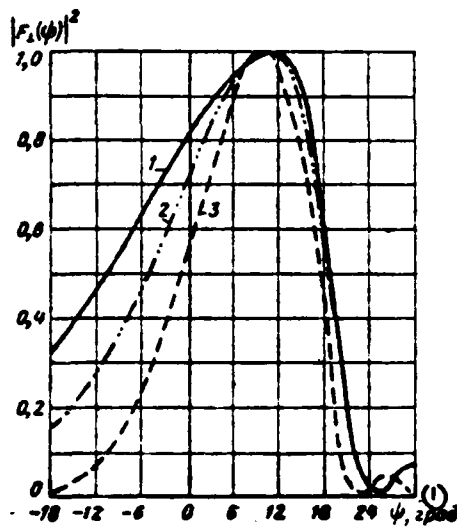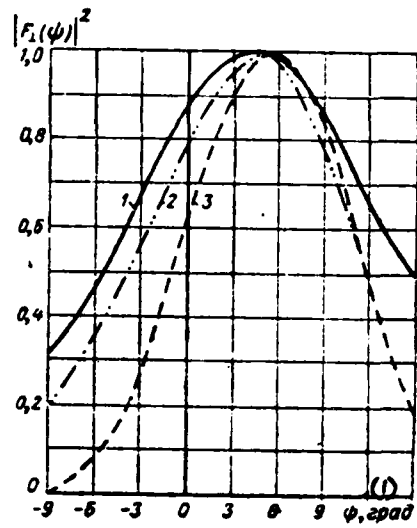


Fig. 6.18.                          Fig. 6.19.

Fig. 6.18. Form of antenna radiation pattern, arranged/located on parabolic cylinder at different values of parameter г:

_1) Г/λ=0; 2) Г/λ=2; 3) Г/λ=10._

Key: (1). deg.

Fig. 6.19. Effect on form of radiation pattern of parameter p: 1) p/λ=10; 2) p/λ=20; 3) p/λ=100.

Key: (1). deg.

Page 151.


Let us examine the antenna of fixed/recorded length (L/λ=5) with

the constant amplitude distribution without supplementary phase

change (β=k). Polarization let us accept perpendicular. In order to

have the possibility to analyze not only the form of radiation

pattern, but also the divergence of diagram from the conducting

surface, let us introduce coordinate $\psi$, connected with the angle φ

with the relationship/ratio

$$\psi = \varphi_0|_{s=\Gamma+L} - \varphi, \qquad (6.49)$$

where $\varphi_0|_{s=\Gamma+L}$ - tangent inclination plane to the surface of parabolic

cylinder at the point, which coincides with the end/lead of the

antenna.


In Fig. 6.18 are constructed the standardized/normalized

radiation patterns $|F_\perp(\psi)|^2$, corresponding p=λ and to different values

Γ. With an increase in distance $\Gamma$ the radiation pattern becomes

narrow, its maximum approaches an "axis" of antenna $(\psi=0)$, and when

$\Gamma/\lambda \to \infty$ the form of diagram emerges by the same as in the antenna,

arranged/located on the plane. Effect on the form of the radiation

pattern $|F_\perp(\psi)|^2$ of parameter p (when $\Gamma=2\lambda$) is illustrated by Fig.

6.19. The character of the curves, depicted in Fig. 6.18 and 6.19, is

located in accordance with the results of the preceding/previous
paragraph.

7.
Radiation patterns of emitters, which are located on the elliptical
cylinder and the spheroid.

Calculation of the emitters, arranged/located on the elliptical
cylinder, gives the possibility to trace, as depends the radiation
pattern of surface antenna on the form of object, antenna position on
the surface of variable/alternating curvature. The analysis of the
diagrams of emitters, which are located on the elliptical cylinder,
will make it possible to incidentally rate/estimate the degree of
approximation of method, described in S 6.4.

Page 152.

The investigation of the radiation characteristics of the
sources, placed on the surface of thin elliptical cylinder (band),
will supplement information about the antennas, which radiate from
the surface of flat/plane screen, and also it will make it possible
to rate/estimate the limits of the applicability of the methods of
the physical theory of diffraction and approximation/approach of
Kirchhoff in the problem about the surface emitter.

Together with radiators, which are located on the elliptical cylinder, in this chapter will be examined spheroidal antennas.

7.1. Calculated relationships/ratios for the antenna radiation patterns, which are located on the surface of elliptical cylinder.

The radiation patterns of the surface antennas, arranged/located on the elliptical cylinder, can be designed with the aid of the reciprocity theorem (1.6) and expressions (1.53), (1.58) for the tangential components of magnetic field $H_z$, $H_\eta$ on the surface of cylinder.

Page 153.

After substituting (1.58), (1.53) in (1.6), we will obtain after simple conversions the following expressions for the radiation patterns of the surface antenna:

$$U_{\perp}(\eta) = \int\limits_{\eta_1}^{\eta_2} A_1(\eta_0) \left\{ \sum_{m=0}^{\infty} P_m \frac{ce_m(\eta_0, q) \, ce_m(\eta, q)}{\partial \, hc_m^{(1)}(\xi_0, q)/\partial \xi_0} + \right.$$

$$\left. + \sum_{m=0}^{\infty} Q_m \frac{se_m(\eta_0, q) \, se_m(\eta, q)}{\partial \, hs_m^{(1)}(\xi_0, q)/\partial \xi_0} \right\} d\eta_0; \qquad (7.1)$$

$$U_{\parallel}(\eta) = \int\limits_{\eta_1}^{\eta_2} A_2(\eta_0) \left\{ \sum_{m=0}^{\infty} P_m \frac{ce_m(\eta_0, q) \, ce_m(\eta, q)}{hc_m^{(1)}(\xi_0, q)} + \right.$$

$$\left. + \sum_{m=0}^{\infty} Q_m \frac{se_m(\eta_0, q) \, se_m(\eta, q)}{hs_m^{(1)}(\xi_0, q)} \right\} d\eta_0, \qquad (7.2)$$

where

$$P_m = \begin{cases} A_1^{(2k)} & \text{при } m = 2\kappa, \\ A_1^{(2k+1)} & \text{при } m = 2\kappa + 1; \end{cases}$$

$$Q_m = \begin{cases} B_1^{(2k+1)} & \text{при } m = 2\kappa + 1, \\ B_2^{(2k+2)} & \text{при } m = 2\kappa + 2; \end{cases}$$

$$\mathrm{ce}_m(\eta, q) = \sum_{r=0}^{\infty} A_r^{(m)}(q) \cos r\eta;$$

$$\mathrm{se}_m(\eta, q) = \sum_{r=0}^{\infty} B_r^{(m)}(q) \sin r\eta;$$

$$\int_0^{2\pi} [\mathrm{ce}_m(\eta, q)]^2 \, d\eta = \int_0^{2\pi} [\mathrm{se}_m(\eta, q)]^2 \, d\eta = 1;$$

$$\mathrm{hc}_{2\varkappa}^{(1)} = \sum_{r=0}^{\infty} (-1)^r A_{2r}^{(2k)} J_r(v_1) H_r^{(1)}(v_2);$$

$$\mathrm{hc}_{2\varkappa+1}^{(1)} = \sum_{r=0}^{\infty} (-1)^r A_{2r+1}^{(2k+1)} \{J_r(v_1) H_{r+1}^{(1)}(v_2) + J_{r+1}(v_2) H_r^{(1)}(v_1)\};$$

$$\mathrm{hs}_{2\varkappa+1}^{(1)} = \sum_{r=1}^{\infty} (-1)^r B_{2r+1}^{(2k+1)} \{J_r(v_1) H_{r+1}^{(1)}(v_2) - J_{r+1}(v_2) H_r^{(1)}(v_1)\};$$

$$\mathrm{hs}_{2\varkappa+2}^{(1)} = \sum_{r=0}^{\infty} (-1)^r B_{2r+2}^{(2k+2)} \{J_r(v_2) H_{r+2}^{(1)}(v_2) - J_{r+2}(v_2) H_r^{(1)}(v_1)\};$$

Key: (1). with.


$A_{1,2}(\eta_0)$ - field in antenna aperture;

$$v_{1,2} = \sqrt{q}\, e^{\mp \xi_0}.$$

Radiation pattern $U_{\parallel}(\eta)$ corresponds to parallel, and $U_{\perp}(\eta)$ - perpendicular relative to the generatrix of the cylinder of the orientation of the electric vector of field in antenna aperture,

which is located on the surface of elliptical cylinder when
$\xi = \xi_0$, $\eta_0^{(1)} < \eta_0 < \eta_0^{(2)}$ (Fig. 7.1).

Page 154.

The designations, used in formulas (7.1) and (7.2), are clarified in
S 1.3. It is not difficult to ascertain that in the limit when
$\xi_0 \to \infty$ expressions (7.1) and (7.2) pass into formulas (6.1), (6.4),
describing antenna radiation patterns, which is located on the
circular cylinder. With $\xi_0 \to 0$ the elliptical cylinder is converted
into the band. In this case expressions (7.1), (7.2) take the
following form:

$$U_{\perp}(\eta) = \int_{\eta_0^{(1)}}^{\eta_0^{(2)}} A_1(\eta_0) \left\{ \sum_{m=0}^{\infty} P_m \frac{-ce_m(\eta_0, q) ce_m(\eta, q)}{[\partial bc_m^{(1)}(\xi_0, q)/\partial \xi_0]_{\xi_0=0}} + \right.$$
$$\left. + \sum_{m=0}^{\infty} Q_m \frac{se_m(\eta_0, q) se_m(\eta, q)}{[\partial hs_m^{(1)}(\xi_0, q)/\partial \xi_0]_{\xi_0=0}} \right\} d\eta_0; \qquad (7.3)$$

$$U_{\parallel}(\eta) = \int_{\eta_0^{(1)}}^{\eta_0^{(2)}} A_1(\eta_0) \left\{ \sum_{m=0}^{\infty} P_m \frac{ce_m(\eta_0, q) ce_m(\eta, q)}{hc_m^{(1)}(0, q)} + \right.$$
$$\left. + \sum_{m=0}^{\infty} Q_m \frac{se_m(\eta_0, q) se_m(\eta, q)}{hs_m^{(1)}(0, q)} \right\} d\eta_0. \qquad (7.4)$$
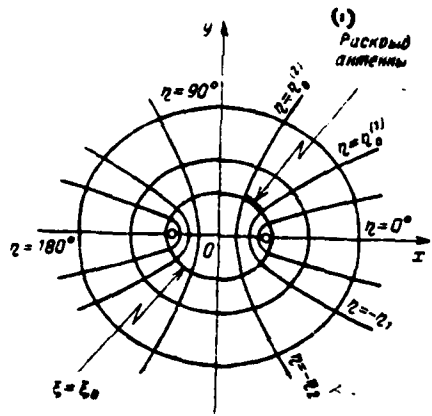
Fig. 7.1. On the calculation of the antenna radiation pattern, which is located on the elliptical cylinder.

Key: (1). Antenna aperture.

Page 155.


Relationships/ratios (7.1)-(7.4) make it possible to calculate

the antenna radiation patterns, which correspond to different

amplitude-phase field distributions in the aperture, for different

values of parameters $\xi_0$, $\eta_1$, $\eta_2$, $q$. However, in view of the complexity of

calculating the Mathieu functions we will be restricted subsequently

to the interpretation of results of computations, which relate,

mainly, to the elementary slotted emitter.

### 7.2.
Radiation patterns of emitters, which are located on the band.


Will examine first of all the emitters, arranged/located on the

surface of thin elliptical cylinder (band) (Fig. 7.2). According to

formulas (7.3) and (7.4) were designed the radiation patterns of

elementary slotted emitters for the bands of different width in

several positions of slot on the band. Fig. 7.3 and 7.4 show the

radiation patterns of slot $|u_\perp(\theta)|$ (Fig. 7.3) and $|u_\parallel(\theta)|$ (Fig. 7.4),

the corresponding to position slots in the center of band. In the

illuminated region the radiation patterns are formed/shaped as a

result of the interference of the field of slot and

radiation/emission of the edges of screen. In the case of parallel

polarization (slot is gashed perpendicularly to the edges of band)

edges of band are excited weakly and therefore diagram $u_{\parallel}(\theta)$

insignificantly differs from the appropriate radiation pattern of

slot, which is located on the plane.
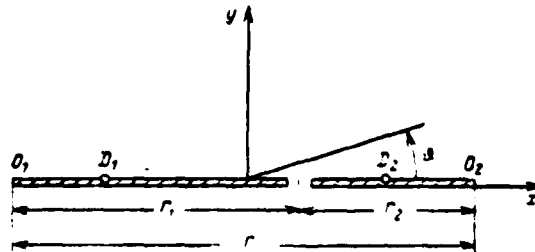
Fig. 7.2. On the calculation of slotted emitters on the band.


Page 156.


At the perpendicular polarization (slot is parallel to the edges of screen) and sufficiently high values $\Gamma_1 = \Gamma_2 \geqslant \lambda$ · in the region of light/world appear the interference maximums, oriented in directions $\vartheta_{max}$, of those corresponding to the cophasal addition of the field of slot and radiation/emission of one of the edges when

$$\kappa \Gamma_{1,2} \sin \vartheta_{max} = n\pi + \kappa \Gamma_{1,2}$$
$$(n = 0, \pm 1, \pm 2, ...).$$

In the shadow zone radiation level of slot depends on the polarization of field and removal/distance of slot from the edges of band. During the parallel polarization radiation level of slot in the shadow zone is considerably lower than with the perpendicular.
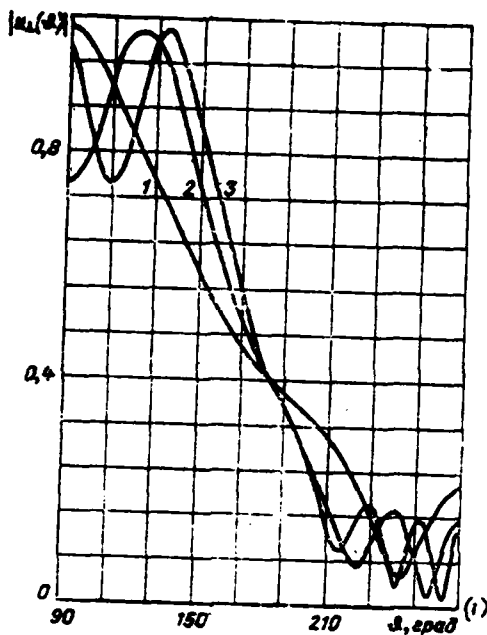
Fig. 7.3. Radiation pattern $|u_\perp(\Phi)|$ of the longitudinal slot, arranged/located symmetrically relative to the edges of the band:

1) $\Gamma=\lambda$; 2) $\Gamma=2\lambda$; 3) $\Gamma=3\lambda$.

Key: (1). deg.

Page 157.

The interference maximums of radiation pattern $|u_\perp(\vartheta)|$ in the shadow zone occur with

$$\kappa\Gamma\sin\vartheta_{max}=n\pi \quad (n=0,\ \pm1,\ \pm2,\ \ldots).$$

With an increase in distances $\Gamma_1 = \Gamma_2$ the values of interference maximums in the shadow zone diminish inversely proportional to $\sqrt{\Gamma_{1,2}/\lambda}$. If slot is distant up to the different distances from the edges of band ($\Gamma_1 \neq \Gamma_2$), its diagram becomes asymmetric, moreover during the perpendicular polarization asymmetry is expressed considerably stronger.
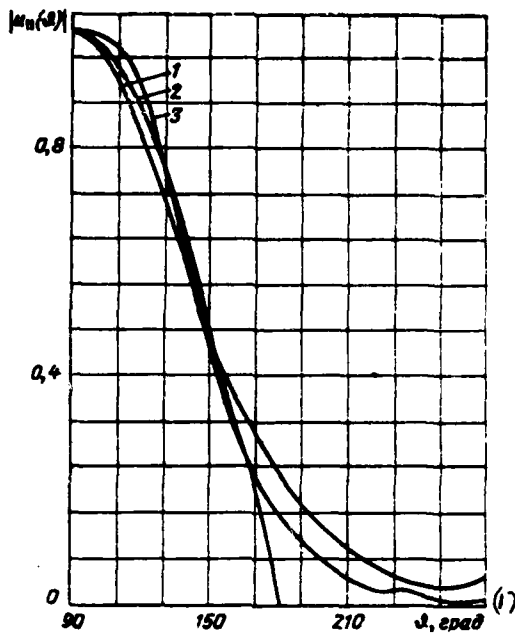
Fig. 7.4. The radiation pattern $|u_{\parallel}(\vartheta)|$ of the transverse slot, arranged/located it is symmetrically relative the edges of the band:

1) $\Gamma=\lambda$; 2) $\Gamma=2\lambda$; 3) $\sin\vartheta$.

Key: (1). deg.

Page 158.

In the region of light/world diagram $|u_{\perp}(\vartheta)|$ has maximums in directions $\vartheta_{max}$ for which

$$\kappa \Gamma_1 \sin \vartheta_{max} \approx n\pi + \kappa \Gamma_1,$$
$$\kappa \Gamma_2 \sin \vartheta_{max} \approx n\pi + \kappa \Gamma_2$$
$$(n = 0, \pm 1, \pm 2, ...).$$

Radiation pattern $|u_\parallel (\vartheta)|$ in the illuminated region virtually does not depend on the position of slot on the band. In the shadow zone of diagram $|u_\perp (\vartheta)|$ have the maximums in directions $\vartheta_{max}$ of such, that

$$\kappa \Gamma \sin \vartheta_{max} = n\pi + \kappa (\Gamma_1 - \Gamma_2)$$
$$(n = 0, \pm 1, \pm 2, ...).$$

In order to rate/estimate the role of joint action of the edges of band on the radiation pattern of surface emitter, Fig. 7.5 and 7.6 compare the diagrams of longitudinal and transverse slots, which are located on the band (Fig. 7.2), the half-planes (see Fig. 3.1) and planes.
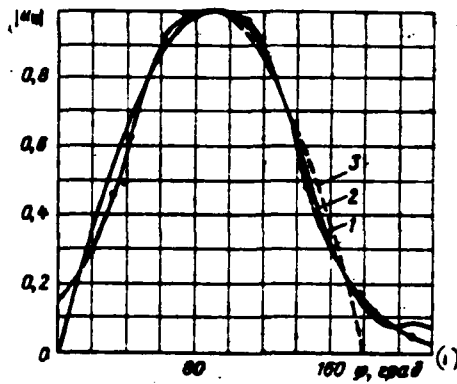
Fig. 7.5. Radiation pattern of the transverse slot, which is located on the band (curve 1), half-plane (curve 2) and plane (curve 3).

Key: (1). deg.

Page 159.

Curves in Fig. 7.5 and 7.6 correspond $\Gamma_1 = \Gamma_2 = \lambda$ (for the band) and $\Gamma = \Gamma_1 = \Gamma_2 = \lambda$ (for the half-plane). During parallel polarization fringe effect is small. During the perpendicular polarization their effect on the radiation pattern of slot is substantial; however, already when $\Gamma_{1,2} \geqslant \lambda$ the edges of band virtually do not interact, i.e., each edge of band emits as the edge of half-plane. In connection with this is justified the use/application of approximation methods of the physical theory of diffraction [26] for calculating the radiation

patterns of emitters, which are located on the surface of band.

In the approximation/approach of physical theory the diffractions of the radiation pattern of longitudinal and transverse slots on the band are designed with the aid of the reciprocity theorem and approximate solution of the corresponding diffractive problem. For the determination of approximate solution of the problem of diffraction they assume that edge/fin $O_1$ of band (Fig. 7.2) emits just as the edge of half-plane $y=0$; $0 \leqslant x < \infty$; and edge/fin $O_2$ as the edge of half-plane $y=0$; $-\infty < x \leqslant 0$.
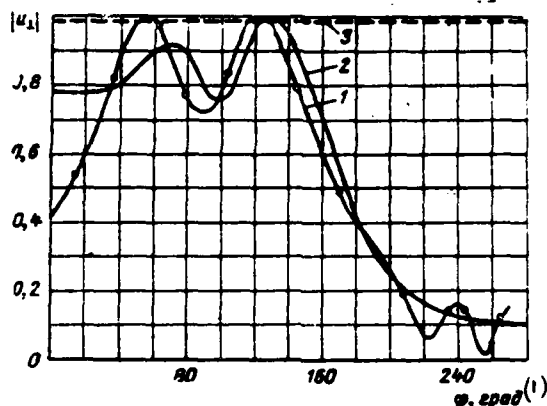
Fig. 7.6. Radiation patte n of the longitudinal slot, which is located on the band (curve 1), half-plane (curve 2) and plane (curve 3).

Key: (1). deg.

Page 160.

Then the solution of diffraction problem can be represented in the following form:

during the parallel polarization

$$G_{\parallel}(\vartheta)|_S = H_x(\vartheta,\ x) =$$

$$= \sqrt{2}\, e^{-i\frac{\pi}{4}} e^{-i\kappa x \cos\vartheta} \left\{ F_1\left(2\sqrt{\frac{\kappa x}{\pi}}\cos\frac{\vartheta}{2}\right) + \right.$$

$$+ F_1\left(2\sqrt{\frac{\kappa(\Gamma - x)}{\pi}}\sin\frac{\vartheta}{2}\right) + \frac{i \exp\left(2i\kappa x \cos^2\frac{\vartheta}{2}\right)}{2\sqrt{\pi\kappa x}\cos\frac{\vartheta}{2}} +$$

$$\left. + \frac{1}{2\sqrt{\pi\kappa(\Gamma - x)}\sin\frac{\vartheta}{2}}\exp\left[i\kappa(\Gamma - x)\sin^2\frac{\vartheta}{2}\right]\right\} \quad (7.5)$$

- on the illuminated side of band,

$$G_{\parallel}(\vartheta)|_S = H_x(\vartheta,\ x) =$$

$$= e^{-i\kappa x \cos\vartheta} \left\{ 2 + \sqrt{2}\, e^{-i\frac{\pi}{4}} \left[ F_1\left(2\sqrt{\frac{\kappa x}{\pi}}\cos\frac{\vartheta}{2}\right) - \right.\right.$$

$$- F_1\left(2\sqrt{\frac{\kappa(\Gamma - x)}{\pi}}\sin\frac{\vartheta}{2}\right) + \frac{i \exp\left(2i\kappa x \cos^2\frac{\vartheta}{2}\right)}{2\sqrt{\pi\kappa x}\cos\frac{\vartheta}{2}} -$$

$$\left.\left. - \frac{i \exp\left[2i\kappa(\Gamma - x)\sin^2\frac{\vartheta}{2}\right]}{2\sqrt{\pi\kappa(\Gamma - x)}\sin\frac{\vartheta}{2}}\right]\right\}$$

- on the shadow side of band;


during the perpendicular polarization

$$G_{\perp}(\vartheta)|_S = H_z(\vartheta,\ x) =$$

$$= \sqrt{2}\, e^{-i\frac{\pi}{4}} e^{-i\kappa x \cos\vartheta} \left\{ F_1\left(2\sqrt{\frac{\kappa x}{2}}\cos\frac{\vartheta}{2}\right) + \right.$$

$$\left. + F_1\left(2\sqrt{\frac{\kappa(\Gamma - x)}{\pi}}\sin\frac{\vartheta}{2}\right)\right\} \quad\quad (7.6)$$

- on the illuminated side of band,

$$G_{\perp}(\vartheta)|_s = H_z(\vartheta,\ x) =$$

$$= e^{-i\kappa x \cos\vartheta} \left\{ 2 + \sqrt{2}\, e^{-i\frac{\pi}{4}} \left[ F_1\left( 2\sqrt{\frac{\kappa x}{\pi}} \cos\frac{\vartheta}{2} \right) - \right.\right.$$

$$\left.\left. - F_1\left( 2\sqrt{\frac{\kappa(\Gamma - x)}{\pi}} \sin\frac{\vartheta}{2} \right) \right] \right\}$$

- on the shadow side of band.

Page 161.

In expressions (7.5) and (7.6)

$\vartheta$ - angle of incidence in the plane wave on the band;

$x$ - coordinate of observation point.

The reference directions of coordinates $\vartheta$, x are shown in Fig. 7.2.

Using expressions (7.5), (7.6) and by reciprocity theorem, we obtain the following approximations for the radiation patterns of longitudinal and transverse slots on the band:

$$u'_{\parallel}(\theta) = \sqrt{2}\, e^{-i\frac{\pi}{4}} e^{-i\kappa\Gamma_1\cos\theta}\left\{ F_1\left(2\sqrt{\frac{\kappa\Gamma_1}{\pi}}\cos\frac{\theta}{2}\right) + \right.$$

$$+ F\left(2\sqrt{\frac{\kappa\Gamma_2}{\pi}}\sin\frac{\theta}{2}\right) + \frac{i}{\pi}\frac{\exp\left(2i\kappa\Gamma_1\cos^2\frac{\theta}{2}\right)}{2\sqrt{\kappa\Gamma_1}\cos\frac{\theta}{2}} +$$

$$\left. + \frac{i}{\sqrt{\pi}}\frac{\exp\left(2i\kappa\Gamma_2\sin^2\frac{\theta}{2}\right)}{2\sqrt{\kappa\Gamma_2}\sin\frac{\theta}{2}}\right\} \quad \overset{(1)}{\text{при}}\ 0<\theta<\pi,$$

$$u'_{\parallel}(\theta) = e^{-i\kappa\Gamma_1\cos\theta}\left\{2 + \sqrt{2}\, e^{-i\frac{\pi}{4}}\left[ F_1\left(2\sqrt{\frac{\kappa\Gamma_1}{\pi}}\cos\frac{\varphi}{2}\right) - \right.\right.$$

$$- F_1\left(2\sqrt{\frac{\kappa\Gamma_2}{\pi}}\sin\frac{\theta}{2}\right) + \frac{i}{\sqrt{\pi}}\frac{\exp\left(2i\kappa\Gamma_1\cos^2\frac{\theta}{2}\right)}{2\sqrt{\kappa\Gamma_1}\cos\frac{\theta}{2}} -$$

$$\left.\left. - \frac{i}{\sqrt{\pi}}\frac{\exp\left(2i\kappa\Gamma_2\sin^2\frac{\theta}{2}\right)}{2\sqrt{\kappa\Gamma_2}\sin\frac{\theta}{2}}\right]\right\} \quad \overset{(1)}{\text{при}}\ \pi<\theta<2\pi; \quad (7.7)$$

$$u'_{\perp}(\theta) = \sqrt{2}\, e^{-i\frac{\pi}{4}} e^{-i\kappa\Gamma_1\cos\theta}\left\{ F_1\left(2\sqrt{\frac{\kappa\Gamma_1}{\pi}}\cos\frac{\varphi}{2}\right) + \right.$$

$$\left. + F_1\left(2\sqrt{\frac{\kappa\Gamma_2}{\pi}}\sin\frac{\theta}{2}\right)\right\} \quad \overset{(1)}{\text{при}}\ 0<\theta<\pi; \quad (7.8)$$

$$u'_{\perp}(\theta) = e^{-i\kappa\Gamma_1\cos\theta}\left\{2 + \sqrt{2}\, e^{-i\frac{\pi}{4}}\left[ F_1\left(2\sqrt{\frac{\kappa\Gamma_1}{\pi}}\cos\frac{\theta}{2}\right) - \right.\right.$$

$$\left.\left. - F_1\left(2\sqrt{\frac{\kappa\Gamma_2}{\pi}}\sin\frac{\theta}{2}\right)\right]\right\} \quad \overset{(1)}{\text{при}}\ \pi<\theta<2\pi.$$

Key: (1). with.

Page 162.

Fig. 7.7 compares precise and approximate radiation patterns $|u_{\perp}(\theta)|$ and $|u'_{\perp}(\theta)|$, the corresponding to removal/distance slots up to the equal distances from the edges of band $\Gamma_1=\Gamma_2=\lambda$. The comparison of diagrams shows that the physical theory of diffraction gives satisfactory results, if the source of field is distant from the edges of screen up to distance $\Gamma_{1,2}\geqslant\lambda$.
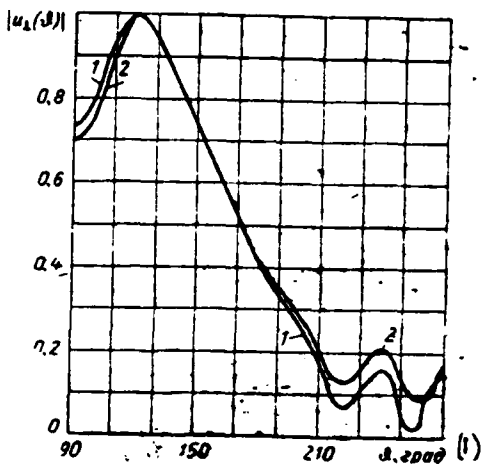
Fig. 7.7. To the evaluation of the approximation/approach of the physical theory of the diffraction: 1 - precise radiation pattern $u_\perp(\vartheta)$; 2 - approximate diagram $u_\perp(\vartheta)$.

Key: (1). deg.

Page 163.

Using the method examined, let us produce the calculation of the antenna radiation pattern, which radiates from the surface of band (Fig. 7.2). Let in antenna aperture $0 \leqslant x \leqslant \Gamma$ be created one of following field distributions:

$$\vec{E} = A_\parallel(x)\vec{e}_z \quad \text{(parallel polarization)}, \qquad (7.9)$$

$$\vec{H} = A(x)\,\vec{e_z} \quad \text{(perpendicular polarization)}, \qquad (7.10)$$

where
$$A(x) = 1 - q_1 \cos\frac{2\pi}{\Gamma}x; \; 0 \leqslant x \leqslant \Gamma.$$

Using formulas (7.7), (7.8), it is not difficult to calculate the antenna radiation patterns, which is located on the band, during the parallel and perpendicular polarizations. For this should be to use the relationship/ratio

$$V(\Phi) = \int_0^\Gamma u(\Phi, \; \Gamma_1)\, A(\Gamma_1)\, d\Gamma_1, \qquad (7.11)$$

by formulas (7.7), (7.8) and produced the operation/process of integration in expression (7.11). Fig. 7.8 for value $\gamma = \Gamma/\lambda = 5$ compares radiation patterns $|V_\perp(\Phi)|$ and $|V_\parallel(\Phi)|$ designed with $q_1 = 0$.
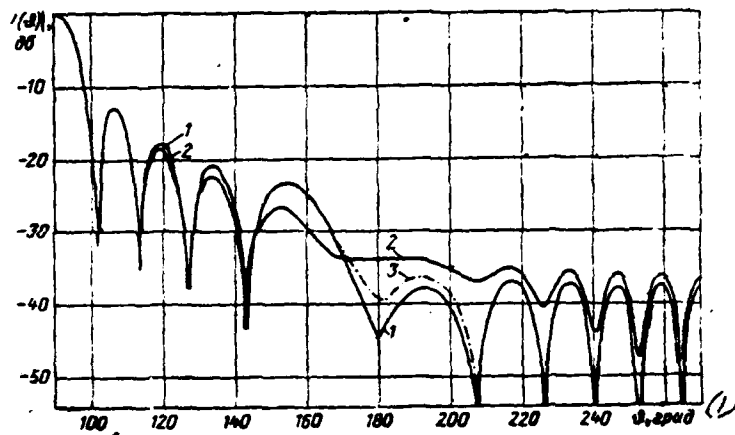
Fig. 7.8. The standardized/normalized radiation patterns $|V(\Phi)|$: 1 - perpendicular polarization; 2 - parallel polarization; 3 - radiation pattern $|V(\Phi)|$ taking into account interaction of the edges of band.

Key: (1). deg.

Page 164.

Fig. 7.9, besides diagrams $|V_\perp(\Phi)|$ and $|V_{||}(\Phi)|$, depicts the radiation patterns of the antenna in question, designed in the approximation/approach of Kirchhoff (aperture method). According to the aperture method of the antenna radiation pattern with the assigned field in aperture (7.9), (7.10) they take the following form:

$$V_a(\vartheta) = \frac{\sin^2 u}{u^2}\left(1 - q_1\,\frac{\pi^2}{u^2 - \pi^2}\right) \varkappa(\Phi), \qquad (7.12)$$

where          $u = \frac{\pi l}{2}\cos\vartheta;\ \varkappa_{||}(\vartheta) = \sin^2\vartheta,\ a\ \varkappa_\perp(\vartheta) = 1.$
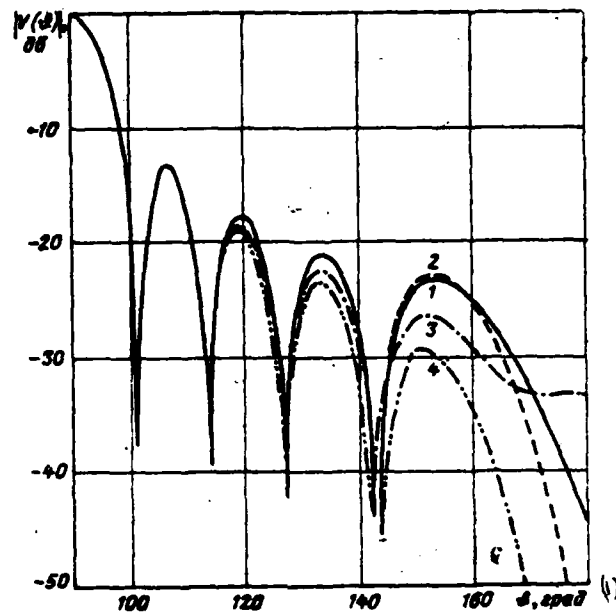
Fig. 7.9. Antenna radiation pattern, which is located on the band: 1,
3 - calculated by formula (7.11) for the perpendicular and parallel
polarizations respectively: 2, 4 - designed in the
approximation/approach of Kirchhoff for the perpendicular and
parallel polarizations, $\gamma=5$, $q=0$.

Key: (1). deg.

Page 165.

From Fig. 7.8 and 7.9 it follows that radiation of the antenna in

question in the illuminated region can be designed with the
satisfactory accuracy in the aperture method, if $\gamma \gtrsim 5$ and $\vartheta \neq 0$ or $\pi$.
During the perpendicular polarization aperture method gives the best
accuracy, than with the parallel. Near the boundaries of shadow $\vartheta = 0$
and $\pi$ and in the shadow zone where is substantial the phenomenon of
diffraction on the edges of band, aperture method it goes without
saying is unsuitable. The radiation patterns $V_{\perp}(\vartheta)$ and $V_{\parallel}(\vartheta)$ in the
illuminated region virtually coincide (with exception of the
directions, close to the boundaries of shadow), and in the shadow
zone they noticeably differ from each other. The difference between
diagrams $V_{\perp}(\vartheta)$ and $V_{\parallel}(\vartheta)$ is caused by the structure of the
diffraction waves, emitted by the edges of band during parallel and
perpendicular polarizations. From Fig. 7.8 and 7.9 it follows that
during both polarizations the antenna in question has virtually
constant maximum radiation level in the region of shadow. This means
that heterogeneous cylindrical waves, emitted by the edges of band,
with the assigned amplitude-phase characteristic in antenna aperture
possess interesting special feature/peculiarity. In proportion to
removal/distance from the boundaries of shadow ($\vartheta \rightarrow 3\pi/2$) the
three-dimensional/space phase shift between the fields of
heterogeneous cylindrical waves vanishes; at the same time with
$\vartheta \rightarrow 3\pi/2$ decrease wave amplitudes, emitted by the edges of band.
Consequently, as is shown calculation, the phenomena indicated during
the addition of diffraction waves average out, and therefore the

maximums of rear antenna lobes have a level, virtually not depending on angle $\vartheta$.

The level of the envelope of the maximums of the rear lobes of the antenna in question it is not difficult to determine, after calculating the value of the lobe/lug, oriented in the direction $\vartheta = 3\pi/2$. Calculation shows that the values of maximum radiation level of the antenna in question in the shadow zone comprise:

$$\Delta_\perp \approx \frac{1}{4\pi\gamma} \left|(1-iq_1)\left\{1 - \frac{2}{\pi\sqrt{2\gamma}} \times \right.\right.$$

$$\left.\left.\times \exp\left[i\left(2\pi\gamma + \frac{\pi}{4}\right)\right]\right\}\right| + O\left(\gamma^{-\frac{5}{2}}\right); \qquad (7.13)$$

$$\Delta_\parallel = \frac{1-q_1}{4\pi\gamma} + O\left(\gamma^{-\frac{5}{2}}\right). \qquad (7.14)$$

Page 166.

Radiation level in formulas (7.13) and (7.14) is read relative to the value of the principal maximum of radiation pattern.

From expressions (7.13) and (7.14) it follows that in the antenna in question the level of rear radiation/emission during the parallel polarization is more than with the perpendicular. At the same time, it was above noted that the radiation/emission of elementary transverse slot, which is located on the band, in the

shadow zone considerably the low-level radiation of the longitudinal slot.

In order to explain the obtained result [expressions (7.13) and (7.14)], let us examine the antenna whose aperture $(D_1 \leqslant x \leqslant D_2)$ occupies the part of the surface of band $(0 \leqslant x \leqslant \Gamma)$ (Fig. 7.2). The level of rear lobe/lug $(\vartheta = 3\pi/2)$ of this antenna according to (7.7), (7.8) and (7.11) comprises

$$\Delta'_\perp = \frac{1}{k(D_2 - D_1)} \int\limits_{D_1}^{D_2} A(x) \Big\{ 1 - \sqrt{2} e^{-i\frac{\pi}{4}} \times$$

$$\times \Big[ F_1 \Big( \sqrt{\frac{2\kappa x}{\pi}} \Big) + F_1 \Big( \sqrt{\frac{2\kappa(\Gamma - x)}{\pi}} \Big) \Big] \Big\} dx, \quad (7.15)$$

$$\Delta'_\parallel = \frac{1}{\kappa(D_2 - D_1)} \int\limits_{D_1}^{D_2} A(x) \Big\{ 1 - \sqrt{2} e^{-i\frac{\pi}{4}} \times$$

$$\times \Big[ F_1 \Big( \sqrt{\frac{2\kappa x}{\pi}} \Big) + F_1 \Big( \sqrt{\frac{2\kappa(\Gamma - x)}{\pi}} \Big) \Big] \Big\} dx -$$

$$- \frac{e^{i\frac{\pi}{4}}}{2\kappa(D_2 - D_1)} \int\limits_{D_1}^{D_2} A(x) \Big[ \frac{e^{i\kappa x}}{\sqrt{\pi\kappa x}} +$$

$$+ \frac{\exp[i\kappa(\Gamma - x)]}{\sqrt{\pi\kappa(\Gamma - x)}} \Big] dx = \Delta'_\perp - \delta. \quad (7.16)$$

In expression (7.16) value $\delta$, to which differs $\Delta'_\parallel$ from $\Delta'_\perp$, it is determined by integral on radiating antenna aperture from two waves, which run along the band and its radiating in direction edges. This means that the amount of radiation of edges and value $\delta$ depend substantially on size/dimension $(D_2 - D_1)$ of radiating antenna aperture.

Page 167.


Therefore depending on the size/dimension of antenna aperture with the fixed/recorded bandwidth value $\Delta'_{\parallel}$ can both exceed and be less than the value $\Delta'_{\perp}$. This confirm the results of calculation. Fig. 7.10 gives the values of the levels $\Delta'$ of the lobe/lug, oriented in the direction $\vartheta = 3\pi/2$, constructed in the dependence on

$$\xi = \frac{\Gamma - (D_2 - D_1)}{\Gamma} \; \underset{\text{для}}{\overset{(1)}{}} \; \gamma = 5 \text{ и } q_1 = 0.$$

Key: (1). for.


If $\xi = 0.5$, which corresponds to elementary slot $\Delta'_{\parallel} < \Delta'_{\perp}$, whereas with $\xi = 0$ [is excited entire/all surface of band, which corresponds to conditions (7.9), (7.10)] $\Delta'_{\parallel} > \Delta'_{\perp}$.
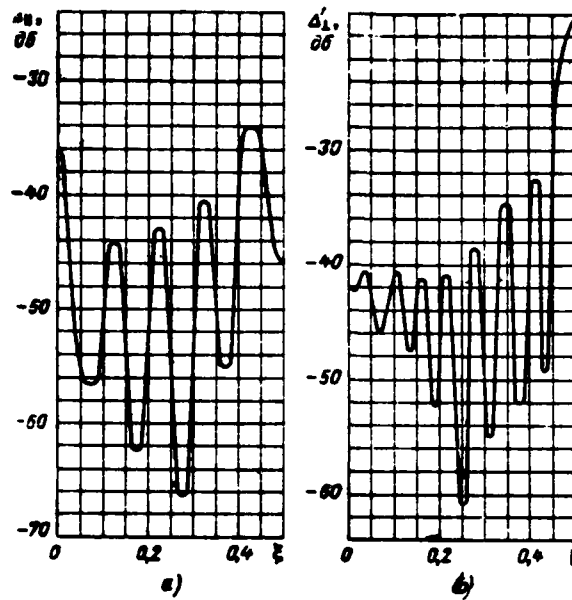
Fig. 7.10. Level values of the rear lobe/lug of broadside antenna array, which is located on the band, with $\gamma=5$, $q=0$: a) - during the parallel polarization; b) - during the perpendicular polarization.

Page 168.

The given results of calculating the broadside antenna array, which is located on the band, were obtained in the approximation/approach of the physical theory of diffraction without taking into account interaction of the edges of band. Neglect of interaction leads to the imprecise determination of radiation pattern near the boundaries of shadow $\vartheta=0$ and $\vartheta=\pi$. In order to refine

radiation pattern and in the region indicated, should be considered interaction of the edges of band. Kray bands $O_1$ and $O_2$ emit heterogeneous cylindrical waves $u_1$ and $u_2$. As a result of wave diffraction $u_1(u_2)$ on edge $O_2(O_1)$ is excited the diffraction wave $u_{12}(u_{21})$, emitted by edge $O_2(O_1)$ which, in turn, diffracts on edge $O_1$ $(O_2)$ and so forth. In the problem about the antenna, arranged/located on the band, we will be restricted to the account only of secondary diffraction, i.e., wave diffraction $u_1$ and $u_2$ on the edges of band $O_2$ and $O_1$ respectively. The effect of the subsequent diffractions on the antenna radiation pattern decreases proportional $\gamma^{-n/2}$, where n=1, 2, 3, .... For the secondary diffraction n=1.

Since the zone of edge effect during the parallel polarization has the insignificant width (for example, see [13]), we will be restricted to the account of interaction of edges only for perpendicular polarization. Examining the diffraction of heterogeneous cylindrical waves $u_1$ and $u_2$ on the edges of band $O_2$ and $O_1$, we will assume that these waves diffract as flat/plane, arriving from the directions $\vartheta_0=0$ and $\vartheta_0=\pi$ and having amplitudes, equal to values of $|u_1|$ and $|u_2|$ on the edges of band $O_2$ and $O_1$. In accordance with the assumptions indicated was designed the antenna radiation pattern for $\gamma=5$ and $q_1=0$. The comparison of the curves, depicted in Fig. 7.8, shows that the account of secondary diffraction on the edges of band makes it possible to refine the antenna radiation

pattern only in the narrow sector of angles, which is adjacent to the

boundary of shadow.


The radiation patterns of cophasal slot antenna (Fig. 7.8, 7.9)

and elementary sources (Fig. 7.3, 7.4) are formed/shaped with

simultaneous fringe effect of band. If antenna, which is located on
the band, is excited by the traveling field and in its aperture
Fig.  7.2) the distribution' of field

$$\vec{H}(x) = A(x) e^{-i\beta x} \vec{h}_\tau. \qquad (7.17)$$

is created
one should expect that effect of one of the edges of band will be

considerably weakened.


Page 169.


In order to be convinced of this, let us calculate the antenna

radiation pattern of the traveling wave in aperture of which is

excited field (7.17) when

$$\vec{h}_\tau = \vec{e}_z$$

$(\vec{e}_z -$ the unit vector, directed along axis Oz),

$$A(x) = 1 + q \cos \frac{\pi (2x - D_2 - D_1)}{D_2 - D_1}. \qquad (7.18)$$

Expressions (7.17), (7.18) describe the wave, which encounters

to edge $O_1$ of bands (Fig. 7.2). It is obvious that at $\beta = k$ and

sufficiently high value of $k(D_2 - D_1)$ edge/fin $O_1$ will be excited

considerably stronger than another edge of band, and therefore it is

possible to assume that the radiation pattern of this antenna will be

close to the diagram of antenna, which is located on the half-plane.

Utilizing relationships/ratios (1.6), (1.53), (7.17) and (7.18), let us represent in the following form the radiation pattern $F_\perp(\theta)$ of traveling-wave antenna, which radiates from the surface of the band:

$$F_\perp(\theta) = \int\limits_{\eta_0^{(1)}}^{\eta_0^{(2)}} A(x)\, e^{i\beta x} \left\{ \sum_{m=0}^{\infty} P_m \frac{ce_m(q,\eta_0)\, ce_m(\theta,q)}{hc_m^{(1)\prime}(0,q)} \right\} d\eta_0 +$$

$$+ \int\limits_{\eta_0^{(1)}}^{\eta_0^{(2)}} A(x)\, e^{i\beta x} \left\{ \sum_{m=0}^{\infty} Q_m \frac{se_m(\eta_0,q)}{hs_m^{(1)\prime}(0,q)} se_m(\theta,q) \right\} d\eta_0. \quad (7.19)$$

The results of calculation according to this formula are shown in Fig. 7.11 (curve 1). The same figure depicts also the antenna radiation pattern (curve 2), which is located on the half-plane.

Calculation shows that in the region of major lobe, shadow slope and first minor lobes the antenna radiation patterns, which are located on the band and the half-plane, differ little from each other.

Page 170.

The characteristic feature of diagram $F_\perp(\theta)$ is the brokenness of its shadow slope, caused by the interference of the fields, scattered by

the edges of band, while the antenna radiation pattern, which is located on the half-plane, monotonically it decreases with $\vartheta > \pi$.

If the length of traveling-wave antenna $D_2 - D_1 \gtrsim 2\lambda$ and $\sigma \gtrsim 0$, for calculating the diagrams of antenna, which is located on the band, instead of formula (7.19) it is possible to use the simpler correlations, obtained in Chapter 3 for the antenna, arranged/located on the half-plane.
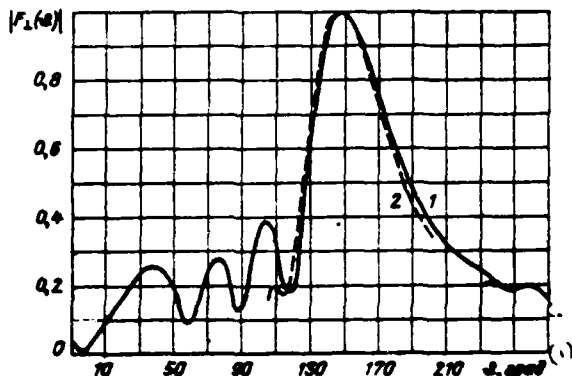
Fig. 7.11. Antenna radiation patterns of the traveling wave, arranged/located on the band and the half-plane. The results of calculation correspond: $D_1=0, D_1=2\lambda, r=2\lambda$ - in the case of band; $\sigma=0, q=0, \zeta=0, l=1$ - in the case of half-plane.

Key: (1). deg.

7.3. Radiation pattern of slot, which is located on the surface of elliptical cylinder.

In view of the complexity of numerical calculations according to formulas (7.1) and (7.2) we will be restricted to the examination only of the nondirectional emitters (longitudinal and transverse slot), which are located on the elliptical cylinder.

Fig. 7.12 and 7.13 show radiation patterns $|U_\perp(\theta)|$ and $|U_\parallel(\theta)|$.

corresponding to the symmetrically arranged ($\eta_0=90°$) transverse and longitudinal slots on the elliptical cylinders with the identical major axes $a=2\lambda$ and different minor axes b.

Page 171.

The results of calculation, given in Fig. 7.12 and 7.13, make it possible to trace, as change radiation patterns $|U_{\parallel}(\Phi)|$ in the dependence on the shape of surface of elliptical cylinder upon transfer from band (b=0) to circular cylinder (b=a). As one would expect, diagram $U_{\parallel}(\Phi)$ changes insignificantly with $0\leqslant b\leqslant a$. On the contrary, the diagram of the longitudinal slot depends substantially on the value of ratio b/a (with a=const). With change b/a from 0 to 1 disappears failure/dip/trough on major lobe of diagram, grow/rise supplementary maximums, is expanded major lobe.
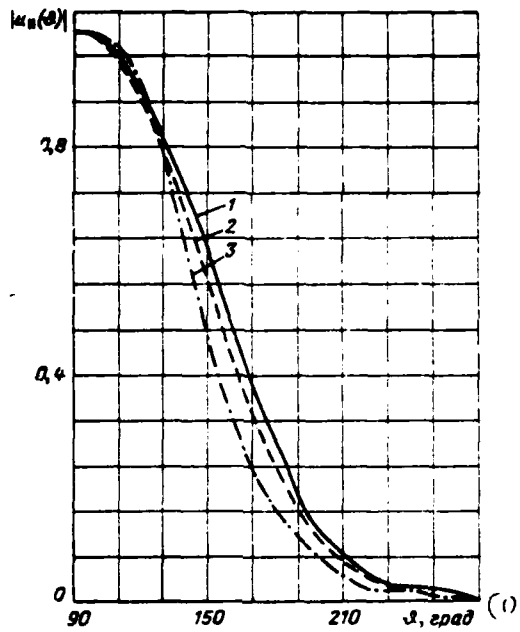
Fig. 7.12. Radiation patterns $|U_\text{в}(\theta)|$ of the transverse slot on the elliptical cylinder, which correspond $a=2\lambda$; $\eta_0=90°$ and to different relations: 1) $b/a=0$; 2) $b/a=0.5$; 3) $b/a=1$.


Key: (1). deg.


Page 172.


The changes in the radiation pattern indicated clearly reflect the character of the dependence of current distribution on the convex body on the radius of curvature of its surface.

Fig. 7.14 and 7.15 show radiation patterns $|U_\perp(\psi)|$ and $|U_\shortparallel(\psi)|$, corresponding to two positions of longitudinal and transverse slots on the elliptical cylinder with axes $a=2\lambda$; $b=\lambda$. Radiation patterns $|U(\psi)|$ are constructed depending on angular coordinate $\psi$, which is counted off in the direction $\vartheta>0$ from normal to the surface of elliptical cylinder at the point where is located slot.
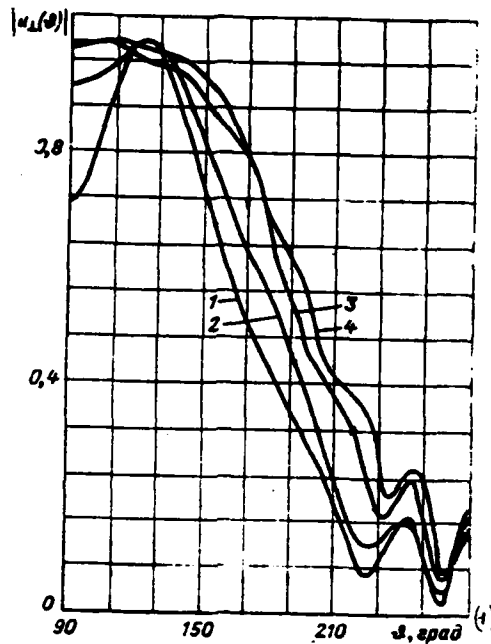
Fig. 7.13. Radiation patterns $|U_\perp(\Phi)|$ of the longitudinal slot on the elliptical cylinder, which correspond $a=2\lambda$; $\eta_0=90°$ and to different relations: 1) b/a=0; 2) b/a=0.25 3) b/a=0.5 4) b/a=1.

Key: (1). deg.

Page 173.

The comparison of Fig. 7.14 and 7.15 with the appropriate results for the slot on the band shows that with an increase in ratio b/a of radiation pattern $U(\psi)$ become less susceptible to the position the slots on the surface of elliptical cylinder. This is natural, since in the limit with b/a→1 diagram $U(\psi)$ not at all depend on the position of slot.
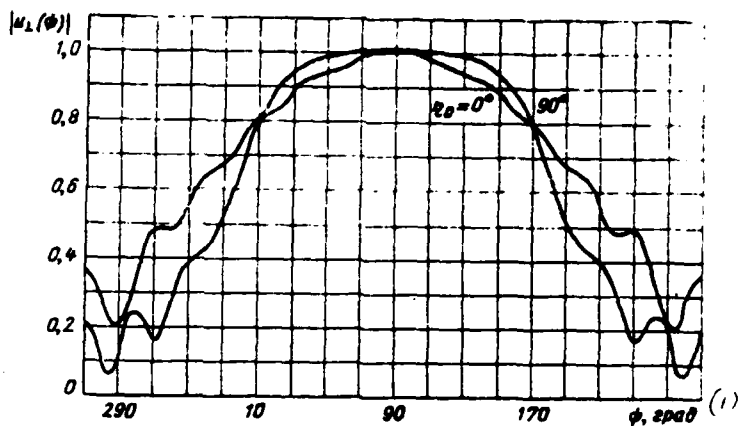
Fig. 7.14. Radiation patterns $|U_\perp(\phi)|$.
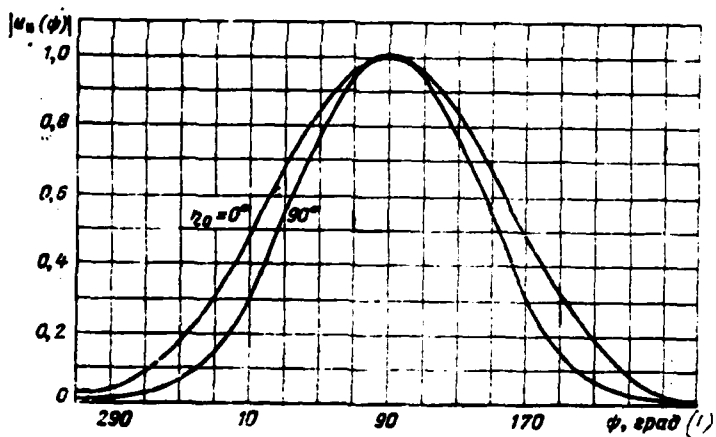
Key: (1). deg.



Fig. 7.15. Radiation patterns $|U_{\|}(\phi)|$.

Key: (1). deg.

Page 174.


Graphs/curves in Fig. 7.3, 7.4, 7.12-7.15 show that the form of
the radiation patterns of elementary sources complicatedly depends on
all parameters of the surface of elliptical cylinder, on the position
of slot on the cylinder. This, in the first place, to relate to the
longitudinal slot, since radiation pattern $U_{\parallel}(\vartheta)$ depends on
parameters $q, \xi_0, \eta (\eta \neq 0$ or $\pi)$ weaker.


Let us examine one of the characteristics of radiation pattern

$$\Delta_{\perp}(q, \xi_0, \eta) = \frac{\left| U_{\perp}\left(\vartheta_{max} \pm \frac{\pi}{2}\right)\right|}{|U_{\perp}(\vartheta_{max})|}$$

- radiation level of the longitudinal slot in the direction of the
boundary of shadow ($\vartheta=0$ or $\pi$ for the symmetrically arranged/located
slot). In special cases $\xi_0 = 0$ (strip) and $\xi_0 \to \infty$ (circular cylinder)
(see Chapter 3 and 6):

$$\Delta_{\perp}(q, 0, \eta) \approx 0.42 \ (\text{если}^{(I)} q \geqslant 10, \ \eta = \pi/2),$$
$$\Delta_{\perp}(q, \infty, \eta) \approx 0.7.$$


Key: (1). if.


Fig. 7.16 shows the values of radiation level of the
longitudinal slot in the elliptical cylinder, designed depending on
the radius of curvature of the edges of elliptical cylinder for
symmetrically arranged/located slot $(\eta = \pi/2)$ and $a = 2\lambda$. From the figure
one can see that already when $\rho \geqslant \lambda/2 \ \Delta_{\perp}(\rho) \approx 0.7$.
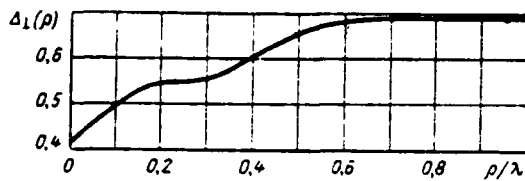
Fig. 7.16. Radiation level of the longitudinal slot in elliptical cylinder $\Delta_\perp (q, \xi, \eta) = \Delta_\perp (\rho)$ in the direction of the boundary of shadow with different radii of curvature of the edges of cylinder $\rho = b^2/a$.

Page 175.

In view of the complexity of calculating the radiation patterns of the sources of field, which are located on the elliptical cylinder according to precise formulas, is of interest the examination of the approximation methods, which make it possible to avoid the cumbersome calculations, connected with the use of Mathieu functions. For this purpose we will use the method, presented in §6.4.

If the radius of curvature R of the surface of elliptical cylinder at the point where is located slot, exceeds wavelength $\lambda$, the radiation pattern of slot $U(\vartheta)$ in the illuminated region insignificantly differs from the diagram of slot, which is located on the circular cylinder whose radius is equal to R. This confirm the results of calculation, given in Fig. 7.17, where are compared

precise (curve 1) and approximated (curve 2) of the radiation pattern of the longitudinal slot, which is located on the elliptical cylinder with the sizes/dimensions of axes $a=2\lambda$, $b=\lambda$, at point $\eta_0=\pi/2$. Precise and approximate radiation patterns noticeably differ only in the shadow zone.
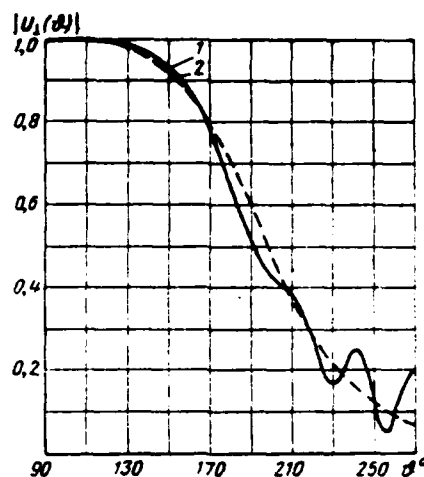
Fig. 7.17. Precise and approximated radiation pattern of the longitudinal slot, which is located on the elliptical cylinder.

Page 176.


7.4. Radiation patterns of spheroidal antennas.


The vast class of the surfaces of the real objects, which have variable/alternating curvature, can be approximated by the surface of spheroid. A strict solution of the problem about the radiation/emission of arbitrary system of sources, which is located on the surface of spheroid, is known [61, 62]. However, the possibilities of the numerical calculation of spheroidal antennas are at present limited by a special case of symmetrical excitation in view of the absence of a sufficient quantity of tabulated spheroidal functions. The most detailed results of the numerical calculation of the radiation patterns of symmetrical spheroidal antennas are given in works [62] (for the flattened spheroid) and [7] (for the prolate spheroid).


Let us examine how affects the surface of the prolate spheroid the radiation patterns of surface emitters, after using the results of work [7]. Let in the surface of spheroid $\xi=\xi_0$ (Fig. 7.18) be gashed the thin annular slot whose position on the surface is characterized by coordinate $\eta=\eta'$. Since is examined symmetrical problem, field distribution along the slot is even.
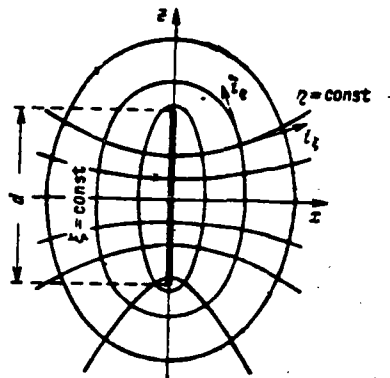
Fig. 7.18. On calculation of spheroidal antenna.


Page 177.


In the remote zone the electric field of annular slot has unique component $E_\eta$, value of which is determined as follows [7]:

$$E_\eta = -iI_\varphi^m \frac{e^{ih\xi}}{\xi} \frac{2}{d} \sqrt{\frac{1-(\eta')^2}{\xi_0^2-1}} \times$$

$$\times \sum_{l=1}^\infty \frac{S_{1l}(h,\eta)}{N_{1l}\left\{\frac{\xi_0}{\xi_0^2-1} \, \mathrm{he}_{1l}^{(1)}(h,\xi_0) + \frac{\partial}{\partial\xi}[\mathrm{he}_{1l}^{(1)}(h,\xi)]_{\xi=\xi_0}\right\}} \, \eta' e^{\frac{i\pi}{2}(l+1)}, \quad (7.20)$$

where $I_\varphi^m$ – magnetic current strength in the slot;


$\mathrm{he}_{1l}^{(1)}(h,\xi)$ – radial spheroidal third-order functions;


$S_{1l}(h,\eta)$ – angular spheroidal functions;

$$N_{1l} = \int_{-1}^{+1} [S_{1l}(h,\eta)]^2 \, d\eta;$$

$$h = \kappa d/2;$$

d – focal length of spheroid.
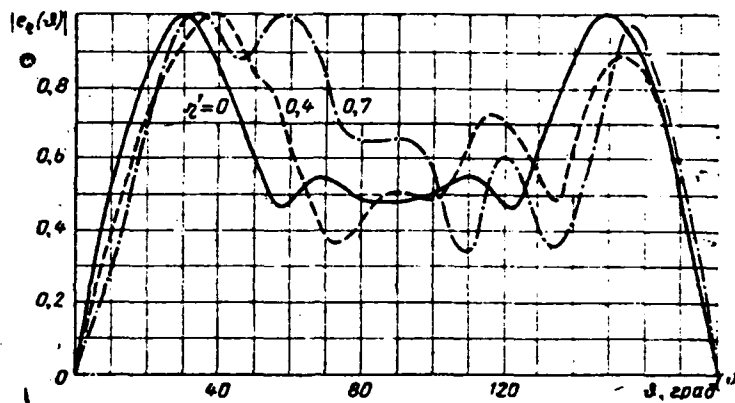
Fig. 7.19. Radiation patterns of annular slot on spheroid with h=7, $\xi_0$=1.077. Length of spheroid L=2.4 $\lambda$; $\eta'$=0; 0.4 and 0.7.

Key: (1). deg.

Page 178.

Fig. 7.19 gives the results of the numerical calculation of the standardized/normalized radiation patterns

$$e_\eta(\vartheta) = \left| \frac{E_\eta(\vartheta)}{E_\eta(\vartheta_{max})} \right|,$$

where $\vartheta$-vectorial angle in the spherical coordinates. From the figure one can see that the displacement of slot over the surface of spheroid leads to the contraction of the lobe/lug of diagram, turned to the side, opposite to displacement. Simultaneously this lobe/lug is sloped toward the axis of spheroid. The changes in the radiation

END

DATE
FILMED

10.82

DTIC

pattern $e_\eta(\theta)$ indicated are caused by the radiation/emission of the current wave, which runs along the large arm of spheroid. Diagrams, turned toward the displacement of slot, on the contrary, is expanded, its amplitude can exceed the amplitude of the lobe/lug, oriented in the direction, opposite to the displacement of slot.

8.

Radiation ████████ from the waveguide, ███████ located on the half-plane.

Is of interest the study of the radiation characteristics of the antennas whose aperture does not coincide with the surface of conductive body, but it is located in immediate proximity of it. In present chapter is examined a special case of the task indicated: the calculation of the radiation pattern of flat/plane waveguide, which is located on the half-plane.

8.1. Formulation of the problem and calculated relationships/ratios.

Let us examine the flat/plane semi-infinite waveguide, arranged/located on the half-plane at a distance of a from its edge (Fig. 8.1). The walls of waveguide we consider ideally conducting and negligibly thin. Let us assume that in the waveguide to the side of the open end/lead (in the negative direction of x axis) is propagated one type wave.

Page 179.

A strict solution of the problem indicated with a=0 is given in work [63]. Together with a strict solution work [63] examines the approximate methods of calculating the radiation/emission of waveguide, and also are compared the results of a precise and proximate analysis. On the basis of comparison it is shown, in particular, that use of approximation/approach of Kirchhoff for the solution of the problem about the radiation/emission from the flat/plane waveguide gives satisfactory results during the computation of field in the front/leading half-space x<0.

In present chapter the method of calculation is based on the use/application of an approximation method of Kirchhoff. Approximation/approach lies in the fact that the field in the aperture of waveguide takes as the equal to the field of incident wave and are not considered currents on the outer side of the upper wall of waveguide. It is obvious that under the assumptions indicated the greatest error in the calculation should be expected in the region the angles $\vartheta > \pi/2$ (Fig. 8.1).

Let us determine the radiation field of the waveguide, arranged/located on the half-plane, in the cases of perpendicular $(E_\perp)$ and by parallel $(E_\parallel)$ of polarizations.

Perpendicular polarization.

In the case of a wave of the type TEM, which is propagated in the waveguide, tangential field in aperture x=0; $0 \leqslant y \leqslant b$ takes the following form:

$$E_y = 1; \quad H_z = -\zeta_1, \qquad (8.1)$$

where $\zeta_1 = \sqrt{\epsilon_1/\mu_1}$. - conductivity of the medium, which fills waveguide.
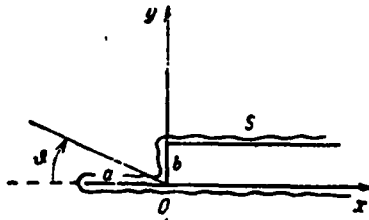
Fig. 8.1. Waveguide on half-plane. Coordinate system.

Page 180.

Unique component $H_z$ of the magnetic field, emitted by waveguide, can be found, after using reciprocity theorem (1.5) and relationships/ratios (1.35), (1.37). Disregarding the radiation/emission of the current, which flows in to the outer side of the wall of waveguide (y=b), we obtain, according to expression (1.5) the following value of the field, created by waveguide in the direction, characterized by angle $\vartheta$:

$$H_z(\vartheta) = \frac{1}{4\pi} \int_0^b (E_y H_{1z} - H_z E_{1y})|_{x=0} \, dy, \qquad (8.2)$$

where $E_{1y}, H_{1z}$ - plane waves, field component, which diffracts on the half-plane [see expressions (1.35)-(1.37)].

Subsequently there will be examined the radiation pattern of single waveguides, which are located on the half-plane, and also diagrams of two identical waveguides, arranged/located symmetrically

relative to half-plane. We will consider that field distribution in the aperture of the waveguide, located under the half-plane, with x=0,−b≤y≤0 is described by expression (8.1).

The radiation patterns of single waveguides, which are located from above or from below from the half-plane, we will note respectively by the sign plus (+) or minus (−). The radiation patterns of two symmetrically arranged/located waveguides during the cophasal excitation let us designate by letter $\Sigma$, and with the antiphase − by letter $\Delta$.

Page 181.

Making integration in expression (8.2), we obtain the following expressions for the radiation patterns of the single waveguides:

$$f_1^+(\theta) = (1 + \zeta_1 \cos\theta)\frac{\sin u}{u} + F_\perp(\theta), \qquad (8.3)$$

$$f_1^-(\theta) = (1 + \zeta_1 \cos\theta)\frac{\sin u}{u} - F_\perp(\theta),$$

where

$$F_\perp(\theta) = \frac{1}{2u}(1+i)(1 + \zeta_1 \cos\theta)\left[F_1(v_1)e^{-iu} - \right.$$

$$- F_1(v_2)e^{iu}] - (1+i)e^{-iu}e^{i2\pi\gamma} \times$$

$$\times \left[\frac{1 + \zeta_1 \cos\theta}{u}\cos\frac{\theta}{2} + \frac{\zeta_1}{2\pi h}\sin\frac{\theta}{2}\right]F_1(q); \qquad (8.4)$$

$\gamma = a/\lambda$ and $h = b/\lambda$ − referred to the wavelength the length of the projecting plate and the height/altitude of waveguide;

$$u = 2\pi h \sin\vartheta; \quad v_1 = p\sin\frac{\vartheta}{2} + q\cos\frac{\vartheta}{2}; \qquad (8.5)$$

$$w = 2\pi\gamma\cos\vartheta; \quad v_2 = p\sin\frac{\vartheta}{2} - q\cos\frac{\vartheta}{2};$$

$$p = 2\sqrt{\sqrt{\gamma^2 + h^2} + \gamma}; \quad q = 2\sqrt{\sqrt{\gamma^2 + h^2} - \gamma}.$$

Angle $\vartheta$ is counted off clockwise from the negative semi-axis x in the coordinate system, shown in Fig. 8.1.

Parallel polarization.

Parallel polarization corresponds to propagation in the waveguide of magnetic waves. Let us examine only a wave of the type $H_{01}$, which creates in aperture $x=0; 0 \leqslant y \leqslant b$ field distribution

$$E_z = \frac{1}{\zeta_z}\sin\frac{\pi y}{b}; \quad H_y = \sin\frac{\pi y}{b};$$

$$\zeta_z = \frac{\beta}{\kappa}\sqrt{\frac{\varepsilon_1}{\mu_1}}, \qquad (8.6)$$

where $\beta$ – wave propogation constant $H_{01}$ in the waveguide.

For determining the unique component of electric field $E_z$ we will use relationships/ratios (1.4), (1.38) and (1.40):

$$E_z(\vartheta) = \frac{1}{4\pi}\int_0^b (E_z H_{1y} - H_y E_{1z})|_{x=0}\, dy. \qquad (8.7)$$

Page 182.

After integration in expression (8.7) we will obtain

$$f_2^+(\theta) = \left(1 + \frac{1}{\zeta_2}\cos\theta\right)\frac{\pi \sin u}{u^2 - \pi^2} + F_{\parallel}(\theta);$$

$$f_2^-(\theta) = -\left(1 + \frac{1}{\zeta_2}\cos\theta\right)\frac{\pi \sin u}{u^2 - \pi^2} + F_{\parallel}(\theta).$$

$$(8.8)$$

where

$$F_{\parallel}(\theta) = (1+i)\frac{1 + \frac{1}{\zeta_2}\cos\theta}{u^2 - \pi^2}\left\{\frac{\pi}{2}\left[F_1(v_1)e^{-iu} - \right.\right.$$

$$\left. - F_1(v_2)e^{iu}\right] + e^{-iw}\left[\pi J_2\cos\frac{\theta}{2} + iuJ_1\sin\frac{\theta}{2}\right]\right\} +$$

$$+ (1-i)e^{-iw}\frac{J_1\cos\frac{\theta}{2}}{2\pi h\zeta_2};$$

$$(8.9)$$

$$J_1 = e^{-i2\pi\gamma}\int_{2\sqrt{2\gamma}}^{p}e^{i\frac{\pi}{2}t^2}\sin\left(\frac{\pi t}{4h}\sqrt{t^2 - 8\gamma}\right)dt;$$

$$J_2 = e^{i2\pi\gamma}\int_{0}^{q}e^{i\frac{\pi}{2}t^2}\cos\left(\frac{\pi t}{4h}\sqrt{t^2 + 8\gamma}\right)dt; \quad (8.10)$$

$$\zeta_2 = \frac{\beta}{\kappa}\sqrt{\frac{\varepsilon_2}{\mu_2}} = \sqrt{\varepsilon_2 - \frac{1}{4h^2}}; \quad (\mu_2 = 1).$$

## 8.2. Analysis of the obtained results.

Utilizing expressions (8.3), (8.8) for the radiation patterns of single waveguides, it is possible to obtain total field for two waveguides, symmetrically arranged/located relative to half-plane and having the arbitrarily assigned excitation, i.e., any amplitude and the phase of the incident waves. Let us examine two simple ones and

important ones of the case when the amplitudes of the incident waves in these waveguides are identical, and phases either are equal ("cophasal excitation" - electric vectors $\vec{E}_{\text{пад}}$ in the apertures have identical direction)or opposite (" antiphase excitation" - vectors $\vec{E}_{\text{пад}}$ have opposite orientation).

Perpendicular polarization.

In this case during the cophasal excitation of two waveguides. the plate to the "total diagram" effect does not exert and field coincides with the field of two waveguides in the absence of half-plane, i.e.

$$f_{1z}(\theta) = f_1^+(\theta) + f_1^-(\theta) = 2(1 + \zeta_1 \cos\theta)\frac{\sin u}{u}. \quad (8.11)$$

Page 183.

Thus, the cophasally excited waveguides during the perpendicular polarization are equivalent to one waveguide with a height/altitude of 2b, equal to the doubled height/altitude of single waveguide. Diagram (8.11) coincides with field expression of the radiation/emission of the radiation/emission of this waveguide, obtained in the approximation/approach of Huygens-Kirchhoff [63]. During the antiphase excitation of symmetrical waveguides with the wave of the type $E_{**}$ in each, the resulting "differential" diagram

$$f_{1a} = f_1^+(\theta) - f_1^-(\theta) = 2F_\perp(\theta) \qquad (8.12)$$

is formed/shaped with the essential effect of half-plane.

Parallel polarization.

During the cophasal excitation of the upper and lower waveguides [field in the aperture of lower waveguide differs from that described by expression (8.6) only by sign] total field is equal

$$f_{2z}(\theta) = f_2^+(\theta) + f_2^-(\theta) = 2F_{\parallel}(\theta). \qquad (8.13)$$

This means that the projecting plate distorts the total radiation pattern of waveguides during the parallel polarization. At the same time differential radiation pattern (antiphase excitation) half-plane does not affect:

$$f_{2a}(\theta) = f_2^+(\theta) -$$
$$-f_2^-(\theta) = 2\left(1 + \frac{1}{\backslash_2}\cos\theta\right)\frac{\pi \sin u}{u^2 - \pi^2}. \qquad (8.14)$$

It is not difficult to see that formula (8.14) coincides in by the expression, obtained in the approximation/approach of Huygens-Kirchhoff [63] for the waveguide with the doubled height/altitude 2h and the excited by the wave type $H_{\bullet z}$, the propagation constant of which in the waveguide $\beta = \kappa \sqrt{1 - 1/(2h)^2}$ coincides with the wave propogation constant $H_{\bullet 1}$ in the waveguide

with a height/altitude of h.

Page 183.

Thus, the comparison of formulas (8.11) and (8.14) with (8.3) and
(8.8) shows that the first terms of right sides in expressions (8.3
and (8.8) correspond to the approximation/approach of
Huygens-Kirchhoff for the waveguide and his mirror image. Terms $F_\perp$
and $F_\parallel$ in these formulas consider fringe effect of half-plane.

The radiation patterns, described in S 8.1, are obtained without
taking into account the currents, which flow in to the outer side of
the walls of waveguides. Analysis of the radiation patterns of single
waveguides makes it possible to rate/estimate the error, connected
with the approximation/approach indicated. For this in expressions
(8.3), (8.8) one should assume $\gamma=0$ that it corresponds to the
symmetrical task about the radiation/emission from the flat/plane
waveguide. However, there is no complete symmetry of diagrams (8.3),
(8.8) in this case, since are not considered the currents flowing in
to the top wall of waveguide. The degree of asymmetry of radiation
patterns with $\gamma=0$ can serve as qualitative evaluation of the
admissibility of the made simplification.

8.3. Results of calculating the radiation patterns.

According to the formulas, obtained in S 8.1, was produced the calculation of the radiation patterns of the paired waveguides, arranged/located on the half-plane, for the different values of parameters $h=b/\lambda$ and $\gamma=a/\lambda$.

In the case of perpendicular polarization was examined the antiphase excitation of waveguides, in the case of parallel - cophasal. The amplitude and phase radiation patterns $f_{1,2}^{+}$, $\Phi_{1,2}^{+}$ of single waveguides, arranged/located on the half-plane, can be used for obtaining the radiation patterns of two waveguides with arbitrary excitation. For this to the expression of the radiation pattern of upper waveguide $f_{1,2}^{+}(\theta)$ should be added the expression, which characterizes the diagram of lower waveguide $f_{1,2}^{-}(\theta)=f_{1,2}^{+}(-\theta)$, multiplied by certain complex coefficient of B, i.e.,

$$f_{1,2}(\theta)=f_{1,2}^{+}(\theta)+$$
$$+Bf_{1,2}^{-}(\theta)=f_{1,2}^{+}(\theta)+Bf_{1,2}^{+}(-\theta). \qquad (8.15)$$

Page 185.

During the calculation of these diagrams to the parameters $\zeta_1$ and $\zeta_2$ were attached importance, which correspond to different phase wave velocity in the waveguide, by different from the velocity in the

free space. The latter was reached by the filling of waveguide with dielectric or with the selection of the width of waveguide. In the case of perpendicular polarization the calculations were carried out for the values of the conductivity $\zeta_1$, equal to 0.82 and 1-2.8.

The value of conductivity $\zeta_1=0.82$ corresponds phase wave velocity of the type $H_{10}$, which is propagated in rectangular waveguide without the filling with the wide wall, which has size/dimension of $d=0.875\lambda$. Remaining values of $\zeta_1$ correspond to the semi-infinite flat/plane waveguide with the wave of the type TEM, filled with dielectric with permeability $\varepsilon_1$ from 1 to 8. The height/altitude of waveguide varied within the limits $0.25 \leqslant h \leqslant 1.25$.

In the case of parallel polarization the calculations were performed for wave $H_{01}$ and values $\zeta_2$, which correspond to the values of height/altitude h=0.75; 1, 1.25 with the filling of waveguide with dielectric with permeability $\varepsilon_1$ from 1 to 8. During calculations in all cases it was accepted $\mu_1=1$. Giving to the parameters $\zeta_1$ and $\zeta_2$ complex values, it is possible to consider the effect of the fundamental wave reflected on the radiation pattern. In this case $\zeta_1$ and $\zeta_2$ are connected with the complex coefficient of reflection $\Gamma$ by the relationship/ratio

$$\zeta_{1,2} = \zeta_{1,2} \frac{1-\Gamma}{1+\Gamma}. \qquad (8.16)$$

where the values of $\zeta_{1,2}$ are determined by formulas (8.1) and (8.6).

Antiphase excitation of two waveguides. Perpendicular polarization.

Amplitude radiation pattern in this case is the symmetrical function of angle $\vartheta$, it has two major lobes, radiation/emission along half-plane ($\vartheta=0$) is absent. Phase diagram $\Phi_1(\vartheta)$ is also symmetrical, but its part in the region of the negative values $\vartheta$ is shifted value $\pi$ relative to its part with $\vartheta>0$.

Page 186.

Amplitude diagrams for several values of the height/altitude of waveguide h are depicted in Fig. 8.2-8.4. As the parameter is undertaken the ratio of the length of plate to the height/altitude of waveguide $\gamma/h$. With an increase in this relation major lobe approaches an axis of antenna, its width decreases, grow/rise the slope/transconductance of diagram on the slope, turned to the axis, and side-lobe level.
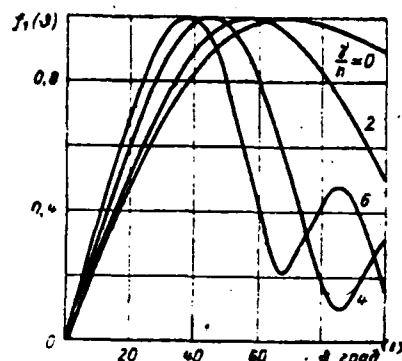
Fig. 8.2.
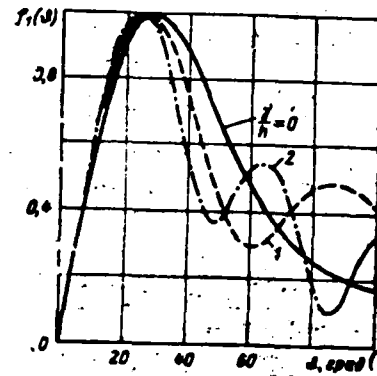


Fig. 8.3.

Fig. 8.2. Amplitude radiation patterns of two waveguides with antiphase excitation with h=1.25.

Key: (1). deg.

Fig. 8.3. Phase radiation patterns of two waveguides with antiphase excitation with h=0.75.

Key: (1). deg.

Page 187.

The effect of ratio $\gamma/h$ on the radiation pattern weakens with an increase in altitude of waveguide h. With $\gamma/h=0$ phase diagrams (Fig. 8.5) are in effect constant, which corresponds to the location of the phase center of system in the beginning of coordinates (Fig. 8.1), i.e., in the foundation of radiating apertures on the half-plane.
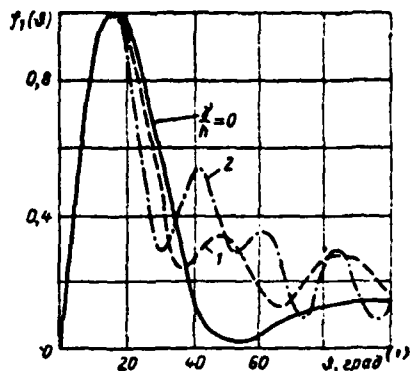
Fig. 8.4.
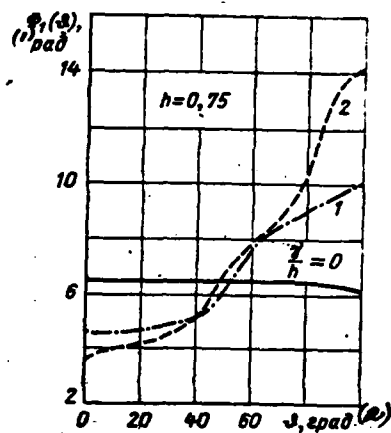


Fig. 8.5.

Fig. 8.4. Amplitude radiation patterns of two waveguides with antiphase excitation with h=1.25.

Key: (1). deg.

Fig. 8.5. Phase radiation patterns of two waveguides with antiphase excitation with h=0.75.

Key: (1). rad. (2). deg.

Page 188.

With an increase in the parameter $\gamma/h$ in the phase diagrams appears characteristic sagging/deflection in the center (with small ones $\vartheta$).

This corresponds to the carrying out of phase center forward from the aperture to the edge/fin of half-plane. Strictly speaking, this system does not have phase center and it is possible to speak only about certain effective phase center. The coordinates of the effective phase center $x_0$, $y_0$ can be found, if real phase response in certain selected interval of angles is represented in the form of the curve

$$\varphi(\vartheta) = \psi_0 + \kappa x_0 \cos\vartheta + \kappa y_0 \sin\vartheta, \qquad (8.17)$$

where $\psi_0 = const.$ In the region of major lobe where the phase changes sufficiently smoothly, the approximation of phase response $\Phi(\vartheta)$ by function $\varphi(\vartheta)$ with a good accuracy it is possible to produce with the aid of their join at three points $\vartheta_i$.

Fig. 8.6 gives the graph/diagram of dependence on $\gamma/h$ that found with such method of the relative coordinate of effective phase center $\gamma_0 = x_0/\lambda$ for different values of h.
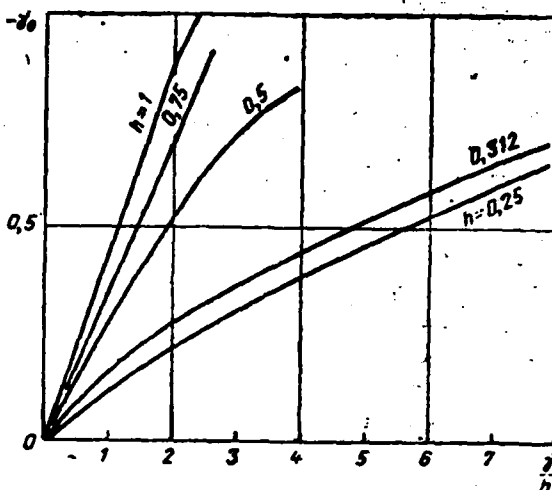
Fig. 8.6. Graph/diagrams of dependence of position of effective phase center on ratio $\gamma/h$ during perpendicular polarization.


Page 189.


In view of symmetry the approximation was conducted in the sector of angles - $\vartheta_0 \leqslant \vartheta \leqslant \vartheta_0$, where $\vartheta_0$ corresponds to the first minimum of diagram, but do not exceed 90°.


From Fig. 8.6 it follows that for values of h=0.25-1.25 the coordinate of phase center is connected with value $\gamma$ with relationship/ratio $\gamma_0 \sim (0.35-0.5)\gamma$. Thus, the obtained effective phase center of system is located near the middle of the projecting plate. Let us note that with an increase in the length of plate to the sizes/dimensions, many the high altitudes of waveguide ($\gamma/h \gg 1$), phase center again approach an aperture. The phase diagrams of waveguides as this converted to the effective center is simple to show, it is actually/really close to the constants.
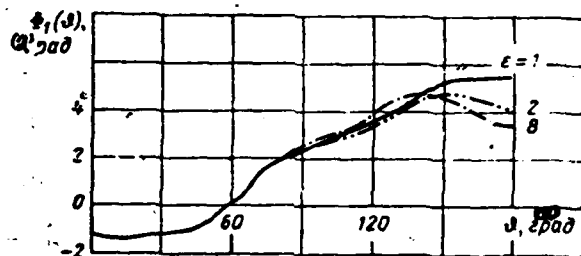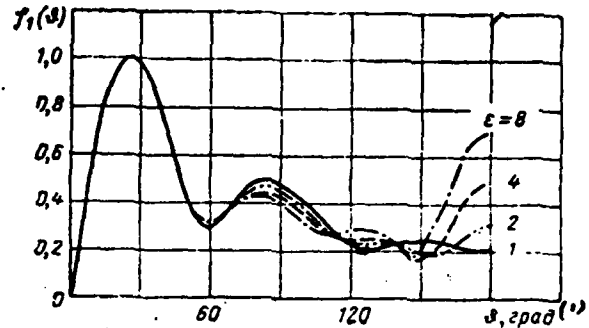
Fig. 8.7. Amplitude and phase radiation patterns of waveguides, filled with dielectric (during perpendicular polarization).

Key: (1). deg. (2). rad.

Page 190.

It is established/installed, that the filling of waveguide with dielectric virtually does not affect the position of maximum and the width of radiation pattern. The effect of filling proved to be essential only in the region of the rear radiation/emission where the

results of calculations were imprecise. As the illustration Fig. 8.7
for h=0.75 and γ/h=0.75 shows the amplitude and phase diagrams of the
waveguides, filled with dielectric with different values ε.-

Cophasal excitation of two waveguides.

Parallel polarization.

In the case of the amplitude and phase diagram of the cophasal
waveguides parallel to polarization, symmetrically arranged/located
relative to half-plane, they are the even functions of angle θ. Major
lobe is directed along the half-plane and is expanded with an
increase in the length of plate γ. Simultaneously increase minor
lobes. With an increase in value γ the first minor lobe can achieve
the level of the main thing and exceed it, which makes it possible to
create radiation pattern close one in form to the table-shaped.
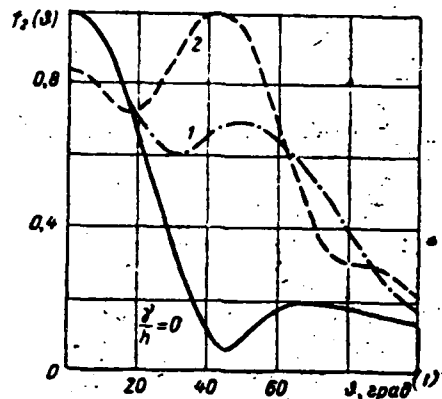
Fig. 8.8. Amplitude radiation patterns of two cophasal waveguides with h=0.75 and different values γ/h.

Key: (1). deg.

Page 191.

With an increase in altitude of waveguide h at the constant value γ the radiation pattern becomes narrow, and side-lobe level decreases (Fig. 8.8-8.10).
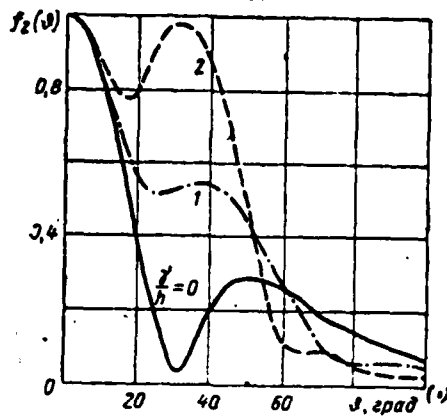
Fig. 8.9. Amplitude radiation patterns of two cophasal waveguides with h=1 and different values γ/h.
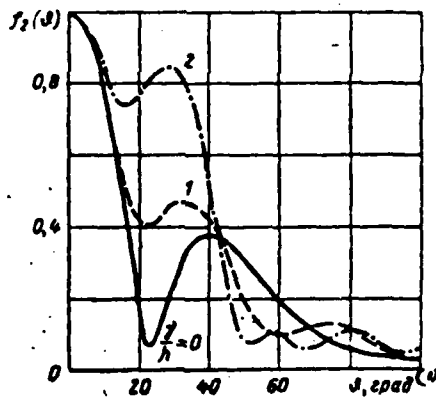
Key: (1). deg.



Fig. 8.10. Amplitude diagrams of two cophasal waveguides with h=1.25 and different values γ/h.

Key: (1). deg.

Page 192.


Phase diagrams in the region of major lobe are close to the constants. The filling of waveguide with dielectric in this case also weakly affects diagram, at least in the region of major lobe. In the region of minor lobes the effect of filling somewhat stronger than in the preceding case. But difference is most substantial in the region of the rear radiation/emission where initial relationships/ratios (8.8) for the radiation field as a result of the allowed approximations/approaches become imprecise. For the illustration Fig. 8.11 shows the amplitude and phase diagrams of the waveguide, filled with dielectric.


Radiation from the single waveguide during the perpendicular and parallel polarizations.


The amplitude and phase diagrams of the single waveguide, arranged/located on the half-plane, for the perpendicular polarization are shown in Fig. 8.12-8.14.
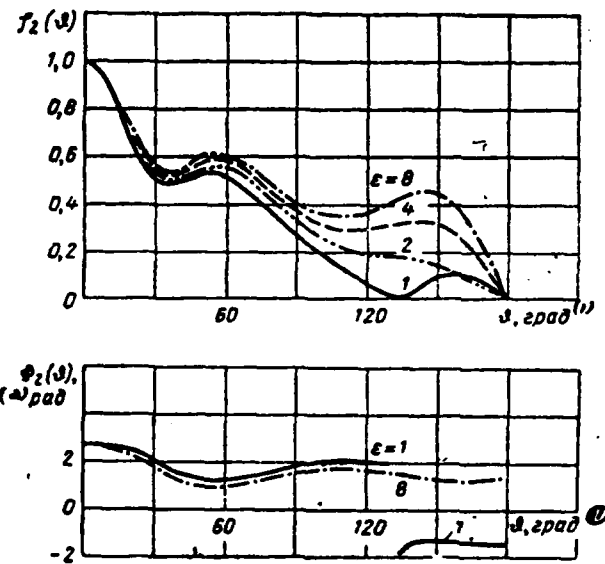
Ϡϧ ϧ. Ϭ.11.        Amplitude and phase diagrams of cophasal waveguides with dielectric filling with h=0.75; γ/h=0.75 and parallel polarization.

Key: (1). deg. (2). rad.

Page 193.

Analogous diagrams for the parallel polarization are given in Fig. 8.15-8.17. Utilizing these diagrams, it is possible with the aid of expression (8.15) to calculate the radiation pattern of two waveguides with the arbitrary excitation.
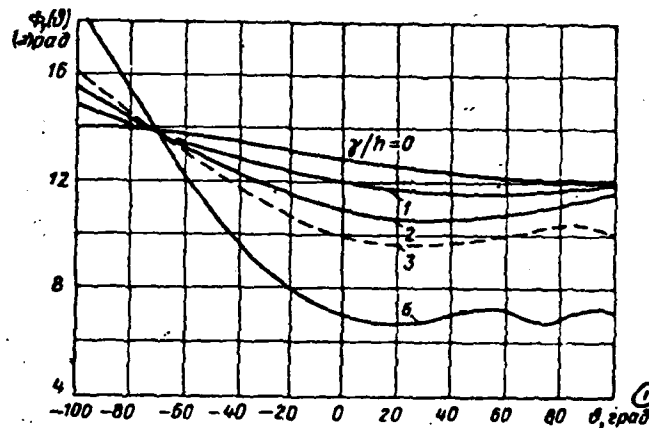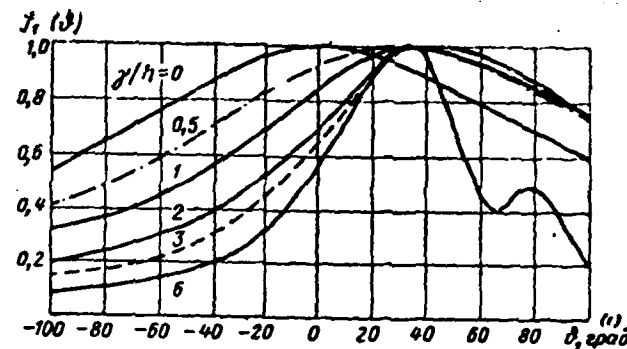
Fig. 8.12. Amplitude and phase diagrams of waveguide on half-plane with h=0.25.

Key: (1). deg. (2). rad.

Page 194.

The amplitude radiation pattern of single waveguide for both polarizations with $\gamma>0$ is deflected upward from the direction $\vartheta=0$.

The amount of deflection of the maximum of the radiation pattern of single waveguide $\vartheta^+_{max}$ from the axis at different relative lengths of plate $\gamma$ for both polarizations is given in Fig. 8.18 (see page 199), where solid lines correspond to perpendicular polarization, and broken lines - parallel.
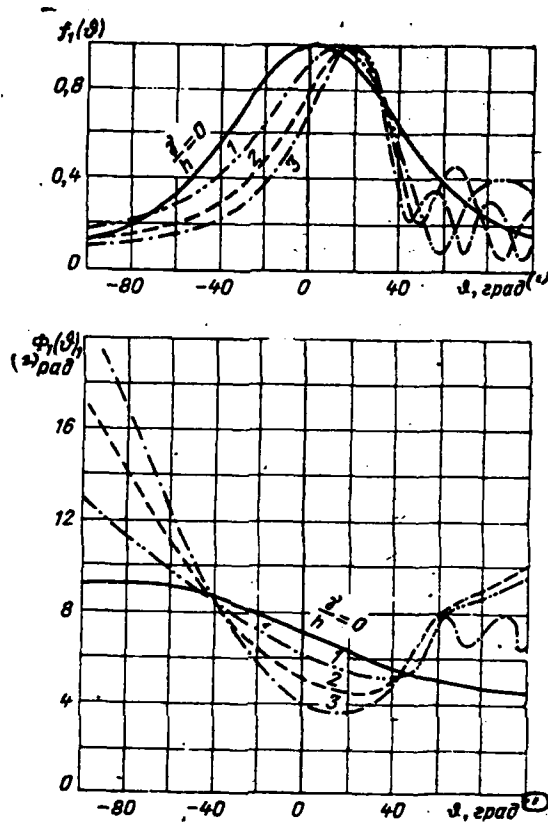
Fig. 8.13. Amplitude and phase diagrams of waveguide on half-plane with h=0.75.

Key: (1). deg. (2). rad.

Page 195.

The width of radiation pattern decreases with an increase $\gamma$. A number of minor lobes on top from the half-plane and their level they

increase with the increase/growth $\gamma$, which is especially noticeable in the case of perpendicular polarization. In the region $\vartheta < 0$ the diagram monotonically drops more rapidly, the larger is $\gamma$.
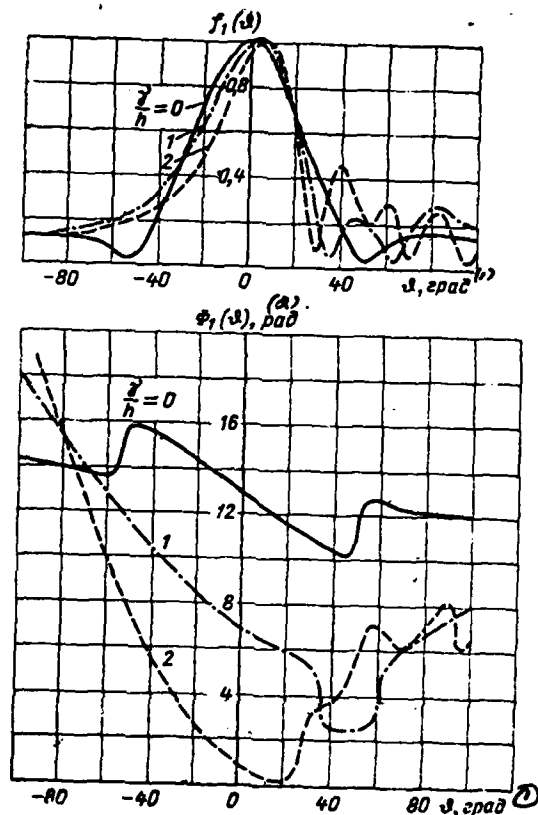
Fig. 8.14. Amplitude and phase diagrams of waveguide on half-plane with h=1.25.

Key: (1). deg. (2). rad.

Page 196.

The phase diagrams, depicted in Fig. 8.12-8.17 (Fig. 8.17 cm. on page 198) with $\gamma/h=0$ have certain inclination/slope which is

explained by the fact that the reference point is arranged/located not in the center of aperture, but in its foundation. With the increase/growth $\gamma$ phase diagrams are distorted. This corresponds to certain displacement of phase center towards the edge/fin of half-plane. The jumps of phase diagram coincide with the minimums of amplitude diagram.

The analysis of calculations for different values $\varepsilon$ showed that the effect of dielectric filling on the radiation pattern of single waveguide so is small, as in the case of two waveguides.
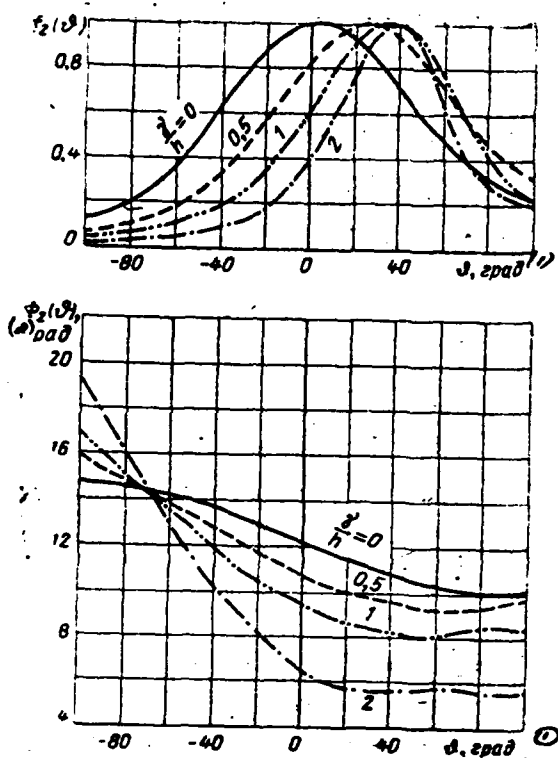
Fig. 8.15. Amplitude and phase diagrams of waveguide on half-plane with h=0.75.

Key: (1). deg. (2). rad.

Page 197.

8.4. Comparison of the results of calculation with the experimental data.

Together with the calculations of radiation patterns $f_1(\theta)$ and $f_2(\theta)$ were carried out the measurements of these diagrams.
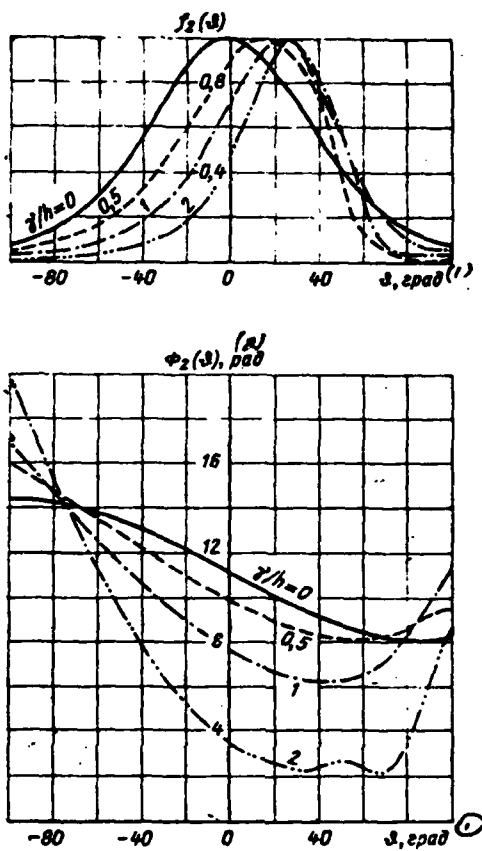
Fig. 8.16. Amplitude and phase diagrams of waveguide on half-plane with h=1.

Key: (1). deg. (2). rad.

Page 198.

In the case of perpendicular polarization the relative height/altitude of waveguide h=0.341; the relative length of plate $\gamma$ took values from 0 to 2.46. During the parallel polarization h=0.752, and $\gamma$ was changed from 0 to 2.3.

The width of waveguide d and the transverse size/dimension l of plate comprised in the first case (in the portions $\lambda$) $d_\perp = 1.11$, $l_\perp = 1.9$, the secondly $d_\parallel = 3.27$, $l_\parallel = 4.25$.
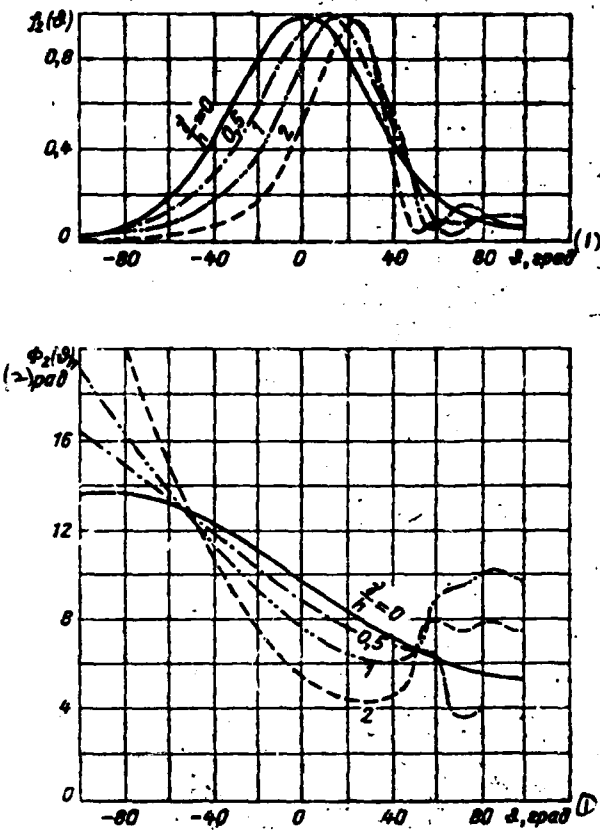
Fig. 8.17. Amplitude and phase diagrams of waveguide on the half-plane with h=1.25.


Key: (1). deg. (2). rad.


Page 199.


Amplitude and phase radiation patterns were taken/removed in the mock-up (Fig. 8.19) in principal plane, normal to the edge/fin of

plate. The projecting plate to the radiation pattern during the cophasal excitation of waveguides in the case of perpendicular polarization $(E_{\perp})$ and antiphase during parallel polarization $(E_{\shortparallel})$ virtually does not affect [see formulas (8.13) (8.16)].
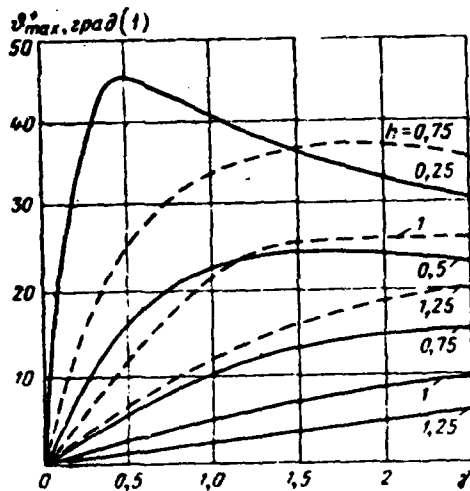
Fig. 8.18.
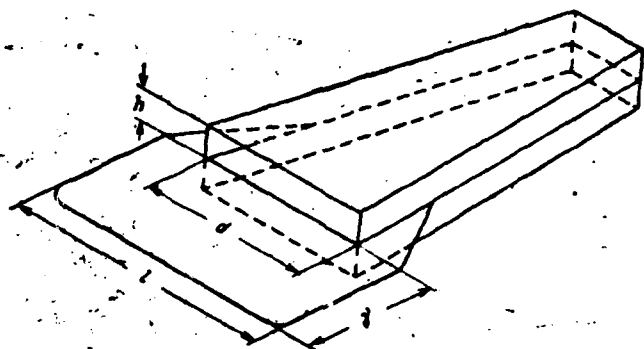
Fig. 8.19.

Fig. 8.18. Graph/diagrams of dependence of direction of maximum of radiation pattern of waveguide on relative length of plate γ.

Key: (1). deg.

Fig. 8.19. General view of mock-up.

Page 200.
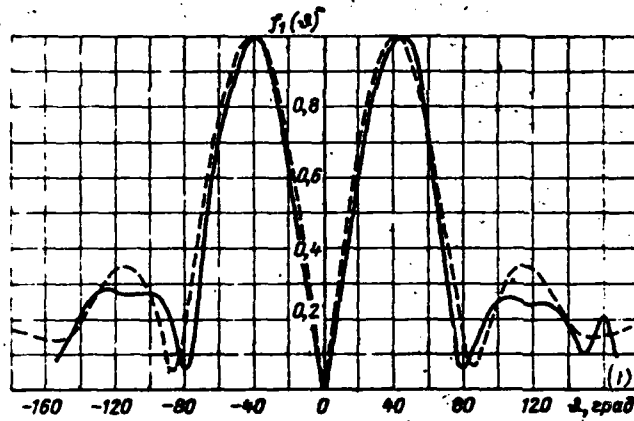


Fig. 8.20. Comparison of experimental (unbroken curve) and calculated (dotted line) radiation patterns for perpendicular polarization with h=0.34, $\gamma$/h=2.7.

Key: (1). deg.
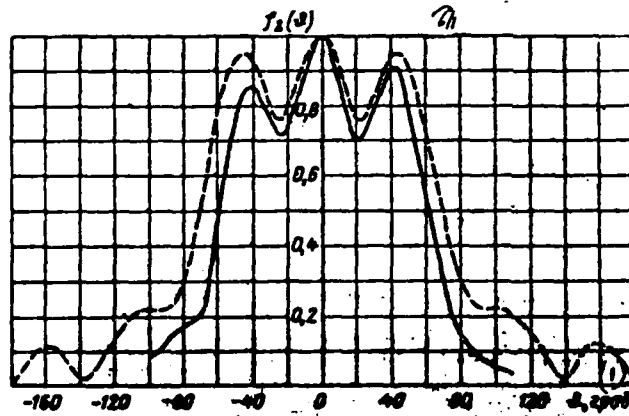


Fig. 8.21. Comparison of experimental (unbroken curve) and calculated (dotted line) radiation patterns for parallel polarization with h=0.75, $\gamma$/h=1.5.

Key: (1). deg.

Page 201.

From the graphs/curves Fig. 8.20 it is evident that in the
sector of angles of $-90° \leqslant \vartheta \leqslant 90°$ occurs the satisfactory coincidence of
experimental diagrams with the calculated ones; coincide position
both the value of maximums and minimums and also the width of diagram
on the level of half power. With an increase in the relative length
of plate $\gamma$ the region of coinciding experimental and calculation data
is expanded. The experimental and calculated amplitude radiation
patterns of two waveguides with the cophasal excitation during the
parallel polarization are shown in Fig. 8.21. Experimental and
calculated radiation patterns for the parallel polarization with
small $\gamma/h$ coincide in the larger sector of angles and it is
considerably more precise than during the perpendicular polarization.
This is connected with the smaller flowing in of currents to the
external walls in the case of parallel polarization.

9.

Three-dimensional ████ radiation patterns of elementary emitters,
which are located on the half-plane.

The results of calculation, obtained in chapters 3-8, to the
equal degree are valid also for the antenna with the two-dimensional
aperture, if discussion deals with the main section of its radiation
pattern (see S 1.2) and is satisfied condition (1.30). However,
frequently the information about the main section of diagram it is
insufficient. In connection with this is of interest the examination
of the three-dimensional/space vector antenna radiation pattern with
the two-dimensional aperture.

In Chapter 3 it was shown that, if surface antenna was distant
up to the sufficient distance from the edge of half-plane, its
radiation pattern can be represented in the form of the product of
two factors one of which corresponds to the diagram of slot, which is
located within the limits of antenna aperture, and another - to
antenna radiation pattern in the free space.

Page 202.

Analogous confirmation is correct for the radiation pattern of the
two-dimensional aperture, which radiates from the surface of
semi-infinite screen. Therefore special importance acquires the
analysis of the radiation patterns of elementary sources,
arranged/located on the half-plane.

9.1. Radiation patterns of elementary slots and electric dipole, that
are located on the half-plane.

Let us determine the radiation patterns of three fundamental
simplest emitters, which are located on the surface of half-plane
(Fig. 9.1): the longitudinal slot, the transverse slot and vertical
electric dipole. To the emitters indicated correspond the following
conditions for excitation:

$$\vec{E}_{1_1}|_s = \delta(x - x_0)\,\delta(z - z_0)\vec{e}_z \qquad (9.1)$$

- for the longitudinal slot,

$$\vec{E}_{1_1}|_s = \delta(x - x_0)\,\delta(z - z_0)\vec{e}_z \qquad (9.2)$$

- for the transverse slot;

$$\vec{H}_{1n}|_s = \delta(x - x_0)\,\delta(z - z_0)\vec{e}_y \qquad (9.3)$$

- for the vertical dipole.
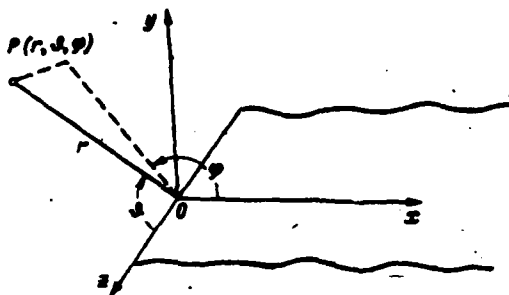
Fig. 9.1. On the calculation of the radiation patterns of elementary sources.

Page 203.

In expressions (9.1)-(9.3):

x, z - coordinate of observation point in the Cartesian system (Fig. 9.1);

$x_0$, $z_0$ - coordinate of the source of field.

In order to calculate the radiation patterns of the emitters in question, we will use relationships/ratios (1.24), (1.25), obtained in $\S$ 1.2 [1].

FOOTNOTE [1]. For calculating the radiation patterns it is possible to

use also the results of work [64]. ENDFOOTNOTE.

Calculation shows that in the remote zone spherical components of the electric field of the sources indicated take the following form:

$$E_{\varphi \parallel} = \sin \vartheta e^{-i\alpha} \left\{ 1 + \sqrt{2}^{-i\frac{\pi}{4}} F_1(v) \right\} =$$

$$= 2 \sin \vartheta e^{-i\alpha} w_{\varphi \parallel}(\vartheta, \varphi) = V_{\varphi \parallel}(\vartheta) W_{\varphi \parallel}(\vartheta, \varphi); \qquad (9.4)$$

$$E_{\vartheta \parallel} = 0$$

- for the longitudinal slot.

$$E_{\vartheta \perp} = \sin \varphi e^{-i\alpha} \left\{ 1 + \sqrt{2}^{-i\frac{\pi}{4}} F_1(\vartheta) + \right.$$

$$\left. + \frac{\sqrt{2} e^{i\frac{\pi}{4}}}{\pi} \frac{e^{i\frac{\pi}{2}\sigma^3}}{v} \right\} =$$

$$= 2 \sin \varphi e^{-i\alpha} W_{\vartheta \perp}(\vartheta, \varphi) = V_{\vartheta \perp}(\vartheta) W_{\vartheta \perp}(\vartheta, \varphi), \qquad (9.5)$$

$$E_{\varphi \perp} = \cos \varphi \cos \vartheta e^{-i\alpha} \left\{ 1 + \sqrt{2} e^{-i\frac{\pi}{4}} F_1(\vartheta) + \right.$$

$$\left. + \frac{\sqrt{2} e^{i\frac{\pi}{4}}}{\pi} \frac{e^{i\frac{\pi}{4}\sigma^3}}{v} \frac{1 + \cos \varphi}{\cos \varphi} \right\} =$$

$$= 2 \cos \varphi \cos \vartheta e^{-i\alpha} W_{\varphi \perp}(\vartheta, \varphi) = V_{\varphi \perp}(\vartheta, \tilde{\tau}) \times$$

$$W_{\varphi \perp}(\vartheta, \varphi)$$

- for the transverse slot

$$E_\vartheta = -\sin\varphi\cos\vartheta\, e^{-iu}\left\{1 + \sqrt{2}\,e^{-i\frac{\pi}{4}}F_1(v) + \right.$$

$$\left. +\frac{\sqrt{2}\,e^{-i\frac{\pi}{4}}}{\pi}\,\frac{e^{i\frac{\pi}{2}v^2}}{v}\right\} =$$

$$= -2\sin\varphi\cos\vartheta\, e^{-iu}\, W_\vartheta\,(\vartheta,\varphi) = V_\vartheta\,(\vartheta,\varphi)\,W_\vartheta\,(\vartheta,\varphi); \quad (9.6)$$

$$E_\varphi = -\cos\varphi\, e^{-iu}\left\{1 + \sqrt{2}\,e^{-i\frac{\pi}{4}}F_1(v) + \right.$$

$$\left. +\frac{\sqrt{2}\,e^{i\frac{\pi}{4}}}{\pi}\,\frac{e^{i\frac{\pi}{2}v^2}}{v}\,\frac{1+\cos\varphi}{\cos\varphi}\right\} =$$

$$= -2\cos\varphi\, e^{-iu}\, W_\varphi\,(\vartheta,\varphi) = V_\varphi\,(\vartheta,\varphi)\,W_\varphi\,(\vartheta,\varphi)$$

- for the vertical electric dipole.


Page 204.


In expressions (9.4)-(9.6) are introduced the following designations:

$$v = 2\sqrt{\frac{\kappa x_0\sin\vartheta}{\pi}}\cos\frac{\varphi}{2};$$

$$u = \kappa x_0\sin\vartheta\cos\varphi + \kappa z_0\cos\vartheta;$$

$\vartheta$, $\varphi$ - angles in the spherical coordinates, shown in Fig. 9.1.


The given relationships/ratios make clear physical sense: each of them can be represented in the form of the product of two factors one of which [V, ($\vartheta$, $\varphi$)] describes the radiation pattern of elementary source in the free space, and another [W($\vartheta$, $\varphi$,] characterizes the effect of semi-infinite screen on the radiation

pattern of emitter. In the main sections $\vartheta=\pi/2$ of radiation pattern
(9.4)-(9.6) they coincide with the appropriate expressions for the
radiation patterns of the elementary cylindrical sources of field,
led in Chapter 3. With the aid of formulas (9.4)-( 9.6) it is
possible to calculate the three-dimensional/space radiation patterns
of the emitters in question.

Page 205.

9.2. Results of the numerical calculation of the radiation patterns
of elementary sources.

The calculated radiation patterns of elementary sources are
shown in Fig. 9.2-9.9. Diagrams correspond to the position of
elementary sources at point $x_{e}=2\lambda$, $z_{e}=0$ on the surface of
semi-infinite screen.

The results of calculations Fig. 9.2-9.6 depicts in the form of
the lines of level of the constant values of the spherical components
of standardized/normalized radiation patterns according to the power.

The radiation patterns, depicted in Fig. 9.2-9.6, are calibrated
relative to the maximum power coefficients, emitted by elementary
sources, which are located on the infinite flat/plane screen.

Fig. 9.2. Lines of level $|E_{\varphi\|}(\vartheta, \varphi)|^2 = \mathrm{const}$ of the radiation pattern of the longitudinal slot. This diagram is calibrated to its own maximum, and remaining (Fig. 9.3-9.6) to maximums $|V(\vartheta, \varphi)|^2$.
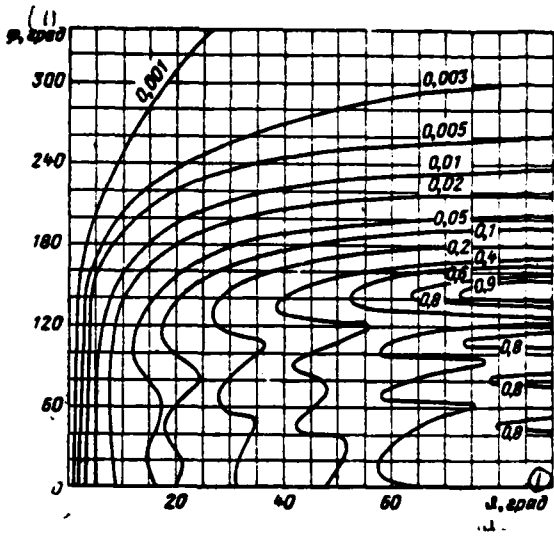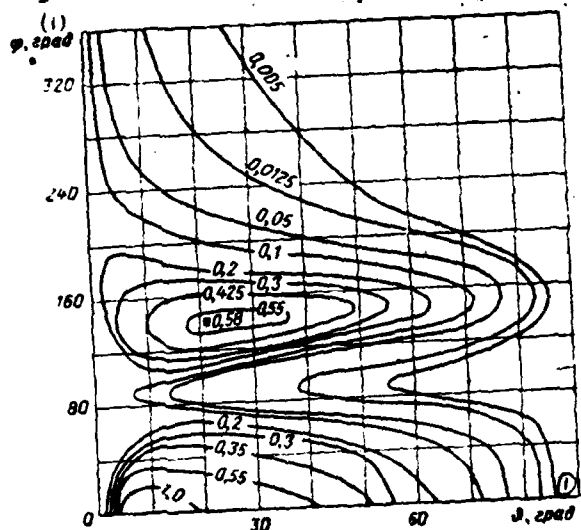
Key: (1). deg.

Page 206.



Fig. 9.3. Lines of level $|E_{\varphi 1}(\theta, \varphi)|^2 = \text{const}$ of radiation pattern of transverse slot.

Key: (1). deg.
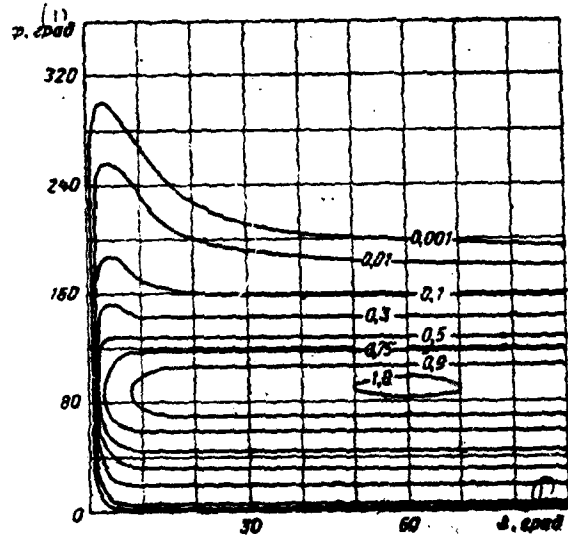
Fig. 9.4. Lines of level $|E_{\theta\perp}(\theta, \varphi)|^2 = \text{const}$ of the radiation patterns of the transverse slot.

Key: (1). deg.

Page 207.
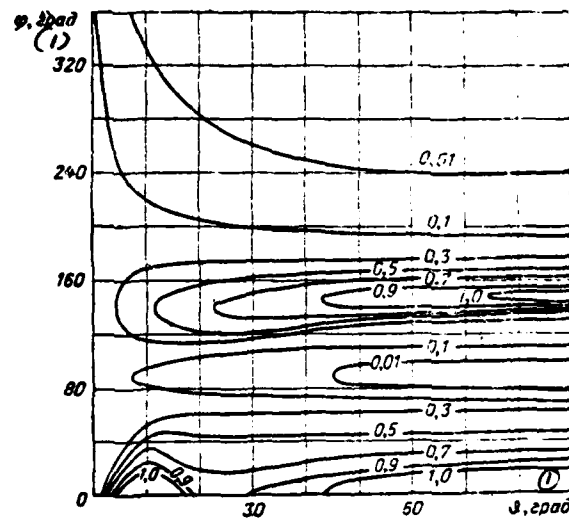


Fig. 9.5. Lines of level $|E_\vartheta(\vartheta, \varphi)|^2 = \mathrm{const}$ of radiation pattern of vertical dipole.
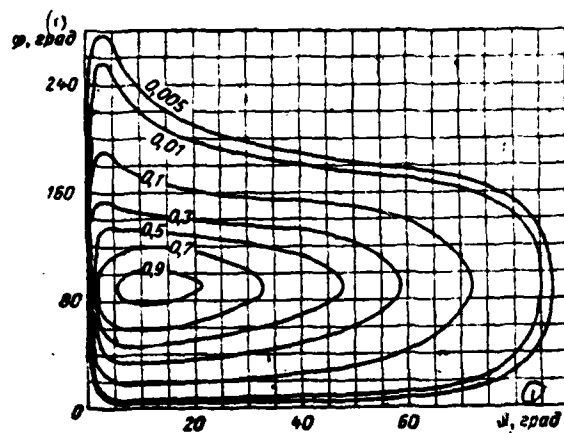
Key: (1). deg.



Fig. 9.6. Lines of level $|E_\varphi(\vartheta, \varphi)|^2 = \mathrm{const}$ of radiation pattern of vertical dipole.

Key: (1). deg.

Page 208.
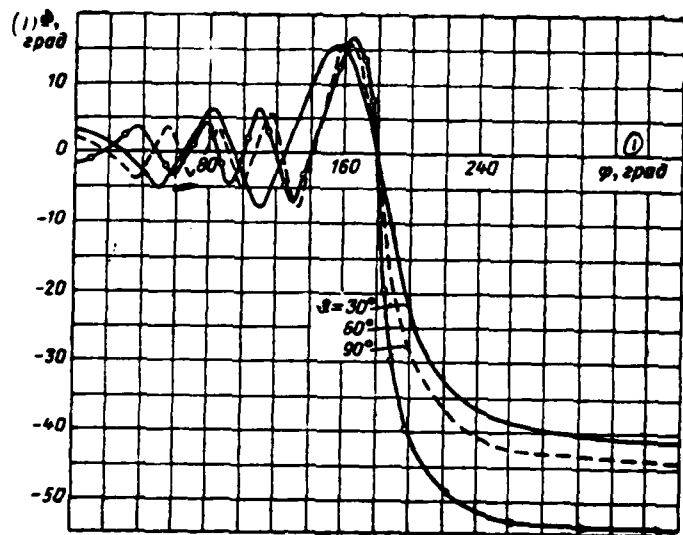


Fig. 9.7. Phase diagrams $\Phi_{\varphi\|}(\varphi, \vartheta) = \arg E_{\varphi\|}(\vartheta, \varphi)$.

Key: (1). deg.
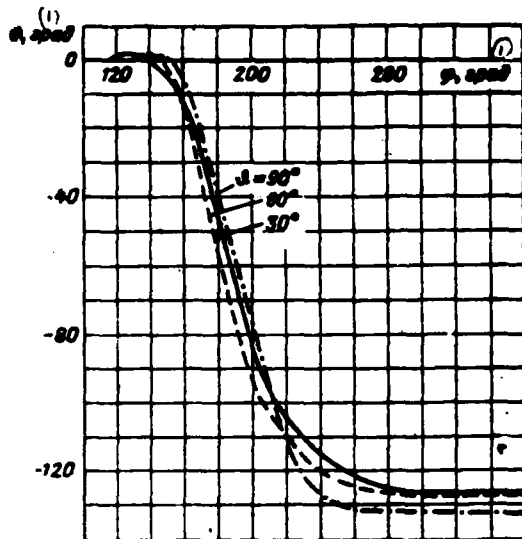
Fig. 9.8. Phase diagrams $\Phi_{\varphi\perp}(\varphi,\vartheta) = \Phi_{\varphi}(\varphi,\vartheta) = \arg E_{\varphi}(\upsilon,\varphi)$.

Key: (1). deg.

Page 209.

From Fig. 9.2-9.6 it is evident that in the shadow zone of radiation pattern monotonically they decrease, and in the region of light/world - they oscillate as a result of the interference of the fields, emitted by elementary sources and edge of screen. The greatest brokenness of radiation patterns with $\varphi < \pi$ is observed in the main sections $\vartheta = \pi/2$. On the measure the removals/distances from the boundary of shadow in the region of the light/world of radiation

pattern approach the values, which correspond to the position of emitters on the plane. The radiation patterns of the transverse slot and vertical dipole with $\vartheta=0$; $\pi$ unlimitedly grow/rise. The special feature/peculiarity of the radiation patterns of the transverse slot and dipole indicated is caused by the action of the edge of screen, along which flows the current with infinite surface density [65]. It should be noted that, in spite of the special feature/peculiarity indicated, power in the diagrams of the transverse slot and dipole have completely specific values.
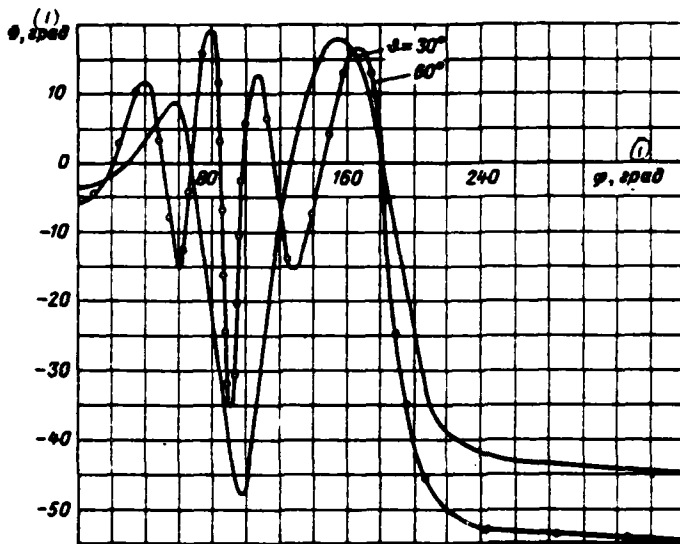
Fig. 9.9. Phase diagrams $\Phi_{\phi\perp}(\varphi, \vartheta) = \Phi_{\varphi}(\varphi, \vartheta) = \arg E_{\varphi}(\vartheta, \varphi)$   $\Phi_{\varphi}(\varphi, \vartheta) = \arg E_{\varphi}(\varphi, \vartheta)$.

Key: (1). deg.

Page 210.

Under the actual conditions when the transverse slot or dipole is located on finite baffle, their radiation pattern will as before have peaks in the directions $\vartheta=0$ and $\pi$ (since edge will operate as traveling-wave antenna); however, the values of these peaks will be final. Let us note that the region of the increase of diagram, which corresponds with $x_\bullet=2\lambda$ to directions of $\theta<1°$, in Fig. 9.3-9.6 is not noted.

Fig. 9.7-9.9 depicts the phase diagrams, designed depending on angular coordinate $\varphi$ for several sections of radiation pattern $\vartheta$=const. From the diagrams it is evident that the phase center of radiation/emission in the shadow zone is arranged/located at point z=0; x=0 on the edge of screen. In the illuminated region phase center is within the limits $0<x<x_\circ$; $0<z<x_\circ$ctg$\vartheta$, moreover its position is different for different sections of radiation pattern.

Page 211.


Appendix I.


Asymptotic formulas for the radiation pattern of slot, which is located on the key.


In order to find asymptotic formulas for diagram u(φ), which correspond to the sufficient removal/distance of slot from the edge of key $(\kappa\Gamma \gg 1)$, let us represent expressions (1.41) and (1.44) for both polarizations in the following form:

$$G = \frac{1}{2a} \left\{ \int\limits_{C_1+C_2} e^{-i\kappa\rho'\cos w} \frac{e^{-i\frac{\pi}{a}w}}{e^{-i\frac{\pi}{a}w} - e^{i\frac{\pi}{a}\xi}} dw \mp \right.$$

$$\left. \mp \int\limits_{C_1+C_2} e^{-i\kappa\rho'\cos w} \frac{e^{-i\frac{\pi}{a}w}}{e^{-i\frac{\pi}{a}w} - e^{i\frac{\pi}{a}\eta}} dw \right\}, \qquad (\text{I.1})$$

where during parallel polarization $G = G_{\parallel} = E_z$, and with perpendicular $G = G_{\perp} = H_z$ [see expressions (1.41) and (1.44)];

$$\xi = \varphi - \varphi', \quad \eta = \varphi + \varphi';$$

$C_1$ and $C_2$ - ducts/contours of integration on the complex plane w, shown in Fig. I.1.


Since us interests the field of slot, which is located on the

key, in expression (I.1) it is possible to assume $\xi \approx \eta \approx \zeta$. Bearing in mind that $\kappa \rho' \gg 1$, for computing the integrals in expression (I.1) is convenient to use the steepest descent method, converting the ducts/contours of integration $C_1$ and $C_2$ into the ways of the fastest descent, passing through saddle points $w = -\pi$; 0; $\pi$ integrands in expression (I.1). However, before carrying out strain of ducts/contours $C_1$ and $C_2$ into paths of steepest descent of integration $W_1$ and $W_2$ (Fig. I.1), it is necessary to explain, what special features/peculiarities possess integrands in formula (I.1) and as are arranged/located these special features/peculiarities on plane w.

Page 212.

Of fundamental interest are those special features/peculiarities which are arranged/located either within the range

$$-\pi \leqslant w \leqslant \pi,$$

or outside it, but near its ends $w = +-\pi$. The presence of such special features/peculiarities must be considered during the conversion of ducts/contours $C_1$ and $C_2$ and during the integration for the steepest descent method. Under sign of both integrals in expression (I.1) stands the function of the following form:

$$S(w, \varkappa) = \frac{1}{1 - \exp\left[1\frac{\pi}{a}(w + \varkappa)\right]},$$

which has simple poles at the points

$$w_n = -x + 2an \quad (n = 0, \pm 1, \pm 2, \ldots).$$

Let us examine how are arranged/located poles $w_n$. Pole $w_0$, which corresponds n=0, is located at point $w_0 = -x$. If we are restricted to the examination of the key whose exterior angle $\pi < \alpha < 2\pi$, will seem that

$$-\pi \leqslant w_0 \leqslant 0.$$
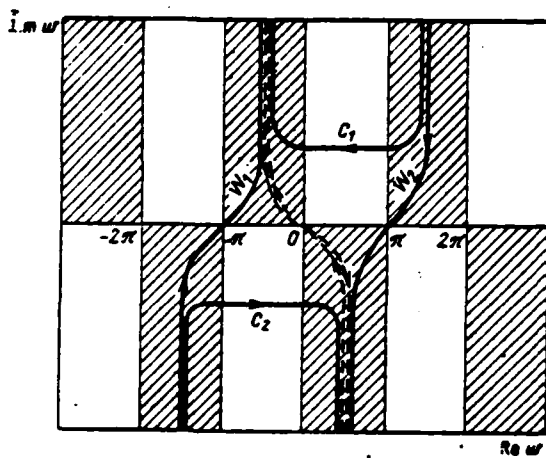
Fig. I.1. Ducts/contours of integration on plane w.

Page 213.

Pole $w_1(n=1)$ is located at the point

$$w_1 = 2a - \varkappa.$$

Since it is assumed that $\alpha \geqslant \pi$, pole $w_1$ cannot prove to be inside the interval $(-\pi, \pi)$. However, with $\alpha \to \pi$ and $\varkappa \to \pi$ pole $w_1$ approaches saddle point $w = \pi$. It is analogous, if $\varkappa \to \pi$ ($\varkappa = \pi$ — boundary of shadow), pole $w_0$ approaches saddle point $w = -\pi$. Remaining special features/peculiarities $w_n(n \neq 0; 1)$ of function $S(w, \varkappa)$ are located out of the interval $(-\pi, \pi)$ far from its ends/leads. Therefore during the conversion of the ducts/contours of integration $C_1$ and $C_2$ in the way of the fastest descent $W_1$ and $W_2$ and the integration for the steepest descent method it is necessary to consider the simple poles $w_0$ and $w_1$

of integrand. The conversion of ducts/contours $C_1$ and $C_2$ into paths
of steepest descent of integration is shown in Fig. I.1. If $0 \leqslant \varkappa \leqslant \pi$
the region of light/world), during the strain of duct/contour $C_2$ it
is necessary to add in expression (I.1) deduction in pole $w = w_*$ which
proves to be within the region, limited by duct/contour $C_2 = W_1 + W'_1$.
When $\varkappa > \pi$ (shadow zone) pole $w = w_*$ proves to be out of the interval
$(-\pi, \pi)$. The contribution, introduced by pole $w = w_*$, corresponds to
geometric-optical component of diffraction field. Since branches $W'_{12}$
of the converted ducts/contours $C_{12} = W_{12} + W'_{12}$ coincide, and the
directions of circuit/bypass along $W'_1$ and $W'_2$ are opposite,
expression (I.1) taking into account the aforesaid can be represented
in the following form:

$$G = h(\xi) e^{-i\varkappa\rho'\cos\xi} \mp h(\eta) e^{-i\varkappa\rho'\cos\eta} +$$

$$+ \frac{1}{2\alpha} \left\{ \int_{W_1 + W_2} e^{-i\varkappa\rho'\cos w} \frac{e^{-i\frac{\pi}{\alpha}w}}{e^{-i\frac{\pi}{\alpha}w} - e^{i\frac{\pi}{\alpha}\xi}} dw \mp \right.$$

$$\left. \mp \int_{W_1 + W_2} e^{-i\varkappa\rho'\cos w} \frac{e^{-i\frac{\pi}{\alpha}w}}{e^{-i\frac{\pi}{\alpha}w} - e^{i\frac{\pi}{\alpha}\eta}} dw \right\}, \qquad (I.2)$$

$$h(\varkappa) = \begin{cases} 1 & \text{при } 0 < \varkappa < \pi, \\ 0 & \text{при } \varkappa > \pi. \end{cases}$$

Page 214.


So that the ducts/contours $W_1$ and $W_2$ would be by paths of steepest
descent of integration, their inclination/slope at saddle points
$w = +-\pi$ to axis Re w must compose angle in 45°. Taking into account
this and taking into account the direction of circuit/bypass $W_1$ and

$W_1$, let us make the following replacement of variable/alternating:

$$w = se^{i\frac{5\pi}{4}} + \pi \overset{(1)}{\text{для}} W_1;$$

$$w = se^{i\frac{\pi}{4}} - \pi \overset{(1)}{\text{для}} W_2. \qquad (I.3)$$

Key: (1). for.

Since it is assumed that $\kappa\rho' \gg 1$, replacement (I.3) makes it possible to convert expressions (I.2) to the following form:

$$G = h(\xi) e^{-i\kappa\rho'\cos\xi} \mp h(\eta) e^{-i\kappa\rho'\cos\eta} +$$

$$+ \frac{1}{2\alpha} \exp\left[i\left(\kappa\rho' - \frac{\pi}{4}\right)\right]\left\{\left[\int_{-\infty}^{+\infty} \frac{\exp\left(-\frac{\kappa\rho'}{2}s^2\right)ds}{1 - \exp\left[i\frac{\pi}{\alpha}\left(se^{i\frac{\pi}{4}} + \xi - \pi\right)\right]} - \right.\right.$$

$$\left. - \int_{-\infty}^{+\infty} \exp\left(-\frac{\kappa\rho'}{2}s^2\right) \frac{ds}{1 - \exp\left[i\frac{\pi}{\alpha}\left(se^{i\frac{5\pi}{4}} + \xi + \pi\right)\right]}\right] \mp$$

$$\mp \left[\int_{-\infty}^{+\infty} \exp\left(-\frac{\kappa\rho'}{2}s^2\right) \frac{ds}{1 - \exp\left[i\frac{\pi}{\alpha}\left(se^{i\frac{\pi}{4}} + \eta - \pi\right)\right]} - \right.$$

$$\left.\left. - \int_{-\infty}^{+\infty} \exp\left(-\frac{\kappa\rho'}{2}s^2\right) \frac{ds}{1 - \exp\left[i\frac{\pi}{\alpha}\left(se^{i\frac{5\pi}{4}} + \eta + \pi\right)\right]}\right]\right\}. \qquad (I.4)$$

Page 215.

In this recording Green's functions are represented in the form of the combination of the integrals

$$I = \int_{-\infty}^{+\infty} \exp\left(-\frac{\kappa\rho'}{2}s^2\right) \frac{ds}{1 - \exp\left[-\gamma_{1,2}(s + b_{1,2})\right]}. \qquad (I.5)$$

where

$$\gamma_1 = -i\,\frac{\pi}{a}\,e^{i\frac{\pi}{4}j};$$

$$b_1 = e^{-i\frac{\pi}{4}}\,(x - \pi);$$

$$\gamma_2 = -i\,\frac{\pi}{a}\,e^{i\frac{5\pi}{4}};$$

$$b_2 = e^{-i\frac{5\pi}{4}}\,(x + \pi - 2a).$$

Integrand in (I.5) has simple ones of pole at points $s=-b_{1,2}$. If $b_1$ or $b_2 \to 0$, the pole of integrand approach appropriate saddle points and the function

$$f(s) = \frac{1}{1 - e^{-\gamma_{1,2}(s + b_{1,2})}}$$

stops the rapidly changing in the vicinity point $s=0$. Therefore for computing the integrals of form (I.5) it is not possible to directly use the usual method of steepest descent [66]. The difficulty indicated during the computation of integral can be bridged, after isolating the part of function $f(s)$ oscillating near the poles, after presenting $f(s)$, as follows:

$$f(s) = \frac{1}{1 - e^{-\gamma(s+b)}} = \frac{1}{\gamma(s+b)} + T(s), \qquad (I.6)$$

where

$$T(s) = \frac{1}{1 - e^{-\gamma(s+b)}} - \frac{1}{\gamma(s+b)}.$$

In expression (I.6) function $T(s)$ will always be that slowly changing and therefore, substituting (I.6) in (I.5), we will obtain:

$$I_1 = \int\limits_{-\infty}^{+\infty} e^{-\frac{\pi \rho'}{2}s} \left[ \frac{1}{\gamma(s+b)} + T(s) \right] ds =$$

$$= \frac{1}{\gamma} \int\limits_{-\infty}^{+\infty} \frac{e^{-\frac{\pi\rho'}{2}s}}{s+b}\, ds + T(0) \sqrt{\frac{2\pi}{\pi\rho'}}. \qquad (I.7)$$

Page 216.

For computing the integral

$$I^{(1)} = \frac{1}{\gamma} \int_{-\infty}^{+\infty} \frac{e^{-\frac{\pi \rho'}{2} s^2}}{s+b} ds \qquad (1.8)$$

we will use the reception/procedure, proposed by Felsen [67].

Let us represent

$$\frac{1}{s+b} = -\frac{1}{b} \left( \frac{s^2 - sb}{s^2 - b^2} - 1 \right).$$

Then

$$I^{(1)} = -\frac{2}{\gamma b} \left\{ \int_0^{\infty} \frac{s^2 e^{-\frac{\pi \rho'}{2} s^2}}{s^2 - b^2} ds - \frac{1}{2} \sqrt{\frac{2\pi}{\kappa \rho'}} \right\}.$$

In order to calculate the integral

$$I^{(2)} = \int_0^{\infty} \frac{s^2 e^{-\frac{\pi \rho'}{2} s^2}}{s^2 - b^2} ds,$$

let us enter as follows. It is not difficult to ascertain that

$$\frac{d}{dx} \left[ e^{x b^2} I^{(2)}(x) \right] = - e^{x b^2} \int_0^{\infty} s^2 e^{-x s^2} ds =$$

$$= -\frac{1}{2} e^{x b^2} x^{-\frac{3}{2}} \Gamma \left( \frac{3}{2} \right) = -\frac{\sqrt{\pi}}{4} e^{x b^2} x^{-\frac{3}{2}}. \qquad (1.9)$$

Integrating expression (I.9) on x from $-xb^2$ to $\infty$, we obtain

$$I^{(2)}(x) = \frac{1}{2}\sqrt{\frac{\pi}{x}} - \frac{1}{2}V\overline{-\pi b^2}\,e^{-xb^2}\int\limits_{-xb^2}^{\infty} e^{-t}t^{-\frac{1}{2}}\,dt.$$

Thus,

$$I^{(2)} = \frac{1}{2}\sqrt{\frac{2\pi}{\kappa\rho'}} - \frac{\pi V\overline{-b^2}}{2}\left\{1 - V\overline{2}\,e^{-i\frac{\pi}{4}}\times\right.$$
$$\left.\times F_1\left(\sqrt{\frac{-i\kappa\rho' b^2}{\pi}}\right)\right\} \qquad (I.10)$$

and then

$$I = \int\limits_{-\infty}^{+\infty} e^{-\frac{\kappa\rho'}{2}s^2}\frac{ds}{1 - e^{-\gamma(s+b)}} =$$
$$= -\frac{i\pi}{\gamma}\operatorname{sign} b\, e^{-\frac{\kappa\rho'}{2}b^2}\left\{1 - V\overline{2}\,e^{-i\frac{\pi}{4}}\times\right.$$
$$\left.\times F_1\left(e^{-i\frac{\pi}{4}}|b|\sqrt{\frac{\kappa\rho'}{\pi}}\right)\right\} + \sqrt{\frac{2\pi}{\kappa\rho'}}\left(\frac{1}{1 - e^{-\gamma b}} - \frac{1}{\gamma b}\right). \quad (I.11)$$

Page 217.

Substituting expressions (I.5)-(I.11) into formula (I.4) and by defining concretely values of $\gamma_{1,2}$ and $b_{1,2}$, we will obtain the following asymptotic representations for Green's functions $G_{\parallel,\perp}$ in the regions of light/world and the shadows, which correspond $\kappa\rho' \gg 1$.

1. Region of light/world $0 \leqslant \xi \leqslant \pi;\ 0 \leqslant \eta \leqslant \pi)$

$$G_{\shortparallel, \perp} = e^{-i\kappa\rho'\cos\xi} \mp e^{-i\kappa\rho'\cos\eta} + \frac{1}{2a} e^{i\left(\kappa\rho' + \frac{\pi}{4}\right)} \times$$

$$\times \left[ \frac{\sin\frac{\pi^2}{a}}{\cos\frac{\pi^2}{a} - \cos\frac{\pi}{a}\xi} \mp \frac{\sin\frac{\pi^2}{a}}{\cos\frac{\pi^2}{a} - \cos\frac{\pi}{a}\eta} \right] \sqrt{\frac{2\pi}{\kappa\rho'}} -$$

$$- \frac{i}{2\pi} e^{i\left(\kappa\rho' - \frac{\pi}{4}\right)} \left\{ \pi e^{-i\frac{\pi}{4}} e^{-\frac{i\kappa\rho'}{2}(\pi-\xi)^2} \times \right.$$

$$\times \left( 1 - \sqrt{2} e^{-i\frac{\pi}{4}} F_1\left[ \sqrt{\frac{\kappa\rho'}{\pi}}(\pi-\xi) \right] \right) -$$

$$- \frac{1}{\pi-\xi} \sqrt{\frac{2\pi}{\kappa\rho'}} - \pi e^{-i\frac{\pi}{4}} e^{-\frac{i\kappa\rho'}{2}(2a-\xi-\pi)^2} \times$$

$$\times \left( 1 - \sqrt{2} e^{-i\frac{\pi}{4}} F_1\left[ \sqrt{\frac{\kappa\rho'}{\pi}}(2a-\xi-\pi) \right] \right) +$$

$$+ \frac{1}{2a-\xi-\pi} \sqrt{\frac{2\pi}{\kappa\rho'}} \mp \pi e^{-i\frac{\pi}{4}} e^{-i\frac{\kappa\rho'}{2}(\pi-\eta)^2} \times$$

$$\times \left( 1 - \sqrt{2} e^{-i\frac{\pi}{4}} F_1\left[ \sqrt{\frac{\kappa\rho'}{\pi}}(\pi-\eta) \right] \right) \pm$$

$$\pm \frac{1}{\pi-\eta} \sqrt{\frac{2\pi}{\kappa\rho'}} \pm \pi e^{-i\frac{\pi}{4}} e^{-i\frac{\kappa\rho'}{2}(2a-\eta-\pi)^2} \times$$

$$\times \left( 1 - \sqrt{2} e^{-i\frac{\pi}{4}} F_1\left[ \sqrt{\frac{\kappa\rho'}{2}}(2a-\eta-\pi) \right] \right) \mp$$

$$\mp \frac{1}{2a-\eta-\pi} \sqrt{\frac{2\pi}{\kappa\rho'}} \right\}. \qquad (1.12)$$

Page 218.

2. Shadow zone $(\pi < \xi < a, \ \pi < \eta < a)$

$$G_{\shortparallel,\perp} = \frac{1}{2\pi} e^{i\left(\kappa\rho' + \frac{\pi}{4}\right)} \times$$

$$\times \left( \frac{\sin \frac{\pi^2}{\alpha}}{\cos \frac{\pi^2}{\alpha} - \cos \frac{\pi}{\alpha} \xi} \mp \frac{\sin \frac{\pi^2}{\alpha}}{\cos \frac{\pi^2}{\alpha} - \cos \frac{\pi}{\alpha} \eta} \right) \sqrt{\frac{2\pi}{\kappa\rho'}} -$$

$$- \frac{i}{2\pi} e^{i\left(\kappa\rho' + \frac{\pi}{4}\right)} \left\{ -\pi e^{-i\frac{\pi}{4}} e^{-i\frac{\kappa\rho'}{2}(\xi-\pi)^2} \times \right.$$

$$\times \left( 1 - \sqrt{2} e^{-i\frac{\pi}{4}} F_1\left[ \sqrt{\frac{\kappa\rho'}{\pi}} (\xi - \pi) \right] \right) +$$

$$+ \frac{1}{\xi - \pi} \sqrt{\frac{2\pi}{\kappa\rho'}} - \pi e^{-i\frac{\pi}{4}} e^{-i\frac{\kappa\rho'}{2}(2\alpha-\xi-\pi)^2} \times$$

$$\times \left( 1 - \sqrt{2} e^{-i\frac{\pi}{4}} F_1\left[ \sqrt{\frac{\kappa\rho'}{\pi}} (2\alpha - \xi - \pi) \right] \right) -$$

$$- \frac{1}{2\alpha - \xi - \pi} \sqrt{\frac{2\pi}{\kappa\rho'}} \pm \pi e^{-i\frac{\pi}{4}} e^{-i\frac{\kappa\rho'}{2}(\eta-\pi)^2} \times$$

$$\times \left( 1 - \sqrt{2} e^{-i\frac{\pi}{4}} F_1\left[ \sqrt{\frac{\kappa\rho'}{\pi}} (\eta - \pi) \right] \right) \mp$$

$$\mp \frac{1}{\eta - \pi} \sqrt{\frac{2\pi}{\kappa\rho'}} \pm \pi e^{-i\frac{\pi}{4}} e^{-i\frac{\kappa\rho'}{2}(2\alpha-\eta-\pi)^2} \times$$

$$\times \left( 1 - \sqrt{2} e^{-i\frac{\pi}{4}} F_1\left[ \sqrt{\frac{\kappa\rho'}{\pi}} (2\alpha - \eta - \pi) \right] \right) \mp$$

$$\mp \frac{1}{2\alpha - \eta - \pi} \sqrt{\frac{2\pi}{\kappa\rho'}} \right\}. \qquad (1.13)$$

Page 219.


Appendix II.


Calculation of fields, created by slot, which is located on the impedance plane.


Let the slot in the impedance plane (Fig. II.1) be excited by the field

$$H_m = -\delta(z' - \Gamma)\vec{e}_y. \qquad (\text{II.1})$$

(Plane coordinates x=0 in contrast to the coordinates in half-space x>0, they will be noted by primes, i..., with x=0 z=z', y=y').


For the convenience we will consider that the surface impedance Z of plane can be represented in the following form:

$$Z = \bar{\eta} Z_0, \qquad (\text{II.2})$$

where

$$Z_0 = \sqrt{\frac{\mu_0}{\varepsilon_0}} = 120\pi \text{ ohm}$$

- impedance of free space.


Disregarding ohmic losses, let us assume

$$\bar{\eta} = i\eta, \qquad (\text{II.3})$$

$\eta = \text{const}$ — real value.
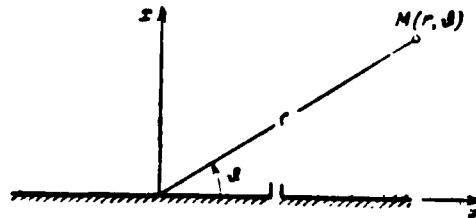
Fig. II.1. On the calculation of the radiation/emission of slot in the impedance plane.

Page 220.

Taking into account boundary condition in the impedance surface, we obtain

$$\left[\frac{\partial H}{\partial n} + \kappa \eta H\right]_{x=0} = i\omega\delta(z' - \Gamma),\qquad(\text{II}.4)$$

where $\vec{n} = \vec{e}_x$ - unit vector of normal to the surface of screen. According to the formula of Kirchhoff and the conditions for radiation/emission, magnetic field H(x, z) at any point (x, z) of half-space x⩾0 can be represented in the following form:

$$H(x,\ z) = \frac{1}{4}\int_{-\infty}^{\infty}\left[H(0,\ z')\frac{\partial\psi}{\partial n} - \psi\left(\frac{\partial H}{\partial n}\right)_{x=0}\right]dz'.\quad(\text{II}.5)$$

As auxiliary function $\psi=\psi(x,z,x',z')$ in expression (II.5) let us select the combination of the following form:

$$\psi = H_0^{(1)}[\kappa\sqrt{(x-x')^2+(z-z')^2}] +$$
$$+ H_0^{(1)}[\kappa\sqrt{(x+x')^2+(z-z')^2}].\qquad(\text{II}.6)$$

Substituting function $\psi$ and value $(\partial H/\partial n)_{x=0}$, found from condition

(II.4), into expression (II.5), we obtain

$$H(x, z) = \frac{1}{2}\left\{ -i\omega\mu H_0^{(1)}(\kappa\sqrt{x^2+(z-\Gamma)^2}) + \right.$$

$$\left. + \kappa\eta\int_{-\infty}^{\infty} H_0^{(1)}[\kappa\sqrt{x^2+(z-t')^2}] \right\} H(0, t')\,dt'. \quad \text{(II.7)}$$

In view of the uniform relative to X convergence of integral in
(II.7) admissibly to pass in this expression to the limit with x→0,
in consequence of which there will be obtained following integral
equation for the value of magnetic field on the surface of screen
x=0:

$$H(0, z') = \frac{1}{2}\left\{ -i\omega\mu H_0^{(1)}(\kappa|z'-\Gamma|) + \right.$$

$$\left. + \kappa\eta\int_{-\infty}^{\infty} H_0^{(1)}(\kappa|z'-t|) H(0, t)\,dt \right\}. \quad \text{(II.8)}$$

Page 221.


The obtained integral equation has differential nucleus and therefore
for solving it it is expedient to use Fourier transform, having
temporarily assumed that k - is complex and Imk>0. In view of the
made assumption the Fourier transform equation (II.8) is holomorphic
in the band

$$-\operatorname{Im}\kappa \leqslant \operatorname{Im}\zeta \leqslant \operatorname{Im}\kappa. \quad \text{(II.9)}$$

Actually/really, the left side of equation (II.8) with |z'| →∞ behaves
as exp(+-iβz') (β - propagation constant of ground wave), and
therefore its Fourier transform is holomorphic in the band

$$-\operatorname{Im}\beta \leqslant \operatorname{Im}\zeta \leqslant \operatorname{Im}\beta. \quad \text{(II.10)}$$

The Fourier transform of the right side of equation (II.8) is regular in band (II.9). Therefore in view of the fact that $\beta \geqslant \kappa$ (ground wave retarded), the Fourier transform for equation (II.8) as a whole is holomorphic in band (II.9). Equation (II.8) modified according to Fourier takes the following form:

$$\overline{H(0, \zeta)} = \frac{1}{2} \left\{ -\frac{i\omega\epsilon}{\sqrt{2\pi}} \int_{-\infty}^{\infty} e^{i\zeta z'} H_0^{(1)}(\kappa|z'-\Gamma|) dz' + \right.$$

$$\left. + \frac{\kappa\eta}{\sqrt{2\pi}} \int_{-\infty}^{\infty} e^{i\zeta z'} \left[ \int_{-\infty}^{\infty} H(0, t) H_0^{(1)}(\kappa|z'-t|) dt \right] dz', \quad (II.11) \right.$$

where $\overline{H(0, \zeta)}$ - Fourier transform for $H(0, \zeta)$.

Page 222.

Taking into account that [63]

$$\int_{-\infty}^{\infty} e^{i\zeta z'} H_0^{(1)}(\kappa|z'-\Gamma|) dz' = e^{i\zeta\Gamma} \frac{2}{\sqrt{\kappa^2 - \zeta^2}}$$

and

$$H(0, t) = \frac{1}{\sqrt{2\pi}} \int_{-\infty}^{\infty} e^{-i\zeta t} \overline{H(0, \zeta)} d\zeta,$$

we obtain with the aid of formula (II.11)

$$\overline{H(0, \zeta)} = \frac{1}{2} \left\{ -\frac{2}{\sqrt{2\pi}} \frac{i\omega\epsilon}{\sqrt{\kappa^2 - \zeta^2}} e^{i\zeta\Gamma} + \right.$$

$$\left. + \frac{\kappa\eta}{2\pi} \int_{-\infty}^{\infty} \overline{H(0, \zeta)} W(\zeta, \zeta) d\zeta \right\}, \qquad (II.12)$$

where

$$W(\xi,\ \zeta) = \int\limits_{-\infty}^{\infty} e^{i\zeta z'} \left[ \int\limits_{-\infty}^{\infty} e^{-i\xi' t'} H_0^{(1)}(\kappa|z'-t|)dt \right] dz' =$$

$$= \int\limits_{-\infty}^{\infty} e^{i(\zeta-\xi) z'} \left[ \int\limits_{-\infty}^{\infty} e^{i\zeta u} H_0^{(1)}(k|u|)du \right] dz' =$$

$$= \frac{2}{\sqrt{\kappa^2-\xi^2}} \int\limits_{-\infty}^{\infty} e^{-i(\zeta-\xi) z'}\,dz' = \frac{4\pi\delta\,(\zeta-\xi)}{\sqrt{\kappa^2-\xi^2}}.$$

Therefore

$$\overline{H(0,\ \zeta)} = i \left\{ -\frac{1}{\sqrt{2\pi}}\, \frac{i\omega\epsilon}{\sqrt{\kappa^2-\zeta^2}}\, e^{i\zeta\Gamma} + \frac{\eta\kappa\,\overline{H(0,\ \zeta)}}{\sqrt{\kappa^2-\zeta^2}} \right\}$$

and, therefore,

$$\overline{H(0,\ \zeta)} = \frac{\omega\epsilon}{\sqrt{2\pi}}\, \frac{1}{\sqrt{\kappa^2-\zeta^2}-i\kappa\eta}\, e^{i\zeta\Gamma}. \qquad (\text{II.13})$$

As a result of holomorphy of both parts of the latter/last equality in band (II.9) admissibly inverse transformation of Fourier expression (II.13). Thus, the solution of integral equation (II.8) takes the following form:

$$H(0,\ z') = \frac{\omega\epsilon}{2\pi} \int\limits_{-\infty}^{\infty} \frac{\exp\left[-i\zeta\,(z'-\Gamma)\right]d\zeta}{\sqrt{\kappa^2-\zeta^2}-i\kappa\eta}. \qquad (\text{II.14})$$

We convert the obtained solution of equation (II.8), taking into account the special features/peculiarities of integrand in (II.14) on the plane $\zeta=\zeta_1+i\zeta_2$. For this let us lock the real axis $O\zeta_1$ by the semicircumference of a large radius, which lies at the lower half-plane $\zeta_2<0$ for $z'-\Gamma>0$, and at the upper for $z'-\Gamma<0$ (Fig. II.2). During the conversion of the duct/contour of integration in (II.14) it is necessary to consider the special features/peculiarities of integrand.

Page 223.

It is not difficult to ascertain that it has two simple poles at the points

$$\zeta_{1,2} = \pm \kappa \sqrt{1 + \eta^2} \qquad (\text{II.15})$$

and branch point

$$\zeta^{\text{I, II}} = \pm \kappa. \qquad (\text{II.16})$$

In view of the Cauchy theorem about the deductions the integral in (II.14) taking into account special features/peculiarities (II.15) and (II.16) can be represented in the following form:

$$\left\{ \int_{-\infty}^{\infty} + \int_{S_{R+}} + \int_{S_{r+}} + \int_{S'_{+}} + \int_{S''_{+}} + \int_{c_{r+}} + \int_{c'_{+}} + \right.$$
$$\left. + \int_{c''_{+}} \right\} \frac{\exp[-i\zeta(z'-\Gamma)]\,d\zeta}{\sqrt{\kappa^2 - \zeta^2} - i\kappa\eta} = 0 \qquad (\text{II.17})$$

with $z' - \Gamma < 0$;

$$\left\{ \int_{-\infty}^{\infty} + \int_{S_{R-}} + \int_{S_{r-}} \int_{S'_{-}} + \int_{S''_{-}} + \int_{c_{r-}} + \int_{c'_{-}} + \right.$$
$$\left. + \int_{c''_{-}} \right\} \frac{\exp[-i\zeta(z'-\Gamma)]\,d\zeta}{\sqrt{\kappa^2 - \zeta^2} + i\kappa\eta} = 0 \qquad (\text{II.18})$$

when $z' - \Gamma > 0$.

The sections of the duct/contour of integration in expressions (II.17) and (II.18) are shown in Fig. II.2.

As a result of the selected location of the ducts/contours of integration for $z' - \Gamma < 0$ and $z' - \Gamma > 0$ the integrands in (II.17) and

(II.18) satisfy Jordan's lemma on semicircumferences $S_{R\pm}$ respectively
and therefore integrals lengthwise $S_{R\pm}$ vanish with R→∞. Furthermore,
it is obvious, that

$$\left\{\int_{S'_\pm}+\int_{S''_\pm}\right\}\frac{e^{-i\kappa z'}d\zeta}{\sqrt{\lambda^2-\zeta^2}-i\kappa\eta}=0,$$

since the directions of circuit/bypass on $S'_\pm$ and $S''_\pm$ during the
integration are opposite, and integrands on $S'_\pm$ and $S''_\pm$ have identical
values. Integrals in infinitesimal circles/circumferences $S_{r\pm}$
according to the Cauchy theorem are equal to the deductions of the
corresponding integrals in poles (II.15), multiplied on - $2\pi$i.
Integrals in circles/circumferences $C_{r\pm}$ around branch points (II.16)
are equal to zero.

Page 224.

During the integration for the coasts of sections/cuts $C'_\pm$ and $C''_\pm$ it
is necessary to consider sign change of root upon transfer from one
shore of section/cut to another, i.e., upon transfer from one branch
of root to another as a result of the circuit/bypass of branch point.
Taking into account the noted special features/peculiarities of
integration in (II.17) and (II.18), we obtain:

for $z'-\Gamma>0$

$$H(0, z') = \frac{\omega\varepsilon}{2\pi} \Big[ \int_{C'_-} + \int_{C''_-} + \int_{S_{r-}} \Big] \frac{\exp\left[-i\zeta(z'-\Gamma)\right] d\zeta}{\sqrt{\kappa^2-\zeta^2}-i\kappa\eta} =$$

$$= \frac{\omega\varepsilon}{2\pi} \Big\{ \int_{-\varkappa-i\infty}^{-\varkappa} \frac{\exp\left[-i\zeta(z'-\Gamma)\right] d\zeta}{-\sqrt{\kappa^2-\zeta^2}-i\kappa\eta} +$$

$$+ \int_{-\varkappa}^{-\varkappa-i\infty} \frac{e^{-i\zeta(z'-\Gamma)} d\zeta}{\sqrt{\kappa^2-\zeta^2}-i\kappa\eta} - 2\pi i \operatorname*{res}_{\zeta=-\zeta_0} \frac{\exp\left[-i\zeta(z'-\Gamma)\right]}{\sqrt{\kappa^2-\zeta^2}-i\kappa\eta} \Big\} =$$

$$= \omega\varepsilon \Big\{ \frac{1}{\pi} \int_{1}^{1+i\infty} \frac{\exp\left[i\kappa(z'-\Gamma)t\right]}{t^2-1-\eta^2} \sqrt{t^2-1} \; dt +$$

$$+ \frac{\eta}{\sqrt{1+\eta^2}} \exp\left[i\kappa\sqrt{1+\eta^2}(z'-\Gamma)\right] \Big\}. \qquad (\text{II.19})$$

for $z'-\Gamma < 0$

$$H(0, z') = \frac{\omega\varepsilon}{2\pi} \Big[ \int_{C'_+} + \int_{C''_+} + \int_{S_{r+}} \Big] \frac{\exp\left[-i\zeta(z'-\Gamma)\right] d\zeta}{\sqrt{\kappa^2-\zeta^2}-i\kappa\eta} =$$

$$= \frac{\omega\varepsilon}{2\pi} \Big\{ \int_{\varkappa+i\infty}^{\varkappa} \frac{\exp\left[-i\zeta(z'-\Gamma)\right] d\zeta}{-\sqrt{\kappa^2-\zeta^2}-i\kappa\eta} + \int_{\varkappa}^{\varkappa+i\infty} \frac{\exp\left[-i\zeta(z'-\Gamma)\right] d\zeta}{\sqrt{\kappa^2-\zeta^2}-i\kappa\eta} -$$

$$- 2\pi i \operatorname*{res}_{\zeta=\zeta_1} \frac{\exp\left[-i\zeta(z'-\Gamma)\right]}{\sqrt{\kappa^2-\zeta^2}-i\kappa\eta} \Big\} =$$

$$= \omega\varepsilon \Big\{ \frac{1}{\pi} \int_{1}^{1+i\infty} \frac{\exp\left[-i\kappa(z'-\Gamma)t\right]}{t^2-1-\eta^2} \sqrt{t^2-1} \; dt +$$

$$+ \frac{\eta}{\sqrt{1+\eta^2}} \exp\left[-i\kappa\sqrt{1+\eta^2}(z'-\Gamma)\right] \Big\}. \qquad (\text{II.20})$$
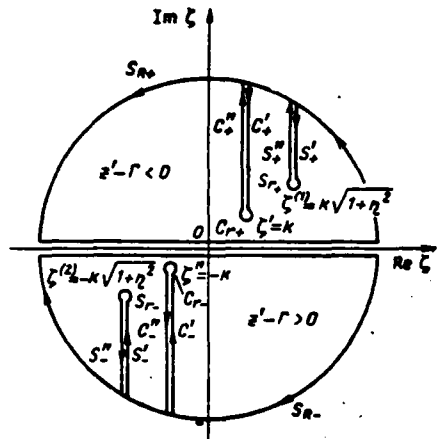
Fig. II.2. To the conversion of the duct/contour of integration.

Page 225.

After combining expressions (II.19) and (II.20), we will obtain the following representation for the field, created by slot on the impedance plane:

$$H(0, z') =$$

$$= \omega\varepsilon \left\{ \frac{i}{\pi} \int\limits_{1}^{1+i\infty} \frac{\exp(i\varkappa t \,|\, z' - \Gamma \,|)}{t^2 - 1 - \eta^2} \sqrt{t^2 - 1} \; dt + \right.$$

$$\left. + \frac{\eta}{\sqrt{1+\eta^2}} \exp(i\varkappa \sqrt{1+\eta^2} \,|\, z' - \Gamma \,|) \right\}. \quad (\text{II.21})$$

In expression (II.21) the first term corresponds to the value of radiation field on the surface of impedance screen, and the second describes two ground waves, which spread from the slot. Expression (II.21) can be used for calculating the radiation pattern of slot on the impedance half-plane in the approximation/approach of Kirchhoff.

DOC = 82036110          PAGE 358

Pages 226-228.

REFERENCES.

1. «Дифракция электромагнитных волн на некоторых телах вращения». Сборник статей. Изд-во «Советское радио», 1957.
2. Пистолькорс А. А. ЖТФ, 1947, т. 17, № 3.
3. Резников Г. Б. Антенны летательных аппаратов. Изд-во «Советское радио», 1967.
4. Уэйт Д. Р. Электромагнитное излучение из цилиндрических систем. Изд-во «Советское радио», 1963.
5. Кочержевский Г. Н. «Радиотехника», 1955, № 10.
6. Hurd R. A. Canad. J. Phys., 1956, v. 34, № 4.
7. Дупленков Д. А., Иванов С. Н. «Известия вузов», Радиофизика, 1964, т. 7, № 3.
8. Sinclair G. Proc. IRE, 1948, v. 36, № 12.
9. Bailin L. L., Silver S. Trans. IRE, 1956, v. AP-4, № 1.
10. Морс П. М., Фешбах Г. Методы теоретической физики, т. I и II. Изд-во иностранной литературы, 1958.
11. Фельд Я. Н. Основы теории щелевых антенн. Изд-во «Советское радио», 1948.
12. Вайнштейн Л. А. Электромагнитные волны. Изд-во «Советское радио», 1957.
13. Потехин А. И. Некоторые задачи теории дифракции электромагнитных волн. Изд-во «Советское радио», 1948.
14. Бриллюэн Л. Б., Пароди М. Распространение волн в периодических структурах. Изд-во иностранной литературы, 1953.
15. Фок В. А. ЖЭТФ, 1945, т. 15, вып. 12.
16. Фок В. А. «Известия АН СССР», 1946, т. 10, № 2.
17. Зоммерфельд А. Оптика. Изд-во иностранной литературы, 1953.
18. Oberhettinger F. Comm. on Pure and Appl. Math., 1954, v. 7, № 3.
19. Хенл Х., Мауэ А., Вестпфаль К. Теория дифракции Изд-во «Мир», 1964.
20. Мак-Лахлан Н. В. Теория и применение функций Матье. Изд-во иностранной литературы, 1953.
21. Франк Ф., Мизес Р. Дифференциальные и интегральные уравнения математической физики, часть вторая. ОНТИ, 1937.

22. Фок В. А. ЖЭТФ, 1949, т. 19, вып. 10.

23. Белкина М. Г., Вайнштейн Л. А. Дифракция электромагнитных волн на некоторых телах вращения. Сборник статей. Изд-во «Советское радио», 1957.

24. Baker B. B., Copson E. T. The mathematical theory of Huygens'principle. Oxford, 1939.

25. Фок В. А. Таблицы функций Эйри, 1946.

26. Уфимцев П. Я. Метод краевых волн в физической теории дифракции. Изд-во «Советское радио», 1962.

27. Васильев Е. Н. ЖТФ, 1967, т. 37, вып. 3.

28. Тихонов А. Н. ДАН СССР, 1963, т. 151, № 3.

29. Сазонов Д. М. Третий Всесоюзный симпозиум по дифракции волн. Рефераты докладов. Изд-во «Наука», 1964.

30. Айзенберг Г. З. Антенны ультракоротких волн. Связьиздат, 1957.

31. Hines J. N., Rumsey V. H., Walter C. H. Proc. IRE, 1953, v. 41, № 11.

32. Honey R. C. Trans. IRE, 1959, v. AP-7, № 4.

33. Kiely D. G. Dielectric Aerials. Lnd, 1953.

34. Цейтлин Н. М. Применение методов радиоастрономии в антенной технике. Изд-во «Советское радио», 1966.

35. Фельд Я. Н., Бененсон Л. С. Антенны сантиметровых и дециметровых волн, ч. I. ВВИА им. Жуковского, 1955.

36. Фельд Я. Н., Бененсон Л. С. Антенно-фидерные устройства, ч. II. ВВИА им. Жуковского, 1959.

37. Hansen W. W., Woodyard J. R. Proc. IRE, 1938, v. 26, № 3.

38. Кузнецов В. Д. «Радиотехника», 1950, т. 5, № 5.

39. Chernin M. G., Bickmore R. W. IRE Conv. Rec., 1956, part I, v. 4.

40. Broussaud J. Ann. de Radioélectr., 1956, № 43.

41. Cullen A. L., Goward F. K. J. IEE, 1946, v. 93, part IIIA, № 4.

42. Dion A. Trans. IRE, 1958, v. AP-6, № 4.

43. Gruenberg H. Trans. IRE, 1954, v. AP-2, № 4.

44. Ramsay J. F., Popovich B. V. IEEE Intern. Conv. Rec., 1963, part I, p. 30—55.

45. Griffits H. D. Canad. J. Phys., 1953, v. 31, № 4.

46. Simmons A. J., Giddings O. M., Diamond M., Gindsberg J. IEEE Intern. Conv. Rec., 1963, part I, p. 56—69.

47. Miller J. R., Forman R. J. Trans. IEEE, 1966, v. AP-14, № 5.

48. Гринева К. И. «Радиотехника», 1969, т. 11, № 12.

49. P a u l i W. Phys. Rev., 1938, v. 54, № 11.
50. O b e r h e t t i n g e r F. J. of Math. and Phys., 1956, v. 34, № 4.
51. S e n i o r T. B. A. Comm. on Pure and Appl. Math., 1959, v. 12.
52. Т р е н е в Н. Г. «Радиотехника и электроника», 1958, т. 3, вып. 2.
53. G o u b a u G. Proc. IRE, 1952, v. 40, p. 865.
54. E l l i o t t R. S. Trans. IRE, 1954, v. AP-2, № 2.
55. T a i C. T. J. of Appl. Phys., 1951, v. 22, № 4.
56. B r i c k Proc. IRE, 1955, pt. C, № 1.
57. W a i t J. R., O k a s h i m o K. Canad. J. Phys., 1956, Feb., v. 34.
58. W a i t J. R. Proc. IRE, 1956, v. 44, p. 694.
59. К и н г Р., У Т а й - ц з у н ь. Рассеяние и дифракция электромагнитных волн. Изд-во иностранной литературы, 1962.
60. Г о р я н н о в А. С. ДАН СССР, 1956, т. 109.
61. М а р к о в Г. Т. Труды МЭИ, 1958, вып. 30.
62. Б е л к и н а М. Г. Дифракция электромагнитных воли на некоторых телах вращения. Сборник статей, стр. 148. Изд-во «Советское радио», 1957.
63. В а й н ш т е й н Л. А. Теория дифракции и метод факторизации. Изд-во «Советское радио», 1966.
64. В а н д а к у р о в Ю. В. ЖЭТФ, 1954, т. 26, № 3.
65. M e i x n e r J. Ztschr. f. Naturforschung, 1948, Bd. 3a, S. 506.
66. Л а в р е н т ь е в М. А., Ш а б а т Б. В. Методы теории функций комплексного переменного. Физматгиз, 1958.
67. F e l s e n L. B. J. of Appl. Phys., 1955, v. 26, № 2.

Pages 229-231.


No typing.